Title
POSITIVE MUONS AND MUONIUM IN MATTER

Authors
Brewer, J.H.
Crowe, K.M.
Gygax, F.N.
et al.

Publication Date
1974-03-01

To be published as a chapter in
"Muon Physics," Vernon W. Hughes
and C.S. Wu, eds., Academic Press

LBL-2424
Preprint c. 2

POSITIVE MUONS AND MUONIUM IN MATTER

J. H. Brewer, K. M. Crowe, F. N. Gygax and A. Schenck

March 1974

Prepared for the U. S. Atomic Energy Commission
under Contract W-7405-ENG-48

DISCLAIMER

LBL-2424

POSITIVE MUONS AND MUONIUM IN MATTER

J. H. BREWER

University of British Columbia, Department of Chemistry and TRIUMF

K. M. CROWE

University of California, Berkeley and Lawrence Berkeley Laboratory

F. N. GYGAX

Lawrence Berkeley Laboratory and
Swiss Institute for Nuclear Research, Villigen

and

A. SCHENCK

Institut for High Energy Physics, ETH Zurich

March 1974

POSITIVE MUONS AND MUONIUM IN MATTER

CONTENTS

ABSTRACT

This paper is a review of recent progress in the study of interactions of polarized positive muons and muonium ($\mu^+ e^-$) atoms in matter. These studies are made possible by the asymmetric decay of the muon, in which the easily detected positron is emitted preferentially along the muon spin. A wide range of phenomena are discussed, ranging from chemical reactions of muonium to uses of the μ^+ magnetic moment as a microscopic probe of local magnetic fields in solids. Finally, the acronym "μSR" is suggested to describe such studies, in the context of their relationship with various NMR and ESR techniques.

I. INTRODUCTION

The purpose of this paper is to provide a status report on a field of muon physics which is in a state of rapid expansion: the study of interactions of positive muons and muonium with matter. We have chosen to concentrate on recent results currently under extensive study instead of providing an historical account of progress to date. We apologize in advance to those whose pioneering work will be mentioned only briefly, with the excuse that they have led the way to so many new and exciting topics that sometimes there is only room left for a brief reference to the early publications. We shall also take generous advantage of descriptions in other texts; these will provide, from time to time, the framework necessary for the reader to become his own innovator. Finally, we will often refer to original papers, which, of course, must be the ultimate source for the serious reader. At times we will only be able to provide a brief sketch to show the way and to convey our excitement about this relatively new field.

The first step of an experimental study in this field is to bring polarized positive muons to rest in condensed or gaseous matter. The usual μ^+ beam characteristics and the involved stopping mechanism leave the thermalized muons distributed over an extended macroscopic zone of the target. They can, therefore, be used as a probe for testing the bulk properties of the target material. Unlike the μ^-, the μ^+ will not be captured in atomic or molecular orbits, and will have no nuclear interactions. Until its decay, the implanted positive muon behaves much like a proton, playing the role of the nucleus of muonium, a "light isotope of atomic hydrogen." We will be mainly interested in the muon spin's magnetic interaction with the target medium. The muon will "see"--through its magnetic moment--all the magnetic field components

at its location. These local fields may originate from nuclei, electrons, paramagnetic ions, or a variety of hyperfine interactions, all of which may be influenced by externally controlled parameters, such as temperature and applied magnetic field. When the μ^+ decays, the direction of positron emission is correlated with the direction of the muon magnetic moment. Thus, counting decay positrons in a given direction as a function of the time spent by the muons in the medium provides information about the evolution of their polarization. If many muons see an identical local field, the energy of interaction between that field and the μ^+ magnetic moment may be observed as a precession frequency; random or time-dependent local fields will cause relaxation of the monitored polarization.

In Section II we will discuss how the polarized muon is obtained, how it is detected, and how it decays. Section III will deal with the process by which a high-energy μ^+ comes to rest in matter, and the consequences thereof. Sections IV through VI will treat muonium--its formation, its depolarizing effect on the μ^+, and its chemical reactions. We will then discuss experimental studies of muonium chemistry in Section VII and of muonium in solids in Section VIII. Section IX will treat the interactions of quasi-free muons in matter.

The properties of the positive muon are well measured and understood; we will start by mentioning only those that are relevant to a phenomenological understanding of the complex interactions of positive muons with their environment.

II. PHENOMENOLOGICAL DESCRIPTION OF PRODUCTION AND BEHAVIOR OF POLARIZED POSITIVE MUONS

Table II.1 contains the basic information about muons relevant to this section.

TABLE II.1 - Muon Properties.

Spin: 1/2

Mass: $m_\mu = 105.6595(3)$ MeV $= 206.7684(6)\ m_e = 0.1126123(6)\ m_p$

Magnetic moment: $\mu_\mu = \left| g_\mu S_z \right| \frac{e\hbar}{2m_\mu c} = 3.183347(9)\ \mu_p = 28.0272(2) \times 10^{-18}$ MeV/gauss

Bohr radius: $a_B^\mu = \frac{\hbar^2}{m_\mu e^2} = 255.927$ fm $= 2.55927 \times 10^{-11}$ cm

Compton wavelength: $\lambda\!\!\!^{-}_\mu = \frac{\hbar}{m_\mu c} = 1.86758$ fm

Lifetime: $\tau_\mu = 2.1994(6) \times 10^{-6}$ sec

Apart from its mass and lifetime, the positive muon is in nearly every respect similar to a positron. In the following discussions, however, the proton-like aspects of its behavior, which have received relatively minor attention in the past, will emerge as more important to an understanding of its interactions with matter. The muonium atom (Mu), as a light radioactive isotope of hydrogen, promises to greatly supplement the information obtained from studies of tritium and positronium. Negative muons play an entirely different role in matter from that of positive muons; it is not the purpose of this paper to cover that field.

The theory of the production and decay of the muon is well established; a few words are appropriate here about the mechanism by which nature has contrived to provide almost completely

polarized muon beams. The earliest source of positive muons is, of course, cosmic rays; and even they are polarized. See, for example, Bradt and Clark (BC 63). Artificially produced muons arising from pion decay, $\pi^+ \rightarrow \mu^+ + \nu_\mu$, are 100% polarized opposite to their momentum in the pion c.m. frame. In the laboratory frame, where the pions are relativistic, a muon beam arises from disintegrations at various decay angles. Preservation of a high average polarization requires only that one establish geometrical conditions that accept a reasonably narrow decay cone in the c.m. system. Fortunately, the momentum of the decay muon in the c.m. system (29 MeV/c) is large enough to separate forward decays from backward decays by simply requiring the muon to have either a higher magnetic rigidity than the pion or a longer range than the backward decay; the situation can easily be reversed. This argument assumes, of course, that the pion beam is monoenergetic. In fact, for a continuous spectrum of decaying pions, the muons are polarized only if the pion momentum spectrum has a steep slope in the region from which the observed muons originate.

The first cyclotrons operating in the meson-producing region yielded pion beams from internal targets located in the main circulation field. Positive pions usually can escape only if they are produced in the backward direction. Here the spectrum drops rapidly with momentum, producing highly polarized beams. Negative muon beams coming from pions produced in forward directions off internal targets will be less polarized.

With externally produced pions, a polarized muon beam can be made by providing a crude pion momentum selection and tuning the last elements of the channel for muons away from the mean pion momentum. Many muon channels also have sufficiently narrow momentum transmissions to provide excellent polarized beams simply by specifying the final muon range (see, for example, Culligan *et al.* (CL 64).

Thus, using parity violation in π-μ decay and taking reasonable pains in the beam design, one can produce muon beams with polarizations typically between 60 and 90%. The direction of polarization can even be reversed, by tuning the muon momentum to be either above or below the mean pion momentum. The tighter the geometry and momentum resolution, the higher the polarization --at the expense, of course, of net flux.

The muon is decelerated in matter by normal collisions with electrons; the resultant multiple Coulomb scattering produces a broadened beam, but the muon's spin is unaffected by the electrostatic interactions and remains pointed in its initial direction. Let us assume that the muon has come to rest, still unaffected by local magnetic fields in the medium. This assumption will be justified in the next section.

If the muon is in a vacuum, it precesses in a magnetic field B at the classical Larmor frequency

$$|\nu^{\mu}| = \left|\frac{2\mu_{\mu} B}{h}\right| = \left|\frac{g_{\mu} eB}{4\pi m_{\mu} c}\right| = 13.55 \frac{\text{kHz}}{\text{G}} \times |B| \cdot \qquad (2.1)$$

Table II.2 shows the frequency and time scales corresponding to the range of fields we shall consider.

TABLE II.2 - Observable muon and muonium precession frequencies and the corresponding cycle periods for a magnetic field strength B.

B	(kG)	0.01	0.1	1	10	100
$\|\nu^{\mu}\|$	(MHz)		1.355	13.55	135.5	1355
$T_{\mu} = 1/\|\nu^{\mu}\|$	(nsec)		740	74	7.4	0.74
$\|\nu^{Mu}\|$	(MHz)	13.94	139.4	1394		
$T_{Mu} = 1/\|\nu^{Mu}\|$	(nsec)	72	7.2	0.72		

In Table II.2 we have included for future reference the corresponding periods for the muonium atom.

The decay of the μ^+ lepton goes via the reaction $\mu^+ \rightarrow e^+ + \bar{\nu}_\mu + \nu_e$. The positron spectrum--treated in Chapter III--is described by

$$\frac{dN(w,\theta)}{dw d\Omega} = \frac{w^2}{2\pi}\left[(3-2w) - \xi\,(1-2w)\cos\theta\right] = \frac{C}{2\pi}\left[1 + D\cos\theta\right], \quad (2.2)$$

where $w = E/E_{max}$ is the positron energy, measured in units of $E_{max} = m_\mu/2$, θ is the angle between the spin of the μ^+ and the e^+ momentum, and ξ stands for the degree of polarization of the decaying muons. The spectrum is shown in Fig. 2.1.

In practice, the positrons are detected with an efficiency $\varepsilon(w)$ which is not constant over their entire energy range. The observed probability is then

$$\left\{\int_0^1 \varepsilon(w)\left[\frac{dN(w,\theta)}{dw d\Omega}\right] dw\right\}\frac{d\Omega}{4\pi} = \tilde{\varepsilon}\left[1 + \tilde{A}\cos\theta\right]\frac{d\Omega}{4\pi}\,. \quad (2.3)$$

If positrons of all energies were detected with the same efficiency, the observed average asymmetry $\tilde{A}$ would be $\frac{1}{3}\xi$. As the detection efficiency for low-energy e^+ is reduced, the observed $\tilde{A}$ increases from $\frac{1}{3}\xi$ toward the limiting value of ξ. Although this effect has been exploited only in a few experiments, it is especially valuable for detecting very small muon polarizations.

In addition to reduction of the asymmetry by kinematic depolarization ($\xi < 1$) and by the average over positron energy, one observes an experimental asymmetry A smaller than $\tilde{A}$ because of the inevitable finite detection angle.

A related effect of detector geometry is the average effective misalignment of the muon spin with respect to the axis of symmetry of the positron telescope. To illustrate this effect, first consider the idealized case in which all the muons stop at the same site and the positron detector subtends a very small solid angle. We then consider only those decays in

which the positron is coplanar with the telescope axis and the muon spin direction. The angle θ between muon spin and positron directions cannot generally be measured directly, since the muon spin direction is often the unknown we seek to define by experiment. It is in principle the angle θ' between the telescope axis and the e^+ direction which is directly observable. For events in the plane defined above, these two angles are related by $\theta' = \theta + \theta_o$ where θ_o is the angle between the telescope axis and the muon polarization, as shown in Fig. 2.2. Since decays are only detected if $\theta' = 0$, the counting rate in the positron detector will depend on geometry as

$$R(\theta_o) \sim 1 + A \cos \theta_o. \tag{2.4}$$

An actual experimental apparatus, of course, has a finite stopping target and a finite positron detector, as shown in Fig. 2.3. The effect of each departure from the ideal is to require definition of an average effective θ_o. The typical experiment also involves application of a magnetic field to the region, which further complicates the definition of θ_o due to the curved paths of incoming muons and decay positrons. In the end, however, Eq. (2.4) will always hold with an appropriate definition of A and θ_o, the latter being considered as an empirical parameter.

One experimental approach to studying the muon polarization is to place two positron telescopes at approximately $\theta_o = 0$ and $\theta_o = \pi$. The difference between the properly normalized positron detection rates in these two directions will be proportional to the muon asymmetry A, which may be a function of time, A(t), due to spin relaxation by interactions with the medium. The application of a magnetic field parallel to the muon polarization often has dramatic effects on the muon asymmetry, as will be seen later. This "longitudinal field technique" has been used extensively in measuring the muonium hyperfine splitting (see Chapter II), and for studying certain interactions of muons with the medium.

However, with somewhat greater experimental effort one can often obtain more information by using the "transverse field technique" described below.

In transverse field experiments, an external field B is applied perpendicular to the mutual plane of the muon polarization and the detector axis, causing the muon spins to precess at an angular frequency

$$\omega^{\mu} = \frac{\mu_{\mu} B}{\hbar} = \frac{g_{\mu} \mu_{o}^{\mu} B}{\hbar} = \frac{g_{\mu} eB}{2m_{\mu} c} \quad . \tag{2.5}$$

This causes θ_o to be replaced by $\theta_o + \omega^{\mu}(t_1 - t_o)$ in Eq. (2.4), where t_o is the time of the muon's entry into the stopping target and t_1 is the time of the decay. The distribution of positron detections thus becomes oscillatory in time.

This distribution also decays exponentially with a lifetime $\tau_{\mu} = 2.2$ μsec due to the disintegration of the muon, and in some cases has a time dependence A(t) of the envelope of the oscillations, which reflects a relaxation of the average polarization due to interactions with the medium and/or inhomogeneities in the external field.

The distribution can be expressed by the following formula, which incorporates all the effects mentioned above:

$$\frac{dN(t)}{dt} = N_o e^{-t/\tau_{\mu}} \left\{1 + A(t) \cos \left[\omega^{\mu} t + \phi\right]\right\} + BG, \tag{2.6}$$

where $t = t_1 - t_o$ and $\phi = \theta_o + \Delta\phi$, in which $\Delta\phi$ represents medium-dependent shifts of the apparent initial phase of the precession, to be discussed later. The term BG accounts for additional events, accidentals, and electronic breakthroughs, which occur generally at random and are usually rare. N_o is a normalization factor, essentially determined by the solid angle of the e^+ detector, its average detection efficiency, and the total number of stopped muons.

Experimentally, one collects data by recording the arrival time t_o of the muon and the decay time t_1, and constructing an elapsed-time histogram for $t = t_1 - t_o$, an example of which is shown in Fig. 2.4. In this situation, the ensemble of events are collected one at a time; the event signature is constructed so that only a single muon may be in the sample at once, and subsequently only one positron may appear. The time interval resolution Δt can be set either electronically or in the binning program, and is typically on the order of 10^{-9} sec. The expected number of counts in a histogram bin of width Δt at t_i is given by $[dN(t_i)/dt]\,\Delta t$; by varying the parameters N_o, $A(t)$, ω^μ, ϕ and BG, the optimal fit of Eq. (2.6) to the entire histogram is determined, defining the best values for these parameters. Usually $A(t)$ is expressed as Ae^{-t/T_2} in terms of the two independent parameters A and T_2. Of the four parameters A, T_2, ω^μ and $\Delta\phi = \phi - \theta_o$, each represents a piece of valuable information about the interactions of the positive muon.

The asymmetry A is proportional to the apparent initial muon polarization. As an indication of the amount of polarization one observes in practice, Table II. 3 shows a number of results for asymmetries measured in various materials. The data shown fall into three general groups. One group is essentially completely polarized ($A \tilde{\sim} 1/3$), the second group is roughly 50% depolarized, and the third has a polarization of 10% or less.

Relaxation times in the range $10^{-7} < T_2 < 10^{-5}$ sec can easily be measured by this technique, providing information complementary to proton NMR data. These phenomena will be discussed in Section IX.

The fitted phase ϕ consists of two parts: the average effective angle θ_o between the positron telescope axis and the mean polarization of the stopping muon, and the medium-dependent apparent phase shift $\Delta\phi$. Since in the usual situation muons of various polarizations stop over an extended

target volume, θ_o may be a poorly calculable quantity; it is usually left as an empirical parameter. Experimental uncertainties in t_o are usually also absorbed into the definition of θ_o. The additional apparent phase shift $\Delta\phi$ is due exclusively to interactions of the muon in the target medium after it comes to rest. A nonzero value of $\Delta\phi$ generally reflects a very short-lived formation of muonium just after the μ^+ enters the target. During this brief episode, rapid precession takes place, which sometimes will leave the muons in their ultimate diamagnetic environment with somewhat rotated spins. All this happens too quickly to be directly observable, but the resultant $\Delta\phi$ provides very useful information about the fast processes involved. In Section VI we will discuss some of the recent applications of this phase data.

The precession frequency of a single muon in a magnetic field B is given by Eq. (2.5). Equation (2.6) embodies the assumption that all the muons see the same field B. Occasionally, in addition to small field inhomogeneities and local effects leading to muon spin relaxation by dephasing, there may be several distinct local fields seen by separate ensembles of muons. In this case $\cos(\omega^\mu t + \phi)$ must be replaced by $\sum_i P_i \cos(\omega_i^\mu t + \phi_i)$ to preserve the generality of Eq. (2.6) (P_i = fraction of the muons precessing at the frequency ω_i^μ). Often it is advantageous to perform a simple Fourier analysis of the time histogram (after subtracting background and dividing out the exponential decay). This treatment may reveal precession signals which otherwise might go unsuspected.

In the brief discussion above we have attempted to use only classical concepts; in our detailed discussions of these phenomena we will attempt to be more precise.

III. DECELERATION AND THERMALIZATION OF POSITIVE MUONS IN MATTER

A qualitative understanding of how a fast μ^+ slows down and stops in a target is essential to a complete picture of the behavior of muons in matter. Several questions relating to this process are of basic importance: (1) What are the essential states of the deceleration process? (2) What is the time scale for each state? (3) Is the muon polarization affected? (4) In what state or states does the muon finally thermalize? In this Section we will deal with these questions in some detail. Other questions, related to problems which are not yet well understood, can also be raised: What sorts of radiation damage are caused by the muon, and how might they influence the muon after it stops? In what media could there be significant exceptions to the established rules of how a μ^+ slows down? We will not attempt to answer these questions in the absence of specific experimental evidence, but in some instances interesting conjectures can be made.

The most important gross features of the energy loss process are displayed as a flow diagram in Fig. 3.1. The boxes represent the various stages of deceleration and contain descriptions of the mechanisms involved. On the right side are time estimates for the duration of the different stages, and the approximate kinetic energy at each stage is also indicated.

A muon entering a target with a kinetic energy of $\sim$50 MeV (momentum 115 MeV/c) will first lose energy by scattering with electrons, until its velocity approaches that of the valence electrons of the target atoms (corresponding to an energy of 2-3 keV). During this stage, the energy loss per unit time is given by the Bethe formula. The total time it takes the μ^+ to slow down to 2-3 keV in condensed matter is thus estimated to be about 10^{-10} - 10^{-9} sec; this time is probably somewhat longer in gases. Depolarization during this stage could only be due to spin dependent forces in the

scattering processes with electrons or nuclei. In both cases, as Ford and Mullin (FM 57) and Wentzel (WE 49) have shown, such depolarizing effects are extremely small and can be neglected.

For muon energies of less than 2 keV, or for muon velocities smaller than valence electron velocities, the Bethe formula no longer represents a useful approximation. The deceleration of negative muons from this energy range down to thermal velocity has been treated by Fermi and Teller (FT 47). They estimate a typical slowing-down time in condensed matter of several times 10^{-14} sec. Energy loss is again due to collisions with electrons, where the electrons are now treated as a degenerate gas. In principle, positive muons would slow down through this energy range in similar times if the same mechanisms were in effect. However, there are drastic qualitative differences between the behavior of negative and positive muons at these energies. The most important one is that positive muons capture electrons from the medium to form neutral atoms. This is known to happen for protons, from studies of proton beams traversing condensed or gaseous matter, in which the positive beam is partially neutralized (AG 62). As the velocity of the positive particle drops below that of an electron in the ground state of hydrogen ($\sim\alpha c$), corresponding to a kinetic energy of 3 keV for the muon, the proton (or muon) begins to capture and lose electrons in rapid succession. As the velocity decreases further, the neutral state begins to dominate; at a velocity of about 10^8 cm/sec the beam is more than 80% neutralized. This is shown in Fig. 3.2 for protons traversing aluminum or O_2 gas. It can be inferred that a positive muon beam will become almost completely neutralized at an energy of about 200 eV, forming stable atoms of muonium (MB 52). Direct confirmation that positive muon beams end up as muonium atoms was obtained from the muonium studies that have been performed by Hughes *et al.*,

in gaseous argon targets (HM 60).

To our knowledge, no calculations have been made of the time the positive muon takes to decelerate from 3 keV to 200 eV. Allison (AL 58) has estimated that a μ^+ slowing down through this energy range in hydrogen gas at 1 atm will spend about 2×10^{-10} sec as muonium, passing through about 100 cycles of muonium formation and ionization. The number of capture-loss cycles should not be too dependent on the medium, but the time scale might be expected to be a factor of 1000 shorter ($\sim 2 \times 10^{-13}$ sec) in solid or liquid targets. According to Fermi and Teller, a free μ^- would slow down through this energy range in several 10^{-14} sec. One may thus safely assume that the total time the positive muon spends in the energy range 3 keV - 200 eV is less than 5×10^{-13} sec.

This has important consequences with regard to the depolarization that will occur in this stage. As will be seen in the next Section, the spins of only half of the muons in the ground state of muonium will show a changing orientation in time. They will reverse their directions periodically at a frequency of ~ 4.6 GHz, due to their contact interaction with the magnetic moment of the electron. This modulation is often described qualitatively as the precession of the μ^+ spin in the effective hyperfine field (about 160 kG) produced by the electron's magnetic moment. The spins of these muons will have reversed direction in about 2×10^{-10} sec. Since 5×10^{-13} sec is only a tiny fraction of this period, the depolarization in condensed media during deceleration from 3 keV to 200 eV is totally negligible, even if a single muonium atom remains intact for the entire period; if we take into account the repeated breakup and reformation of muonium, we would expect depolarization during this phase to be negligible even in gases.

At a kinetic energy of 200 eV, practically all muons are in the muonium state. Subsequent deceleration to thermal energies proceeds by collisions of muonium atoms with target atoms or molecules. Mobley (MO 67) has treated thermalization of muonium in argon gas as a purely kinematic process of elastic collisions, in which the average fractional energy loss per collision is constant,

$$\frac{\overline{\Delta E}}{E} = -2\frac{m}{M} ,$$

where m is the mass of muonium and M is the mass of a target atom or molecule. In this picture, the time T_{el} to decelerate from E_1 to E_2 in a gas of density n molecules per unit volume is given by

$$T_{el} = \frac{M}{2^{5/2} n\sigma\sqrt{m}} \left(\frac{1}{\sqrt{E_2}} - \frac{1}{\sqrt{E_1}} \right) , \qquad (3.1)$$

where σ is the cross section for elastic collisions. Note that muonium slows down faster in collisions with lighter atoms. Mobley calculates a time of 1.5×10^{-11} sec for slowing down from 200 to 0.04 eV in argon gas at 35 atm. The number of collisions in this process is about 2.5×10^{3}, independent of pressure.

In gases of large molecules or in condensed media, this model is of questionable validity. Many inelastic energy-loss processes doubtless exist, whose net effect can only be to speed up the deceleration process. Thus the thermalization time in condensed media with molecular weights similar to argon will generally be shorter than $\sim 10^{-12}$ sec, the estimate obtained by simply scaling Mobley's result with density.

As in the initial muonium formation stage, this time is too short to cause any appreciable depolarization. Thus the muons will still be fully polarized immediately following their thermalization in muonium atoms.

Another process is often quite significant during this thermalization state: while a muonium atom still has an epithermal energy in the range of roughly 20 eV - 1 eV, it may participate in so-called "hot atom" reactions. These are chemical reactions that are usually forbidden in the thermal region for lack of energy to overcome potential barriers (high activation energies). Hot atom reactions of tritium (like muonium a radioactive isotope of hydrogen) have been widely studied in gases (RO 70). There are also a number of studies of hot tritium reactions in aqueous solutions, which may be used as a guide for conjecture regarding the outcome of hot muonium reactions in liquids. It should be mentioned that hot atom reactions of positronium in aqueous solution have also been studied in a number of cases (BN 72). However, the analogy between positronium and the various isotopes of hydrogen is much weaker.

The most common hot atom reactions of muonium can be classified as follows:

1. Substitution reactions of the type

   $XH + Mu^* \rightarrow XMu + H$, where X is some radical species;

2. Abstraction reactions such as

   $XH + Mu^* \rightarrow X + MuH$;

3. Addition reactions:

   $X + Mu^* \rightarrow XMu$.

The third type of reaction requires a deexcitation mechanism to carry away the excess energy; it is very likely to produce a chemical radical if X is a molecule with saturated bonds. The other types may also lead to paramagnetic molecules incorporating muons, since there is a lot of energy available and the final products may be in excited triplet states.

So far, as will be shown later, only the first type of reaction has been experimentally verified in the hot atom chemistry of muonium. In this type,

muonium is built into a molecule with saturated bonds, and the total spin density of electrons at the muon site is zero. With respect to magnetic interactions the muon can be considered as quasi-free. These muons have, of course, lost none of their polarization up to the time they become part of a molecule. This is true, in fact, for all the muons that have proceeded through the hot atom channel, independent of their final chemical status.

The situation just after thermalization may be summarized as follows:

1. The total elapsed time since the muon entered the target is between 10^{-10} sec (in condensed media) and 10^{-9} sec (in dilute gases).
2. Regardless of the muon's chemical state, its polarization is completely conserved.
3. The muon may be in any of the following states, listed in approximate order of decreasing likelihood:
   A. A thermalized muonium atom.
   B. Part of a molecule with saturated bonds. In this diamagnetic environment the muon can be considered quasi-free.
   C. Part of a paramagnetic molecule (e.g., a radical or an excited triplet state). Here the environment is magnetically similar to muonium.
   D. A free muon. This state can only occur in the rare cases where the ionization potential of the medium is greater than that of muonium (e.g., in the case of helium).

While there is much evidence to support the validity of this general picture of how a μ^+ slows down in matter, very little is known about the details of the mechanism involved and the possible implications. For instance,

a better understanding of the dynamics of hot atom reactions of muonium might lead to further elucidation of isotopic effects in hot atom chemistry in general. However, in spite of the important role played by hot atom reactions in the chemistry of muonium (as described in Section VII), these phenomena are not yet well understood. The rest of this chapter deals with the behavior of muons in their various states in the few microseconds of their remaining lifetime after thermalization.

IV. QUALITATIVE BEHAVIOR OF THE MUON SPIN IN MUONIUM

Before we embark upon a rigorous derivation of the evolution of a μ^+ spin in a muonium atom, it is conceptually helpful to describe this behavior in semiclassical terms. To this end, we recall from Chapter II the Hamiltonian for the hyperfine interaction between μ^+ and e^- magnetic moments in the presence of an external magnetic field B; this operator can be written

$$H^{Mu} = \frac{\hbar}{4}\omega_o(\vec{\sigma^\mu}\cdot\vec{\sigma^e}) + \frac{\hbar}{2}\vec{\omega^\mu}\cdot\vec{\sigma^\mu} + \frac{\hbar}{2}\vec{\omega^e}\cdot\vec{\sigma^e}\,, \tag{4.1}$$

where $\hbar\omega_o$ is the hyperfine energy splitting, $\vec{\sigma^\mu}$ and $\vec{\sigma^e}$ are muon and electron Pauli spin operators, and $\vec{\omega^\mu}$ and $\vec{\omega^e}$ are muon and electron Larmor frequencies, given by $\hbar\vec{\omega^\mu} = g_\mu \mu_o^\mu \vec{B}$ and $\hbar\vec{\omega^e} = g_e \mu_o^e \vec{B}$. Here $g_\mu \approx -2$ and $g_e \approx +2$ are the muon and electron g-factors, μ_o^μ and μ_o^e are their respective Bohr magnetons ($\mu_o = e\hbar/2mc$). Note that $\vec{\omega^\mu}$ and $\vec{\omega^e}$ are antiparallel.

The eigenvalues of this Hamiltonian are given by the familiar Breit-Rabi formula. To avoid the sometimes misleading practice of labelling the energy levels by total angular momentum eigenvalues (which are good quantum numbers only in zero field), we write out the energy eigenvalues individually:

$$\begin{aligned}
\omega_1 &= E_1/\hbar = \frac{\omega_o}{4} + \omega_-\,,\\
\omega_2 &= E_2/\hbar = -\frac{\omega_o}{4} + \sqrt{\frac{\omega_o^2}{4} + \omega_+^2}\,,\\
\omega_3 &= E_3/\hbar = \frac{\omega_o}{4} - \omega_-\,,\\
\omega_4 &= E_4/\hbar = -\frac{\omega_o}{4} - \sqrt{\frac{\omega_o^2}{4} \pm \omega_+^2}\,,
\end{aligned} \tag{4.2}$$

where $\omega_\pm = \frac{1}{2}\left(|\vec{\omega^e}| \pm |\vec{\omega^\mu}|\right)$. These levels are shown in Fig. 4.1 as

functions of the "natural" specific field $x = 2\omega_+/\omega_o = |\vec{B}|/B_o$, where $B_o = 1585$ G. We will later refer to the transition frequencies $\omega_{ij} = \omega_i - \omega_j$.

The energy eigenstates can be expressed most simply in terms of the "natural" specific field x and the "natural" basis $|m_\mu\ m_e\rangle_{||}$, where the subscript "$||$" indicates explicitly that the axis of quantization is along the magnetic field:

$$\begin{aligned}
|E_1\rangle &= |++\rangle_{||} &&= && |F=1,\ m_F=+1\rangle\ , \\
|E_2\rangle &= s|+-\rangle_{||} + c|-+\rangle_{||} && \xrightarrow[x\to 0]{} && |F=1,\ m_F=0\rangle\ , \\
|E_3\rangle &= |--\rangle_{||} &&= && |F=1,\ m_F=-1\rangle\ , \\
|E_4\rangle &= c|+-\rangle_{||} - s|-+\rangle_{||} && \xrightarrow[x\to 0]{} && |F=0,\ m_F=0\rangle\ ,
\end{aligned} \tag{4.3}$$

$$\text{where} \quad c = \frac{1}{\sqrt{2}}\left(1 + \frac{x}{\sqrt{1+x^2}}\right)^{\frac{1}{2}} \tag{4.4}$$

$$\text{and} \quad s = \frac{1}{\sqrt{2}}\left(1 - \frac{x}{\sqrt{1+x^2}}\right)^{\frac{1}{2}}\ ;$$

we have used the compact notation $|+-\rangle \equiv |m_\mu = +\tfrac{1}{2},\ m_e = -\tfrac{1}{2}\rangle$, etc.

The muon is always assumed (without loss of generality) to be initially completely polarized, while the electron it captures is generally unpolarized. This is assumed throughout, although one can imagine situations in which a certain fraction of the electrons might have a significant polarization [e.g., in ferromagnetic media (IV 73)]. Always choosing the quantization axis along the initial muon polarization, we can thus express the initial conditions as follows: half of the muonium ensemble is formed in the state $|a_o\rangle = |++\rangle$ and half in the state $|b_o\rangle = |+-\rangle$. Note that we have not specified by a subscript whether the quantization axis is along the field. We shall treat the

two orthogonal possibilities separately.

Now, working in the Schrödinger picture, we are prepared to describe the evolution of the muonium spin state.

A. Longitudinal Field

If the magnetic field is parallel to the initial muon polarization, the first half of the ensemble is in an eigenstate, $|a_o\rangle = |++\rangle_{\|} = |E_1\rangle$, and is therefore stationary; the second half, however, is in a superposition of two eigenstates, $|b_o\rangle = |+-\rangle_{\|} = s\,|E_2\rangle + c\,|E_4\rangle$. The time dependence of this state will be

$$\begin{aligned} |b(t)\rangle &= se^{-i\omega_2 t}\,|E_2\rangle + ce^{-i\omega_4 t}\,|E_4\rangle\,, \\ &= e^{-i\omega_2 t}\left(s\,|E_2\rangle + ce^{i\omega_{24} t}\,|E_4\rangle\right)\,, \\ &= e^{-i\omega_2 t}\left[\left(s^2 + c^2 e^{i\omega_{24} t}\right)|+-\rangle_{\|} + sc\left(1 - e^{i\omega_{24} t}\right)|-+\rangle_{\|}\right]\,, \end{aligned} \tag{4.5}$$

where $\omega_{24} = \omega_2 - \omega_4$.

In zero field, $c = s = 1/\sqrt{2}$, and $\omega_{24} = \omega_o$, so that (4.5) becomes

$$|b(t)\rangle = \frac{e^{-i\omega_2 t}}{2}\left[\left(1 + e^{i\omega_o t}\right)|+-\rangle_{\|} + \left(1 - e^{i\omega_o t}\right)|-+\rangle_{\|}\right].$$

That is, neglecting the physically insignificant overall phase, the state $|b(t)\rangle$ oscillates at frequency ω_o between the original state $|+-\rangle_{\|}$ and the state $|-+\rangle_{\|}$, in which the spins are reversed. The muon polarization in this half of the ensemble thus oscillates between +1 and -1, averaging to zero. Combined with the constant polarization +1 for the first half of the ensemble, this produces a net muon polarization which oscillates between 0 and +1 at frequency ω_o, averaging to $\overline{P}^{\mu}(x = 0) = 1/2$. In vacuum, the

period of these oscillations is 0.224 nsec, too short to be resolved with any existing experimental apparatus, so that the apparent effect of muonium formation is reduction of the muon polarization by a factor of 2.

In nonzero longitudinal field, this apparent loss of muon polarization is alleviated. The muon polarization for the first half of the muonium ensemble is still a constant +1, while the polarization of the second half now oscillates between P_{min} and +1, where $P_{min} = \frac{(x^2 - 1)}{(x^2 + 1)}$ can be derived from Eq. (4.5) with Eq. (4.4). Thus the net muon polarization oscillates at angular frequency ω_{24} between $x^2/(x^2 + 1)$ and +1, resulting in an average of

$$\overline{P}^{\mu}_{\parallel}(x) = \frac{1}{2} + \frac{1}{2} \cdot \frac{x^2}{1 + x^2} \quad . \tag{4.6}$$

The apparent depolarization of muons in muonium is thus "quenched" by strong magnetic fields ($B >> B_o$). This phenomenon has been the subject of many experimental studies. It is important to remember that the μ^+ polarization is not actually lost in muonium, but only shared with the electron to an extent which depends upon the external field. If quantum irreversible processes cause relaxation of the electron spin by interaction with the medium, all the polarization eventually disappears; but in the simple case described above, the muon polarization always returns to +1 periodically. Equation (4.6) is exact for free muonium, but refers to the average of the muon polarization over times long compared to the hyperfine period. Normally the time resolution of the apparatus forces such an average, but we will later encounter situations in which the strength of the equivalent hyperfine interaction is greatly reduced, increasing the hyperfine period to the point where these oscillations can be observed directly by the techniques described here.

B. Transverse Field

When the magnetic field is perpendicular to the initial muon polarization neither of the states $|a_o\rangle = |++\rangle_\perp$ and $|b_o\rangle = |+-\rangle_\perp$ is an eigenstate, since the axis of quantization is no longer along the field. This situation is formally more complicated, and a thorough treatment will have to wait until the next Section. However, a semiclassical model can give us a qualitative picture of the behavior.

In weak transverse fields ($B << B_o$), we may treat the effect of the external field as a perturbation on the zero-field eigenstates. In this approximation, the two halves of the muonium ensemble in states $|a\rangle$ and $|b\rangle$ represent, respectively, a polarized spin-1 (triplet) system in which muon and electron spins are "locked" together by the hyperfine interaction, and a spin-0 (singlet) system in which the muon polarization oscillates about zero at high frequency, somewhat as in the field-free case. The triplet state, with a magnetic moment dominated by the electron, will precess in the external field at its Larmor frequency, in a sense opposite to that of the free muon in the same field:

$$\vec{\omega}^{Mu} = \frac{1}{2}(\vec{\omega}^{e} + \vec{\omega}^{\mu}) \approx -103\ \vec{\omega}^{\mu}. \tag{4.7}$$

Note that $|\vec{\omega}^{Mu}| = \omega_-$. Since the muon and electron spins are "locked" together, this precession frequency can be observed in the muon's decay pattern. The motion of the muon polarization in muonium in a weak transverse field thus consists approximately of rapid hyperfine oscillations superimposed upon a slower muonium precession. The actual time dependence of the projection of the μ^+ polarization along its original axis is shown in Fig. 4.2, for a transverse field of 100 G. The qualitative features described above are evident. Note that the mean amplitude of the muonium precession,

averaged over the hyperfine oscillations, is 1/2. In low field ($B \lesssim 100$ G) this precession can be observed directly (GI 71).

When the transverse field is no longer very small compared to $B_o = 1585$ G, the naive picture used above is no longer adequate. The splitting of both the muonium precession and the hyperfine oscillation frequencies can no longer be ignored. As is generally the case, these frequencies correspond to $\Delta m = \pm 1$ transitions between Zeeman eigenstates, in this case ω_{12}, ω_{23}, ω_{14}, and ω_{34}. The selection rules that govern which frequencies actually appear are a function of the field. The limiting cases are

$$\begin{aligned} \Delta m_F &= \pm 1 \text{ for } B << B_o \\ \Delta m_\mu &= \pm 1 \text{ for } B >> B_o. \end{aligned} \tag{4.8}$$

Thus for $B << B_o$ all the four frequencies appear with the same amplitude, whereas only ω_{12} and ω_{34} remain for $B >> B_o$. The frequency splittings have been observed and analyzed to extract the hyperfine frequency of muonium in various media. This new and rapidly expanding branch of μ^+ spin physics will be discussed in more detail in Section VIII.

In this section we have defined a number of useful quantities and described the behavior of the μ^+ polarization in a free muonium atom, taking advantage of a few simplifying approximations. In the next section we will construct the formalism necessary for an exact description of the evolution of muonium in an external field, including interactions of the electron with the medium. Section VI will be devoted to a description of the effect on the muon polarization of formation of muonium for very short times, and the implications for the study of muonium chemistry.

V. MUON SPIN EVOLUTION IN QUASI-FREE MUONIUM: AN ADVANCED TREATMENT

In the previous section we described the time dependence of the spin state of muonium in semiclassical terms; for a few simple cases, that description was complete, but in transverse field or in cases where the muonium electron interacts with the medium, a somewhat more elaborate formalism must be developed. This will be the task of this section.

A. Free Muonium in Longitudinal Field

For the time dependence of the muon polarization in this simplest system, the treatment of the previous section is exact. The polarization of the muon in the second half of the ensemble (state $|b\rangle$) is given by $\vec{P}^{\mu}_{b,\parallel}(x,t) = P^{\mu}_{b,\parallel}(x,t)\,\hat{z} = \langle b(t)|\sigma^{\mu}_{3}|b(t)\rangle\,\hat{z}$, where $\vec{B} = B\,\hat{z}$, $\vec{\sigma}^{\mu}$ is the Pauli spin operator for the muon, and $|b(t)\rangle$ is given by Eq. (4.5). The muon polarization for the entire ensemble is $\vec{P}^{\mu}_{\parallel}(x,t) = P^{\mu}_{\parallel}(x,t)\,\hat{z} = 1/2\,[1 + P^{\mu}_{b,\parallel}(x,t)]\,\hat{z}$. The result is

$$P^{\mu}_{\parallel}(x,t) = \frac{1}{2} + \frac{1}{2}\left[\frac{x^2 + \cos(\omega_{24}t)}{1 + x^2}\right]. \tag{5.1}$$

B. Free Muonium in Transverse Field

The exact time dependence of the muon polarization in muonium in a transverse magnetic field can be obtained in similar fashion as long as the muonium atom does not interact with its material environment. For this we must construct a few 4×4 matrices for changes of basis.

We can most easily describe the initial state in the "transverse" basis $|m_{\mu}\,m_{e}\rangle_{\perp}$ (formally written $|T\rangle$), in which the axis of quantization is

along the initial muon polarization, as in Section IV. A matrix of Clebsch-Gordan coefficients, J, transforms this basis into the basis $|F, m_f\rangle_\perp$ in which the total angular momentum along the same quantization axis is diagonal. If we write $|F, m_F\rangle_\perp$ formally as $|F_\perp\rangle$, then $J_{ij} = \langle F_\perp^i | T_j \rangle$. It is easy to find the rotation matrix R which transforms vectors from the $|F_\perp\rangle$ basis into the basis $|F, m_F\rangle_\parallel$, or $|F_\parallel\rangle$, with the new quantization axis along the magnetic field. The inverse matrix of Clebsch-Gordan coefficients, J^{-1}, then transforms the $|F_\parallel\rangle$ basis into $|m_\mu m_e\rangle_\parallel$, or $|L\rangle$, in terms of which the energy eigenstates $|E\rangle$ can be described by the matrix $\epsilon_{jk} = \langle E_j | L_k \rangle$ implicit in Eqs. (4.3). We can thus expand the initial states in energy eigenstates, allow the stationary components to evolve in time as $\exp(i\omega_j t)$, and then re-expand the result in a basis in which the muon polarization can easily be expressed. A convenient final-state basis will be $|L\rangle$, or $|m_\mu m_e\rangle_\parallel$, where the effect of the operator $\vec{\sigma}^\mu$ is obvious. Thus the equations of motion for the first half of the muonium ensemble can be written

$$|a(t)\rangle = |L_i\rangle \langle L_i | E_j\rangle \exp(i\omega_j t) \langle E_j | L_k\rangle \langle L_k | F_\parallel^\ell\rangle \times \langle F_\parallel^\ell | F_\perp^m\rangle \langle F_\perp^m | T_n\rangle \langle T_n | a(o)\rangle , \quad (5.2)$$

or

$$|a(t)\rangle = |L_i\rangle \epsilon_{ij}^+ \exp(i\omega_j t) \epsilon_{jk} J_{kl}^+ R_{lm} J_{mn} \langle T_n | a(o)\rangle ,$$

where summation over repeated indices is understood. The time evolution of the second half of the muonium ensemble, $|b(t)\rangle$, is obtained by following the same steps.

The two transverse components of muon polarization can be expressed simultaneously in terms of the complex quantity $\tilde{P}_\perp^\mu(x,t)$, whose real part is the μ^+ polarization along the initial direction $\hat{x}$ and whose imaginary part is the μ^+ polarization along the direction $\hat{y}$ perpendicular to both $\hat{x}$ and $\hat{z}$, the field direction, chosen so that $\hat{x} \times \hat{y} = \hat{z}$. The time dependence of this

complex polarization is given by

$$\tilde{P}_{\perp}^{\mu}(x,t) = \frac{1}{2}\langle a(t)|(\sigma_1^{\mu} + i\,\sigma_2^{\mu})|a(t)\rangle + \frac{1}{2}\langle b(t)|(\sigma_1^{\mu} + i\,\sigma_2^{\mu})|b(t)\rangle . \tag{5.3}$$

The explicit expressions of the matrices J, R. and ϵ allow solution of Eq. (5.3) in terms of (5.2). The final result takes the form

$$\begin{aligned}\tilde{P}_{\perp}^{\mu}(x,t) &= P_x^{\mu}(x,t) + i\,P_y^{\mu}(x,t)\\ &= \tfrac{1}{4}[(1+\delta)\,e^{i\omega_{12}t} + (1-\delta)\,e^{i\omega_{23}t} + (1+\delta)\,e^{-\omega_{34}t} + (1-\delta)\,e^{i\omega_{14}t}] \qquad (5.4)\\ &= e^{i\omega_- t}\cos\frac{\omega_o}{2}t\,[\cos(\frac{\omega_o}{2}+\Omega)\,t - i\delta\sin(\frac{\omega_o}{2}+\Omega)t],\end{aligned}$$

where

$$\delta = c^2 - s^2 = \frac{x}{\sqrt{1+x^2}},$$

$$\omega_- = \frac{1}{2}(\omega_{12}+\omega_{23}) = \frac{1}{2}(|\vec{\omega}^{e}| - |\vec{\omega}^{\mu}|) \qquad \text{(see Section IV);}$$

and $$\Omega = \frac{1}{2}(\omega_{23} - \omega_{12}) = \frac{\omega_o}{2}(\sqrt{1+x^2} - 1).$$

In weak fields ($x << 1$) Eq. (5.4) can be approximated by

$$\tilde{P}_{\perp}^{\mu}(x,t) \approx \frac{1}{2}e^{i\omega_- t}[\cos\Omega t + \cos(\omega_o + \Omega)t], \tag{5.5}$$

and then its real part takes the form

$$P_x^{\mu}(x,t) \approx \frac{1}{2}\cos\omega_- t\,[\cos\Omega t + \cos(\omega_o + \Omega)t], \tag{5.5a}$$

which is shown in Fig. 4.2. Since the frequency $(\omega_o + \Omega)$ is too high to observe experimentally, this appears as "muonium precession" at frequency ω_-, modulated at the "beat frequency" Ω, with half the initial μ^+ polarization amplitude. This pattern is clearly shown in a measurement by Gurevich et al. (GI71), who observed muonium precession in quartz and germanium

at 98 gauss (Fig. 5.1). From the precession frequency ω_- and the beat frequency Ω, the hyperfine frequency ω_o can be calculated:

$$\omega_o \approx \omega_-^2 / \Omega.$$

At early times or in very weak fields, the condition $\Omega t << \pi/2$ is fullfilled. Equation (5.5) can then be written

$$\tilde{P}_\perp^\mu(x, t) \tilde{=} \frac{1}{2} e^{i\omega_- t} (1 + \cos \omega_o t). \tag{5.6}$$

That is, the motion consists of a comparatively slow "muonium precession" at frequency ω_-, superimposed upon a "hyperfine modulation" at frequency ω_o. This is just the behavior described semiclassically in the previous section.

C. Quasi-Free Muonium

A muonium atom embedded in matter can rarely be considered "free"; usually we will have to account for the perturbing effects of its material environment.

The first such effect we must consider is the possible collective action of charge carriers or of an ionic crystal field upon the Coulomb attraction in the electron-muon charge system. A large local dielectric polarizability of the medium, due to collective shielding effects, can change the size of the muonium atom, thus drastically modifying the hyperfine coupling constant. Effects of this sort, observed mainly in semiconductors, will be treated in Section VIII. Since these interactions change only the value of ω_o, we will consider them only implicity in this section. It should be kept in mind, however, that ω_o can be a function of the medium; since this hyperfine frequency determines the time scale in muonium, such effects influence the μ^+ depolarization rate.

An interaction with the medium which we must treat explicitly is the coupling of the muonium electron's magnetic moment with those of charge carriers or with the crystal field. (We may neglect direct coupling of the μ^+ magnetic moment to such fields in the medium, at least on the time scale of muonium precession, since these interactions are at least ~ 200 times smaller than those of the electron.) In order to take that interaction into account, we must turn to the elegant and general formalism used by Ivanter and Smilga (IS 68), also illustrated in a paper by Fischer (FI 73). Their descriptions are based on earlier work by Nosov and Iakovleva (NY 63), who in turn used an approach introduced by Wangsness and Bloch for treatment of depolarization by quantum irreversible processes (WB 53). Here we briefly summarize that formalism and its predictions; the results will be used in the next section in connection with μ^+ depolarization related to chemical reactions of muonium.

We start by defining the 4×4 density matrix for the muonium spin system in terms of the Pauli spin matrices $\vec{\sigma}^{\mu}$ and $\vec{\sigma}^{e}$ for the muon and electron:

$$\rho^{Mu} = \frac{1}{4}\left[1 + \vec{P}^{\mu}\cdot\vec{\sigma}^{\mu} + \vec{P}^{e}\cdot\vec{\sigma}^{e} + \sum_{i,j=1}^{3} p_{ij}\,\sigma_i^{\mu}\,\sigma_j^{e}\right] = \frac{1}{4}\sum_{i,j=0}^{3} p_{ij}\,\sigma_i^{\mu}\,\sigma_j^{e}, \qquad (5.7)$$

where $\vec{P}^{\mu}$ is the muon polarization vector, with components p_{10}, p_{20}, p_{30} (x, y, z), and $\vec{P}^{e}$ is the electron polarization vector, with components p_{01}, p_{02}, p_{03}. The quantities σ_o^{μ} and σ_o^{e} are 2×2 unit matrices. Thus the 16 matrices $\sigma_i^{\mu}\cdot\sigma_j^{e}$ (i, j = 0-3) form a complete orthonormal basis for the space subtended by the spin 1/2 ⊗ spin 1/2 system.

For free muonium, the equation of motion of this density matrix is

$$\frac{\partial \rho^{Mu}}{\partial t} = -\frac{i}{\hbar}\left[H^{Mu},\ \rho^{Mu}\right], \qquad (5.8)$$

where H^{Mu} is given by Eq. (4.1). In the quasi-free case, however, the Hamiltonian of the whole system has to be considered. One must add to H^{Mu} a term V representing an "electron-lattice" interaction, whereby polarization is transferred by the electron to the immediate environment, and a term H^{L} for the "lattice-lattice" interaction which distributes the transferred polarization throughout the medium:

$$H = H^{Mu} + V + H^{L}. \tag{5.9}$$

We must now also consider the density matrix ρ^{tot} for the combined system, muonium and medium. Following the development used by Wangsness and Bloch (WB 53) and by Fano (FA 57) we can write the time evolution of ρ^{Mu} as follows:

$$\frac{d\rho^{Mu}}{dt} = -\frac{i}{\hbar}[H^{Mu}, \rho^{Mu}] - \frac{\pi}{\hbar} Tr_{L}[\bar{V}, [\bar{V}, \rho^{Mu} \cdot \rho_{o}^{L}]], \tag{5.10}$$

where Tr_{L} is the trace over that part of the total density matrix which describes the surrounding medium "L," ρ_{o}^{L} is the equilibrium density matrix of the medium, and $\bar{V}$ is the portion of V which is diagonal in the total energy.

Following Nosov and Iakovleva (NY 63), we can express the effect of the double commutator phenomenologically in terms of a relaxation rate ν imposed upon the electronic components of the polarization. Writing out the commutator of Eq. (5.10) and equating coefficients of orthogonal operators, we are led to the system of 15 Wangsness-Bloch equations:

$$\dot{p}_{ko} = -\frac{\omega_o}{2}\sum_{i,j=1}^{3}\epsilon_{ijk}\,p_{ij} + \sum_{i,j=1}^{3}\epsilon_{ijk}\,\omega_i^{\mu}\,p_{jo},$$

$$\dot{p}_{ok} = \frac{\omega_o}{2}\sum_{i,j=1}^{3}\epsilon_{ijk}\,p_{ij} + \sum_{i,j=1}^{3}\epsilon_{ijk}\,\omega_i^{e}\,p_{oj} - 2\nu\,p_{ok}, \qquad (5.11)$$

$$\dot{p}_{ij} = \frac{\omega_o}{2}\left(\sum_{n=1}^{3}\epsilon_{nij}\,p_{no} - \sum_{n=1}^{3}\epsilon_{nij}\,p_{on}\right)$$

$$- \sum_{m,n=1}^{3}\epsilon_{mni}\,\omega_n^{\mu}\,p_{mj} + \sum_{m,n=1}^{3}\epsilon_{mnj}\,\omega_m^{e}\,p_{in} - 2\nu\,p_{ij},$$

where $\vec{\omega}^{e}$ and $\vec{\omega}^{\mu}$ were defined in the previous section, and ϵ_{ijk} is the antisymmetric unit tensor. If $\nu = 0$, so that the two electron-damping terms can be neglected, Eqs. (5.11) are the same as we obtain from Eq. (5.8) for free muonium.

The system of Eqs. (5.11) can be separated into two irreducible subsystems, one involving only the components of muon and electron polarization along the magnetic field direction $\hat{z}$ (longitudinal subsystem), and the other involving only the components of $\vec{P}^{\mu}$ and $\vec{P}^{e}$ perpendicular to $\vec{B} = B\hat{z}$ (transverse subsystem). We will now treat each of these subsystems in more detail.

1. Longitudinal Subsystem

The equations of motion for those components of polarization coupled to p_{30}, the muon polarization along the field, are

$$\dot{p}_{30} = -\frac{\omega_o}{2}(p_{12} - p_{21}),$$

$$\dot{p}_{03} = \frac{\omega_o}{2}(p_{12} - p_{21}) - 2\nu\, p_{03},$$

$$\dot{p}_{11} = -\omega_e\, p_{12} + \omega_\mu\, p_{21} - 2\nu\, p_{11}, \tag{5.12}$$

$$\dot{p}_{22} = \omega_e\, p_{21} - \omega_\mu\, p_{12} - 2\nu\, p_{22},$$

$$\dot{p}_{12} = \frac{\omega_o}{2}(p_{30} - p_{03}) + \omega_e\, p_{11} + \omega_\mu\, p_{22} - 2\nu\, p_{12},$$

$$\dot{p}_{21} = -\frac{\omega_o}{2}(p_{30} - p_{03}) - \omega_e\, p_{22} - \omega_\mu\, p_{11} - 2\nu\, p_{21},$$

where we have used $\omega_e \equiv |\vec{\omega}^e| = \omega_3^e$ and $\omega_\mu \equiv |\vec{\omega}^\mu| = -\omega_3^\mu$.

Solution of these equations in the general case is rather involved. We will mention here only two limiting cases where good approximate solutions can be found. These cases were described by Nosov and Iakovleva (NY 63) and by Ivanter and Smilga (IS 71).

For very fast "spin-flipping" of the electron,

$$\nu >> \omega_o \sqrt{1 + x^2},$$

the time dependence of the μ^+ polarization is

$$P_{11}^\mu(x, t) \approx \exp(-t/\tau_1), \tag{5.13}$$

where

$$\tau_1 = 4\nu/\omega_o^2. \tag{5.14}$$

That is, the muon spin is exponentially damped at a rate which does not depend upon the field, but which decreases with increasing ν. This can be explained qualitatively as a weakening of the μ-e coupling by excessive electron relaxation (NY 63). The limiting case $\nu \to \infty$ corresponds to the situation in metals, where the μ^+ behaves as if free.

At the other extreme is the case of very mild electron relaxation,

$$\nu << \omega_o \sqrt{1 + x^2} \ .$$

Here we average the time dependence over the hyperfine oscillations--that is, over a time interval Δt satisfying

$$\nu << \frac{1}{\Delta t} << \omega_o \sqrt{1 + x^2} \ .$$

The experimentally observable result is

$$\overline{P}^{\mu}_{\parallel}(x, t) \approx P_o \ \exp(-t/\tau_2), \tag{5.15}$$

where P_o is given by Eq. (4.6), and

$$\tau_2 = \frac{1 + x^2}{\nu} \ . \tag{5.16}$$

Not surprisingly Eq. (5.15) depicts an exponential decay of the μ^+ polarization, whose initial (average) value is the same as for free muonium in longitudinal field. The decay time τ_2 can, however, be lengthened by increasing the magnetic field. Experimental observations of such field dependence of τ_2 constitute evidence for the presence of this sort of depolarization mechanism.

2. Transverse Subsystem

Following Ivanter and Smilga (IS 68), we introduce the complex four-component vector

$$\tilde{P} \equiv \begin{pmatrix} p_{10} + i\, p_{20} \\ p_{01} + i\, p_{02} \\ p_{13} + i\, p_{23} \\ p_{31} + i\, p_{32} \end{pmatrix} , \tag{5.17}$$

whose first component is the complex transverse muon polarization $\tilde{P}_{\perp}^{\mu}(x, t)$ defined earlier. The time dependence of the transverse components in Eq. (5.11) can then be written

$$\frac{d\tilde{P}}{dt} = i A \tilde{P}, \tag{5.18}$$

where A is the 4×4 complex matrix

$$A = \frac{\omega_o}{2} \begin{pmatrix} -2\zeta X & 0 & 1 & -1 \\ 0 & (i\gamma + 2X) & -1 & 1 \\ 1 & -1 & (i\gamma - 2\zeta X) & 0 \\ -1 & 1 & 0 & (i\gamma + 2X) \end{pmatrix} \tag{5.19}$$

where

$$\zeta \equiv |\vec{\omega}^{\mu}| / |\vec{\omega}^{e}| = \left| \frac{g_{\mu}\mu_o^{\mu}}{g_e \mu_o^{\mu}} \right| = 1/206.77 \approx \frac{m_e}{m_{\mu}} \tag{5.20}$$

$$\gamma \equiv 4\nu/\omega_o , \tag{5.21}$$

and

$$X = |\vec{\omega}^{e}| / \omega_o = \frac{g_e \mu_o^{e}}{\hbar \omega_o} |\vec{B}| = |\vec{B}| / B_o^{*} , \tag{5.22}$$

an alternative version of the "specific field" discussed in Section IV. The "effective hyperfine field" B_o^{*} has a value of 1593 G for free muonium. The two versions of specific field are very simply related:

$$X = x/(1 + \zeta).^{\dagger}$$

Since the polarization components parallel to the field evolve independently of the transverse components considered here, we may assume without loss of generality the initial condition

---

†Ivanter and Smilga refer exclusively to X in their works.

$$\tilde{P}(0) = \begin{pmatrix} 1 \\ 0 \\ 0 \\ 0 \end{pmatrix} . \qquad (5.23)$$

That is, the muon is initially fully polarized in the $\hat{x}$ direction and there is no initial electron polarization or correlation between electron and muon spins.

The equation of motion (5.18) with the initial condition (5.23) is solved by diagonalizing the matrix A. The orthogonal matrix M which diagonalizes A,

$$M^{-1} A M = \Lambda , \qquad (5.24)$$

and the resulting eigenvalues $\Lambda_{kk} = \lambda_k^m$ can be found by standard but tedious manipulations. We will not describe this process in detail, but simply proceed to the results.

The simplest case, of course, is that in which $\nu = o$, so that A is a real symmetric matrix. Here, as expected, the result contains Eq. (5.4) for $P_\perp^\mu (x, t)$.

For the general case ($\nu \neq o$), several limiting cases have been calculated and discussed by a number of authors.

As for longitudinal fields, extremely fast "spin-flipping" of the electron ($\nu >> \omega_o \sqrt{1 + x^2}$) serves to weaken the coupling between the muon and the electron, allowing the μ^+ to precess almost as if free. Nosov and Iakovleva (NY 63) showed that the muon polarization in this case evolves as

$$\tilde{P}_\perp^\mu (x, t) \approx \exp[(-i\omega_\mu - \frac{1}{\tau_1})t] , \qquad (5.25)$$

where τ_1 is given by Eq. (5.14). That is, as in longitudinal field, the muon polarization relaxes at a rate inversely proportional to ν.

When $\nu \sim \omega_o$, neither μ^+ nor muonium precession is experimentally observable; the muon polarization is lost to the medium through the electron in times shorter than the apparatus can resolve. It may prove necessary to treat this most difficult case in detail if electron "spin-flipping" is to be studied in cases where ω_o is drastically reduced, lengthening the hyperfine time scale to observable intervals.

In the case of very mild relaxation $[\nu^2 << (\frac{\omega_o}{2})^2 x^4]$, Gurevich et al. (GI 71) have calculated the time dependence of the x-component of the μ^+ polarization, averaged over the unobservable hyperfine oscillations as for Eq. (5.15). Their result is

$$\bar{P}_x^{\mu}(x,t) \approx \frac{1}{2} e^{-t/\tau_3} \left[(\cos \Omega_\gamma t + \frac{\Omega \sin \Omega_\gamma t}{3 \tau_3 \Omega_\gamma^2}) \cos \omega_- t + (\frac{2 \omega_+ \Omega^2}{\omega_o \Omega_\gamma^2}) \sin \Omega_\gamma t \sin \omega_- t \right], \tag{5.26}$$

where the expected exponential damping factor is related to ν as

$$\tau_3 \equiv \frac{2}{3\nu} \tag{5.27}$$

and the beat frequency is also relaxation dependent:

$$\Omega_\gamma \equiv \Omega \sqrt{1 - \frac{\nu^2}{4\Omega^2}} \, . \tag{5.28}$$

As will be discussed in the next section, if chemical reactions gradually eliminate free muonium atoms from the ensemble, the observed muonium precession in low fields will be exponentially damped as above, but there will be no shift in the beat frequency. In principle, an observation of this phenomenon, though difficult, would serve to identify the cause of such

relaxation of muonium precession. Such a clue may prove vital to studies of muonium chemistry in the gas phase, where one technique is to add a reactive gas to an inert target gas in weak transverse field and watch the resultant decay of the muonium precession signal.

D. Muonium in an r-f Field

We will briefly mention the effect of one artificially induced perturbation upon the evolution of the μ^+ spin in muonium: the application of a strong r-f field at a frequency near one of the $\Delta m = \pm 1$ transition frequencies of muonium, usually ω_{12}. This technique has been used extensively for measuring the muonium hyperfine interval to extreme precision, and also for studying the chemical and spin-exchange reactions of muonium in gases (MO 67). The analogy with electron spin resonance experiments is nearly perfect, but several distinguishing features should be noticed.

The r-f excitation is almost always superimposed upon a constant longitudinal field. Thus an excitation of the transition $|E_1\rangle \rightarrow |E_2\rangle$ destroys the longitudinal μ^+ polarization in that half of the ensemble which forms in the polarized triplet state. The average polarization is thereby reduced as r-f pumping brings states $|E_1\rangle$ and $|E_2\rangle$ into equilibrium population. Since the population of state $|E_2\rangle$ in the original muonium formation is lower in stronger longitudinal fields [see Eq. (4.5)], the effect of the r-f depolarization increases with field strength. This depolarization is reflected in the ratio of decay positrons detected in forward and backward directions, so that the "resonance signal" is

$$S = \frac{N_f(\text{rf on}) - N_f(\text{rf off})}{N_f(\text{rf on}) + N_f(\text{rf off})} - \frac{N_b(\text{rf on}) - N_b(\text{rf off})}{N_b(\text{rf on}) + N_b(\text{rf off})} . \qquad (5.29)$$

By contrast, the resonance signal in ESR experiments is a bulk absorption of r-f power by the sample.

When the muonium electron is strongly relaxed by the medium, the depolarizing effect of an r-f field is negligible in comparison, leading to a "quenching" of the resonance signal defined above. A fast chemical reaction, placing the μ^+ in a diamagnetic environment before the r-f perturbation can have any effect, will also "quench" the resonant depolarization signal. Measurements of the height and linewidth of $S(\omega_{rf})$ as a function of impurity concentration can be analyzed to yield cross sections for spin exchange and chemical reaction of muonium (MO 67).

VI. CHEMICAL REACTIONS OF MUONIUM AND RESIDUAL MUON POLARIZATION: THEORY

If all thermalized muonium atoms were to preserve their chemical state, most experiments on interactions of the μ^+ spin with matter would involve observation of the sort of phenomena described in the previous section. However, that situation is rather exceptional, since muonium is a radical and therefore has a strong propensity to react chemically. For the time being we shall assume that all such reactions are of the form

$$Mu + X \rightarrow D, \tag{6.1}$$

where X is some reagent and D is an unspecified final state in which the muon is incorporated into a diamagnetic molecule. In most media these reactions occur during the μ^+ lifetime, leaving that particle in a diamagnetic environment, where the rapid spin evolution described in the previous section stops abruptly. Other types of thermalized muonium reactions also occur, and we will describe later the effects of different concurrent reaction channels. In addition, as mentioned in Section III, a substantial fraction (h) of muons usually reaches a diamagnetic environment through hot atom reaction channels, bypassing the muonium stage of spin evolution completely.

Considering for the moment only that fraction (1-h) of the muons which thermalize as free muonium, there are two extreme situations in which chemically meaningful measurements can be made in transverse field. If the Mu atoms remain uncombined for observable times (~100 nsec or more), the "muonium precession" phenomena described in the previous Section can be studied; chemical reactions of Mu atoms are manifested in an exponential decay of that precession. This technique is well suited to gas-phase studies (MO 67), where reaction times are often many nsec. However, since μ^+ stopping density has historically been a severe experimental limitation, most

studies of Mu chemistry have been in condensed matter, especially in liquids, where reaction times are usually much too short for direct observation of muonium precession. In this situation, one looks for μ^+ precession as described in Eq. (2.6). Muons still precessing in muonium (~103 times faster) appear completely depolarized on this time scale, so that muonium is considered as a depolarizing influence upon the muon. In fact, since each muon "emerges" from the muonium stage of spin evolution at a different time (following a probability distribution), the μ^+ ensemble is depolarized (in a thermodynamic sense) by the resultant "dephasing." If τ_m, the mean chemical lifetime of free muonium, is much longer than the period of muonium precession ($2\pi/\omega_-$), this "fast depolarization" is complete, and the muon asymmetry in Eq. (2.6) is zero. However, if $\tau_m \ll 1/\omega_o$, the μ^+ spin has little opportunity to evolve in muonium before entering a diamagnetic state, and the "residual polarization" after its brief stay in muonium approaches unity. In addition, when $\tau_m \sim 1/\omega_-$, the short-lived muonium precession rotates the polarization through an average angle $|\Delta\phi| \sim \omega_- \tau_m$ which is observed as a shift of the apparent initial phase of the μ^+ precession, as described in Section II.

When muonium lasts long enough to destroy the μ^+ precession, but not long enough for Mu precession to be observed directly, no useful information can be obtained in transverse field about the fate of the fraction (1-h) of muons which thermalize as muonium. This limitation does not apply to experiments in longitudinal field, and in general the two techniques are complementary. However, the residual polarizations and apparent phase shifts in transverse field, when observable, provide the most revealing experimental test of very fast chemical reactions. The emphasis in this section will therefore be upon a precise theoretical prediction of these quantities in terms of the properties of the medium.

A. Proper Muonium Mechanism

Muonium reacts with the reagent X at a constant rate Λ. The probability m(t) that a given muonium atom is still free at time t therefore obeys the rate equation

$$\frac{dm(t)}{dt} = -\Lambda m(t), \tag{6.2}$$

so that the probability m(t) decays exponentially with a mean lifetime

$$\tau_m = 1/\Lambda; \tag{6.3}$$

if the origin of time is chosen to be the instant of thermalization (approximately when the μ^+ enters the target, since the stopping time can be neglected in comparison with the time scale of μ^+ polarization evolution in muonium), then m(t) is given by

$$m(t) = e^{-t/\tau_m}. \tag{6.4}$$

The probability dn that the reaction (6.1) occurs within an interval dt' at time t' is given by

$$dn = \frac{1}{\tau_m} e^{-t'/\tau_m} dt'. \tag{6.5}$$

At the time of the reaction, the complex μ^+ polarization in the transverse subsystem (defined as in the previous sections) is just $\tilde{P}_\perp^\mu(x, t)$, the first component of $\tilde{P}$ in Eq. (5.17). Following reaction (6.1), the μ^+ will precess at essentially the free Larmor frequency, ω_μ. Thus the polarization of such a muon at any time $t > t'$ is

$$\tilde{P}_\perp^\mu(x, t') e^{-i\omega_\mu (t-t')}.$$

Such a fate befalls a fraction dn of all the muons in the ensemble.

These muons thus contribute

$$dP(t) = dn\, \tilde{P}_{\perp}^{\mu}(x, t')\, e^{-i\omega_{\mu}(t-t')} \tag{6.6}$$

to the net ensemble muon polarization, P(t). Summing all such contributions leads to an integral over dt'. By the same token, we must include in P(t) the contribution from Mu atoms which have not yet reacted; this is given by the product of the probability e^{-t/τ_m} of Mu surviving reaction for a time t, and the polarization of such muons, $\tilde{P}_{\perp}^{\mu}(x, t)$. The global μ^+ polarization at time t is thus given by

$$P(t) = \int_0^t \tilde{P}_{\perp}^{\mu}(x, t')\, e^{-i\omega_{\mu}(t-t')}\, \frac{e^{-t'/\tau_m}}{\tau_m}\, dt + \tilde{P}_{\perp}^{\mu}(x, t)\, e^{-t/\tau_m}. \tag{6.7}$$

For $t >> \tau_m$, the second term vanishes and (6.7) can be written in the form

$$P(t >> \tau_m) \approx e^{-i\omega_{\mu} t}\, R_{\perp}, \tag{6.8}$$

where

$$R_{\perp} = \int_0^{\infty} \tilde{P}_{\perp}^{\mu}(x, t')\, e^{i\omega_{\mu} t'} \left(\frac{e^{-t'/\tau_m}}{\tau_m} \right) dt. \tag{6.9}$$

That is, long after all muonium atoms have reacted, the muons precess just as if they had begun at $t = 0$ with an initial polarization $R_{\perp}$. This apparent initial μ^+ polarization is called the "residual polarization;" it is generally reduced and rotated with respect to the actual inital polarization. $R_{\perp}$ can be calculated in several ways. If $P_{\perp}^{\mu}(x, t)$ is given by a manageable explicit formula such as (5.4), the integral in (6.9) can be performed directly. Alternatively, if the diagonalization of the matrix A as in Eq. (5.24) is known, the time dependence of $\tilde{P}_{\perp}^{\mu}(x, t)$ can be written formally as

$$\tilde{P}^{\mu}_{\perp}(x,t) = \sum_k F_k e^{i\lambda^m_k t}, \tag{6.10}$$

where

$$F_k = M_{1k}(M^{-1})_{k1}. \tag{6.11}$$

This formula can be substituted into Eq. (6.9) and integrated easily. The result is

$$R_{\perp} = \frac{1}{\tau_m} \sum_k \frac{F_k}{\alpha_k}, \tag{6.12}$$

where

$$\alpha_k = -\frac{1}{\tau_m} + i(\lambda^m_k + \omega_{\mu}). \tag{6.13}$$

This approach is useful in more complicated situations, as we shall see later. However, the most elegant approach to this problem is that used by Ivanter and Smilga (IS 68), who noted that Eq. (6.9) simply expresses $R_{\perp}$ in terms of the Laplace transform of the first component of $\tilde{P}$. This allows solution for $R_{\perp}$ by transforming the differential equations (5.18) into a system of linear equations:

$$(A = u\,I)\ \mathcal{L}(u) = -\tilde{P}(0), \tag{6.14}$$

where

$$\mathcal{L}(u) = \int_0^{\infty} e^{-ut}\,\tilde{P}(t)\,dt,$$

with $u = 1/\tau_m - i\omega_{\mu}$, and I the identity matrix. Thus $R_{\perp}$ is just $1/\tau_m$ times the first component of the four-component transformed vector $\mathcal{L}(u)$. The linear system is easily solved by matrix methods, giving the general result

$$R_{\perp} = \frac{1}{1 - i\tau(A+B)B/(AB^2 - A - B)}, \tag{6.15}$$

where $$\tau = \frac{\omega_o}{2}\,\tau_m, \tag{6.16}$$

$$A = -\,i\,\alpha, \tag{6.17}$$

$$\alpha = \gamma + 1/\tau, \tag{6.18}$$

and $$B = A - 2x. \tag{6.19}$$

The longitudinal subsystem of polarization components parallel to the magnetic field is unaffected by μ^+ or Mu precession. Here the time dependence of the μ^+ polarization in muonium generally consists of an exponential decay, either in $P_{||}^{\mu}(x,t)$ [as in Eq. (5.13)] or in its average over hyperfine oscillations [as in Eq. (5.15)]. As muons react chemically, they are spared from this depolarization; the ensemble time dependence thus has a form analogous to Eq. (6.7). Such an integral is easily performed in the simple case

$$1/\tau_m << \omega_o\sqrt{1+x^2} << \nu, \tag{6.20}$$

where $P_{||}^{\mu}(x,t)$ is given by Eq. (5.13). The result is

$$P(t) = \frac{\tau_1}{\tau_m+\tau_1} + \frac{\tau_m}{\tau_m+\tau_1}\exp\left[-\left(\frac{1}{\tau_m}+\frac{1}{\tau_1}\right)t\right] \tag{6.21}$$

where τ_1 is given by Eq. (5.14). The effective depolarization time $\tau_{eff} = \left(\frac{1}{\tau_m}+\frac{1}{\tau_1}\right)^{-1}$ is sometimes long enough to be observed directly (GM 68).

In the case of slow reactions and mild relaxation,

$$1/\tau_m << \omega_o\sqrt{1+x^2} \quad \text{and} \quad \nu << \omega_o\sqrt{1+x^2}\ , \tag{6.22}$$

integration of $\overline{P}_{||}^{\mu}(x,t)$ from Eq. (5.15) yields

$$\bar{P}(t) = \frac{\tau_2 P_o}{\tau_m + \tau_2} + \frac{\tau_m P_o}{\tau_m + \tau_2} \exp\left[- \left(\frac{1}{\tau_m} + \frac{1}{\tau_2}\right) t \right], \tag{6.23}$$

with P_o from Eq. (4.6) and τ_2 from Eq. (5.16). Conditions (6.22) are often fulfilled in gas phase reactions.

In general, however, we may only observe the residual μ^+ polarization $R_{||}$ at times $t >> \tau_m$, long after all Mu atoms have reacted. The expression for $R_{||}$ is analogous to that for $R_\perp$:

$$R_{||} = \int_0^\infty P_{||}^{\mu}(x, t') \frac{e^{-t'/\tau_m}}{\tau_m} dt', \tag{6.24}$$

where $P_{||}^{\mu}(x, t)$ is just $p_{30}(t)$ as in Eq. (5.12). After some manipulations with the Fourier transform (IS 68), one obtains the general result

$$R_{||} = \frac{x^2 + 1/2 + (\alpha^2/4)}{x^2 + 1 + \nu \tau_m + (\alpha^2/4)}, \tag{6.25}$$

where α is given by Eq. (6.18).

In the limiting case (6.20), the result is $R_{||} = \tau_1/(\tau_m + \tau_1)$, as evident from Eq. (6.21).

In another simple limiting case

$$\nu << 1/\tau_m << \omega_o \sqrt{1 + x^2}, \tag{6.26}$$

we have $\alpha \to 0$ and (6.25) reduces to

$$\lim_{\alpha \to 0} R_{||} = \frac{x^2 + 1/2}{x^2 + 1 + \nu \tau_m}. \tag{6.27}$$

This result can also be obtained by integrating $\bar{P}_{||}^{\mu}(x, t)$ from Eq. (5.15) (NY 65).

The oblique field case can easily be handled as a superposition of longitudinal and transverse subsystems: if the original μ^+ polarization is in the x-z plane at an angle ψ to the z-axis, the net residual polarization is

$$\vec{R} = \hat{x}\, \mathrm{Re}\,(p_{10}(0)\, R_\perp) + \hat{y}\, \mathrm{Im}\,(p_{10}(0)\, R_\perp) + \hat{z}\, p_{30}(0)\, R_{\parallel}\,, \tag{6.28}$$

where $p_{10}(0) = \sin\psi$ and $p_{30}(0) = \cos\psi$.

The above description pertains to that fraction (1-h) of muons which thermalize as free muonium. In general there is also a fraction h which react through epithermal channels, essentially at t = 0, and propagate throughout their existence as quasi-free muons. To obtain the experimentally observed residual polarization, $\vec{P}_{res}$, one must combine these two components:

$$\vec{P}_{res} = h[\, p_{10}(0)\, \hat{x} + p_{30}(0)\, \hat{z}\,] + (1-h)\, \vec{R}. \tag{6.29}$$

The pure transverse field case, where $p_{30}(0) = 0$ and $p_{10}(0) = 1$, can thus be expressed as

$$P_{\perp_{res}} = h + (1-h)\, R_\perp\,. \tag{6.30}$$

If we then observe the positrons from μ^+ decay long after all Mu atoms have reacted, the experimental asymmetry A and the phase shift $\Delta\phi$ in Eq. (2.6) will be given by

$$A = A_o\, |P_{\perp_{res}}| \tag{6.31}$$

$$\text{and}\quad \tan\Delta\phi = \frac{\mathrm{Im}\,(P_{\perp_{res}})}{\mathrm{Re}(P_{\perp_{res}})}, \tag{6.32}$$

where A_o is a constant factor equivalent to the effective asymmetry when no polarization is lost in the target. This factor, like θ_o in Eq. (2.6), depends

upon beam polarization, counter geometry, and the details of the decay. Both are usually fitted as empirical parameters. Figure 6.1 shows the dependence of $|P_{\perp_{res}}|$ and $\Delta\phi$ upon the average chemical lifetime τ_m for a perpendicular field of 100 G, assuming $\nu = 0$. The dashed curves are for the case without hot atom chemistry, where $P_{\perp_{res}} = R_\perp$, and the solid curves show the results for h = 0.5. At very short chemical lifetime ($\tau_m << 1/\omega_o$) the average muon's stay in muonium is so brief as to have no effect on the polarization, leaving $P_{\perp_{res}} = 1$ and $\Delta\phi = 0$. For $\tau_m \sim 1/\omega_o$, muons "drop out" of muonium over one or two hyperfine periods, causing $R_\perp$ to drop to ~ 0.5; this situation persists for τ_m intermediate between $1/\omega_o$ and $1/\omega_-$, giving the "plateau" effect seen in $|P_{\perp_{res}}|$ in Fig. 6.1. When $\tau_m \sim 1/\omega_-$, muons leave muonium during approximately the first quarter cycle of muonium precession, leading to a rotation of the residual polarization in the opposite sense to μ^+ precession as well as a net attenuation which is essentially complete for $\tau_m >> 1/\omega_-$. In this final limit, the phase of $R_\perp$ goes to - 90° (positive $\Delta\phi$ being defined here in the sense of free μ^+ precession) while $|R_\perp| \to 0$; $P_{\perp_{res}}$, however, contains the constant unrotated vector h, and so its phase returns to zero as the magnitude of the rotated component vanishes.

As we have seen, irreversible depolarization of the muons is brought about by the "dephasing" of their spins due to chemical reaction of Mu atoms at random times. This is referred to as the "proper muonium mechanism" for fast μ^+ depolarization. The "plateau" in $|P_{\perp_{res}}|$ and the "phase dip" in $\Delta\phi$ are particularly characteristic of this mechanism; these phenomena are not predicted in oversimplified models such as that used by Firsov and Byakov (FB 65).

A convenient experimental method for testing these predictions can

be used in dilute solutions of a highly reactive scavenger compound (X) in a solvent (S) which is inert to thermal reactions with Mu, but in which epithermal reactions have a finite probability h. The reaction rate $\Lambda = 1/\tau_m$ is assumed to be proportional to the concentration $[X]$ of the reagent:

$$\Lambda = k[X], \tag{6.33}$$

where k, the constant of proportionality, is called the chemical rate constant. Thus, by varying the reagent concentration $[X]$, one can change the chemical lifetime τ_m to produce curves of $P_{\perp_{res}}$ vs $[X]$ such as those shown in Fig. 6.2, where a rate constant $k = 10^{10}$ liter/mole-sec and a "hot fraction" $h = 0.5$ are assumed. The solid curves in Fig. 6.2 are for an external field of 100 G, corresponding to the solid curves in Fig. 6.1. The dotted curves are for B = 10 G, and show that slowing down the muonium precession broadens the plateau. The dashed curves are for $B = B_o = 1585$ G, where ω_- becomes comparable to ω_o and the plateau disappears. Here the amplitude of the phase dip is reduced and the positive excursion for very short reaction times is much more noticeable than in lower fields. The reversal of the sign of $\Delta\phi$ can be understood in terms of Eq. (5.4) for $\tilde{P}_\perp^\mu(x,t)$. For high fields, $\delta \approx 1$ and the first motion of the μ^+ spin includes a rotation in the normal sense of μ^+ precession. The contrary precession of the electron moment then carries the μ^+ spin along with it. For fields stronger than B_o, the dip in the phase of $P_{\perp_{res}}$ becomes too small to measure conveniently, especially when h is large. The positive excursion increases somewhat with field, but is never large enough to observe easily.

In Fig. 6.2 it is assumed that $\nu = 0$; any significant relaxation rate for the muonium electron would disrupt the muonium precession, as in Eq. (5.25), causing the plateau effect and the phase dip, both results of coherent Mu precession, to be more or less spoiled. Equation (6.15) gives the depen-

dence of $P_{\perp_{res}}$ upon $\gamma = 4\nu/\omega_o$; one can envision a situation in which τ_m is constant while ν depends upon the concentration of a paramagnetic species (SC 71). More generally, both τ_m and ν would vary with [X]. However, there is no evidence for non-negligible spin-flipping in even strongly paramagnetic solutions (SC 71). so we may assume that $\nu << \omega_o$ in liquids.

B. Radicals and Two-Stage Mechanisms

It was assumed in the preceding description that all chemical reactions of muonium leave the μ^+ in a diamagnetic environment. This is not generally true. Since muonium is itself a paramagnetic atom, at least one of the products of its reaction with an ordinary diamagnetic molecule will be a paramagnetic molecule, or radical. If the radical product incorporates the muon, then a hyperfine interaction between the μ^+ and any unpaired electron will lead to motions of the coupled spins quite like those in muonium. The simplest sort of radical contains one unpaired electron in an s-orbital; in this case the spin system is identical to muonium except that the strength of the hyperfine coupling is greatly reduced. That is, the hyperfine frequency in the radical, ω_r, is generally much less than that in muonium, ω_o.

Radicals created in epithermal reactions, if all of the same species, could be observed directly by virtue of their muonium-like behavior, described most generally by Eq. (5.18), in which A is now A_r, the radical version of the matrix A_m defined by Eq. (5.19); A_r differs from A_m in the substitution of ω_r for ω_o everywhere (including the definition of X). If a fraction r of incoming muons enter identical radicals in this way, essentially at t = 0, they can be detected only if they remain chemically free for an observable time (~ 100 nsec or more); such "radical precession" has never yet been observed.

Fast thermal reaction of an epithermally formed muon-bearing radical R leads to a μ^+ depolarization mechanism perfectly analogous to the proper muonium mechanism described earlier, provided that the thermal reaction leaves the muon in a final diamagnetic environment D:

$$R + X \rightarrow D. \tag{6.34}$$

However, if the radical itself arises from thermal reaction of muonium, as in

$$Mu + X \rightarrow R, \tag{6.35}$$

then the μ^+ spin has already evolved in muonium for an arbitrary time before entering the radical environment. If the radical subsequently reacts as in (6.34), and if both reactions occur swiftly enough, some μ^+ polarization still remains; but the simple Laplace transform technique described above will not suffice to solve for the residual polarization which here involves an integral over two exponentially distributed reaction times.

A flow diagram of this "two-component mechanism" along with other competing mechanisms of μ^+ depolarization, is shown in Fig. 6.3. The possibility of reactions of Mu with the solvent S are also included in this picture; these are assumed to be of the form

$$Mu + S \rightarrow D \tag{6.36}$$

or

$$Mu + S \rightarrow R. \tag{6.37}$$

With the variety of reactions given by (6.1) and (6.34-6.37), an assortment of chemical rate constants must be defined. Table VI.1 lists rate constants and chemical lifetimes for the various reactions in Fig. 6.3, using an obvious mnemonic prescription for subscript labels. To maintain a semblance of simplicity, the possibilities of more than one reagent or of multiple radical species are not mentioned. In fact, Fig. 6.3 does not include more than a repre-

sentative selection of reaction channels. For instance, we have not mentioned the possibility of formation of unstable diamagnetic compounds which decompose spontaneously, releasing free Mu atoms again. Ivanter and Smilga (IS 71) showed that the process of multiple formations of unstable diamagnetic compounds has the same effect upon the muon as the process of repeated ionization and electron capture known as charge exchange. The effect of either process is generally the same as for continuous depolarization of the muonium electron by the medium, with an appropriate definition of ν. We have also neglected such three-stage depolarization mechanisms as $Mu \rightarrow R \rightarrow R' \rightarrow D$.

The residual polarization following the two-component depolarization process $Mu \rightarrow R \rightarrow D$ can be obtained by solving a set of coupled integro-differential equations which reduce to an equivalent set of Volterra integral equations. Fischer (FI 73) found the solution for the case in which the unpaired electron in the radical is initially unpolarized. He also pointed out that the problem could be solved similarly for the case in which the radical simply adopts the muonium electron as its unpaired electron, so that the electron polarization [components $p_{oi}(t)$] is transferred smoothly from Mu to R. The advantage of the integro-differential method is that the residual polarization emerges as an explicit (if somewhat unwieldy) function of the applied field, the hyperfine coupling in the radical, the electron depolarization rates ν_m and ν_r in muonium and the radical, and the chemical parameters listed in Table VI.1.

Another calculational technique is sometimes convenient when several complicated competitive reaction schemes are to be treated, or when A_m and A_r can be diagonalized easily (e.g., by numerical techniques using a computer). This approach, described in detail in Ref. (BG 73), is an extension of the derivation described in Eqs. (6.10) through (6.13). The residual polarization is expressed as a generalized sum of contributions from

all possible histories of μ^+ spin evolution, each contribution consisting of a product of the probability of that history and the final μ^+ polarization resulting from that history, as in Eq. (6.6). This leads to integrals over reaction times as in Eq. (6.7). When formal solutions for time dependence such as Eq. (6.10) are substituted into these integrals, they can be performed easily. The residual polarization is then expressed in terms of eigenvalues, reaction rates, and diagonalizing matrices.

Assuming that A_r is diagonalized by the matrix R [in analogy to equation (5.24)], so that

$$R^{-1} A_r R = \Lambda^r, \tag{6.38}$$

with $\Lambda^r_{kk} = \lambda^r_k$, the residual polarization in the transverse subsystem for the model described by Fig. 6.3 and Table VI.1 can be expressed as

$$\begin{aligned} P_{\perp_{res}} = h &- \frac{(1 - h - r)}{\tau_{md}} \sum_k \frac{F_k}{\alpha_k} \\ &- \frac{r}{\tau_{rd}} \sum_k \frac{G_k}{\beta_k} \\ &+ \frac{(1 - h - r)}{\tau_{mr}\,\tau_{rd}} \sum_{ik} \frac{W_{ik}}{\alpha_k\,\beta_i}\,, \end{aligned} \tag{6.39}$$

where F_k is given by Eq. (6.11), α_k by Eq. (6.13),

$$G_k = R_{1k} (R^{-1})_{k1}\,, \tag{6.40}$$

$$\beta_k = -1/\tau_{rd} + i(\lambda^r_k + \omega_\mu), \tag{6.41}$$

and W_{ik} is given by different expressions, depending upon whether the

electron polarization is lost or transmitted as Mu → R; if the radical starts over with a new unpolarized electron, then

$$W_{ik} = G_i F_k. \tag{6.42}$$

If the radical picks up the muonium electron with no loss of polarization, then

$$W_{ik} = \sum_j R_{1i} (R^{-1})_{ij} M_{jk} (M^{-1})_{k1} . \tag{6.43}$$

This latter formulation is less elegant, in that the dependence of $P_{\perp_{res}}$ upon ν_m, ν_r, ω_r and B remains implicit in the diagonalization of A_m and A_r. However, this approach has certain practical advantages. To construct a diagram such as that in Fig. 6.3 which includes all conceivable reaction schemes would be sheer folly, since the results are totally insensitive to processes which only involve a minute fraction of the μ^+ ensemble. However, different situations call for different treatments; for instance, depolarization in solids encompasses a wide range of mechanisms which are unimportant in liquids and completely absent in gases. Thus a formalism which can be easily modified to include new or exotic channels is sometimes more convenient in constructing "made-to-order" models.

To visualize the observable effects of radical formation, we recall the dependence of $|P_{\perp_{res}}|$ and $\Delta\phi$ upon reagent concentration for the proper muonium mechanism (without radicals). In Fig. 6.2 we showed the characteristic "plateau" and phase dip for several magnetic fields. Radicals, with substantially smaller hyperfine frequencies than muonium, produce these effects at proportionally lower fields, which are usually experimentally impractical. Thus a field which is "low" for muonium may be "high" for the radical, facilitating an experimental test for the presence of radicals. Figure 6.4 shows several examples of physical interest. All are for B = 100 G,

$h = 0.5$, and $r = \nu_m = \nu_r = 0$. The solid curves show the proper muonium mechanism (no radicals) with $k_{mxd} = 10^{10}$ liter / mole-sec and all other rate constants zero. These are the same as the solid curves in Fig. 6.2. The other sets of curves show situations involving a radical with $\omega_r = 0.1\ \omega_o$. For the dashed curves, the radical is formed from reaction of Mu with X, and the only nonzero rate constants are $k_{mxd} = 10^{10}$ liter / mole-sec, $k_{mxr} = 10^{11}$ liter / mole-sec, and $k_{rxd} = 10^{10}$ liter / mole-sec. For the dotted curves the radical is formed from reaction of Mu with the solvent, and the nonzero rate constants are $k_{mxd} = 10^{10}$ liter /mole-sec, $[S]k_{msr} = 10^{11}$ sec^{-1}, and $k_{rxd} = 10^{10}$ liter / mole-sec. In all examples the muonium electron is assumed to be transferred "gently" to the radical with no loss of polarization [see Eq. (6.43)]. The loss of the plateau effect with the addition of radicals is apparent in both situations. This is due to the shifting of the upper, "hyperfine" part of the depolarization curve towards lower concentrations (longer times).

It should be noted that while other phenomena could cause a curve of $|P_{\perp_{res}}|$ with no plateau in low field, they would also destroy the phase deviation, which persists in the situations depicted in Fig. 6.4. For instance, a large value for ν_m would disrupt the coherent precession of the muonium system, thereby destroying the plateau, but necessarily eliminating the phase deviation at the same time. Similarly, a mechanism consisting only of a dependence of the hot fraction h upon [X] could cause a plateau-free "repolarization" but could not result in any phase deviation. Observation of phase deviations without concomitant plateaus in $|P_{\perp_{res}}|$ thus serves as a specific experimental test for the presence of radicals in the depolarization mechanism.

VII. MEASUREMENTS OF REACTIONS OF MUONIUM

The Mu atom, being paramagnetic and highly reactive, interacts chemically and/or magnetically in most media, as discussed in the preceding section. The quantities τ_m (mean chemical lifetime of free Mu) and ν (relaxation rate of the Mu electron) generally characterize these interactions; for certain ranges of τ_m and ν, phenomena can be observed which provide information about the reactions of Mu and the properties of the medium. In this section we will give a brief survey of such experimental results.

In transverse field, Mu precession cannot be observed unless both τ_m and $1/\nu$ are larger than $\sim 10^{-8}$ sec, the smallest time interval over which measurements are practical. These conditions have thus far been satisfied only for muonium in noble gases, insulators, and some semiconductors at low temperature. When Mu precession is observable, its amplitude generally relaxes; measurements of the relaxation rate are reliable in the region from about 10^5 sec^{-1} to 10^8 sec^{-1}. This method is thus convenient for measuring rates of moderately slow chemical reaction and electron relaxation processes such as spin exchange.

Free μ^+ precession at the muon Larmor frequency, at the other extreme, is only visible if Mu reacts in very short times ($\tau_m \lesssim 1/\omega$) via epithermal or fast thermal processes, or if the electron's relaxation rate is so high ($\nu \gg \omega_o$) that it is effectively decoupled from the muon. The former situation occurs in many liquids, while the latter is characteristic of conductors. As mentioned in the preceding section, τ_m can be manipulated by varying reagent concentration in solutions, and the residual polarization fitted to determine chemical rate constants. Determinations of ν by transverse field techniques are apparently limited to gases in which $\nu \ll \omega_o$ and solids with $\nu \gg \omega_o$,

since Mu precession has not been observed in any liquid, and even the strongest paramagnetic solutions do not show fast enought relaxation of muonium to significantly effect the residual μ^+ polarization. (BC 74)

In longitudinal field, the dephasing effect of Mu precession is absent, and the presence of muonium is signalled by a reduced value of the apparent initial polarization $R_{||}$ and/or an exponential decay of the time-averaged polarization, as in (5.13), (5.15), (6.21) or (6.23). Muonium formation alone can never "destroy" more than 50% of the muon polarization in longitudinal field [see Eq. (4.6)]. However, in gases or other media where muonium is long-lived, relaxation processes (e.g., spin-exchange collisions) can bring about complete depolarization of the μ^+. Chemical reactions can only serve to reduce the amount of depolarization, but can speed up the apparent rate of that depolarization which does occur, as is evident from Eq. (6.21). These phenomena can also be studied by virtue of their quenching effect upon the resonant depolarization produced by an r-f field, as discussed in section V.

We turn now to a survey of experimental results.

A. Reactions of Mu in Gases

Mobley et al. (MO 67, MB 66, MA 67) have conducted a series of experiments on chemical and spin exchange reactions of muonium with impurity gases in high-pressure (40 atm) argon. To our knowledge these are the only studies of muonium chemistry in gases to date. They are of three types: relaxation of Mu precession in transverse field, directly observed relaxation in longitudinal field, and quenching of resonant r-f depolarization in longitudinal field.

1. Transverse Field

Mu precession was observed in a very weak transverse field (~2 G).

The rate λ of relaxation of the precession signal was measured and compared with that observed in pure argon, $\lambda_o \approx 0.2\ \mu sec^{-1}$, which was probably due to minute O_2 impurities. Examples of Mu precession signals are shown in Fig. 7.1. The most reliable results were:

Added Gas	Partial Pressure (mm Hg)	$\lambda\ (\mu sec^{-1})$
O_2	0.255	4.4 ± 1.8
C_2H_4	10.4	5.8 ± 1.7
CH_3Cl	705	1.5 ± 0.5

The relaxation rate due to interactions with reagent X is proportional to the concentration [X], usually expressed in moles/liter (at 300°K, 1 mm Hg partial pressure is equivalent to a concentration of 5.87×10^{-5} moles/liter):

$$\lambda = k\,[X]. \tag{7.1}$$

The constant of proportionality, k , is a second-order rate constant. Again following the chemist's convention, we express k in liter / mole-sec.

Interpretation of Eq. (7.1) is not unambiguous. The quantity λ is the rate of loss of polarized muonium; this may result from loss of muonium itself by chemical reaction ($k = k_{ch}$) or from depolarization of free muonium ($k = k_d$). In general $k = k_{ch} + k_d$. The mean chemical lifetime and an effective spin-flip frequency in transverse field can be expressed in terms of these rate constants as $1/\tau_m = k_{ch}\,[X]$ and $\nu_{eff} = \frac{2}{3} k_d\,[X]$ -- see Eq. (5.27).

Depolarization of free muonium in gases is believed to proceed by spin exchange: in a glancing collision between a Mu atom and a paramagnetic molecule, the wave function of the muonium electron briefly overlaps that of the unpaired molecular electron(s), making possible an exchange of electrons with opposite spins. The average depolarizing effect of a spin exchange

process depends upon the available molecular electron spin states (exchange of electrons with like spins has no effect). In general we can write $k_d = f k_{se}$, with $f < 1$. For spin $\frac{1}{2}$ molecules, $f = \frac{1}{2}$; for spin 1 molecules, $f = \frac{1}{2}(32/27)$. (MA 67) By contrast, a "charge exchange" process ($Mu \rightarrow \mu^+ \rightarrow Mu$) always results in a 50% polarization loss (unless its rate competes with ω_o): $k_d = \frac{1}{2} k_{ce}$. These relations are somewhat modified in longitudinal field, as will be seen.

Relaxation in C_2H_4 and in CH_3Cl is taken to be due only to chemical reactions, $k = k_{ch}$. From Eq. (7.1) we obtain

$$k_{ch}(Mu + C_2H_4) = (0.95 \pm 0.28) \times 10^{10} \text{ liter / mole-sec} \qquad (7.2)$$

and

$$k_{ch}(Mu + CH_3Cl) = (3.6 \pm 1.2) \times 10^{7} \text{ liter / mole-sec.} \qquad (7.3)$$

In O_2, both chemical reactions and spin exchange collisions are important. The experimental result cannot be separated into chemical and spin exchange parts on the basis of this measurement. Since O_2 is a spin 1 molecule, the result can be written

$$k(Mu + O_2) = k_{ch}(Mu + O_2) + \tfrac{1}{2}(32/27)\, k_{se}(Mu + O_2) = (2.9 \pm 1.2) \times 10^{11} \text{ liter / mole-sec.} \qquad (7.4)$$

2. Longitudinal Field

In longitudinal field, chemical reactions of Mu do not cause relaxation in any sense; it is easy, then, to make the mistake of equating the observed relaxation rate with a depolarization rate. However, as can be seen clearly from Eq. (6.21), the removal of muons from relaxing muonium causes an

apparent increase in the relaxation rate for that part of the μ^+ ensemble which does relax. Thus Eq. (7.1) is valid for longitudinal as well as transverse field, with the more general prescription

$$k = k_{ch} + k_D. \tag{7.5}$$

The longitudinal field depolarization rate constant k_D is related to the transverse or zero field depolarization rate constant k_d as follows [recall Eq. (5.16)]:

$$k_D = \frac{k_d}{1 + x^2} \tag{7.6}$$

Mobley analyzed his longitudinal field results with the assumption $k = k_D$. In the most important cases, O_2 and NO, chemical reactions are significant and this assumption is not valid.

The field dependence of the measured rate constants is not described well by Eq. (7.6) in most cases, as can be seen from Fig. 7.2. The fit is best for O_2 and NO, where spin exchange is probably dominant. Even in these cases, however, the data are fitted to the dependence (7.6), neglecting the constant term proportional to k_{ch}. Judging from the high-field values of λ/n (= k in cm^3/sec), this term is relatively small. Its effect would be to reduce the fitted values of k_d slightly. Keeping in mind this questionable extrapolation, we can express Mobley's results as follows:

$$\begin{aligned} \lim_{x \to 0} k(Mu + O_2) &= k_{ch}(Mu + O_2) + \tfrac{1}{2}(32/27)\, k_{se}(Mu + O_2) \\ &= (1.7 \pm 0.2) \times 10^{11} \text{ liter /mole-sec;} \end{aligned} \tag{7.7}$$

$$\lim_{x \to 0} k(\mathrm{Mu} + \mathrm{NO}) = k_{ch}(\mathrm{Mu} + \mathrm{NO}) + \tfrac{1}{2} k_{se}(\mathrm{Mu} + \mathrm{NO})$$

$$= (1.7 \pm 0.25) \times 10^{11} \text{ liter / mole-sec.} \qquad (7.8)$$

The result (7.7) agrees with the transverse field result (7.4) within the errors.

Relaxation was also observed with NO_2, C_2H_4, C_2H_6, CH_3Cl, CO_2, and Cl_2 impurities. As can be seen from Fig. 7.2, the field dependence of λ/n does not fit the form (7.6) for NO_2 or for C_2H_4. Radical formation is likely in these cases, probably via $Mu + NO_2 \rightarrow MuO\cdot + NO$ and $Mu + C_2H_4 \rightarrow MuC_2H_4\cdot$; however, since some depolarization mechanism is necessary if relaxation is to be observed [Eq. (6.21) shows this explicitly], the overall mechanism is unclear in all these cases.

3. Signal Quenching

The quenching effect of impurities upon the resonant r-f depolarization in longitudinal field was analyzed by Mobley to extract rate constants for chemical reaction. (MO 67) We will not discuss the method in detail, but simply list the more interesting results:

$$k_{ch}(\mathrm{Mu} + O_2) = (2.6 \pm 0.6) \times 10^{11} \text{ liter / mole-sec ,} \qquad (7.9)$$

$$k_{ch}(\mathrm{Mu} + \mathrm{NO}) = (1.15 \pm {}^{1.1}_{0.4}) \times 10^{11} \text{ liter / mole-sec ,} \qquad (7.10)$$

$$k_{ch}(\mathrm{Mu} + C_2H_4) = (1.4 \pm 0.4) \times 10^{10} \text{ liter / mole-sec ,} \qquad (7.11)$$

$$k_{ch}(\mathrm{Mu} + NO_2) > 1.1 \times 10^{12} \text{ liter / mole-sec ,} \qquad (7.12)$$

and

$$k_{ch}(\mathrm{Mu} + H_2,\ N_2, \text{ or } SF_6) < 5 \times 10^{8} \text{ liter / mole-sec.} \qquad (7.13)$$

The result (7.9) for $k_{ch}(Mu + O_2)$ is larger than the most precise value (7.7) for the total rate constant for O_2, which was expected to be dominated by the spin exchange rate. There is not yet a satisfactory explanation for this discrepancy. The results (7.10) and (7.8) for NO are consistent and can be combined to yield a spin exchange rate constant of

$$k_{se}(Mu + NO) + (1.1 \,^{+2.3}_{-0.9}) \times 10^{11} \text{ liter /mole-sec}, \qquad (7.14)$$

but the uncertainties in this result are too large for it to be very meaningful.

4. Comparison with Hydrogen Atoms

Unlike positronium, which has no nucleus, muonium fits neatly into the theoretical structures of physical chemistry as a light isotope of the hydrogen atom ($m_{Mu} = 0.113\ m_H$). Predictions of isotopic differences in reaction rates, already tested with the trio (H, D, T), can thus be extended in a new direction with Mu. This may lead to a deeper understanding of the most basic types of reactions in physical chemistry.

For these studies the gas phase is ideal, since atoms and molecules can legitimately be thought to "collide" in gases. The purely kinetic isotope effect arising from the $m^{-\frac{1}{2}}$ mass dependence of the mean thermal velocity can thus be separated easily from more interesting dynamic isotope effects. In liquids, comparison of Mu and H reaction rates is generally more qualitative, as we shall see later. Even in gases, however, some care must be taken in reducing rate constants to more fundamental quantities.

For quasi-elastic two-body collisions such as the spin exchange process

$$Mu + O_2 \xrightarrow{\text{spin exchange}} Mu + O_2, \qquad (7.15)$$

or for two-body abstraction reactions such as

$$Mu + NO_2 \rightarrow MuO\cdot + NO, \tag{7.16}$$

the rate constant can be reduced to a cross section by using the definition

$$k\ (\text{liter/mole-sec}) = N_o \times 10^{-3}\ \bar{v}\ (\text{cm/sec})\ \sigma\ (\text{cm}^2), \tag{7.17}$$

where $N_o = 6.022 \times 10^{23}$ mole^{-1} and $\bar{v}$ is the mean thermal velocity of Mu atoms relative to impurity molecules, given by

$$\bar{v} = \sqrt{\frac{8k_BT}{\pi\mu}}, \tag{7.18}$$

where $\mu = [(1/m_{Mu}) + (1/m_X)]^{-1}$ is the reduced mass. In most cases $m_{Mu} << m_X$ and $\mu \approx m_{Mu}$, so that $\bar{v} \propto m_{Mu}^{-\frac{1}{2}}$. This gives the aforementioned kinetic isotope difference between k(Mu) and k(H) attributable to

$$\bar{v}(Mu) \approx 2.98\ \bar{v}(H). \tag{7.19}$$

At room temperature, $\bar{v}(Mu) \approx 0.75 \times 10^6$ cm/sec. Further differences must come from σ in the form of "dynamic" isotope effects.

In a formation reaction such as

$$Mu + C_2H_4 \rightarrow C_2H_4Mu^*, \tag{7.20}$$

the excited complex $C_2H_4Mu^*$ is long-lived enough to be considered a stable

reaction product, (TH 65) allowing definition of a cross section as in (7.17). However, in highly exothermic formation reactions such as the chemical reaction of Mu with NO, the intermediate excited complex MuNO* is so unstable that a third body must actually participate in the collision to absorb the kinetic energy released. Otherwise there is simply a resonant scattering. Rate constants for these reactions cannot legitimately be expressed in terms of cross sections. For such 3-body processes as

$$Mu + NO + Ar \rightarrow MuNO + Ar \ , \tag{7.21}$$

the more basic quantity is the third-order rate constant κ (given in liter^2/mole^2-sec), defined by

$$k_{ch}(Mu + NO) = \kappa(Mu + NO + Ar\ \ ) \ [Ar\ ]. \tag{7.22}$$

At 40 atm and room temperature, [Ar] = 1.7 moles/liter. Although the pressure dependence (7.22) was not checked experimentally, the H atom reaction analogous to (7.21) is known to be a 3-body process, (TH 65) so we must assume that (7.21) is the correct reaction. Naturally, κ will still be proportional to $\bar{v}$, so we expect the same kinetic isotope effect in 3-body reactions as in the binary collisions.

Those of Mobley's results which can be compared with measured H atom cross sections and rate constants are summarized in Table VII. 1. From these limited data we can only remark on two qualitative trends: the cross sections for spin exchange reactions seem to be significantly smaller for Mu than for H while chemical reaction cross sections and 3-body rate constants are larger for Mu than for H. This information shows clearly that one can

practically measure reaction rates of Mu in gases and compare them with analogous reaction rates of H, D, and T, illuminating the role of isotope effects in the theory of absolute reaction rates. However, Mobley's results were derived from data with very low statistics, making the uncertainties too large to allow critical quantitative comparison of Mu and H rates.

With the advent of μ^+ beams of higher stopping density, (KE 72) gas phase studies of muonium chemistry are bound to become more popular, and high-statistics determinations of rate constants, cross sections, and their pressure and temperature dependences will probably be made. Reactions such as $Mu + H_2 \rightarrow MuH + H$ or $Mu + Cl_2 \rightarrow MuCl + Cl$, perhaps the most interesting for comparison of (Mu, H, D, T), may soon be observed and studied. These reactions were too slow at room temperature to have been detectable in Mobley's apparatus.

B. Reactions of Mu in Liquids

Most studies of muonium chemistry have been made in the liquid phase. Here, as explained in Section VI, one varies accessible parameters such as the magnetic field and the reagent concentration [X], and compares the behavior of the residual μ^+ polarization $\vec{P}_{res}$ with theory to determine rate constants and other physical quantities. For these studies, longitudinal field measurements are often very useful; for instance, when radical formation is important, the field dependence of $P_{\parallel res}$ can be fitted to a form similar to (6.27) to determine the hyperfine frequency ω_r. (GF 71) However, rate constants for diverse processes are best determined from the concentration dependence of A and $\Delta\phi$ in transverse field [see Eq. (6.31) and (6.32)].

In a series of experiments performed at the 184-inch Cyclotron in Berkeley, muons were stopped in solutions in a uniform transverse field, and time histograms of the μ^+ stop - e^+ emission interval fitted to the form (2.6), as described in Section II. The resultant values for A and $\Delta\phi$ as functions of [X] were fitted to the theory [Eq. (6.31) and (6.32)], where $P_{\perp res}$ is given by Eq. (6.39).

Several simplifying restrictions were imposed upon the general theory (6.39) in these fits. First, "hot" reactions were presumed to lead only to diamagnetic compounds incorporating muons (r = 0); radicals were assumed to form only in thermal chemical reactions. Second, relaxation of the spin of the muonium electron was assumed to be slow by comparison with the electron Larmor frequency, and was therefore neglected ($\nu_m \approx 0$). This assumption is supported by ESR data on hydrogen atoms in solution. (NF 71) Relaxation of the unpaired electron in radicals was likewise presumed to be negligible ($\nu_r \approx 0$). As noted by Fischer, (FI 73) this assumption is questionable in the

case of radicals whose unpaired electron may have hyperfine couplings with several nuclei; however, in most cases the effects of $\nu_r < \omega_r$ would be difficult to detect except in very weak fields. Third, it was assumed that only one species of radical incorporating the muon is present in a given type of solution and that it is formed by chemical reaction with either the reagent ($k_{msr} = 0$) or the solvent ($k_{mxr} = 0$), but never both in the same solution. Fourth, the form (6.43) was chosen for W_{ik}, assuming "gentle" transfer of the Mu electron to the unpaired electron in the radical. The results are actually rather insensitive to the choice of (6.42) or (6.43). Finally, neither muonium nor the radical was presumed to react thermally with the solvent to form a diamagnetic species incorporating the muon, except at negligible rates ($< 10^7$ liters/mole-sec). These assumptions gave the simplest form of the theory which permitted a good fit to all the data. Justifications and possible exceptions will be discussed below.

When the radical species "R" was assumed to be known, the hyperfine frequency ω_r in the radical was obtained by multiplying the ratio $\mu_\mu/\mu_p = 3.18$ of muon and proton magnetic moments into the measured value of the hyperfine frequency for the analogous radical in which the muon is replaced by a proton; these values were obtained from Landolt and Börnstein. (LB 65) When the radical species was unknown, ω_r was fitted by trial and error, and the optimal value used to make the best determinations of the parameters described above. In such cases, the choice of ω_r dramatically affects the fitted values of the rate constants. This is because ω_r sets the time scale for depolarization in the radical, while the rate constants determine the duration of that chemical state. In general, when fitting data in which the radical stage plays an important role, if one changes ω_r by some factor, the resultant change in the fitted value of a given rate constant is never more than a similar multiplicative

value. In the cases where ω_r was chosen by trial and error, the specified uncertainties in the rate constants shown below represent only the tolerance of the fits for the specified choice of ω_r. An additional uncertainty, which could in some cases be as large as an order of magnitude, is implicit in the crude determination of ω_r. However, this degree of accuracy is still sufficient to allow many interesting comparisons with H atom chemistry, as will be seen later. Most importantly, the qualitative conclusion that a radical depolarization mechanism is involved remains unaffected by these uncertainties. Further experiments may allow positive identification of the radical species or direct measurement of ω_r, thereby eliminating these ambiguities.

1. Results

a. Example of the Proper Muonium Mechanism: I_2 in CH_3OH

Figure 7.3 shows the observed dependence of $|P_{\perp_{res}}|$ and $\Delta\phi$ upon the concentration of iodine in methanol solution in a field of 102 G. The leftmost point in this and all such graphs corresponds to the result for the pure solvent; due to the log scale of the concentration, the point is actually infinitely far off scale to the left. The curve through the points is the best fit to Eq. (6.30) where $R_\perp$ is given by (6.12), the case of (6.39) in which the muons are depolarized by the proper muonium mechanism (i.e., when no radical formation is involved). The chemical reaction involved is presumed to be

$$Mu + I_2 \xrightarrow{(k_{mxd})} MuI + I. \qquad (7.23)$$

The fraction of muonium atoms reacting epithermally with CH_3OH is $h \approx \frac{1}{2}$. The phase variation is striking, and the "plateau" in $|P_{\perp_{res}}([I_2])|$ is noticeable. Both of these phenomena are due to the coherent precession of free muonium

atoms in the magnetic field, as explained in Section VI, and constitute proof of the central role of muonium in the depolarization mechanism. If a substantial number of muons were placed in radicals, the effect [see Fig. 6.4] would be to decrease the amplitude of the phase dip and to destroy the plateau. There does in fact seem to be a slight lessening of the plateau effect, and this may be due to a small but finite probability of reaction of muonium with CH_3OH to form a radical containing the muon, probably in epithermal collisions. This would constitute an exception to the assumption that $r = 0$. The quality of the fit is improved slightly by allowing some radical formation, but the correction is so small that the result is insensitive to the source, type, and fate of the radicals involved. Thus, since the mechanism is clearly dominated by reaction (7.23), this case may be practically considered to be an example of the proper muonium mechanism.

Similar results were obtained (BC 71) for I_2 in CH_3OH at fields of 1000 and 4500 G. The 100 G results are consistent with these, but are much more conclusive, since the phase dip and plateau are most evident at low fields [see Fig. 6.2]. The numerical results of these and other fits are listed in Tables VII. 2 and VII. 3.

b. Evidence for Radical Formation in Benzene

The muon asymmetry in benzene (C_6H_6) has long been known (SW 58) to be exceptionally low, implying a hot fraction $h \approx 1/8$, as compared to $h \approx \frac{1}{2}$ for methanol or water. This property makes benzene an attractive solvent for studies of muonium chemistry, since the range (1-h) through which $|P_{\perp_{res}}|$ can be varied by chemical means is near maximum, and the amplitude of the phase dip is increased accordingly. Bromine was chosen as a muonium scavenger because of its virtually unlimited solubility in benzene and because of the

analogy with iodine; the expected reaction in this case is

$$Mu + Br_2 \xrightarrow{(k_{mxd})} MuBr + Br. \qquad (7.24)$$

Data were taken in a 200 G magnetic field so that the "plateau" would be visible.

However, as can be seen in Fig. 7.4 , the results were in strong disagreement with the predictions of the proper muonium mechanism, the best fit for which is indicated by the dashed lines. There is no discernible plateau, and the phase variation is much less sharp than predicted by the simple theory. This behavior resembles the predictions of the proper muonium mechanism in a stronger magnetic field. Since the criterion for a "strong" field is that it be comparable with the effective hyperfine field, it was this observation which led to consideration of environments similar to muonium but with lower values of the effective hyperfine field (i.e., radicals).

On the basis of other chemical studies, (SW 67, MH 70) the following assumptions were made about the chemical processes involved: first, that the reaction

$$Mu + C_6H_6 \xrightarrow{(k_{msr})} C_6H_6Mu^{\cdot}, \qquad (7.25)$$

forming the muonium analog of the radical cyclohexadienyl ($C_6H_7^{\cdot}$), is in competition with reaction (7.24) for muonium. Second, that the radical reacts subsequently with bromine to place the muon in a diamagnetic compound, according to

$$C_6H_6Mu^{\cdot} + Br_2 \xrightarrow{(k_{rxd})} D \text{ (unidentified)} \qquad (7.26)$$

The isotropic average effective hyperfine field at the unpaired electron due to the extra proton in cyclohexadienyl is 47.71 G, (LB 65) as compared with 1593 G in muonium; thus the ratio of the hyperfine frequency ω_r in $C_6H_6Mu^{\cdot}$ to the hyperfine frequency ω_o in muonium was taken to be

$$\frac{\omega_r}{\omega_o} = \frac{(47.71 \times \mu_\mu/\mu_p)}{1593} = 0.095. \qquad (7.27)$$

This value was used to obtain the best fit to the data [solid lines in Fig. 7.4] corresponding to the best values for the fitted parameters, as listed in Tables VII. 2 and VII. 3; a trial and error search for the best empirical value for ω_r/ω_o gave a minimum χ^2 for $\omega_r/\omega_o \approx 0.03^{+0.04}_{-0.02}$. A study of the field dependence of the residual polarization in benzene in longitudinal field (GF 71) yielded an estimate of $\omega_r/\omega_o = 0.054 \pm 0.004$. A new fit to the data using this value gives estimates for the rate constants $\{k(7.24) \approx 5.5,\ k(7.25) \approx 0.10,$ and $k(7.26) \approx 0.57\} \times 10^{10}$ liter /mole-sec.

Although it was not possible to dissolve enough iodine in benzene to achieve full "repolarization", it was possible to study the dependence of $P_{\perp res}$ upon $[I_2]$ in C_6H_6 over a large enough region to determine that the results were consistent with those observed for Br_2 in C_6H_6. These results are also listed in Tables VII. 2 and VII. 3.

c. Mu Chemistry in Aqueous Solutions

In spite of its rather large hot fraction ($h \sim \frac{1}{2}$), water has proved to be a nearly optimal solvent for muonium chemistry. Most importantly, these results show that H_2O is more or less inert with respect to thermal chemical reactions with Mu -- that is, any reaction of Mu + H_2O has a rate constant $< 10^7$ liter /mole-sec. Thus all significant thermal reactions of muonium are

with the reagent. This situation would be expected to favor many examples of the proper muonium mechanism, but instead we have found a number of more complicated mechanisms, all involving radicals.

(1) Hydrogen Peroxide

Perhaps the most elegant system studied was Mu with H_2O_2 in H_2O. The experimental dependence $P_{\perp_{res}}([H_2O_2])$ at a field of 100 G is shown in Fig. 7.5 along with the best fits to the data. Again, the dashed curve is the best fit with the proper muonium mechanism, and the solid curve is the best fit with the general mechanism, including radicals. Clearly radicals are present. In this case the muonium is presumed to react with hydrogen peroxide to form a diamagnetic compound containing the muon, presumably according to

$$\mathrm{Mu} + \mathrm{H_2O_2} \xrightarrow{(k_{mxd})} \mathrm{HO^{\cdot}} + \mathrm{MuHO}, \tag{7.28}$$

and (competitively) to form a muonic radical, presumably according to

$$\mathrm{Mu} + \mathrm{H_2O_2} \xrightarrow{(k_{mxr})} \mathrm{MuO^{\cdot}} + \mathrm{H_2O}\,. \tag{7.29}$$

The radical $MuO^{\cdot}$ subsequently reacts with H_2O_2 to leave the muon in a final diamagnetic environment:

$$\mathrm{MuO^{\cdot}} + \mathrm{H_2O_2} \xrightarrow{(k_{rxd})} \mathrm{D'\ (unidentified)}. \tag{7.30}$$

These assumptions are consistent with most interpretations of H atom reactions with H_2O_2, as described later. Nevertheless, it is possible that the

radical species has been misidentified. If, for instance, the predominant radical species were $MuO_2^{\cdot}$ rather than $MuO^{\cdot}$, the value assumed for ω_r would be incorrect, possibly introducing errors of as much as an order of magnitude in the rate constants, as discussed previously. However, regardless of possible ambiguities in the identification of chemical species, the conclusion that the presence of radicals is essential to the overall depolarization mechanism is inescapable.

The effective hyperfine field at the unpaired electron due to the proton in the hydroxyl radical $HO^{\cdot}$ is known (LB 65) to be 41.3 G (isotropic average), which would imply $\omega_r/\omega_o = 0.0825$ for $MuO^{\cdot}$ [recall Eq. (7.27)]. This value was used to obtain the results listed in Tables VII.2 and VII.3. The empirical value giving a minimum χ^2 was $\omega_r/\omega_o = 0.175 \pm 0.1$, consistent with the predicted value.

(2) Strong Acids

Preliminary results show a great deal of variety in the reactions of muonium with various acids. In HCl, as noted earlier by Swanson, (SW 58) there seems to be no "repolarizing" effect at any concentration. The muon precession in 10 M HCl is virtually indistinguishable from that in pure water. Therefore, no combination of reactions between Mu, H^+, and Cl^- leads to a diamagnetic compound containing the muon in times shorter than about 10 nsec. Similar results in concentrated $MnCl_2$ solutions indicate that these conclusions are relatively independent of pH.

However, addition of nitric acid to water causes marked "repolarization", with a maximal asymmetry reached at about 10 M. Experimental results for $P_{\perp_{res}}([HNO_3])$ at 100 G are shown in Fig. 7.6 . It was assumed that HNO_3 dissociates sufficiently that the Mu reacts predominantly with the

anion, NO_3^-. Again, the proper muonium mechanism (dashed curve) is a poor fit, but an excellent fit (solid curve) can be obtained if one assumes the following reactions to be significant: First, the usual direct reaction leading to a diamagnetic compound:

$$Mu + NO_3^- \xrightarrow{(k_{mxd})} D \text{ (unidentified)}; \tag{7.31}$$

in addition, the competitive reaction leading to a muonic radical:

$$Mu + NO_3^- \xrightarrow{(k_{mxr})} R \text{ (unidentified)}, \tag{7.32}$$

followed by the final reaction of the radical to place the muon in a diamagnetic environment:

$$R + NO_3^- \xrightarrow{(k_{rxd})} D' \text{ (unidentified)}. \tag{7.33}$$

Here there has been no attempt to identify any of the product species, but only the types of processes taking place; all the fitted results listed in Table VII. 3, including ω_r/ω_o, were obtained by minimizing χ^2. Results for $P_{\perp_{res}}$-($[HNO_3]$) at a field of 4500 G are consistent with these, but are much less sensitive to the presence of radicals.

Similar results were seen for solutions of $HClO_4$ in water at 4400 G. However, no one has yet undertaken a study of $HClO_4$ at low field, where the results are sensitive to radical formation, so the existing data are interpreted only in terms of the proper muonium mechanism. Such interpretation predicts a rate constant $k(Mu + HClO_4) \approx 10^9$ liter /mole-sec.

(3) Ferric Salts

The quenching effect of ferric ions on μ^+ depolarization in $Fe(NO_3)_3$ solutions at 11 kG were first interpreted strictly in terms of a strong relaxation of the muonium electron by Fe^{3+} ions, assuming the rate ν_m of that relaxation to be proportional to the square of Fe^{3+} concentration (SC 70). Although this mechanism may be present, the model considered in Ref. (NY 65) included the additional assumption that the mean chemical lifetime of muonium was independent of reagent concentration, which is now know to be incorrect. Results for $FeCl_3$ and $Fe(ClO_4)_3$ at 4500 G were later treated as evidence for the proper muonium mechanism, (BC 71) with the assumption that the only important reaction was

$$Mu + Fe^{3+} \overset{(k_{mxd})}{\rightarrow} \mu^+ + Fe^{2+}, \qquad (7.34)$$

where either the free muon itself or the product of its subsequent reaction with anions in the solution constitutes a diamagnetic environment for the muon. In light of the lack of reaction of muonium with HCl, one might expect the system Mu + $FeCl_3$ in H_2O to provide a good example of the proper muonium mechanism. Results at 4500 G are consistent with this assumption, but low-field measurements must be made to test for the presence of radicals in the depolarizing mechanism.

Results for $Fe(NO_3)_3$ and $Fe(ClO_4)_3$ at high field should not be interpreted strictly in terms of the proper muonium mechanism. The evidence for radical formation in nitric acid suggests that muonium might form radicals in $Fe(NO_3)_3$ solutions as well; again, low-field data may resolve this question. For $Fe(ClO_4)_3$ there is no doubt that radical formation is involved. Figure 7.7 shows the experimental dependence $P_{\perp res}([Fe(ClO_4)_3]$ at 100 G. The

best fit without radicals (dashed curve) is very poor; only by assuming that muonium reacts with dissolved $Fe(ClO_4)_3$ to form a muonic radical can one obtain an acceptable fit (solid curve). The situation here is formally the same as in reactions (7.31), (7.32), and (7.33) for NO_3^-, with the additional process (7.34) for Fe^{3+}. Again, no attempt was made to identify chemical species. The results listed in Tables VII. 2 and VII. 3 are obtained by minimizing χ^2. The existence of muonic radicals in $Fe(ClO_4)_3$ solutions leads one to expect that radical formation will be found to play an important role in $HClO_4$ as well; low-field measurements should confirm this.

It should be mentioned here again that the muonium "spin-flip" frequency, ν_m, may not be negligible in solutions of paramagnetic ions. Although the absence of any significant "repolarization" in concentrated Mn^{2+} solutions (BC 71) demonstrates that the repolarizing effect of other paramagnetic reagents are due mainly to the types of chemical mechanisms described above, some concentration-dependent muonium relaxation [as postulated in Ref. (SC 70)] could serve to partially quench the phase variations and generally mimic the effects of radicals shown in Fig. 7.7 . Consequently, estimates of the contribution of radicals to the depolarization mechanism in paramagnetic solutions are to be regarded as tentative, pending further clarifying experiments.

d. Conclusions Regarding the Model

Several of the above results are particularly important in resolving certain controversies about the theory. First, the results for I_2 in CH_3OH at 102 G firmly establish that the residual polarization in pure methanol is due solely to hot atom chemistry. If, as claimed by Babaev et al., (BB 66) $P_{\perp_{res}}(CH_3OH)$ were nonzero due to thermal chemical reaction of the type

$$\mathrm{Mu} + \mathrm{CH_3OH} \xrightarrow{(k_{msd})} \mathrm{D\ (unidentified)}, \qquad (7.35)$$

muonium atoms would never remain uncombined long enough to precess, and there could be no phase dip. In fact, such reactions must be totally unimportant to the mechanism in order to explain the return of the phase to zero as $[I_2] \to 0$. Therefore, we can be sure that $k(7.35) < 10^7$ liter / mole-sec and that the fraction of muonium reacting epithermally with methanol at room temperature is $h(CH_3OH) = 0.53 \pm 0.01$. Similarly, the results for benzene indicate $h(C_6H_6) = 0.13 \pm 0.01$, but are not as conclusive regarding $k_{msd}(C_6H_6)$, due to the small phase dip. However since the asymmetry in pure benzene is so small, it is still fairly certain that $k_{msd}(C_6H_6) < 10^8$ liter / mole-sec.

The incomplete depolarization in water is also exclusively due to hot atom chemistry, as is especially clear from the curves of $P_{\perp_{res}}$ vs hydrogen peroxide concentration in water. The best value for $h(H_2O)$ is 0.55 ± 0.03; the anomalously high value (0.59 ± 0.01) of $h(H_2O)$ obtained in the fit of the H_2O_2 results is probably a reflection of the low value for A_o in the same instance, which in turn could be due to the low density of concentrated H_2O_2 solutions compared to other concentrated aqueous solutions. A higher-density target gives a slightly increased A_o; such variations of A_o with density are not allowed for in the fits. This introduces a systematic error of ~5% in the numerical results for A_o and h, but does not significantly distort the other results.

The second general conclusion to be drawn from these results is that formation of fast-reacting radicals plays a central role in many (if not most) examples of μ^+ depolarization in liquids. If the radicals formed by reactions of Mu were relatively stable, or if radicals were rarely formed at all (proper

muonium mechanism), the model formulated by Ivanter and Smilga in Ref. (IS 69) would be completely adequate for analysis of muonium chemistry. It is clear, however, that the more general case derived in Section VI is necessary for most practical applications.

2. Comparison with Hydrogen Atom Chemistry

Absolute rates of reaction in solution are difficult to estimate reliably from first principles, due to the complexity of the processes involved. It is possible, however, to make some qualitative predictions of how rates will depend upon the mass of one reactant when all other physical parameters are held constant.

As mentioned earlier, rate constants of Mu and H in gases are expected to differ by a factor of 3 due to the kinetic isotope effect in the mean thermal velocity [see Eq. (7.19)]. Additional factors may arise from "dynamic" isotope effects. Unfortunately, such a treatment is only appropriate for gases, where the mean free path is many molecular radii and the concept of a "collision rate" is well defined. In liquids, each reagent molecule is continually surrounded by a "cage" of solvent molecules which severely restrict its thermal motion. (BE 71) The reactants must diffuse through this crowded environment to find each other, and when they do approach they are apt to stay in each other's presence for some time: the probability of reaction in such a prolonged "encounter" is often close to unity. Such reactions are called "diffusion controlled" (DC), since the rate of reaction depends only upon how fast the reactants diffuse through the solvent to meet each other. Since diffusion in liquids proceeds primarily by "squeezing" and "tumbling", such rates are largely determined by the geometrical properties of solvent and reactant molecules, and the mass dependence is generally weaker than

in gases.

A rough estimate of the diffusion controlled rate for reactions of Mu atoms in water or methanol is $k_{DC}(Mu) \approx 10^{11}$ liter / mole-sec. Most of the measured rate constants for Mu in liquids are near this limiting value. Rate constants less the k_{DC} usually reflect an "activation energy" E_a required to form the activated complex $HX^{\ddagger}$ in the reaction $H + X \rightarrow HX^{\ddagger} \rightarrow$ products. (GL 72) The rate constant then acquires an exponential temperature dependence via the Boltzmann distribution: $k \propto \exp(-E_a/k_B T)$. The quantity E_a may depend upon factors such as the vibrational frequencies of bonds formed in the activated complex, which may in turn depend upon the mass of the light atom. Even in the case of diffusion-controlled reactions, the diffusion process itself requires an activation energy (GL 41, WO 72, LO 67) which may depend upon mass. In addition, quantum mechanical tunneling, which may be important for many reactions of H, (LR 68) can be expected to be quite significant for muonium. Such "dynamic" isotope effects can cause dramatic differences between k(Mu + X) and k(H + X).

Table VII. 4 shows a comparison between Mu and H rate constants for some of the more unambiguous reactions studied.

a. Rates Near the Diffusion-Controlled Limit

The rate constant $k(7.23) = (1.33 \pm 0.1) \times 10^{11}$ liter /mole-sec for reaction (7.23) of Mu with I_2 in CH_3OH is near the DC limit for muonium in methanol. The corresponding H atom rate has been measured in aqueous solution (AN 67) to be 4×10^{10} liter / mole-sec, in qualitative agreement with this result. The rate constant $(5.7 \pm 1) \times 10^{10}$ liter / mole-sec for Mu + I_2 in C_6H_6 indicates that diffusion of Mu through benzene is about one-half as fast as through methanol, if reaction (7.23) is truly diffusion-controlled. Such

an assumption is supported by the fact that the rate constant k(7.24) = (9.4 ± 0.3) × 10^{10} liter / mole-sec for reaction of Mu with Br_2 in C_6H_6 is nearly the same as with I_2. This value agrees well with the measured (FA 67) rate (12 ± 6) × 10^{10} liter / mole-sec for H + Br_2 in water.

b. Reactions with Solvents

The rate constant for H + CH_3OH in aqueous solution is (AN 67) (1.6 ± 0.1) × 10^6 liter / mole-sec. While this result cannot rigorously be compared with the rate for Mu in pure CH_3OH, where diffusion is irrelevant, it does qualitatively corroborate the value k(7.35 < 10^7 liter / mole-sec for Mu + CH_3OH. The reaction rate of thermalized H atoms with benzene to form cyclohexadienyl [analogous to reaction (7.25)] was measured by pulsed radiolysis in aqueous solution (SW 58, SW 67) to be about (7 ± 3) × 10^8 liter / mole-sec, whereas for muonium k(7.25) = $(8^{+5}_{-3}) \times 10^8$ liter / mole-sec in the pure solvent. Again, these two rates in different solvents cannot legitimately be compared in an absolute sense; nevertheless, the fact that they agree constitutes some justification for the assumption that the radical is formed by thermal, rather than "hot atom", reactions. In water, the results are consistent with k(Mu + H_2O) < 10^7 liter / mole-sec. We are not aware of any evidence for fast reactions of H with H_2O.

c. Reactions of Muonium in Aqueous Solution

(1) Hydrogen Peroxide

The basic reaction of H with hydrogen peroxide is thought to be (ST 68)

$$H + H_2O_2 \rightarrow HO^{\cdot} + H_2O \,. \qquad (7.36)$$

The rate constant for this reaction has been measured (ST 68) over a range

of pH to be $k(7.36) = (9 \pm 5) \times 10^7$ liter /mole-sec. The reaction is presumed to involve a cleavage of the O-O single bond, but from (7.36) it is impossible to tell whether the original H atom emerges in the H_2O as in reaction (7.28), ("OH abstraction") or in the HO· as in reaction (7.29), ("O abstraction"). For muonium k(7.29) is nearly 4 times higher than k(7.28).

One would expect k(7.28) + k(7.29) to be the Mu rate analogous to k(7.36); instead, $k(7.28) + k(7.29) = (1.09 \pm 0.15) \times 10^{10}$ liter /mole-sec, roughly a factor of 100 higher than the corresponding H atom rate. Such a large anomaly is probably attributable to dynamic isotope effects. Even a gross error in the assumed value of ω_r (caused, for instance, by misidentification of the radical) would not explain such a discrepancy between the two rate constants.

(2) Strong Acids

Since HCl, HNO_3, and $HClO_4$ are all highly dissociated in aqueous solutions, their reactions with Mu can be considered primarily in terms of the ionic species H^+, Cl^-, NO_3^-, and ClO_4^-. As mentioned earlier, HCl solutions up to 10 M do not repolarize the muon; we must conclude that no combination of reactions with H^+ and/or Cl^- leads to a stable diamagnetic environment for the muon in times less than about 10^{-8} sec.

In nitric acid, on the other hand, one finds a net reaction rate $k(Mu + NO_3^-) = k(7.31) + k(7.32) = (1.3 \pm 0.6) \times 10^{11}$ liter /mole-sec, an essentially diffusion-controlled rate. This result is a factor of 10^4 higher than the measured (NS 65) H atom rate constant $k(H + NO_3^-) = (9 \pm 5) \times 10^6$ liter / mole-sec. Assuming that the rates of the same reactions have been measured, such a dramatic isotopic effect probably reflects a tunneling process. (LR 68) As in the case of H_2O_2, such a large discrepancy cannot be explained simply by postulating an error in ω_r.

A solution of concentrated $NaNO_3$ was studied as a test of pH depen-

dence; complete repolarization was observed, as for concentrated HNO_3. While a full curve of $P_{i_{res}}([NaNO_3])$ would be necessary to clarify the details of the chemical processes involved, this single measurement was sufficient to indicate that Mu reacts with NO_3^- at approximately the same rate, independent of the presence of H^+. Also, highly reactive species such as NO_2, O_2, and NO_2^- should not have been present in signficant concentrations in the freshly prepared $NaNO_3$ solution.

The repolarization of muons by $HClO_4$ in high magnetic field was also studied. A fast reaction is suggested, $k(Mu + ClO_4 \rightarrow D) \approx 10^9$ liter / mole-sec, for the complete process leaving the muons in diamagnetic compounds. Until studies are made in low field, the details of the process are uncertain. However, one can predict that radical formation will be important on the basis of results at 100 G with $Fe(ClO_4)_3$, which show a rate constant $k_{mxr} = (3.8 \pm 0.8) \times 10^{10}$ liter / mole-sec. Here Fe^{3+} is unlikely to react with Mu to produce a radical, so we expect that this rate represents k(7.37) for the reaction

$$Mu + ClO_4^- \xrightarrow{(k_{mxr})} (\text{muonium-containing radical}) . \qquad (7.37)$$

Since reactions of H atoms with ClO_4^- are regarded as virtually nil, (AN 67) there is again dramatic disagreement between Mu and H rates.

(3) Ferric Salts

The data for $Fe(ClO_4)_3$ at 100 G provide detailed information about the rates and qualitative features of several reactions, but the large number of species involved complicates the extraction of rates of specific reactions of Mu with Fe^{3+} and/or ClO_4^- to produce both diamagnetic and paramagnetic products. In strong fields, even less detail is available from the data [see

Fig. 6.2], and in the case of $Fe(NO_3)_3$ we can only be sure that a fast reaction does take place.

The situation with $FeCl_3$ solutions should be much simpler, since Mu does not appear to react significantly with Cl^-. Interpreting the high-field data on Mu + $FeCl_3$ strictly in terms of reaction (7.34), one obtains a rate constant $k(7.34) = (2.1 \pm 0.2) \times 10^7$ liter/mole-sec. The H atome rate constant for the direct oxidation-reduction reaction analogous to (7.37) has been measured to be $(9 \pm 1) \times 10^7$ liter/mole-sec (AN 67) in similarly mild acidic solutions. Taken at face value, the muonium rate is 200 times that for hydrogen. However, it is unlikely that the process involved is as simple as reaction (7.34). Ferric ions are known (CW 66) to form complexes in solution, in particular $FeCl^{2+}$ and $FeCl_2^+$, whose rate constants for reaction with H atoms are respectively 4.5 and 9.0×10^9 liter/mole-sec (see Ref. AN 67). It is possible that reactions of Mu with one or both of these species was actually observed.

d. Reactions of Radicals

The μ^+ depolarization technique also allows measurement of rate constants for reactions of various radicals incorporating muonium.

In comparing these rate constants with the corresponding rates for analogous radicals in which the muon is replaced by a proton, the difference in masses of Mu and H should affect only the "dynamics" of the processes. Even MuO$^\cdot$, the lightest muonic radical envisioned, should diffuse through liquids at the same rate as HO$^\cdot$, its protonic analog. Comparisons of reaction rates of muonic and protonic versions of these radicals should therefore admit of straightforward interpretation in terms of the dynamics of the activated complex.

The most serious difficulty with this interpretation is the uncertainty as to which radical is actually being produced. In the cases of HNO_3 and $Fe(ClO_4)_3$ solutions, for instance, no attempt was made to identify the

radical species. The fitted value for ω_r/ω_o, while imprecise, does provide a hint as to likely candidates, suggesting MuO· in the case of HNO_3 and some species with a weaker hyperfine coupling in the case of $Fe(ClO_4)_3$. However, this cannot be regarded as conclusive evidence, and the products of reactions (7.32) and (7.37) must be regarded as unknown. A longitudinal field technique has given an experimental estimate of ω_r in C_6H_6Mu· [reference (GF 71)], and it may prove possible to determine other hyperfine couplings in this way Such studies would be very helpful.

In some cases it is possible to deduce the identity of the radical, if there is only one species of "reagent" and the products of its reaction with H are well known. In hydrogen peroxide solutions, for instance, it seems most probable that reactions (7.28) and (7.29) should dominate, (ST 68) making MuO· the most likely radical species. The value for the rate constant for reaction of MuO· with H_2O_2 is $k(7.30) = (1.4 \pm 0.2) \times 10^9$ liter /mole-sec. The corresponding rate for HO· + H_2O_2 is (AN 67) about $(3 \pm 2) \times 10^7$ liter/ mole-sec, a factor of 50 slower. Unless the radical has been misidentified, this difference is almost certainly due to dynamic isotope effects in the $(MuOH_2O_2)^{\ddagger}$ complex.

The addition of H to benzene to form cyclohexadienyl is also a well established reaction, (MH 70) a fact which lends credence to the assumption that C_6H_6Mu· is the radical involved in reactions (7.25) and (7.26). We are unaware of any measurement of the reaction rates for C_6H_7· with Br_2 or I_2; these measurements of $k(C_6H_6Mu· + Br_2) = (3.6 \pm 1.0) \times 10^9$ liter / mole-sec and $k(C_6H_6Mu· + I_2) = (2 \pm 1) \times 10^9$ liter /mole-sec may represent the only information available on these reactions. In view of the large size of the C_6H_6Mu· molecule and the similarity of the rates with Br_2 and I_2, the reaction is probably diffusion-controlled in liquids.

e. Prospects for Muonium Chemistry in Liquids

In summary, there are evidently a number of startling exceptions to the naive expectation (FB 65, BC 71) that Mu and H should react at similar rates in analogous processes in liquids. The present results, far from settling the issue, call for further investigations, both experimental and theoretical. The accuracy of H atom measurements may also need critical examination. Although experimentally difficult, more attempts should be made to measure radical hyperfine frequencies directly. Such measurements would be quite interesting in their own right, for comparison with hyperfine couplings in protonic versions of the same radicals. It is clear from these results that comparisons of Mu and H atom solution chemistry are feasible, and that one may expect to encounter large differences in rates. The interpretation and final understanding of these differences, presumably in terms of dynamic isotope effects, may be of great significance to the chemical physics community.

3. Muonium Hot Atom Chemistry

The "hot fraction" h has been a source of annoyance in the history of muonium chemistry, largely due to the analysis of many experimental results with the assumption that it was negligible. (GF 71) Now that epithermal reactions have been shown to be important (and their efficiencies easily measurable), this topic becomes a new area of study.

Unambiguous measurements of h are available in only a few substances:

$$h(H_2O \text{ at } 300^\circ K) = 0.55 \pm 0.03$$

$$h(CH_3OH \text{ at } 300^\circ K) = 0.53 \pm 0.01$$

$$h(C_6H_6 \text{ at } 300^\circ K) = 0.13 \pm 0.01.$$

In addition, a preliminary analysis of unpublished $P_{\perp_{res}}([Br_2])$ results in

CS_2 at 300° K indicates a hot fraction in CS_2 similar to that in C_6H_6. These numbers tell us only the efficiency for epithermal formation of stable diamagnetic compounds containing muonium; paramagnetic products (radicals) may also form, and at this stage we can only put weak upper limits on the efficiency of such reactions. Furthermore, we cannot tell which diamagnetic products are formed; however, studies of hot tritium chemistry (RO 70) can help us make intelligent guesses. These guesses can sometimes be complemented by measurement of "chemical shifts" in the μ^+ precession frequency due to diamagnetic shielding by molecular electrons. Each molecular species will have a characteristic chemical shift which can be estimated from theory and/or proton NMR measurements on analogous species. However, these shifts are very small (~ 1 ppm) and their measurement requires extremely precise frequency determinations. Furthermore, when more than one molecular species is present in significant numbers, it is impossible to separate the different frequencies which result. So far the only attempts to sort out such chemical shifts have been in precise measurements of the muon magnetic moment (HM 63, CH 72).

The specification of temperature is not superfluous; although one might naively expect h to be independent of temperature, this is not the case. In water h is a uniformly increasing function of temperature, showing a spectacular rise as the phase changes from ice at 0° C to water at 0° C (MY 67). [See Fig. 7.8] Not surprisingly, these results were first interpreted in terms of thermal reactions. We are now bound to seek an explanation for the phase dependence of hot atom processes. One possibility is that hydrogen-bonded ice is much more efficient than water at slowing down the epithermal Mu atom, which then has fewer collisions in the energy range where reactions are likely.

Very high asymmetries are seen in halogen-substituted methanes (see Table II. 3). To test for a "thermal contribution" to the residual polarization in $CHCl_3$, a series of mixtures of $CHCl_3$ and CH_3OH (known to be thermally inert) were examined; a thermal process would be reflected in a characteristic dip in $\Delta\phi$. The (unpublished) results, shown in Fig. 7.9 , are taken to be good evidence for a purely epithermal reaction with $CHCl_3$. It will also be noticed that the dependence of the asymmetry upon the mole fraction of $CHCl_3$ is not linear. This must be a consequence of the dynamics of the hot atom processes: the cross section for epithermal reaction will have a peak at a different energy for each molecular variety, and the different molecules will have different efficiencies at each energy for slowing down the Mu atoms without reaction. The resultant dependence of the epithermal reaction probability upon mixture can have a variety of shapes.

In Table II.3 we list the muon asymmetries in a variety of pure substances. On the basis of a single measurement, one cannot determine whether the residual asymmetry is strictly due to hot atom chemistry or partially due to thermal reactions; however, a good indication of the dominant mechanism can sometimes be obtained by varying the strength of the transverse magnetic field; for a purely epithermal reaction, the asymmetry should be independent of field strength (except for apparatus effects). In the case of purely thermal reactions, more than 50% depolarization in low fields reflects the brief coherent precession of muonium atoms [see Fig. 6.2]; this depolarizing process can be slowed down (increasing the residual asymmetry) by reducing the field strength. Thus a field-independent asymmetry in low fields (20-500 G) can be taken as an indication of predominantly epithermal processes. (GM 71) In this light, Table II. 3 represents a tremendous amount of information about hot atom reactions of Mu, none of which has yet been satisfactorily

analyzed.

To summarize, we feel that muonium "hot atom" chemistry is a field of great promise (for example, in comparisons with hot tritium reactions to help illuminate the dynamics of epithermal processes) which has suffered from profound theoretical neglect.

C. Reactions of Mu in Solids

Muons exhibit a much more varied behavior in solids than in gases or liquids. The μ^+ may replace a proton constituent (as in gypsum), (SC 71) or the Mu atom may occupy a large interstitial vacancy (as in quartz), (MO 68) or the μ^+ may acquire a screening cloud of conduction electrons (as in most metals) which has an average charge density similar to that of the e^- in the Mu atom, but in which there is no coherently coupled μ^+-e^- spin system in the sense of muonium. A description appropriate to one case is generally a poor way of treating another, and the concept of chemical reactions takes on a rather broad interpretation, restricted to those media in which quasi-free Mu atoms can be said to exist in the familiar sense. In solids, then, we may define a "chemical reaction" as any process which removes the μ^+ from quasi-free muonium and places it in a diamagnetic environment. Any such reaction is assumed to take place at a constant rate $1/\tau_m$.

Because of this diversity, we will leave most of the "chemical" reactions of Mu in solids to be discussed along with other phenomena under the subject headings of the particular media in the last two Sections; however, there are several cases which are appropriately mentioned here.

Epithermal reactions of Mu in frozen liquids (e.g., water) have already been discussed. Thermal reactions of Mu in certain amorphous solids could be studied by "freezing in" varying amounts of a reagent, exactly as in the

liquid phase technique. This sort of investigation involves no new concepts (except perhaps in the interpretation of the results), but has not yet been undertaken.

In sulfur, some very unusual μ^+ behavior has been observed. (GM 68) Since yellow sulfur is an excellent insulator, one might expect to see free Mu precession in crystalline sulfur. On the other hand, Mu might be expected to react rapidly with sulfur, causing Mu precession to be replaced by μ^+ precession with some residual polarization. One in fact observes μ^+ precession, but there seems to be two components to the signal, one long-lived, with an asymmetry of 0.05, and one rapidly relaxing, with an initial asymmetry of 0.16 and a relaxation time of 30 ± 5 nsec.

Gurevich et al. (GM 68) interpreted this as a case of chemical reaction of Mu with $\nu \gg \omega_o \sqrt{1 + x^2}$, in which $P_\mu(t) = P'_\mu(t)e^{-i\omega_\mu t}$, where $P'_\mu(t)$ is given by Eq. (6.21). They extracted a chemical lifetime of $\tau_m = 130$ nsec and an electron relaxation rate $\nu = 270\omega_o$. This interpretation is entirely consistent with the data, but is subject to many reservations. First, the possible presence of hot atom processes weakens the necessary assumption that the polarization of the non-relaxing component is equal to $\tau_1/(\tau_1 + \tau_m)$. Second, one is hard-pressed to imagine a mechanism for such rapid relaxation of the Mu electron in so good an insulator.

An alternate model for μ^+ in sulfur can be proposed: muonium reacts epithermally with the S_8 ring structure to form both diamagnetic (constant polarization) and radical products. For the radical (e.g., $MuS_8^{\cdot}$) one can easily imagine $\nu_r \gg \omega_r$ due to multiple hyperfine couplings. Thus the μ^+ polarization in the radical fraction could well have the time dependence (5.13). In this model no thermal chemical reactions need to be postulated.

Longitudinal field studies of $P_{\parallel\,res}$ in sulfur (EP 66) [see Fig. 7.10]

indicate a low-temperature field dependence vaguely like that described by Eq. (4.6) if an "effective hyperfine field" of ~75 G is assumed in the definition of x. This suggests a depolarizing process including a radical with $\omega_r \sim 0.05\ \omega_o$. At room temperature, the residual polarization is not completely restored even by strong fields; this is consistent with the hypothesis of a relaxing radical.

Neither of the above models is supported by conclusive evidence and the behavior of μ^+ and/or Mu in sulfur must still be regarded as an unresolved mystery.

A somewhat similar behavior is observed for muonium in a number of ionic crystals; in addition, the process by which positive muons replace protons in $CaSO_4 \cdot 2H_2O$ crystals must be in some sense a hot atom reaction. However, the mechanisms acting in these cases are so unclear that we cannot pretend to have understood the "chemistry" involved, and so we will reserve discussion for the Sections dealing more generally with Mu and μ^+ in solids.

VIII. MUONIUM IN SOLIDS

In many solids, the μ^+ captures a single electron to form a muonium atom in some vacancy or interstitial site. The coupled μ^+ and e^- spins then evolve as described in Section V, subject to a variety of interactions causing depolarization or destruction of the muonium spin system. There are also a number of situation in which the μ^+ does not form muonium in this sense; these cases will be discussed in the next section.

We can separate the behavior of Mu in solids into four general categories correlated with the physical characteristics of the solid. In pure nonmagnetic insulators, Mu finds a spacious enough interstitial site that its behavior resembles that of a free muonium atom in vacuum. In other insulators with high densities of paramagnetic impurities, or in ferromagnetic insulators, Mu may find a spacious site, but is subject to rapid "chemical" reactions and depolarizing magnetic perturbations which destroy the Mu precession signal and make direct identification of Mu difficult. In pure semiconductors at low temperature, Mu may be confined to a cramped interstitial site or may have a delocalized electron wave function spanning many lattice sites; in each case it is strongly perturbed by the crystal field and the available conduction electrons. And in warm n-type semiconductors or semimetals with high densities of conduction electrons, muonium suffers such severe perturbations that it exists only by a marginal definition.

Each of these categories will be treated more or less separately in the following discussion.

A. Muonium in Solid Insulators

Muonium precession is directly observable in many pure insulators (MO 68, GI 69, BC 73). In quartz, ice and solid CO_2 the "two-frequency precession" described by Eq. (5.5) has been observed in moderate fields (see, for example, Fig. 5.1). In each case the value of ω_o extracted from the "beat frequency" is consistent with the hyperfine frequency of muonium in vacuum. Since the hyperfine coupling is given by

$$\hbar \omega_o = \frac{8\pi}{3} g_e \mu_o^e g_\mu \mu_o^\mu |\psi_s(0)|^2, \tag{8.1}$$

where

$$|\psi_s(0)|^2 = \frac{1}{\pi r_o^3}, \tag{8.2}$$

one can say that the mean radius r_o of the Mu atom is the same in these insulators as in vacuum. Thus the interstitial sites in such media are both "spacious" (dimensions $> 2r_o$) and "empty" (negligible valence electron densities). This is not the case for some semiconductors, as will be seen later.

Whenever Mu precession has been observed, a fairly rapid damping of the oscillations has been noted. This relaxation may be due to "chemical" reaction of Mu ("τ_m effects"), depolarization of the Mu electron ("ν effects"), or random local magnetic fields (RLMF) which "smear out" the Mu precession frequency. Mu precession is ~100 times more sensitive to RLMF than is free μ^+ precession. In quartz (SiO_2), which should be chemically inert, the damping may be due to RLMF from the ^{29}Si nuclei (μ = -0.55 n.m.) comprising 4.7% of the Si atoms (MM 70). This hypothesis is supported by the fact that the damping is more rapid at 77°K than at 300°K, as shown in Fig. 8.1 (MO 68); this suggests a "motional narrowing" effect: the enhanced diffusion at higher temperature decreases the time of influence of a given local

field. It was also observed that the damping is faster in crystalline quartz than in fused quartz at the same temperature (300°K), as can be seen from Fig. 8.2.

In corundum (Al_2O_3), no Mu precession can be seen, presumably (MM 70) due to the action of RLMF from the ^{27}Al nuclei (μ = +3.64 n.m.). The field dependence of the polarization in longitudinal field, shown in Fig. 8.3, is consistent with Eq. (4.6) for muonium with a "normal" (vacuum-like) size, except for very low fields, where the polarization drops suddenly to zero. This is taken as evidence that the strength of the RLMF is about 50G.

In each of these insulators, a significant free μ^+ precession signal is observed along with the Mu precession. In view of the relatively stable state of muonium, this cannot be due to a fast thermal chemical reaction of Mu. No satisfactory explanation has yet been offered for the general simultaneous presence of stable Mu and μ^+, but there are two attractive conjectures. The μ^+ signal may be due to muons placed in a diamagnetic environment by epithermal processes of an unknown nature, or to a phenomenon analogous to the "Ore gap" for positrons: in some media, a positron must capture an electron while epithermal in order to form positronium; once thermalized, it lacks sufficient ionization potential to steal an electron away from the medium. For muonium, with twice the ionization potential of positronium, such effects could only occur in highly electrophilic media.

As discussed in the previous section, there is no direct evidence for quasi-free Mu in sulfur. Chemical reactions may be expected to play an important role, but the behavior of Mu in sulfur is still an enigma.

1. Alkali Halides

The alkali halides have also proved to be a very interesting environment for muonium. No Mu precession signal can be seen in any of these ionic crystals, but longitudinal field measurements show evidence for muonium.

Perhaps the best-studied (IM 72) example is KCl. Here (as in most cases) a small μ^+ precession signal is seen in transverse field. This component of the polarization is presumably due to some epithermal process, and has been subtracted out of the residual polarization in longitudinal field, which is shown in Fig. 8.4 as a function of the field strength. The residual polarization $R_{||}$ is zero at zero field, but is restored in fields of ~100 G; when a second crystal with higher purity and fewer dislocations was used, this critical field dropped to ~20G. It is concluded (IM 72) that the behavior in weak field is due to RLMF from paramagnetic lattice defects. If the high-field behavior is extrapolated back to zero field, a residual polarization $R_{||}(0) < 0.5$ is obtained. Muonium formation alone can never cause $R_{||}(0) < 0.5$, so the field dependence cannot be fitted to the form (4.6) as could the Al_2O_3 data. However, the shape of $R_{||}(B)$ is clearly that of a hyperfine-coupled spin system, presumably muonium, so it was assumed that muonium itself was being depolarized ($\nu > 0$). This depolarization would always go to completion if it were not cut short by some quasichemical reaction of Mu ($1/\tau_m > 0$), so the data must obey the general form (6.25). Ivanter et al. (IM 72) found an excellent fit to this model for a wide range of values of ω_o, ν, and τ_m; given the additional assumption that conditions (6.26) hold in KCl, it was possible to extract from the resultant dependence (6.27) the following values:

$$\omega_o \text{ (KCl)} = (0.97 \pm 0.04)\, \omega_o(\text{vac}) \tag{8.3}$$

$$\nu\, \tau_m = 1.81 \pm 0.10. \tag{8.4}$$

This fit, subject to the conditions (6.26), is indicated by the solid line in Fig. 8.4. Unfortunately one cannot obtain separate determinations of ν and τ_m from this fit, since the trade-off between the two is very sensitive to the exact value of ω_o in the region $\omega_o \approx \omega_o(\text{vac})$. The fitted value of the

hyperfine frequency (and thus the size of the Mu atom) is consistent with the vacuum value, as in other insulators.

The hydrogen analogue of muonium in ionic crystals is the U_2 center. The ESR measurements on U_2 centers in KCl (SP 66) one obtains a hyperfine frequency for the hydrogen ground state which is 3% smaller than the vacuum value. If we assume this value for muonium also, we obtain a rough estimate of the separate values of ν and τ_m:

$$\nu \approx \frac{1}{\tau_m} \approx 10^9 \text{ sec}^{-1}.$$

Measurements were also made in low field on a sample of KCl with fewer dislocations (IM 72). The extrapolated value of the residual polarization at zero field was the same (within errors) as for the earlier sample. Whenever conditions (6.26) apply,

$$R_{\parallel}(0) = \frac{1}{2(1+\nu\tau_m)};$$

it is concluded that $\nu\tau_m$ is independent of the concentration of lattice defects. There are two plausible explanations for this. In the first picture both ν and $1/\tau_m$ are proportional to the defect density, since Mu interacts with the paramagnetic defects both by spin-exchange collisions and by "chemical" reactions, in which Mu becomes bound to a dislocation. In the second picture neither ν nor τ_m is related to defects at all.

If ν is unrelated to defects then it must be simply the inverse of the spin-lattice relaxation time of the muonium electron. As such, it would be surprisingly large. If muonium were in a pure s-state, no coupling of the electron spin to the diamagnetic lattice should occur; that is, there would be no coupling to phonons, and consequently no relaxation. If the electron spin is coupled to some orbital angular momentum (LS coupling) which in turn is

sensitive to the electric crystal field, then a spin-lattice interaction is possible, due to the time modulation of the crystal field by phonon modes. Hence, for a spin-lattice relaxation to occur, the ground state of Mu in the crystal must contain some admixtures of excited vacuum states such as the 2p state. Such mixing is facilitated by the static part of the electric field. The 3% reduction of the hyperfine frequency of hydrogen atoms (U_2 centers) in KCl is an indication of such a mechanism.

In the original work of Ivanter and Smilga (IS 68) ν is always tacitly assumed to be field independent. This assumption is by no means obvious. Table VIII.1 lists formulas for the relaxation times of paramagnetic impurities in ionic crystals as derived (MA 66) for different phonon processes: 1) the direct process, a one-phonon process; 2) the Raman process, involving two phonons; and 3) the Orbach process, which involves an excited electronic level. Only the Orbach process is field independent. Future μ^+ depolarization measurements promise to shed some light on which phenomena actually occur.

Clearly these processes are not an isolated property of the muon but are relevant to many other solid state phenomena.

Other alkali halides have also been studies with muonium (see Table II.3), with similar but not identical results. The residual asymmetry in transverse field, postulated to be due to hot atom processes, is much larger for LiF than for KCl. This might be expected, since Li and F are so much lighter than K or Cl; however, the "hot fraction" (if such it is) is smaller in NaCl than in KCl. In LiF, one observes a fairly short transverse relaxation time T_2, which decreases with decreasing temperature. A "motional narrowing" effect may be suggested. Uncertainties as to the muon's whereabouts following epithermal processes in these crystals may be alle-

viated by the fact that similar transverse field results are seen in LiF and LiH, which we may regard as an alkali halide of sorts. The analogy is especially good since the magnetic properties of ^{1}H and ^{19}F nuclei are nearly identical. Since the μ^+ surely replaces protons in LiH, one is tempted to conjecture that the epithermal process in LiF is a substitution of μ^+ for Li^+ or Mu^- for F^- at a lattice site. It is expected that further experiments, including new longitudinal field studies, will greatly clarify the processes at work in these crystals.

It is evident that a careful analysis of μ^+ depolarization in the alkali halides leads one to ask important questions about the interactions of impurities with the crystal field. Perhaps, as further measurements provide answers to these questions, muonium will help us understand more about the properties of the crystal itself.

2. Ferromagnetic and Antiferromagnetic Insulators

So far, we have only considered muonium in a nonmagnetic insulator. Some particularly nice effects can be expected for muonium in a ferromagnetic or antiferromagnetic insulator (SS 71, IV 73). The muonium electron will be coupled by an exchange interaction to ferromagnetically ordered spins of the sample; not so, however, the muon. The relevant Hamiltonian would thus be of the form

$$H = A\,\vec{S}_\mu \cdot \vec{S}_e + (g_e \mu_o^e \vec{B}_{loc} + \sum_i J_i \vec{S}_i) \cdot \vec{S}_e + g_\mu \mu_o^\mu \vec{B}_{loc} \cdot \vec{S}_\mu , \qquad (8.5)$$

with J_i being an exchange integral of the muonium electron with a neighbor electron, labeled i, whose spin is S_i. The electron may then see an effective magnetic field which differs dramatically from the field that acts on the muon. An interesting mechanism for relaxation of the muonium electron is also possible in ferromagnetic insulators--the absorption or emission of magnons, the quanta of ferromagnetic spin waves. The measurement of

relaxation times in these substances might lead, for instance, to a determination of magnon scattering cross sections with muonium (SS 71). Further, the presence of a majority spin on a ferromagnet may lead to unequal initial population of the ^1S_o and $^3S_1$ states of muonium. The resultant time dependence of the μ^+ polarization could be very exotic.

So far, very little data exist for muonium in ferro- or antiferromagnetic insulators. It has been noted that both the residual polarization and the transverse relaxation time of the quasi-free μ^+ precession signal in Cr_2O_3 drop dramatically when the powdered sample is cooled below its Néel temperature (307°K). Precession at frequencies other than the free μ^+ Larmor frequency is evidently absent in Cr_2O_3 in a finite external field; but the available data is very limited, and the observation of μ^+ precession in coherent internal fields in Ni and Fe (FH 73, PC 74) encourages further investigation.

B. Muonium in Semiconductors

The study of muons and muonium in semiconductors has been a long, interesting, and fruitful undertaking, which still has only just begun. Much elegant experimental and theoretical work has been done in the last 15 years in an attempt to understand the general features of the behavior of Mu in silicon and germanium, to which most of our discussion will be limited. However, recent results have relieved much of the confusion and ambiguity which plagued the early work, and we will present the data in the context of what is now known to occur, at the risk of some injustice to those who opened up this frontier.

1. Deep Donor Muonium in Germanium and Silicon

Perhaps the most illuminating recent advance in this field has been the detection of "two-frequency Mu precession" in germanium (GI 71) and p-type silicon (CJ 72, BC 73) at 77°K. These observations not only firmly

established the existence of long-lived interstitial muonium atoms in these crystals, but also provided measurements of the hyperfine frequency of the Mu atom in the interstitial site [recall Eq. (5.5)]. The results were

$$\omega_o(\text{Ge})/\omega_o(\text{vac}) = 0.56 \pm 0.01 \tag{8.6}$$

and

$$\omega_o(\text{Si})/\omega_o(\text{vac}) = 0.45 \pm 0.02. \tag{8.7}$$

The latter result is in agreement with that of Andrianov et al. (AM 70) who studied the quenching of the depolarization in longitudinal field for a mildly p-type single crystal of silicon at 300°K. Fitting the field dependence to Eq. (4.6), they found

$$\omega_o(\text{Si})/\omega_o(\text{vac}) = 0.405 \pm 0.026. \tag{8.8}$$

This technique is comparable in accuracy with the two-frequency precession method, but is not nearly as unambiguous. In an earlier longitudinal field study by Eisenstein et al. (EP 66), the field dependence of the polarization in a mildly p-type Si crystal at 300°K was consistent with that observed by Andrianov et al., but at temperatures $\leq$ 77°K a completely different behavior was seen. The field dependence in n-type Si was also quite different. We will return to this point later.

Recalling Eq. (8.2), we see that these Mu atoms have a radius about 1.2 times that of muonium in vacuum, $r_o(\text{vac}) = 0.532$ Å; their dimensions are still much smaller than one lattice parameter ($\sim$ 5 Å). Interstitial muonium is therefore concluded to be a "deep donor" in Si and Ge—that is, the whole atom fits into one interstitial site and has a binding energy of several eV. Wang and Kittel (WK 73) have explained the magnitude of the reduction of ω_o, as well as the small difference between silicon and germanium, in terms of known properties of the crystals. In their model, the potential function for the bound electron is cut off at large radii due to screening by the valence band electrons of the neighboring silicon atoms.

2. Anomalous Muon Precession in Silicon

A further clarification has resulted from the observation of a second type of two-frequency precession in silicon, corresponding to a much weaker hyperfine coupling. This phenomenon has been labelled "anomalous muon precession" for lack of a positive identification of its source; like deep-donor Mu precession, it is observed only in cold p-type silicon crystals.

The square of the Fourier transform of an experimental time histogram (corrected for background and μ decay) yields a power spectrum of precession frequencies, in which two-frequency precession is manifested as a pair of lines. Figure 8.5 shows a comparison between such Fourier spectra for silicon and fused quartz in the same field, demonstrating the absence of anomalous precession in quartz. Whereas the deep-donor muonium frequencies rise approximately linearly with field up to a few hundred gauss, and are independent of the orientation of the crystal in the field, the anomalous frequencies were found to have the field dependence shown in Fig. 8.6, and are slightly anisotropic, as indicated. Deep-donor Mu precession and anomalous precession have lifetimes of about 500 nsec.

The field dependence of the anomalous frequencies is much stronger than that of the free μ^+ precession frequency in weak fields. The muon must therefore be coupled, as in muonium, to a particle or system with a larger magnetic moment than its own. The field dependence of the anomalous frequencies can in fact be fitted to that of transition frequencies ω_{12} and ω_{34} in a modified version of the Breit-Rabi energy levels (4.2), if the different crystal orientations are treated as separate cases. This can be seen qualitatively from Fig. 4.1. [As is implicit in the transverse field selection rules (4.8) and explicit in the equation of motion (5.4), frequencies ω_{12} and ω_{34} should be dominant when $B \gg B_o$.] However, it is necessary to allow both the hyperfine coupling strength and the g-factor of the electron to vary in order to obtain a fit.

For the case of the [111] crystal axis parallel to the field, the best value for ω_o/ω_o (vac) is 0.0198 ± 0.0002; for [100] parallel to the field, the best value is ω_o/ω_o (vac) $= 0.0205 \pm 0.0003$. In both cases the best value for g_e is 13 ± 3. Clearly, the spin g-factor of an electron cannot be much different from 2, nor can a pure contact interaction be anisotropic; this modified Breit-Rabi description is meant only as a phenomenological characterization of the data.

These results can be interpreted in terms of a number of physical models (BC 73). Perhaps the most attractive is shallow-donor muonium. Here the electron wavefunction is spread over many lattice sites, whereas the entire deep-donor muonium atom fits into one interstitial site. An s-state cannot produce the observed behavior, due to the relatively invariable spin g-factor of the electron. However, in an $\ell \neq 0$ state the orbital g-factor can be large and anisotropic: the electron wavefunction for a shallow donor must be a superposition of conduction band states, which may have small anisotropic effective masses. If the spin-orbit coupling for the electron is large, j_e becomes a good quantum number, and $\vec{J}_e$ formally replaces $1/2\ \vec{\sigma}\, e = \vec{S}_e$ in the Breit-Rabi Hamiltonian. For $j_e = 1/2$ the observed field dependence can easily be reproduced. [It should be noted that other components could be formed with $j_e > 1/2$ which might precess at unobserved frequencies or be quickly relaxed (e. g., by transitions to the $j_e = 1/2$ level).] We conclude that the postulated shallow-donor muonium state must contain substantial admixtures of $\ell \neq 0$ excited vacuum states. The stability of this state (lifetime $\sim$ 500 nsec) against radiative transitions to the deep-donor 1s state can be explained by the small overlap between shallow-donor and deep-donor electron wavefunctions.

A conventional phenomenological description for such behavior is provided by the "effective spin Hamiltonian" formalism often used in ESR work on paramagnetic impurities:

$$H = \vec{J}_e \cdot \underset{\sim}{A} \cdot \vec{S}_\mu + \mu_o^e \vec{B} \cdot \underset{\sim}{g}_e \cdot \vec{J}_e + \mu_o^\mu g_\mu \vec{S}_\mu \cdot \vec{B}, \tag{8.9}$$

where $\underset{\sim}{A}$ and $\underset{\sim}{g}_e$ are now tensors and $\vec{J}_e$ is an effective spin. By adopting this phenomenological Hamiltonian, one can consistently describe quite complicated ESR patterns and their dependence upon the orientation of the crystal in the field. A good fit to the data is obtained assuming a scalar $\underset{\sim}{g}_e$ and a minimal anisotropy with symmetry about the [111] axis for $\underset{\sim}{A}$, which has then only two independent nonzero elements: $A_{33} = A_{\parallel}$ and $A_{11} = A_{22} = A_{\perp}$. Postulating $j_e = 1/2$, we can express the results as follows:

$$(\underset{\sim}{g}_e)_{ij} = \delta_{ij} \times (13 \pm 3), \tag{8.10}$$

$$A_{\parallel} = (0.0198 \pm 0.0002)\, A_o(\text{vac}), \tag{8.11}$$

and

$$A_{\perp} = (1.035 \pm 0.02)\, A_{\parallel}, \tag{8.12}$$

where A_o(vac) is the hyperfine coupling of muonium in vacuum.

Whether the "anomalous precession" in silicon is actually due to shallow-donor muonium or to some other spin system (BC 73) is not known; however, its behavior is precisely that of a muonium-like object with $g_e \approx 13$ and $\omega_o \approx \omega_o(\text{vac})/50$, so we will henceforth refer to "shallow-donor Mu precession" for practical and mnemonic reasons.

3. Tenative Model

In all the silicon and germanium samples studied, a quasi-free μ^+ precession signal was observed in transverse field. The asymmetry and relaxation time of this signal vary dramatically with temperature and doping concentration. In the case of cold mildly p-type Si, all three signals (μ^+, deep-donor Mu, and shallow-donor Mu) are present simultaneously. Since all these motions are out of phase with each other within a few nsec, they must each represent an independent component of the muon ensemble, starting out

simultaneously (within ~ 10^{-10} sec) as distinct products of the thermalization process. The measured asymmetries in these signals only account for about 2/3 of the muon polarization; the missing 1/3 must represent a fraction of the ensemble which relaxes within a few nsec of thermalization or precesses at frequencies too high to be resolved. An unpublished observation of a short-lived (T_2 ~ 30 nsec) component in the μ^+ precession signal at 4400 G (p-type Si at 77°K) suggests the following hypothesis: some fourth fraction of the muon ensemble thermalizes as a free μ^+, which soon (but not immediately) captures an electron to form some muonium state. The resultant Mu atoms are out of phase in their subsequent precession and appear depolarized. The long-lived μ^+ signal must represent a fraction of muons which thermalize into fundamentally different circumstances and are immune to the process postulated above.

If we allow ourselves these conjectures, the situation in p-type Si at 77°K can be summarized as follows: a fraction f_+ of the muons thermalize as free μ^+ and wait in interstitial sites for free electrons to come by, which they promptly capture to form some Mu states. Another fraction f_{dd} thermalizes as deep-donor Mu, and a third fraction f_{sd} thermalizes as shallow-donor Mu. The remaining muons (excluding any channels we may have neglected) undergo some unknown epithermal or otherwise very fast process which places them in a stable diamagnetic environment; we retain the symbol h for this fraction, although a "chemical" interaction is not necessarily indicated. This situation is pictured diagrammatically in Fig. 8.7.

Such a model is consistent with observations for p-type Si at 77°K, but how does it work for other Si and Ge crystals at different temperatures and with different dopings? Let us for instance consider the longitudinal-field data on p-type Si at 300°K (AM 70): Andrianov et al. found that the relationship between the zero-field polarization $P_{\parallel}(0)$ and the polarization $P_{\perp}$ of the long-lived

μ^+-precession component in transverse field was $P_{\parallel}(0) = P_{\perp} + 1/2\,(1-P_{\perp})$, within about 2%. Assuming that the f_+ fraction is not much more stable at 300°K than at 77°K, we may equate $P_{\perp}$ with h. Thus the fraction (1 - h) which thermalizes in states other than stable quasi-free μ^+ has a polarization of 1/2 in zero field (averaged over any hyperfine oscillations)—consistent with the assumption that it all forms muonium. The fraction f_+ should be included in this component, since its originally free interstitial muons should quickly capture electrons. (In longitudinal field there are no problems with "dephasing" due to statistically distributed formation times.) All of the polarization is thus accounted for: $P_{\perp} = h$ and $h + f_+ + f_{sd} + f_{dd} \approx 1$.

When a weak longitudinal field is applied, any stable fraction f_{sd}, with its weak hyperfine coupling, should be quickly "repolarized"; no such phenomenon is observed experimentally. In fact, as mentioned earlier, the field dependence is entirely consistent with the assumption that muonium ends up only in the deep-donor state at 300°K. One might then expect to see a large deep-donor Mu precession signal in transverse field; in fact, no such signal has been detected, nor is any shallow-donor Mu signal visible at 300°K. It has been fashionable to explain this absence in terms of a rapid relaxation ($\nu \neq 0$) or charge exchange ($Mu \rightleftarrows \mu^+$) process; however, in this case such a hypothesis is not plausible, due to the behavior in longitudinal field. As discussed for the case of alkali halides, relaxation or charge exchange will lead to complete depolarization even in longitudinal field unless a "chemical" process permanently removes the muon to a diamagnetic environment at a rate $1/\tau_m \sim \nu$. Because no such "extra" depolarization is observed, we are forced to conclude that $1/\tau_m >> \nu$; the disappearance of any transverse-field Mu precession signal must then be due to "chemical" reactions within a few nsec, and not to relaxation or charge exchange at all. It seems much more plausible

in this case to assume that nearly all of the fraction (1 - h) forms initially in the free μ^+ and shallow-donor Mu states, which then undergo transitions to the deep-donor Mu ground state within a few nsec.

Obviously, these arguments cannot be carried much further into the realm of conjecture until more experimental evidence is available. The desirability of an in-depth study of mildly p-type silicon is obvious, for not until one case is thoroughly understood can credible extensions be made to other cases. However, we are compelled to mention some of these other cases in an attempt to put this field in perspective.

Feher, Eisenstein, et al. (FP 60, EP 66) studied a variety of silicon crystals with various dopings in longitudinal field at 300, 77, and ~ 10°K. They also studied the muon polarization in transverse field, but did not watch the precession in the sense of Section II. In both cases a gated scaling technique was used which effectively yielded the <u>average</u> polarization over 1 - 4 μsec. Their polarization measurements are thus subject to serious underestimation when even slow relaxation is present. Nevertheless, a few interesting conclusions can be drawn from their data.

In each of their cold ($\leq$ 77°K) weakly doped silicon samples, Eisenstein et al. measured a zero-field polarization $P_\perp(0) < 0.5$, considerably smaller than that observed in the same sample at 300°K. The missing polarization was restored by weak longitudinal fields (~ 50 G). The low-field "quenching" effect would be expected in p-type Si due to the formation of shallow-donor Mu ($B_o = 32 \pm 1$ G), but a value of $P_{||}(0) < 0.5$ would not. This is probably due to RLMF from ^{29}Si nuclei (recall the relaxation of Mu precession in quartz): if the measured ~ 500 nsec lifetime of Mu precession in p-type Si at 77°K is due to local fields of about 1G, the same relaxation rate would be seen in zero field; such a relaxing signal is averaged over 4 μsec in Eisenstein's technique, yielding a misleading value for $P_{||}(0)$. Thus the low-field

quenching effect in cold n-type samples is not necessarily evidence for shallow-donor muonium.

For increasingly n-type Si samples, more and more polarization is lost, even in strong longitudinal fields, up to the point at which electron wave-functions from adjacent donors begin to overlap, producing an impurity conduction band. These silicon samples are effectively metallic, and the muons are not depolarized significantly. This behavior is entirely consistent with a model in which muonium electrons spin-exchange with conduction band electrons, producing a relaxation rate ν which increases slowly with the density of conduction band electrons until the silicon goes metallic, at which point $\nu >> \omega_o$ and the muonium electron is effectively decoupled from the muon. One may ask whether muonium can be said to exist any more at this stage; the distinction is not entirely academic. In some metals, for instance, long-range screening of the μ^+ by conduction electrons will prevent formation of an atom-like charge density about the muon; in others, the interstitial μ^+ may have a very localized screening charge distribution similar to a Mu atom; and in some cases, the muon may acquire a screening charge distribution rather like that of a Mu^- ion (FR 58). In any case one may think of the μ^+ with the screening charge as a sort of "collective muonium atom," whether deep- or shallow-donor, in which $\nu >> \omega_o$.

With highly p-type Si, not much polarization is lost even in zero field; most is accounted for in the fraction $(h + f_+)$ observed as μ^+ precession in transverse field. Here one might expect that the depletion of available conduction band electrons would make the fraction f_+ more stable and perhaps even inhibit formation of the fractions f_{dd} and f_{sd}. If this is the case, then virtually all the variety evident in μ^+ behavior in silicon could be expressed as a function of conduction electron concentration.

The transverse-field results of Feher et al. for μ^+ in silicon samples at room temperature with various dopings are summarized in Fig. 8.8. Additional data of Eisenstein et al. are given in Table VIII.2.

4. Germanium

The behavior of muons in germanium crystals appears to be very similar to that observed in silicon. As mentioned earlier, deep-donor Mu precession has been studied in Ge at 77°K, and has nearly the same properties as that observed in Si. Attempts to detect shallow-donor Mu precession in Ge crystals have so far been unsuccessful.

Andrianov et al. (AM 69) made a very nice study of the μ^+-precession signal in Ge over a range of temperatures from 77 to 360° K, and found that both the initial asymmetry and the relaxation rate were smooth functions of temperature, as can be seen in Fig. 8.9. In a metallic n-type Ge crystal, virtually no depolarization was seen, either in the initial polarization or in its time dependence, at any temperature. In a moderately p-type Ge crystal at 77 °K, all the polarization can be accounted for in the μ^+ precession asymmetry and the Mu precession asymmetry measured in low field (7 G); the μ^+ precession has no detectable relaxation. As the temperature is raised past ~ 200° K, the asymmetry and relaxation rate of the μ^+ signal begin to rise simultaneously, until at 360° K it accounts for all of the polarization, and relaxes with a lifetime $T_2 \approx 3.5$ μsec.

This behavior is consistent with that observed in similarly doped silicon, and suggests a growth of fractions f_+ and h at the expense of fractions f_{dd} and f_{sd}. Andrianov et al. suggest that the scattering of electrons by phonons may inhibit muonium formation, or that thermal ionization of Mu may become important at high temperatures. The latter hypothesis is questionable, since even temporary ($t > 10^{-10}$ sec) muonium formation leads to depolarization of the μ^+ precession signal in transverse field, and if repeated formation and

ionization (i.e., charge exchange) takes place, all of the polarization will be quickly lost. It seems unlikely that the μ^+ signal is due to an enhanced fraction f_+, since we have already postulated a rapid relaxation of free interstitial μ^+ precession in cold p-type Si due to capture of conduction electrons; at the same temperature, conduction electrons might be expected to be much more available in Ge, with its smaller band gap. The increase of the relaxation rate with temperature could be due to so many different (and contradictory) mechanisms that we must conclude that it is not understood.

5. Summary

We can only reiterate that the study of Mu and μ^+ in semiconductors is by no means finished. Enough evidence has been gathered to suggest that most of the differentiation of the muon ensemble into various components takes place during thermalization, as pictured in Fig. 8.7, but this model is still subject to great confusion. Some fairly straightforward experiments should suffice to clear up many uncertainties.

The eventual value of a more complete understanding of the behavior of muons in semiconductors cannot be assessed in advance, but the general problem of impurity states is of obvious interest. The most elementary natural impurity is hydrogen, of course, but searches for atomic hydrogen in Si and Ge have yielded negative results, even though H is known to diffuse freely through these crystals. Observations of deep-donor Mu have thus helped to clarify the status of hydrogen-like interstitial impurities in Si and Ge; Wang and Kittel (WK 73) concluded that more is known about muonium than about H or H_2 in these crystals upon which most of modern solid state electronics technology depends.

IX. QUASI-FREE MUON PRECESSION AND SLOW DEPOLARIZATION

In this section we will discuss processes involving muons which end up in diamagnetic environments with their initial polarization unaffected by coherent hyperfine interactions. Examples are the quasi-free μ^+ component h produced in hot-atom reactions, and muons in metals, where the screening of the μ^+ charge is accomplished by the collective motion of conduction electrons rather than by a single muonium electron. In the former case the muon is actually part of a diamagnetic molecule, while in the latter case one may think of the μ^+ as being in a muonium atom with $\nu >> \omega_o$ so that the hyperfine coupling is "broken." In either case, the μ^+ loses no polarization in reaching its ultimate environment, and any subsequent relaxation can be observed directly.

The behavior of quasi-free muons in condensed matter has been studied principally by means of their precession in a transverse magnetic field. Therefore only this case will be considered here. We will deal first with quasi-free muons in solids and then with muons in paramagnetic solutions.

A. Muons in Solids

1. Muon Precession Local Fields

In a field $\vec{B}$, the precession frequency $\vec{\omega}^{\mu}$ of a free μ^+ is given by Eq. (2.5), which can be written

$$\vec{\omega}^{\mu} = -\gamma_{\mu}\vec{B}, \quad \text{where } \gamma_{\mu} \equiv \frac{|g_{\mu}|\mu_o^{\mu}}{\hbar} = 0.85\times10^5 \text{ rad/sec·G.} \tag{9.1}$$

We consider several cases in which $\vec{B}$ is not homogeneous throughout the stopping target:

a) Assume that the field $\vec{B}$ seen by a given muon is constant in time, parallel to the external field ($\vec{B} = B\hat{z}$), and has a limited number of discrete magnitudes B_i. One must then replace the cosine in the rate distribution formula (2.6) by a sum over cosines with different discrete frequencies

$\omega_i^\mu = \gamma_\mu B_i$:

$$\cos(\omega^\mu t + \theta_o) \sum_i P_i \cos(\omega_i^\mu t + \theta_o), \tag{9.2}$$

where P_i is the fraction of muons which precess at frequency ω_i^μ. This will obviously result in complicated beat phenomena in the precession pattern.

b) Next let us assume that the fields seen by individual muons are still constant in time and parallel to the external field, but have a continuous distribution of magnitudes $\mathcal{D}(B)$, implying a frequency distribution $f(\omega) \equiv \frac{1}{\gamma_\mu} \mathcal{D}(B)$. The cosine in Eq. (2.6) must then be replaced by an integral:

$$\cos(\omega^\mu t + \theta_o) \rightarrow \int_0^\infty d\omega f(\omega) \cos(\omega t + \theta_o). \tag{9.3}$$

The frequency spectrum $f(\omega)$ is a distribution function of the probability density for finding muons precessing with frequency ω; in an NMR experiment it would be directly observable as the NMR line shape. Thus the μ^+ precession pattern is simply the Fourier transform of the line shape which would be measured if one could perform a conventional (macroscopic power absorption) NMR experiment with stopped muons (AB 70). A muon technique—effectively "trigger" detection of magnetic resonance—used by Coffin et al. (CG 58) in measuring the muon's magnetic moment actually yielded the line shape directly.

The integral in Eq. (9.3) can be expressed in the form

$$\int_0^\infty d\omega f(\omega) \cos(\omega t + \theta_o) = F(t) \cos(\overline{\omega^\mu} t + \theta_o). \tag{9.4}$$

When the variance ΔB of the local field is small compared with the average local field $B_\mu = \overline{\omega^\mu}/\gamma_\mu$, the envelope function $F(t)$ can often be approximated by a Gaussian or exponential decay with relaxation time T_2. Thus $F(t)$ describes a slow relaxation and can be identified with $A(t)/A(0)$ as introduced in Eq. (2.6).

The field distribution $\mathcal{D}(B)$ often represents an average over a spatial field distribution $\mathcal{D}(B,\vec{r})$ weighted according to the spatial muon distribution $\rho_\mu(\vec{r})$:

$$\mathcal{D}(B) = \int_{\text{target vol.}} d^3r\ \rho_\mu(\vec{r})\,\mathcal{D}(B,\vec{r}).$$

In the case where the field strength is a simple function of position, $B(\vec{r})$, one can write $\mathcal{D}(B,\vec{r}) = \delta[B-B(\vec{r})]$ (Dirac delta function); if, in addition, the muons are uniformly distributed throughout the target volume, $\rho_\mu(\vec{r}) = 1$ and one can rewrite the substitution (9.3) as

$$\cos(\omega^\mu t + \theta_o) \rightarrow \int_{\text{target vol.}} dr^3\ \cos[\gamma_\mu B(\vec{r})t + \theta_o].$$

This description is expected to apply in the case of the "fluxoid lattice" in type II superconductors (IV 69). Since the observed time dependence is just the Fourier transform of the field distribution, a μ^+ precession experiment can be used in much the same way as γ-γ angular correlation measurements (AG 68) to study the fluxoid lattice.

c) If the direction of the constant local field seen by a given μ^+ is not fixed, the situation can become quite complicated. However, some qualitative features are evident: the frequency of precession does not depend upon the orientation, but only upon the strength of the local field; the apparent amplitude and the initial phase do, however, depend critically upon the relative orientations of the field, the initial muon polarization, and the observation direction (the axis of symmetry of the positron counter telescope). Thus the net effect of a distribution of field directions will be to reduce the amplitudes and change the phases of different frequency components. If we note that

$$\int_0^\infty d\omega f(\omega)\cos(\omega t + \theta_o) = \text{Re}\int_0^\infty d\omega f(\omega) e^{i(\omega t + \theta_o)}, \qquad (9.5)$$

we can express these effects as follows: distributions of field orientations contribute an imaginary part to $f(\omega)$ and reduce the net amplitude:

$$\int_0^\infty d\omega \left| f(\omega) \right| \leq 1.$$

In the simplest case, an isotropic distribution of field directions, the effect is simply to reduce $f(\omega)$ to $2/3\ [\cos\theta_o e^{-i\theta_o}]$ times its corresponding value when $\vec{B} = B\hat{z}$.

d) Finally, we relax the assumption that the field seen by an individual muon is constant in time. This is most often the result of diffusion of the muons in a medium where the local field varies with position. We will not attempt a quantitative derivation of the consequences of such behavior, but the main qualitative features are obvious: if the muon moves from a position with one local field to a position with a different local field in a time much shorter than the difference between its precession periods in the two fields, it will "see" an adiabatic average field

$$B_\mu \rightarrow \frac{\int \mathcal{D}(B) B dB}{\int \mathcal{D}(B) dB}.$$

For somewhat slower diffusion, the behavior is more complicated, but can generally be approximated by Eq. (9.4), where the damping described by the envelope function $F(t)$ is slower for faster rates of diffusion (generally the consequence of higher temperature). This effect, known in NMR work as motional narrowing (AB 70), has been observed for muons in copper, where the transverse relaxation time T_2 has a marked temperature dependence (GM 72).

2. <u>The Magnetic Field Measured via μ^+ Precession</u>

The magnetic field $B_\mu = \overline{\omega^\mu}/\gamma_\mu$ determined by a measurement of the mean precession frequency is the average local field experienced by the muon at its site. This local field need not be identical with the applied external field; in ferromagnetic materials, for instance, the external field may have very little

net effect. In general, the local field at some position in the crystal can be broken down into the following contributions (SR 68):

$$\vec{B}_\mu = \vec{B}_{ext} + \vec{B}_{DM} + \vec{B}_L + \vec{B}_{dip} + \vec{B}_{hf}, \tag{9.6}$$

where

$\vec{B}_{ext}$ = external applied field,

$\vec{B}_{DM}$ = demagnetization field,

$\vec{B}_L$ = Lorentz field,

$\vec{B}_{dip}$ = field due to nearby magnetic dipoles,

and

$\vec{B}_{hf}$ = corrected hyperfine field.

The external field $\vec{B}_{ext}$ and the demagnetization field $\vec{B}_{DM}$ (determined by the geometry and bulk permeability of the sample) describe the familiar macroscopic features of the field inside a sample. The microscopic features of the magnetic field are accounted for in the other terms, which describe the contributions from the immediate neighborhood of the field probe. Following standard practice, we consider for magnetic media a spherical "Lorentz cavity" centered about the probe (muon), and calculate the effects of its surface and volume field sources upon that probe. The imagined sphere should have a diameter of at least several lattice spacings, in order to include all of the important dipole sources in the volume contribution, but should fit within a single domain. The surface contribution is the Lorentz field, $B_L = (4\pi/3)\vec{M}$, where $\vec{M}$ is the sample magnetization. The volume contribution $\vec{B}_{dip}$ is just the net field due to all the local magnetic dipoles within the Lorentz cavity. Finally, the corrected hyperfine field $\vec{B}_{hf}$ is the effective field due to contact interactions with polarized electrons.

Let us now examine the various contributions to $\vec{B}_\mu$ for a few specific cases.

a. Insulators

In a diamagnetic crystal $\vec{B}_{DM} + \vec{B}_L$ is vanishingly small; contributions to $\vec{B}_{dip}$ arise only from nuclear moments (see the example below). In a paramagnetic crystal $\vec{B}_{DM} + \vec{B}_L$ is still very small and may in many cases be neglected; $\vec{B}_{dip}$ will consist of contributions from the various paramagnetic ions inside the cavity. In some cases these contributions will cancel due to the symmetry of the site, leaving $\vec{B}_{dip} = 0$. For more details see Ref. NA 67.

b. Nonmagnetic Metals

In a metal there is a contribution to $\vec{B}_{hf}$ from the contact interaction with conduction electrons which are polarized by an external magnetic field; this field causes the Knight shift (AB 70, NA 67). In this case $\vec{B}_{hf}$ is given by the expression

$$\vec{B}_{hf} = \vec{B}_{cep} = K\vec{B}_{ext}, \tag{9.7}$$

where K is the Knight shift parameter (or tensor)

$$K = \frac{8\pi}{3} \langle |u(0)|^2 \rangle \chi. \tag{9.8}$$

Here $\langle |u(0)|^2 \rangle$ is the conduction electron density at the muon site, averaged over all states at the Fermi level, and χ is the Pauli parmagnetic susceptibility (per atom).

Conventional measurements of the Knight shift require the performance of NMR with a metal probe. Due to the skin effect, the rf field will only penetrate into a thin surface region, and it may sometimes be questionable whether one measures the bulk Knight shift of the probe material or some surface properties. With the muon one can measure real bulk Knight shifts (HM 63). However, such studies are tedious, requiring accurate measurement of shifts of ~ 100 ppm in the muon precession frequency. The only known measurements were made in conjunction with the first high-precision determination of the magnetic moment of the muon (HM 63). The Knight shift at

the muons was consistently an order of magnitude smaller than that measured or predicted at the lattice nuclei—not surprisingly, since the μ^+ is presumably located at interstitial sites, where enhancement of conduction electron wavefunctions is weak (HM 63). Singlet annihilation rates of positrons stopped in metals (also proportional to the electron probability density) are consistent with this explanation. An unexpectedly large positive frequency shift observed in graphite is unexplained; μ^- precession measurements in the same sample (HS 63) yielded the expected frequency.

c. Ferromagnetic and Antiferromagnetic Metals

Here $\vec{B}_{dip}$ is the usual sum over the dipole fields of the magnetic ions. This term will disappear if the muon occupies a site with cubic symmetry. The hyperfine field seen by the muon is thought to be decomposed as follows (KO 73):

$$\vec{B}_{hf} = \vec{B}_{cep} + \vec{B}_{vep}, \tag{9.9}$$

where $\vec{B}_{cep}$ is the above-mentioned contribution due to the conduction electron polarization, and $\vec{B}_{vep}$ is a positive field produced by the polarized valence electrons shielding the probe charge in its vicinity. The latter term ($\vec{B}_{vep}$) should be small for the muon. As the ferromagnetism of transition elements like Ni, Fe, Co originates mainly from the conduction electrons, $\vec{B}_{cep}$ may be expected to account for most of $\vec{B}_{hf}$ in these substances.

d. Other Solids

Muons may be expected to provide a useful probe for a number of hitherto neglected or poorly understood solids. The μ^+ precession signal in semiconductors, for instance, has been studied in detail, as discussed earlier; however, the state of the quasi-free muon in these crystals is not well enough understood to warrant discussion in this section. The behavior of quasi-free muons in ferromagnetic and antiferromagnetic insulators has not yet been

systematically investigated, but preliminary studies of Cr_2O_3 show a marked difference in the μ^+ signal above and below the Néel temperature (see the previous section). Exceptionally small relaxation times of the μ^+ precession signal have been found in sulfur (see discussion at the end of Section VII), silicon (see Section VIII), $Gd\,NO_3 \cdot 6H_2O$, and $Fe(NO_3)_3 \cdot 6H_2O$ (Table II.3). None of these results are satisfactorily understood and further investigations are needed.

3. Examples

We turn now to descriptions of various recent experiments which can be understood or analyzed in terms of the framework outlined above.

a. Slow μ^+ Depolarization in a Single Crystal of Gypsum

This experiment in gypsum ($CaSO_4 \cdot 2H_2O$), Ref. SC 71, helped to clarify the mechanism for slow μ^+ depolarization in solid crystals. It can be completely understood in terms of muon precession in local fields as described in Section IX. A. 1, in perfect analogy with NMR experiments on the protons of the water molecules in the hydrated form of $CaSO_4$. The interpretation is based on the assumption that the quasi-free μ^+ precession signal comes from muons which replace protons in waters of hydration via hot atom reactions of muonium. Each observable muon thus occupies the lattice site of a proton in one of the two water molecules in the unit cell of the crystal. This assumption draws support from the results in aqueous solutions.

The neighboring proton will create a magnetic dipole field at the site of the muon, given by the expression (SC 71)

$$\delta B_\mu = \pm \frac{\mu_p}{r^3} (3 \cos^2\theta - 1), \qquad (9.10)$$

where μ_p = magnetic moment of proton, θ = angle between the magnetic moment vector of the proton and the muon-proton radius vector, and r = the muon-proton distance = 1.55 Å.

Depending on whether the proton spin is parallel or antiparallel to an external field, the dipole field will either add to or subtract from the external field. Since there are two H_2O molecules oriented differently with respect to the crystal axes, one expects up to four different muon precession frequencies, as shown in Fig. 9.1. ω_2 and ω_3 belong to the first pair; ω_1 and ω_4 belong to the second pair. In addition, the muon will feel the field components due to protons (and perhaps to magnetic impurities) farther away, which will lead to an inhomogeneous broadening of the frequency distribution about each ω_i. From NMR measurements it is inferred that this distribution is Gaussian in shape, with full width $\Delta\omega$.

Taking the Fourier transform of this field or frequency distribution, one obtains the following expression for $F(t)$ [defined as in Eq. (9.4)]:

$$F(t) = \exp\left(\frac{-t^2}{T_2^2}\right) \cos\left(\frac{1}{2}\,\delta\omega_1 t\right) \cos\left(\frac{1}{2}\,\delta\omega_2 t\right), \qquad (9.11)$$

with

$$\delta\omega_1 = \omega_2 - \omega_1 = \omega_4 - \omega_3,$$

$$\delta\omega_2 = \frac{1}{2}(\omega_4 - \omega_1) + \frac{1}{2}(\omega_3 - \omega_2),$$

and

$$T_2 = \frac{4}{\Delta\omega}.$$

The average frequency $\overline{\omega^\mu}$ (Eq. 9.4) is the central frequency

$$\overline{\omega^\mu} = \frac{\omega_1 + \omega_4}{2} = \frac{\omega_2 + \omega_3}{2}.$$

There are actually two beat frequencies, $\delta\omega_1$ and $\delta\omega_2$, and a Gaussian damping function with a relaxation time T_2. The values of the beat frequencies $\delta\omega_1$ and $\delta\omega_2$ depend upon the crystal orientation in the external field and can be calculated without difficulty (PA 48).

Figures 9.2a and b show data for $F(t)$ for two different crystal orientations. The solid lines are calculated curves, not fits. The beat behavior as well as

the damping are clearly visible. In Fig. 9.2b the agreement between the data and the calculated curve is rather poor; however, in this case the crystal orientation in the external field was not accurately known.

The points in Fig. 9.2 were obtained by dividing the experimental histogram into 500 nsec sections and performing a Fourier analysis on each section. This leads to a determination of the amplitude and phase of the precession signal at the central frequency $\overline{\omega^{\mu}}$. For all crystal orientations the experiment showed that $\tau_{\mu} < 2/(\delta\omega_1 + \delta\omega_2)$—that is, that the beating effect was not important for the most statistically significant part of the histograms. Thus the analysis could be simplified. Equation (9.11) can be written:

$$F(t) = \exp\left(-\frac{t^2}{T_2^{*2}}\right), \tag{9.12}$$

with formally

$$\frac{1}{T^{*2}} = \frac{1}{T_2^2} - \frac{1}{t^2}\ln\left[\cos\left(\frac{\delta\omega_1}{2}t\right)\cos\left(\frac{\delta\omega_2}{2}t\right)\right]. \tag{9.13}$$

For early times $(t << 2/\delta\omega_1$ or $2/\delta\omega_2)$,

$$\frac{1}{t^2}\ln\left[\cos\left(\frac{\delta\omega_1}{2}t\right)\cos\left(\frac{\delta\omega_2}{2}t\right)\right]$$

is approximately time independent. A value of T_2^* is therefore obtained by fitting Eq. (9.12) to the measured histogram. Table IX.1 shows the calculated muon NMR spectra, the calculated T_2^* values, and the corresponding values obtained from the fits for the crystal orientations studied. The line width $\Delta\omega = 4/T_2$ is extracted from the data for the third crystal orientation, where the spectrum effectively consists of only one line, implying $T_2 \approx T_2^*$. The other calculated T_2^* values are in good agreement with the measured ones.

The consistency of the results of this experiment shows that slow μ^+ depolarization in solids is often a consequence of the local field distribution

(dipolar line broadening). In this special case it is further demonstrated that quasi-free muons are indeed most likely to be found in proton sites.

b. Slow Depolarization and Muon Diffusion in Copper

In an experiment by Gurevich et al. (GM 72), slow μ^+ depolarization in copper was shown to be due to inhomogeneous local fields from the nuclear magnetic moments. Natural copper consists of the two isotopes ^{63}Cu and ^{65}Cu with abundances of 69.1% and 30.9% respectively. Each has spin $I = 3/2$; the magnetic moments are +2.23 n. m and 2.38 n. m respectively. Thus the two isotopes have almost identical effects upon the muon.

When the external field is much stronger than the dipole field at the muon site and when the muon's gyromagnetic ratio is much greater than that of the nuclei (in this case, $\gamma_\mu/\gamma_I = 11.7$), $F(t)$ is given by the following expression (GM 72):

$$F(t) = \exp(-\Omega^2 t^2), \tag{9.14}$$

where

$$\Omega^2 = \frac{1}{6} I(I+1) \sum_{j=1}^{m} \omega_j^2 \tag{9.15}$$

and

$$\omega_j^2 = (\hbar/r_j^3)\, \gamma_\mu \gamma_I (1 - 3\cos^2\theta_j). \tag{9.16}$$

Here $r_j = |\vec{r}_j|$ and θ_j are respectively the distance from the muon to the j^{th} nucleus and the angle which the vector $\vec{r}_j$ makes with respect to the direction of the external field. For a polycrystalline sample this formula must be averaged over all crystal orientations.

In the derivation of Eq. (9.14) it is assumed that the muon occupies a fixed position. If the muon diffuses through the crystal at a significant rate, $F(t)$ will be modified due to motional narrowing. If $F(t)$ has a Gaussian shape in the absence of diffusion [as in Eq. (9.14)], the inclusion of motional effects leads (AB 70) to the form

$$F(t,\tau_c) = \exp\{-2\sigma^2\tau_c^2[\exp(-t/\tau_c)-1+t/\tau_c]\}, \qquad (9.17)$$

where σ is the relaxation rate in the absence of diffusion, and can be identified with Ω [Eq. (9.15)] properly averaged over all crystal orientations. The correlation time τ_c represents the average time the muon takes to cross a unit cell by diffusion.

Gurevich et al. observed that at 77°K the damping of the muon precession signal had an essentially Gaussian shape; their fit to the data yielded $\sigma = 0.219 \pm 0.008\ \mu\text{sec}^{-1}$. This implies that diffusion of muons at liquid nitrogen temperature is slow compared with the muon decay rate, and is of no importance in the slow depolarization. The measured σ thus gives a good account of the static field distribution from the magnetic moments of the Cu nuclei. However, at higher temperatures the relaxation rate is considerably slower. Figure 9.3 shows the relaxation rate $\Lambda = 1/\tau_r$ as a function of temperature (τ_r is the time at which the muon polarization had decreased by a factor of e). Only diffusion can account for these results, as the relaxation rate for the spins of the copper nuclei is practically constant over the temperature region investigated. By comparing the experimental damping curves for different temperatures with Eq. (9.17), using $\sigma = 0.219\ \mu\text{sec}^{-1}$, the correlation time τ_c as a function of temperature was obtained. Figure 9.4 shows $\ln(1/\tau_c)$ versus $1/T$. The plotted data may be interpolated by a straight line. This dependence is to be expected if the diffusion mechanism is governed by an activation energy E representing the potential barrier between adjacent sites for the muon: the muon is hopping from one crystal site to another. The correlation time should thus be described by

$$\frac{1}{\tau_c} \approx \frac{D_o}{a^2} \exp\left(-\frac{E}{k_B T}\right), \qquad (9.18)$$

where $D_o \exp(-E/k_B T)$ is the diffusion coefficient and a is the lattice parameter of copper. One may interpret D_o as the vibration frequency of the muon in its temporary interstitial site.

From the slope of the straight line in Fig. 9.4 one can deduce an activation energy corresponding to $E/k_B = 540°K$. The deviation from the straight line in Fig. 9.4 may be due to a temperature dependence of the preexponential factor.

It would be very interesting to compare the diffusion coefficients of protons, deuterons, and tritons with that of muons for the purpose of studying isotope effects in diffusion processes. For instance, it is known that $D_T < D_H < D_D$ for palladium (SI 72) but no study has yet been made of muons in Pd. The study of positive muons in metals should in fact be regarded as a vital new part of the expanding field of hydrogen in metals (e. g. Ref. SI 72), with all the concomitant implications for such technological problems as corrosion and embrittlement.

c. Muon Precession in Nickel and Iron

Muon precession studies in ferromagnetic materials are particularly interesting inasmuch as they promise to yield new information about the various contributions to the local field. Ferromagnetism is not yet perfectly understood on a microscopic level, and it is likely that the use of the positive muon as a probe may help to clarify some hitherto unanswered questions. Kossler and collaborators (FH 73) have observed muon precession in polycrystalline nickel and iron over a temperature region encompassing both ferromagnetic and paramagnetic states. The temperature dependence of the precession frequency and the relaxation rate were studied. Similar results were obtained by Crowe et al. (PC 74) for a single crystal of nickel and over a larger range of external fields.

The observed field in paramagnetic Ni is essentially equal to the applied external field. No fast depolarization processes seem to affect $P_{\perp\,res}$, but

slow depolarization with a relaxation time of $T_2 \approx 4$ μsec is evident. $P_{\perp_{res}}$ and B_μ are essentially independent of temperature in the paramagnetic region studied ($T_c = 631°K < T < 705°K$) (FH 73); however, preliminary studies of T_2 just above T_c show evidence for critical phenomena. No measurements were made in paramagnetic iron ($T > T_c = 1043°K$).

All the existing measured values of B_μ for an unsaturated sample of ferromagnetic Ni are shown as a function of temperature in the lower part of Fig. 9.5. For each sample no more than a single B_μ value is observed at each temperature. The solid line in the figure is the magnetization curve for Ni (WF 26), normalized to a saturation field of 1500 G at $T = 0°K$. Thus B_μ has approximately the same temperature dependence as the magnetization of the material. The measured local field is in the same direction as the external field. In order to interpret these results, one must first determine the most probable position of the muon in the unit cell of the crystal. Octahedral and tetrahedral interstitial sites are considered the only likely possibilities, with some indication that the former type would be favored (FH 73).

For B_{ext} too weak to saturate the sample, B_μ is found to be essentially independent of B_{ext}. This is due to the high permeability of nickel: magnetic domain walls move in such a way as to screen out the external field, implying that in Eq. (9.6) $\vec{B}_{ext} + \vec{B}_{DM} = 0$. Since the dipole fields from Ni cores cancel by symmetry at both octahedral and tetrahedral sites ($B_{dip} = 0$), the only remaining contributions are $\vec{B}_\mu = \vec{B}_L + \vec{B}_{hf}$. The larger contribution in this case is $\vec{B}_L = (4\pi/3)\vec{M}_s$, where $M_s = |\vec{M}_s|$ is the saturation magnetization, which has the same value inside every domain. One must, of course, choose the size of the Lorentz cavity smaller than the dimensions of a magnetic domain to preserve the above definition. Below saturation the orientation of $\vec{M}_s$ is obviously different from one domain to another, but $\vec{B}_L$ and $\vec{B}_{hf}$ are always essentially collinear (SR 68). Let us now consider the particular case of the

single crystal at 77°K, where $B_\mu = +1.48$ kG is measured and $B_L = +2.14$ kG is calculated. The difference $B_{hf} = -0.66$ kG must be due to a contact interaction with 4s and 3d conduction electrons. If the muon charge were closely screened by fully polarized 4s electrons we would expect a hyperfine field of +160 kG as in the Mu atom. The reduced value of the measured field arises partly becuase the screening electrons are only partially polarized.

Neutron diffraction studies yield an unperturbed interstitial magnetization of $M_i = -0.85 \times 10^{22}\ \mu_B/cm^3$ (MO 66), i.e., $M_i = -0.079$ kG. For a naive picture in which screening of the muon charge is completely ignored (effectively treating the μ^+ as an uncharged probe), one can compute a contact field $8\pi M_i/3$ of exactly -0.66 kG. It would be unwise to consider this agreement to be other than fortuitous until a detailed calculation of the screening of the interstitial muon charge by the band electrons is available.

For B_{ext} strong enough to saturate the sample, no further domain wall motion can occur and B_{DM} stays at its maximum value, DM_s, where D is the sample demagnetizing factor. In this case B_μ rises linearly with B_{ext} with unit slope. This is demonstrated in Fig. 9.6. The "knee" in the experimental curve occurs at the calculated saturation field of the sample.

The temperature dependence of the residual polarization is of some interest. Figure 9.7 shows results of Kossler et al. (FH 73) for nickel. Since the Ni specimen actually consists of a large number of magnetic domains, the value of $P_\perp$ depends upon the alignment of domains transverse to the initial muon polarization. Whenever the directions of magnetization of the domains differ from the initial muon polarization direction, the muon spins will precess on "cones" with different axes and aperture angles. As discussed in Section IX. A. 1. c, the overall amplitude of the precession is reduced by 2/3 when the magnetization directions are isotropically distributed.

The solid line in Fig. 9.7 is a measure of this domain alignment; it is extracted by dividing the permeability by the macroscopic magnetization and normalizing to the residual polarization. As can be seen, this line accurately represents most of the data. The drop in $P_\perp$ near the Curie temperature is somewhat artificially introduced by assuming a sudden randomization of orientation near this temperature. This assumption, however, needs experimental confirmation. Such measurements may make possible a study of the formation of domains and clusters around the Curie temperature in the absence of an external field (KO 73).

Slow depolarization rates in Ni were also measured by the LBL and SREL groups. Essentially no slow relaxation was observed in the single crystal, even at 77°K (PC 74). By contrast, a very fast relaxation is observed in polycrystalline samples, especially at lower temperatures (FH 73, PO 74). The absence of this relaxation in single-crystal nickel rules out the possibility that slow depolarization is caused primarily by such dynamical mechanisms as creation or destruction of single magnons or multiple magnon processes, such as suggested by Kossler (KO 73). Other relaxation mechanisms, such as electron scattering from the μ^+, lead to very long relaxation times, invisible on the scale of the muon lifetime.

The disappearance of precession in a polycrystalline sample at low temperature must arise from an extremely short depolarization time caused by a large inhomogeneous line width ΔB. T_2 and ΔB are related by $\Delta B = 2/\gamma_\mu T_2$. (A depolarization time of 0.1 μsec implies a ΔB of about 200 gauss.) Figure 9.5 shows values of ΔB calculated from muon T_2 measurements, compared with ^{61}Ni NMR line widths in polycrystalline nickel from Ref. SB 63. The line widths inferred from μ^+ precession signals in the single-crystal sample at 300 and 77°K ($\Delta B_{77} < 18$G, $\Delta B_{300} < 10$G) are an order of magnitude smaller than the narrowest absolute line widths previously observed in nickel (PC 74).

The approximate equality of ΔB as measured with muons and NMR is significant considering that the field at the nickel nuclei is larger than that at the μ^+ by a factor of 50. If the broadening were due to strains in the sample, one would expect the line width to scale approximately with the field measured. It is well known that considerable line-broadening occurs in polycrystalline ferromagnets because of the inhomogeneous fields of randomly oriented crystallites. The general trend of ΔB in Fig. 9.5 toward larger values at lower temperatures may be qualitatively understood in terms of an increase in the anisotropy energy with decreasing temperature (AU 68), causing an increase in magnetization inhomogeneity.

Kossler's ΔB data show a sharp rise about 550°K. Since $B_\mu(T)$ becomes very steep near the Curie temperature $T_c = 631$°K, imperfect temperature regulation and/or homogeneity would produce an effective internal field inhomogeneity which gets worse closer to T_c. Kossler's ΔB data near T_c can be explained if one assumes an experimental temperature spread ~10°K.

In ferromagnetic iron, Kossler et al. (FH 73) have measured B_μ at a number of temperatures between 300 and 675°K. Iron has a bcc crystal structure, so the μ^+ may be found at the interstitial face-centered sites. There, unlike in the case of Ni, B_{dip} would have one of the values +18.8 or -9.4 kG, depending upon whether the nearest iron cores are situated on a line perpendicular or parallel to the magnetization directions in the domain (ST 73). It is known that hydrogen in Fe has a diffusion (hopping) time of about 10^{-9} sec at 300°K (CH 70). The μ^+ will probably diffuse even faster from one face-centered site to another. Since there are twice as many of the second type of site as of the first, the muon will feel an average dipolar field which exactly cancels, provided that the "hopping time" is very small compared with the period of precession ($\sim 10^{-8}$ sec) in the local fields. For the temperature range studied, a unique B_μ is always observed, as in nickel. No detailed information on slow

depolarization in Fe is presently available. Low-temperature studies of single-crystal Fe may thus be expected to greatly clarify the situation, and perhaps reveal exciting new phenomena.

The interstitial magnetization in iron is known to be a highly structured function of position (SM 66). Thus the value B_{hf} = - 3.0 kG extracted from the Fe data using B_{dip} = 0 and B_L = + 7.1 kG cannot be interpreted very meaningfully until a great deal more is understood about the muon's screening charge and position distribution in iron. However, the result is still qualitatively consistent with the naive picture of contact interactions with unperturbed electron bands.

It seems very likely that a great variety of μ^+ precession phenomena await discovery and study in iron; one can imagine a similar wealth of information available from many other such metals. The future seems rich indeed for this latest application of the positive muon as a probe of matter.

B. Slow Depolarization in Paramagnetic Liquids

The NMR line in liquids generally has a Lorentzian shape, the Fourier transform of which is an exponential decay function describing the relaxation of spin components perpendicular to the external magnetic field. Slow muon depolarization in transverse fields is thus expected to obey an exponential decay law:

$$F_{\perp}(t) = e^{-t/T_2} \tag{9.19}$$

where T_2 is the transverse or spin-spin relaxation time. Relaxation in this case means the loss of phase coherence among the spins of the precessing muons. Slow depolarization in a longitudinal field arrangement is also described by an exponential decay law:

$$F_{\parallel}(t) = e^{-t/T_1} \tag{9.20}$$

with T_1 = the longitudinal or spin-lattice relaxation time. Relaxation in this

case consists of transitions between the Zeeman states of the muons, caused by interactions with the lattice, which provides or absorbs the energy quanta involved. No longitudinal slow depolarization has yet been measured in paramagnetic solutions.

As emphasized before, the muons which precess at the free muon Larmor frequency must be in a diamagnetic environment—placed there either by hot-atom reactions or by thermal reactions of muonium. From results on hot-tritium chemistry in aqueous solutions it is known that the molecule THO is formed preferentially (WO 65). It can be assumed that the same mechanism dominates in hot-atom reactions of muonium, so that most of the "hot fraction" in water $[h(H_2O) = 0.55 \pm 0.03]$ represents formation of MuHO molecules—that is, about half of the muons replace protons in water molecules during epithermal collisions. In solutions where thermal Mu does not react rapidly, these are the only muons observed in a precession experiment.

Since the muon takes the place of a proton, it can be assumed that the muon spin will be relaxed in the same way as the proton spin. Proton spin relaxation phenomena in aqueous solutions have been investigated quite extensively, using NMR (AB 70). Particularly susceptible to study with muons are slow relaxation phenomena in paramagnetic aqueous solutions, in which T_2 is usually short enough to be detected within the muon lifetime (PH 62). From the theory of relaxation (AB 70) one expects that

$$\frac{1}{T_2} \approx (\mu)^2, \tag{9.21}$$

where μ is the magnetic moment of the particle involved. When comparing proton and muon relaxation times in the same solution under the same conditions, one thus expects the ratio

$$\frac{T_2(p)}{T_2(\mu)} = \frac{\mu_\mu^2}{\mu_p^2} \approx 10. \tag{9.22}$$

Figure 9.8 shows T_2 data for muons in paramagnetic Fe^{3+} solutions (SC 70); T_2 is plotted versus paramagnetic ion concentration. The lower data points, connected by a solid straight line, were obtained from solutions of $Fe(NO_3)_3$. The upper solid line represents proton NMR results in the same solution. The experimental ratio of proton to muon relaxation times is indeed about 10. No NMR data are available for comparison with the results obtained for muons in $FeCl_3$ and $Fe(ClO_4)_3$ solutions. Differences between the data from $Fe(NO_3)_3$ solutions and data from $Fe(ClO_4)_3$ and $FeCl_3$ solutions is not fully understood and needs further investigation.

The T_2 results for muons in $Gd(NO_3)_3$ solutions of varying concentration were similarly consistent with proton measurements in the same solutions.

As is well known, Fe^{3+} ions usually form $Fe(H_2O)_6^{3+}$ complexes in water, and protons (muons) incorporated into the sphere of hydration are relaxed by the paramagnetic ion. However, the exchange rate for water molecules in the sphere of hydration is slow ($\sim 3\times10^3$ sec^{-1}) (HU 63) compared with the relaxation rate for muons ($\sim 10^5$ sec^{-1}), yet all of the muons appear to relax—not just those "stuck" in the complexes. Furthermore, in concentrated Fe^{3+} solutions a significant fraction of polarized muons reach diamagnetic environments through thermal reactions [recall reaction (7.34)]. The subsequent state of these muons is unknown, and so part of the depolarization mechanism in concentrated Fe^{3+} solutions is not understood. In an attempt to clarify some of these uncertainties, muon precession has been studied in aqueous solutions of $K_3Fe(CN)_6$ (FB 73). In this case the tightly bound complex $Fe(CN)_6^{3-}$ prevents water molecules from closely approaching the Fe^{3+} ion. At the same time, the strong ligand fields cause Hund's rule to be broken, reducing the spin state of Fe^{3+} from d(5/2) to d(1/2); thus, in $Fe(CN)_6^{3-}$ the Fe^{3+} ion has only $\sim 1/5$ as large a magnetic moment as in $Fe(H_2O)_6^{3+}$. In

keeping with expectations, the resultant muon relaxation rate in up to 0.8 M $K_3Fe(CN)_6$ solutions is undetectable in experimental histograms with modest statistics ($T_2 \gtrsim 20$ μsec). A fast thermal reaction of Mu apparently occurs in these solutions, so we can conclude that the ligand fields prevent depolarization of muons both in the epithermally formed MuHO molecules and in the diamagnetic products of the thermal reaction. Further investigations may help to clarify the basic mechanisms involved.

It is important to note that NMR measurements were generally done in solutions with concentrations of $< 10^{21}$ paramagnetic ions/cm^3, because of problems regarding line width, signal strength, rf power, and other experimental considerations. Proton NMR measurements are thus effectively limited to cases with relaxation times $T_2 \gtrsim 10^{-5}$ sec. However, it is easy to measure much shorter relaxation times with muons, and so to study much more concentrated solutions. In principle, transverse or longitudinal relaxation times can be measured down to $\sim 10^{-8}$ sec.

In very concentrated solutions new effects may show up. This is demonstrated by measurements of T_2 for muons in $MnCl_2$ solutions with Mn^{2+} concentration of up to 5 M ($\approx 3\times10^{21}$ ions/cm^3) (SW 72). These studies also provide a good example of the sorts of effects involved and the variety of information which may be extracted from experimental results. At lower concentrations, $MnCl_2$ solutions have been extensively studied with proton NMR by many authors, particularly Bloembergen et al. (BM 61).

Paramagnetic Mn^{2+} ions, like Fe^{3+} ions, are surrounded by six water molecules forming a hydration sphere. In this case the water exchange rate is fast ($\sim 3\times10^{7}$ sec^{-1}) (HU 63), allowing a straightforward treatment of the relaxation process for the entire quasi-free μ^+ ensemble. Protons (or muons) in this hydration sphere are subject to two time-dependent magnetic interactions: the dipole-dipole interaction between the magnetic moments of the

paramagnetic ion and the proton (or muon), and a scalar coupling or spin-exchange interaction caused by the nonvanishing electronic wavefunction of the ion at the site of the proton (or muon) in the hydration sphere. These interactions lead to the following expression for the transverse relaxation time T_2 (BM 61, BB 59):

$$\frac{1}{T_2} = \frac{4}{60}\,\frac{1}{r^6}\,S(S+1)\,\gamma_{p(\mu)}^2\,\gamma_{ion}^2\,h^2[7\tau_c+13\tau_c(1+\omega_s^2\,\tau_c^2)^{-1}]\,P \qquad (9.23)$$

$$+\,\frac{1}{3}\,S(S+1)\,A_{p(\mu)}^2\,h^{-2}[\tau_e+\tau_e(1+\omega_s^2\,\tau_e^2)^{-1}]\,P\,,$$

where S = ion spin (5/2) for Mn^{2+}),

r = internuclear distance between ion and proton (muon),

γ_p (γ_μ) and γ_{ion} = gyromagnetic ratios,

$A_\mu = 3.18\,A_p$ = coupling constant for the exchange interaction,

ω_s = Larmor precession frequency of the ion,

τ_c and τ_e = respective correlation times for dipole-dipole and exchange interactions,

and P = probability of finding a proton (muon) in a hydration sphere, given by

$$P = \frac{\text{(number of water molecules in hydration spheres)}}{\text{(total number of water molecules)}}$$

or $P = 0.108\times$ (molal concentration of Mn^{2+}).

The first term on the right-hand side of Eq. (9.23) is the contribution due to the dipole-dipole interaction; the second term accounts for the spin-exchange interaction.

The correlation times τ_c and τ_e are a measure of the time dependence of the respective interactions; each may be thought of as the duration of the coherent effects of the interaction involved. The time dependence of the dipole-dipole interaction may be caused by rotational diffusion of the Mn^{2+} complex,

by chemical exchange of the H_2O (MuHO) molecules, and by spin relaxation of the paramagnetic ion, parametrized by the respective correlation times τ_r, τ_h, and τ_s:

$$\frac{1}{\tau_c} = \frac{1}{\tau_r} + \frac{1}{\tau_h} + \frac{1}{\tau_s} \tag{9.24}$$

and

$$\frac{1}{\tau_e} = \frac{1}{\tau_h} + \frac{1}{\tau_s} \ . \tag{9.25}$$

(The scalar coupling is not influenced by rotational diffusion.)

The temperature dependence of the correlation times τ_r and τ_h is described by a type of Arrhenius law:

$$\tau = \tau_o \exp(V/RT), \tag{9.26}$$

where V is the activation energy for rotational diffusion or chemical exchange. The temperature dependence of τ_s is more complicated and involves the mechanisms leading to electronic relaxation. (BM 61).

The information contained in Eqs. (9.23 - 26) is typical of what can be obtained from relaxation studies in paramagnetic solutions.

Figure 9.9a shows the experimental data for $T_2(\mu^+)$ as a function of Mn^{2+} concentration along with the overall T_2 (solid curve), the dipole-dipole term (top dashed curve), and the spin-exchange term (lower dashed curve), obtained from Eq. (9.23) by using reasonable values for the respective correlation times and correcting for the larger magnetic moment of the muon. For concentrations below 10^{20} Mn^{2+}/cm^3 there is good agreement between the data and predictions scaled for muons. At higher concentrations the data break sharply alway from the predicted curve, and there seems to be a quenching of the relaxation mechanism. These deviations from Eq. (9.23) can be understood if we assume that some of the correlation times become concentration-dependent at higher concentrations, due to intermolecular interactions of Mn^{2+} complexes. In particular, spin-spin interactions among Mn^{2+} ions might lead to concentra-

tion-dependent correlation times. Indeed, ESR measurements by Garstens and Liebson, and Hinckley and Morgan (HM 66), show a concentration-dependent line width in concentrated Mn^{2+} solutions. Their data (Fig. 9.9b) can be approximated by (solid line in the figure):

$$\tau_s^* = \frac{1.24\times10^{-9}}{N^2} + 1.27\times10^{-11} \text{ sec},$$

where τ_s^* is now used as an additional effective correlation time in the proton (muon)-ion interactions. Here N = ion concentration in moles/liter. The temperature dependence of τ_s^* can also be obtained from Ref. HM 66. For a 3 M solution, one finds

$$\frac{1}{\tau_s^*} = 1.76\times10^{7}\,[\,710 - 2.8\times10^{3}\exp(-\frac{1.26\times10^{3}}{RT})\,]\,. \qquad (9.27)$$

The total correlation time τ_e for the spin-exchange interaction is thus given by

$$\frac{1}{\tau_e} = \frac{1}{\tau_s} + \frac{1}{\tau_s^*} + \frac{1}{\tau_h}\,, \qquad (9.28)$$

where τ_s is the usual electron spin relaxation time and τ_h is the mean time for the muon to remain in the hydration sphere. Similarly, the total correlation time τ_c for the dipole-dipole interaction is given by

$$\frac{1}{\tau_c} = \frac{1}{\tau_r} + \frac{1}{\tau_h} + \frac{1}{\tau_s} + \frac{1}{\tau_s^*}\,, \qquad (9.29)$$

where τ_r is the rotational correlation time. At room temperature

$$\tau_s \approx 3\times10^{-9}, \quad \tau_h \approx 2\times10^{-8}, \quad \tau_r \approx 3\times10^{-11} \text{ sec (BM 61)}.$$

In Fig. 9.10a the data from Fig. 9.9a are shown with the linear concentration dependence (P) divided out. If the correlation times were concentration-independent, $1/T_2P$ would be constant. By inserting the total correlation times τ_e and τ_c [Eqs. (9.28) and (9.29)] into the general expression [Eq. (9.23)] with the other parameters taken from Ref. BB 59, one obtains

the solid line in Fig. 9.10a, which is an excellent fit to the data. The dashed lines in Fig. 9.10a represent spin-exchange and dipole-dipole contributions separately.

However, using Eq. (9.23) together with Eqs. (9.26) and (9.27) and the temperature dependence of τ_r and τ_h from Ref. BM 61, one obtains the dotted curve in Fig. 9.10b for 11 kG, which—as is clearly evident—does not adequately describe the measured temperature dependence of T_2 in a 3 M solution.

If Eq. (9.27) correctly describes the temperature dependence of τ_s^*, and if τ_h behaves normally, we are forced to adopt parameters different from the ones in Ref. BM 61 in the expression

$$\tau_r = \tau_r^0 \exp(V_r(RT) , \tag{9.30}$$

where V_r is the activation energy of the rotational motion of the Mn^{2+} complex. Using V_r = 8.5 kcal/mole and $\tau_r^0 = 1.73 \times 10^{-17}$ sec, we obtain for $1/T_2P$ versus temperature the lower solid curve at 11 kG and the upper one at 4.5 kG external field strength (GM 66).

The large value for the activation energy at 3 M concentrations (as compared with V_r = 4.5 kcal/mole at low concentrations) seem reasonable in view of the greatly increased viscosity of a 3 M $MnCl_2$ solution [η(3 M) ≈ 3.2 centipoises]. It would be of great interest to establish more detailed experimental relationships between these observations and the dynamics of this liquid (GM 66).

There are unfortunately several questionable assumptions in the foregoing analysis, which we will now discuss.

1) The results of Ref. HM 66 for ESR line widths were obtained in an external field of 3 kG. We have neglected any possible field dependence of the ESR line widths and assumed the same values in fields of 4.5 and 11 kG. This is justified only if the relevant correlation time $\tau\omega_s$ (11 kG) < 1 — that is, $\tau < 5 \times 10^{-12}$ sec.

2) The results of Ref. HM 66 were obtained in $Mn(ClO_4)_2$ solutions, whereas the muon relaxation studies were made in $MnCl_2$ solutions.

3) Although it was necessary to change V_r and τ_r^0 in order to fit the temperature dependence of a 3 M solution, we had to assume that τ_r remains relatively independent of concentration at 295°K in order to obtain the fit in Fig. 9.10a.

4) In view of the quality of the fit shown in Fig. 9.10a, τ_h has been assumed to be concentration-independent. This assumption needs further justification. In particular, a concentration-dependent activation energy for chemical exchange might reduce the value of V_r to less than 8.5 kcal/mole.

5) The whole analysis depends upon the basic assumption that $Mn(H_2O)_6^{2+}$ formation continues almost unchanged up to the strongest concentrations.

The testing of these assumptions in further muon-depolarization studies may contribute to our knowledge of the structure and dynamics of fluids. The experimental program in Mn^{2+} solutions should include measurements of relaxation times in longitudinal as well as transverse fields, as a function of varying field strength and temperature, and finally in solution with different anions.

X. CONCLUDING REMARKS

A. μSR—A "Trigger" Detection Technique for Magnetic Interactions

Studies of the precession and depolarization of positive muons and muonium in matter share many characteristics with the associated techniques of NMR and ESR. The important difference is that the more standard resonance techniques involve absorption of macroscopic amounts of power by macroscopic spin ensembles ($\gtrsim 10^{15}$ nuclei or $\gtrsim 10^{12}$ electrons), while as few as 10^6 muons imbedded in the medium can be used to passively detect coherent local fields (through the precession frequency) and random local fields (through the relaxation time). This is possible because the asymmetric decay so efficiently converts information about the muon polarization into an easily detectable external phenomenon (the positron direction). These special features are also shared by a variety of "trigger" detection techniques (AB 70) such as Mössbauer effect; perturbed angular correlations, PAC (SH 72); oriented nuclei; and others. The "coming of age" of such techniques is often marked by the adoption of a suggestive mnemonic acronym; in this context, the applications of muons outlined in this chapter might be referred to as "μSR" studies, where the acronym stands for Muon (or Muonium) Spin Relaxation, Rotation, Resonance, etc., and is intended to suggest the analogy with NMR and ESR.

While other "trigger" detection techniques have advantages similar to those of μSR (e.g., sensitivity), each has its own set of difficulties. Many, for instance, can only be used to study certain substances into which the probe nuclei can be incorporated; ion implantation can sometimes help in this regard, but generates new problems such as radiation damage. Furthermore, in NMR studies involving nuclei other than hydrogen isotopes, the electron core of the probe causes disturbing effects, such as core polarization, which mask or even change the local fields to be measured. Many nuclei also have

electric quadrupole moments, whose interactions complicate measurements of local magnetic fields and contact interactions. The muon, on the other hand, is a bare Dirac particle interacting only through its electric charge and magnetic moment. Thus its "feedback" effects upon local field properties are often small and calculable. The general problems of implanted ion techniques are shared to some extent by the μSR method: the μ^+ or Mu atom may not spontaneously occupy the position one wants to investigate; and radiation damage on a local scale (at the end of a given muon's range) may cause observable effects—although the small number of muons used ($\sim 10^6$) and their distribution throughout an extended bulk sample make cumulative radiation damage a negligible problem.

The μSR technique can be used to study relaxation phenomena over a rather broad range of time scales. In μ^+ precession studies it is possible to directly observe relaxation rates from $\sim 10^4$ to $\sim 10^8$ sec^{-1}, while the relaxation rates ν of the muonium electron can be observed or inferred (with varying degrees of difficulty) over a range from $\sim 10^6$ sec^{-1} ($\nu \ll \omega_o$) to $\sim 10^{14}$ sec^{-1} ($\nu \gg \omega_o$), and in principle even higher [see Eq. (5.13)]. In Fig. 10.1, a comparison (from Ref. WI 68) of time scales accessible to different techniques is supplemented by an indication of the range available with μSR methods. Obviously, the main shortcoming of the μSR technique is caused by the 2.2-μsec muon lifetime, which makes measurement of relaxation times longer than a few lifetimes progressively difficult. {It should be emphasized that this limitation is merely a problem of counting statistics, since the exponential decay in the experimental histogram [see Eq. (2.6)] can be exactly divided out.} In this aspect, NMR and ESR have a tremendous advantage. With NMR one can measure relaxation times on a scale of minutes.

B. The State of the Art

The use of μSR techniques in the study of "ordinary" matter has progressed to that tantalizing stage where its potential in many fields is becoming clear, but where each field of application still suffers from serious gaps of understanding or measurement. We have attempted to survey the current situation in many of these fields; we conclude with brief summaries of a few of them.

1. Muonium Chemistry

Recent advances in theory (IS 72, BG 73, FI 73) and experimental technique (BC 74) have opened up the field of muonium chemistry to extensive and productive study. In the liquid phase, spectacular and unpredicted differences between reaction rates of Mu and H have already been observed (BC 74); it is hoped that further study will generate a deeper understanding in terms of dynamic isotope effects. These studies have also revealed the important roles played by hot-atom reactions of muonium, as well as formation and subsequent reaction of radicals containing muonium, in the "fast" depolarization of positive muons in liquids. Two more fields of chemical research have thus become accessible to μSR techniques.

New techniques (KE 72) also make the study of Mu chemistry in gases a practical reality. In the gas phase, absolute rates of chemical reactions can be treated theoretically (GL 41, WO 72) with much more confidence than in liquids. This nearly untouched field may be expected to bloom with definitive experiments in the next few years.

2. Muons in Solids

The applications of μSR to solid state physics are growing at a nearly explosive rate. Muons have been fruitfully implanted in insulators, semiconductors, metals, and superconductors; in glasses, powders, and crystals; in diamagnetic, paramagnetic, and ferromagnetic media. In each case somewhat different

phenomena are accessible to study, and in each case a slightly different analysis technique must be applied. We have allowed ourselves a good deal of conjecture throughout the text regarding new directions in which solid-state μSR studies are likely to expand; but it is most likely that the next turn in this field will be just as unexpected as those which preceded it, and just as exciting.

ACKNOWLEDGMENTS

No review of such a wide-ranging field as μSR applications could be compiled without the generous assistance of experts in associated fields. We are deeply indebted to many solid-state physicists, in particular Charles Kittel, Alan Portis, and Carson Jeffries of the University of California at Berkeley, for stimulating discussions and helpful suggestions regarding μSR in solids. We are also grateful to David Walker of The University of British Columbia, Dr. M. Anbar of the Stanford Research Institute, Prof. F. S. Rowland of the University of California at Irvine, and several members of the Berkeley Chemistry Department for help with the chemical interpretation of μSR results in liquids. Our colleagues Donald Fleming (U. B. C.), Bruce Patterson (L. B. L.), Richard Johnson (L. B. L.) and Walter Fischer (S. I. N.) deserve special appreciation for their help with this chapter as well as their judicious critical comments. We are all grateful to Don Fleming for tolerating J. H. Brewer's preoccupation with this writing during the critical stages of preparation for a μSR program at TRIUMF, as well as to Dr. J. P. Blaser from SIN for making it possible for F. N. Gygax to extend his stay at LBL on a SIN grant. One of us (JHB) would like to give special thanks to his wife Suzanne for enduring several months of neglect during the writing of this review.

REFERENCES

AB 70 A. Abragam, The Principles of Nuclear Magnetism (Clarendon Press, Oxford, 1970).

AG 62 S. K. Allison and M. Garcia-Munoz, Atomic and Molecular Processes, D. R. Bates, Ed. (Academic Press, New York, 1962), Chap. 19.

AG 68 J. Alonso and L. Grodzins, in Hyperfine Structure and Nuclear Radiations, E. Matthias and D. A. Shirley, Eds. (North Holland, Amsterdam, 1968), p. 549.

AL 58 S. K. Allison, Rev. Mod. Phys. 30, 1137 (1958).

AM 69 D. G. Andrianov, G. G. Myasishcheva, Yu. V. Obukhov, V. S. Roganov, V. G. Firsov, and V. I. Fistul, Sov. Phys. JETP 29, 643 (1969).

AM 70 D. G. Andrianov, E. V. Minaichev, G. G. Myasishcheva, Yu. V. Obukhov, V. S. Roganov, G. I. Savel'ev, V. G. Firsov, and V. I. Fistul', Sov. Phys. JEPT 31, 1019 (1970).

AN 67 M. Anbar and P. Neta, Int. J. Appl. Rad. and Isotopes 18, 493 (1967).

AU 68 G. Aubert, J. Appl. Phys. 39, 504 (1968).

BB 59 R. A Bernheim, T. H. Brown, H. S. Gutowsky, and D. W. Woessner, J. Chem. Phys. 30, 950 (1959).

BB 66 A. I. Babaev, M. Ya. Balats, G. G. Myasishcheva, Yu. V. Obukhov, V. S. Roganov and V. G. Firsov, Sov. Phys. JETP 23, 583 (1966).

BC 63 H. V. Bradt and G. W. Clark, Phys. Rev. 132, 1306 (1963).

BC 71 J. H. Brewer, K. M. Crowe, R. F. Johnson, A. Schenck, and R. W. Williams, Phys. Rev. Lett. 27, 297 (1971).

BC 73 J. H. Brewer, K. M. Crowe, F. N. Gygax, R. F. Johnson, B. D. Patterson, D. G. Fleming, and A. Schenck, Phys. Rev. Lett. 31, 143 (1973).

BC 74 J. H. Brewer, K. M. Crowe, F. N. Gygax, R. F. Johnson, D. G. Fleming, and A. Schenck, Phys. Rev. A9, 495 (1974).

BE 71 S. W Benson, The Foundations of Chemical Kinetics (McGraw-Hill, New York, 1960); E. A. Moelwyn Hughes, The Chemical Statics and Kinetics of Solutions (Academic, New York, 1971).

BG 73 J. H. Brewer, F. N. Gygax, and D. G. Fleming, Phys. Rev. A 8, 77 (1973).

BM 61 N. Bloembergen and L. O. Morgan, J. Chem. Phys. 34, 842 (1961).

BN 72 L. J. Bartal, J. B. Nicholas and H. J. Ache, J. Phys. Chem. 76, 1124 (1972) and Radiochimica Acta 17, 205 (1972).

BO 72 T. Bowen et al., University of Arizona, private communication (1972).

CF 58 T. Coffin, R. C. Garwin, S. Penman, L. M. Lederman, and A. M. Sachs, Phys. Rev. 109, 973 (1958).

CH 70 J. Y. Choi, Metal Trans. 1, 911, (1970).

CH 72 K. M. Crowe, J. F. Hague, J. E. Rothberg, A. Schenck, D. L. Williams, R. W. Williams and K. K. Young, Phys. Rev. D 5, 2145 (1972).

CJ 72 K. M. Crowe, R. F. Johnson, J. H. Brewer, F. N. Gygax, D. G. Fleming, and A. Schenck, Bull. Am. Phys. Soc. 17, 594 (1972).

CL 64 G. Culligan, R. A. Lundy, V. L. Telegdi, R. Winston and D. D. Yovanovitch, in Report of Conference on High Energy Cyclotron Improvement, College of William and Mary, Williamsburg, VA (1964).

CW 66 F. A. Cotton and G. Wilkinson, Advanced Inorganic Chemistry (Interscience, New York, 1966).

EP 66 B. Eisenstein, R. Prepost, and A. M. Sachs, Phys. Rev. 142, 217 (1966).

FA 57 U. Fano, Rev. Mod. Phys. 29, 74 (1957).

FA 67 Farhataziz, J. Phys. Chem. 71, 598 (1967).

FB 65 V. G. Firsov and V. M. Byakov, Sov. Phys. JETP 20, 719 (1965).

FB 73 D. G. Fleming and J. H. Brewer, Bull. Am. Phys. Soc. 18, 1571 (1973).

FH 73 M. L. G. Foy, N. Heiman, W. J. Kossler, and C. E. Stronach, Phys. Rev. Lett. 30, 1064 (1973).

FI 73 W. E. Fischer, SIN-preprint (1973).

FM 57 G. W. Ford and C. J. Mullin, Phys. Rev. 108, 477 (1957).

FP 60 G. Feher, R. Prepost, and A. M. Sachs, Phys. Rev. Lett. 5, 515 (1960).

FR 58 J. Friedel, Nuovo Cimento 7 (Suppl.), 287 (1958).

FT 47 E. Fermi and E. Teller, Phys. Rev. 72, 399 (1947).

GF 71 V. I. Goldanskii and V. G. Firsov, Ann. Rev. Phys. Chem. 22, 209 (1971).

GI 69 I. I. Gurevich, I. G. Ivanter, L. A. Makariyna, E. A. Mel'eshko, B. A. Nikol'skii, V. S. Roganov, V. I. Selivanov, V. P. Smilga, B. V. Sokolov, V. D. Shestakov, and I. V. Takovleva, Phys. Lett. 29B, 387 (1969).

GI 71 I. I. Gurevich, I. G. Ivanter, E. A. Meleshko, B. A. Nikol'skii, V. S. Roganov, V. I. Selivanov, V. P. Smilga, B. V. Sokolov, and V. D. Shestakov, Sov. Phys. JETP 33, 253 (1971).

GL 41 S. Glasstone, K. J. Laider, and H. Eyring, The Theory of Rate Processes (McGraw-Hill, New York, 1941).

GM 66 B. B. Garrett and L. Morgan, J. Chem. Phys. 44, 890 (1966).

GM 68 I. I. Gurevich, L. A. Makar'ina, E. A. Meleshko, B. A. Nikol'skii, V. S. Roganov, V. I. Selivanov, and B. V. Sokolov, Sov. Phys. JETP 27, 235 (1968).

GM 71 I. I. Gurevich, E. A. Meleshko, I. A. Muratova, B. A. Nikol'skii, V. S. Roganov, V. I. Selivanov, and B. V. Sokolov, JETP Lett. 14, 297 (1971).

GM 72 I. I. Gurevich, E. A. Mel'eshko, I. A. Muratova, B. A. Nikol'skii, V. S. Roganov, V. I. Selivanov, and B. V. Sokolov, Phys. Lett. 40A, 143 (1972).

HE 70 See, e.g., K. H. Hellwege, Einführung in die Festkorperphysik II (Springer-Verlag, Berlin, 1970), Chap. 22.1.

HM 60 V. W Hughes, D. W. McColm, K. Ziock, and R. Prepost, Phys. Rev. Lett. 5, 63 (1960).

HM 63 D. P. Hutchinson, J. Menes, G. Shaprio, and A. M. Patlach, Phys. Rev. 131, 1351 (1963).

HM 66 C. C. Hinckley and L. O. Morgan, J. Chem. Phys. 44, 898 (1966).

HS 63 D. P. Hutchinson, J. Menes, and G. Shapiro, Phys. Rev. 131, 1362 (1963).

HU 63 J. P. Hunt, Metal Ions in Aqueous Solutions (Benjamin, New York, 1963), p. 86.

IM 72 I. G. Ivanter, E. V. Minaichev, G. G. Myasishcheva, Yu. V. Obukhov, V. S. Roganov, G. I. Savel'ev, V. P. Smilga, and V. G. Firsov, Sov. Phys. JETP 35, 9 (1972).

IS 68 I. G. Ivanter and V. P. Smilga, Sov. Phys. JETP 27, 301 (1968).

IS 69 I. G. Ivanter and V. P. Smilga, Sov. Phys. JETP 28, 796 (1969).

IS 71 I. G. Ivanter and V. P. Smilga, Sov. Phys. JETP, 33, 1070 (1971).

IV 69 I. G. Ivanter and V. P. Smilga, Sov. Phys. JETP 28, 286 (1969).

IV 73 I. G. Ivanter, Sov. Phys. JETP 36, 990 (1973).

KE 72 K. R. Kendall (thesis), University of Arizona, 1972.

KO 73 W. J. Kossler, private communication (1973).

LB 65 Landolt-Bornstein, in Numerical Data and Functional Relationships in Science and Technology, K. H. Hellwege, Ed., Group II: Atomic and Molecular Physics, Vol. I: Magnetic Properties of Free Radicals (Springer, New York, 1965).

LO 67 S. R. Logan, Trans. Faraday Soc. 63, 1713 (1967).

LR 68 E. S. Lewis and J. K. Robinson, J. Am. Chem. Soc. 90, 4337 (1968).

MA 66 A. A. Manenkov and R. Orbach, Eds. Spin-Lattice Relaxation in Ionic Solids (Harper and Row, New York, 1966).

MA 67 R. M. Mobley, J. J. Amato, V. W. Hughes, J. E. Rothberg, and P. A. Thompson, J. Chem. Phys. 47, 3074 (1967).

MB 52 H. S. W. Massey and E. H. S. Burhop, Electronic and Ionic Impact Phenomena (Clarendon Press, Oxford, 1952), Chap. VIII.

MB 66 R. M. Mobley, J. M. Bailey, W. E. Cleland, V. W. Hughes, and J. E. Rothberg, J. Chem. Phys. 44, 4354 (1966).

MH 70 B. D. Michael and J. Hart, J. Phys. Chem. 74, 2878 (1970).

MM 70 E. V. Minaichev, G. G. Myasishcheva, Yu. V. Obukhov, V. S. Roganov, G. I. Savel'ev, and V. G. Firsov, Sov. Phys. JETP 31, 849, (1970).

MO 66 H. A. Mook, Phys. Rev. 148, 495 (1966).

MO 67 R. M. Mobley (thesis), Yale University, 1967.

MO 68 G. G. Myasishcheva, Yu. V. Obukhov, V. S. Roganov, and V. G. Firsov, Sov. Phys. JETP 26, 298 (1968).

MO 69 G. G. Myasishcheva, Yu. V. Obukhov, V. S. Roganov, L. Ya. Suvorov and V. G. Firsov, High Energy Chemistry 3, 460 (1969).

MO 70 G. G. Myasishcheva, Yu. V. Obukhov, V. S. Roganov, and V. G. Firsov, High Energy Chemistry 4, 398 (1970).

MR 67 G. G. Myasishcheva, Yu. V. Obukhov, V. S. Roganov, and V. G. Firsov, High Energy Chemistry 1, 340 (1967).

MR 70 E. V. Minaichev, G. G. Myasishcheva, Yu. V. Obukhov, V. S. Roganov, G. I. Savel'ev, and V. G. Firsov, Sov. Phys. JETP 30, 230 (1970).

MS 67 G. G. Myasishcheva, Yu. V. Obukhov, V. S. Roganov, L. Ya. Suvorov, and V. G. Firsov, High Energy Chemistry 1, 343 (1967).

MY 67 G. G. Myasishcheva, Yu. V. Obukhov, V. S. Roganov, and V. G. Firsov, High Energy Chemistry 1, 337 (1967).

MY 69 G. G. Myasishcheva, Yu. V. Obukhov, V. S. Roganov, and V. G. Firsov, High Energy Chemistry 3, 463 (1969).

NA 67 A. Narath, in Hyperfine Interactions, A. J. Freeman and K. B. Frankel, Eds. (Academic Press, New York, 1967), p. 287.

NF 71 P. Neta, R. W. Fessenden, and R. H. Schuler, J. Phys. Chem. 75, 1654 (1971).

NS 65 G. Navon and G. Stein, J. Phys. Chem. 69, 1384 (1965).

NY 63 V. G. Nosov and I. V. Yakovleva, Sov. Phys. JETP 16, 1236 (1963); and Nucl. Phys. 68, 609 (1965).

NY 65 V. G. Nosov and I. V. Yakovleva, Nucl. Phys. 68, 609 (1965).

PA 48 G. E. Pake, J. Chem. Phys. 16, 327 (1948).

PC 74 B. D. Patterson, K. M. Crowe, F. N. Gygax, R. F. Johnson, A. M. Portis, and J. H. Brewer, Phys. Lett. 46A, 453 (1974).

PH 62 N. J. Poulis and W. P. A. Hass, Landolt-Bornstein, Zahlenwerte und Funktionen, Vol. II, Part 9, "Magnetic Properties I" (Springer-Verlag, Berlin, 1962).

RO 70 F. S. Rowland, Molecular Beams and Reaction Kinetics, C. Schlier, Ed. (Academic, New York, 1970) (Proceedings of the International School of Physics "Enrico Fermi," Course XLIV), p. 108.

SC 70 A. Schenck, Phys. Lett. 32A, 19 (1970) and unpublished results.

SC 71 A. Schenck and K. M. Crowe, Phys. Rev. Lett. 26, 57 (1971).

SH 72 D. A. Shirley and H. Haas, Ann. Rev. Phys. Chem. 23, 385 (1972).

SI 72 G. Sicking, International Meeting on Hydrogen in Metal, Jülich 1972, Vol. II, p.408 (1972).

SM 66 C. G. Shull and H. A. Mook, Phys. Rev. 16, 184 (1966).

SP 66 J. M. Spaeth, Z. Phys. 192, 107 (1966).

SR 68 D. A. Shirley, S. S. Rosenblum, and E. Matthias, Phys. Rev. 170, 363 (1968).

SS 71 H. C. Siegmann, S. Strassler, and P. Wachter, Proceedings of the Meeting on Muons in Solid State Physics (Burgenstock, Switzerland, 1971), 2. Teil, p. 91.

ST 68 J. P. Sweet and J. K. Thomas, J. Phys. Chem. 68, 1363 (1964); K. Takakura and B. Ranby, J. Phys. Chem. 72, 164 (1968).

ST 73 M. B. Stearns, private communication (1973).

SW 58 R. A. Swanson, Phys. Rev. 112, 580 (1958).

SW 67 M. C. Sauer and B. Ward, J. Phys. Chem. 71, 3971 (1967).

SW 72 A. Schenck, D. L. Williams, J. H. Brewer, K. M. Crowe, and R. F. Johnson, Chem. Phys. Lett. 12, 544 (1972).

TH 65 B. A. Thrush, Prog. React. Kin. 3, 65 (1965).

WB 53 R. K. Wangsness and F. Bloch, Phys. Rev. 89, 728 (1953).

WE 49 G. Wentzel, Phys. Rev. 75, 1810 (1949).

WF 26 P. Weiss and R. Forrer, Ann. Physik 5, 153 (1926).

WI 68 H. H. Wickman, in Hyperfine Structure and Nuclear Radiations, E. Matthias and D. A. Shirley, Eds. (North Holland, Amsterdam, 1968).

WK 73 J. Shy-Yih Wang and C. Kittel, Phys. Rev. B 7, 713 (1973).

WO 65 R. Wolfgang, Progr. Reaction Kinetics 3, 99 (1965).

WO 72 M. Wolfsberg, Accounts Chem. Res. 5, 225 (1972).

Table II.3 - Precession of positive muons and muonium atoms in pure substances in transverse magnetic fields.

Measured asymmetries and relaxation times are arranged loosely according to the type of medium in which the muons are stopped. In each case, the asymmetry is the product of the muon's residual polarization and the maximum effective asymmetry A_o, which is measured when no depolarization occurs in the target. The value of A_o is determined by various experimental characteristics, and generally varies by $\sim$ 20% from experiment to experiment. Care should therefore be taken in comparing asymmetries, especially when measured by different groups. Convenient "reference asymmetries" are carbon, various metals, and bromoform or carbon tetra chloride, in which very little depolarization occurs, or water at 300°K, in which the residual polarization is known to be 0.55±0.03. In some references, residual polarizations are quoted without specifying the experimental value of A_o. In these cases the data are listed as (polarization) A. When no relaxation time is given, or when the field strength is not specified, it is because the value was not mentioned in the reference. In the case of muonium precession at fields of more than 10G, two frequencies are observed. The asymmetry quoted here is the sum of the asymmetries in the two "beating" precession patterns. The final entry, labelled (M′), represents the asymmetry and relaxation time for "anomalous μ^+ precession" in silicon, thought to be shallow-donor muonium precession.

METALS AND SEMIMETALS

TARGET SUBSTANCE	TEMP(K)	FIELD(G)	ASYMMETRY	T2(MICROSEC)	REF
ALUMINUM	300	35	0,27 +/- 0,01	---	EP66
ALUMINUM	300	50	0,209 +/- 0,010	---	SW58
BERYLLIUM	300	50	0,222 +/- 0,012	---	SW58
CARBON (GRAPHITE)	300	50	0,229 +/- 0,008	---	SW58
CARBON (LAMPBLACK)	300	50	0,253 +/- 0,021	---	SW58
CARBON	300	800	0,219 +/- 0,008	---	GM68
CARBON	300	1300	0,225 +/- 0,004	---	GM68
CARBON	300	3500	0,203 +/- 0,008	---	GM68
COPPER	300			> 50.	GM72
COPPER	150			8.80 +/- 0.20	GM72
COPPER	77			4.60 +/- 0.30	GM72
LITHIUM	300	50	0,201 +/- 0,014	---	SW58
MAGNESIUM	300	50	0,254 +/- 0,013	---	SW58
MOLYBDENUM	300	50	0,086 +/- 0,009	---	BB66
IRON (POWDER,SPHERE)	300	50	0,015 +/- 0,003	> 20,	LBL
LEAD	300	350	0,020 +/- 0,006	> 20,	LBL
LEAD	5	350	< 0,01	---	LBL

SEMICONDUCTORS

TARGET SUBSTANCE	TEMP(K)	FIELD(G)	ASYMMETRY	T2(MICROSEC)	REF
SILICON	300	50	0,253 +/- 0,012	---	SW58
SI CRYSTAL (P DOPED)	300	35	0,082 +/- 0,020	---	EP66
SI CRYSTAL (B DOPED)	300	35	0,14 +/- 0,014	---	EP66
SI CRYSTAL (B DOPED)	300	100	0,094 +/- 0,002	> 20,	LBL
SI CRYSTAL (B DOPED)	77	50	0,012 +/- 0,002	> 20,	LBL
SI CRYSTAL (B DOPED)	77	100	0,046 +/- 0,005	10,26 +/- 5,11	LBL
SI CRYSTAL (B DOPED)	77	150	0,014 +/- 0,001	> 20,	LBL
GE CRYSTAL (P DOPED)	300	35	0,25 +/- 0,02	---	EP66
GE CRYSTAL(AS DOPED)	300	50	0,269 +/- 0,068	---	AM69
GE CRYSTAL (IMPURE)	300	50	0,172 +/- 0,012	7, +/- 2,	AM69
SI C	300	50	0,213 +/- 0,011	---	SW58

INSULATORS

TARGET SUBSTANCE	TEMP(K)	FIELD(G)	ASYMMETRY	T2(MICROSEC)	REF
CARBON (DIAMOND)	300	50	0,045 +/- 0,008	---	SW58
SULFUR	300	35	< 0,005	---	EP66
SULFUR	300	50	0,014 +/- 0,011	---	SW58
SULFUR	300	800	0,056 +/- 0,008	---	GM68
SULFUR	300	3500	0,048 +/- 0,009	---	GM68
SULFUR	300	4000	0,046 +/- 0,007	0,03 +/-0,005	GM68
QUARTZ	300	50	0,043 +/- 0,003	---	MR70
FUSED QUARTZ	300	50	0,038 +/- 0,006	---	SW58
FUSED QUARTZ	300	50	0,050 +/- 0,006	---	MO68
FUSED QUARTZ	300	100	0,037 +/- 0,003	> 20,	LBL
QUARTZ CRYSTAL	300	50	0,056 +/- 0,006	---	MO68
QUARTZ CRYSTAL	300	88	< 0,03	---	SW58
QUARTZ POWDER	300	50	0,110 +/- 0,005	---	MO68
AL2 O3	300	35	< 0,07	---	EP66
AL2 O3	300	50	0,022 +/- 0,009	---	SW58
AL2 O3	300	800	0,137 +/- 0,007	---	GM68
AL2 O3	300	3500	0,108 +/- 0,007	---	GM68
AL2 O3 POWDER	300	50	0,111 +/- 0,007	---	MO68
B2 O3 (FUSED)	300	50	0,127 +/- 0,006	---	MO68
LITHIUM HYDRIDE	300	50	0,166 +/- 0,011	5,3 +/- 1,0	MR70
LI H	300	11000	0,127 +/- 0,002	4,51 +/- 0,16	LBL
LITHIUM FLUORIDE	300	35	0,14 +/- 0,03	---	EP66
LI F	300	50	0,169 +/- 0,009	6,7 +/- 1,0	MR70
LI F	300	1000	0,191 +/- 0,004	5,30 +/- 0,33	LBL
LI F	300	11000	0,184 +/- 0,009	5,24 +/- 0,29	LBL
LI F	77	50	0,163 +/- 0,014	1,3 +/- 0,3	MR70
LI F (FUSED)	300	51	0,203 +/- 0,009	6,0 +/- 0,9	MO69
LI F CRYSTAL	300	50	0,148 +/- 0,008	4,6 +/- 0,8	MO69
LI F CRYSTAL	300	405	0,150 +/- 0,006	4,4 +/- 0,6	MO69
K CL CRYSTAL	300		< 0,017	---	MS67
SODIUM CHLORIDE	300	50	0,041 +/- 0,009	---	SW58
NA CL POWDER	300	800	0,035 +/- 0,007	---	GM68
NA CL POWDER	300	3500	0,023 +/- 0,007	---	GM68
NA CL (CRYSTALLINE)	300		< 0,073	---	MS67
NA CL CRYSTAL	300	2	0,099 +/- 0,014	> 15,	IM72
NA CL CRYSTAL	300	50	0,084 +/- 0,005	> 15,	IM72
MG O	300	35	0,12 +/- 0,03	---	EP66
MG O	300	50	0,079 +/- 0,012	---	SW58
MG F2	300	50	0,136 +/- 0,009	---	SW58
CU SO4 (ANHYDROUS)	300	4500	0,156 +/- 0,003	> 20,	LBL
CU SO4	300	11000	0,275 +/- 0,002	13,42 +/- 0,64	LBL
CU SO4*5(H2O)	300	4500	0,261 +/- 0,007	5,04 +/- 0,11	LBL
CU SO4*5(H2O)	300	11000	0,257 +/- 0,002	3,46 +/- 0,06	LBL
NA OH (SOLID)	300	11000	0,191 +/- 0,002	7,53 +/- 0,25	LBL
CA(OH)2 (SOLID)	300	11000	0,177 +/- 0,002	7,51 +/- 0,32	LBL
GYPSUM	300	1000	0,157 +/- 0,003	5,5 +/- 0,5	LBL
GYPSUM (AVG)	300	4500	0,166 +/- 0,002	4,0 +/- 0,6	LBL
GYPSUM	300	11000	0,167 +/- 0,002	5,30 +/- 0,14	LBL
K H2 PO4	300	4500	0,135 +/- 0,004	2,55 +/- 0,15	LBL
K H2 PO4	300	1000	0,122 +/- 0,002	17,65 +/- 2,19	LBL
GD (N O3)3 * 6(H2O)	300	11000		0.04 +/- 0.01	LBL
FE (N O3)3 * 6(H2O)	300	11000		0.04 +/- 0.01	LBL
FE CL2 * 4(H2O)	300	4500	0,159 +/- 0,003	2,88 +/- 0,08	LBL
FE CL3 * 6(H2O)	300	4500	0,224 +/- 0,003	1,99 +/- 0,04	LBL
FE F3	300	4500	0,007 +/- 0,002	4,67 +/- 1,02	LBL
FE BO3	300	1000	0,068 +/- 0,004	5,13 +/- 0,86	LBL
FE BO3	300	4500	0,010 +/- 0,006	1,14 +/- 1,02	LBL
FE BO3	423	4500	0,096 +/- 0,002	5,10 +/- 0,34	LBL
CR2 O3	300	1000	0,037 +/- 0,007	0,81 +/- 0,17	LBL
CR2 O3	310	4500	0,222 +/- 0,003	11,64 +/- 0,70	LBL
SILICONE DC-200	300	50	0,139 +/- 0,010	---	SW58

ASSORTED ELEMENTS AND INORGANIC COMPOUNDS

TARGET SUBSTANCE	TEMP(K)	FIELD(G)	ASYMMETRY	T2(MICROSEC)	REF
BORON	300	1000	0,274 +/- 0,005	3,02 +/- 0,10	LBL
BORON	300	11000	0,312 +/- 0,004	3,13 +/- 0,09	LBL
BORON CARBIDE (B4C)	300	50	0,23 +/- 0,02	6,5 ---	SW58
B4C	300	50	0,295 +/- 0,009	5,3 +/- 0,5	MR70
B4C	300	100	0,286 +/- 0,009	5,3 +/- 0,5	MR70
B4C	300	400	0,295 +/- 0,009	5,6 +/- 0,7	MR70
B4C	300	800	0,225 +/- 0,007	---	GM68
B4C	300	1000	0,286 +/- 0,02	4,5 +/- 0,6	LBL
B4C	300	3500	0,196 +/- 0,007	---	GM68
B4C	300	4500	0,264 +/- 0,003	3,94 +/- 0,10	LBL
B4C	373	11000	0,274 +/- 0,003	4,25 +/- 0,10	LBL
B4C	173	11000	0,266 +/- 0,005	3,13 +/- 0,11	LBL
B4C	77	50	0,286 +/- 0,009	3,6 +/- 0,4	MR70
PHOSPHORUS	300	50	0,025 +/- 0,017	---	SW58
RED PHOSPHORUS	300	35	0,019 +/- 0,038	---	EP66
RED PHOSPHORUS	300	800	0,022 +/- 0,008	---	GM68
BLACK PHOSPHORUS	300	35	0,19 +/- 0,04	---	EP66
LIQUID NITROGEN	77	50	0,037 +/- 0,006	---	MO68
LIQUID NITROGEN	77	50	0,028 +/- 0,002	> 20,	LBL
LIQUID NITROGEN	77	100	0,114 +/- 0,003	9,01 +/- 1,20	LBL
H2O (WATER)	300	50	0,146 +/- 0,003	---	BB66
H2O (WATER)	300	100	0,155 +/- 0,001	> 20,	LBL
H2O (WATER)	300	150	0,154 +/- 0,005	> 20,	LBL
H2O (WATER)	300	1000	0,160 +/- 0,002	> 20,	LBL
H2O (WATER)	300	3500	0,136 +/- 0,011	---	GM68
H2O (WATER)	300		0,176 +/- 0,005	---	MY67
H2O (WATER)	300	4400	0,147 +/- 0,001	> 20,	LBL
H2O (WATER)	300	4500	0,160 +/- 0,001	> 20,	LBL
H2O (WATER)	300	11000	0,165 +/- 0,001	> 20,	LBL
H2O (ICE)	261	11000	0,130 +/- 0,003	5,04 +/- 0,33	LBL
H2O (ICE)	195	3500	0,046 +/- 0,009	---	GI71
H2O (ICE)	77	50	0,066 +/- 0,004	---	MO68
H2O (ICE)	77	50	0,060 +/- 0,006	> 5,	MR70
H2O (ICE)	77		0,066 +/- 0,004	---	MY67
D2O (HEAVY WATER)	300	100	0,139 +/- 0,004	> 20,	LBL
CO2 (DRY ICE)	195	50	0,038 +/- 0,013	---	MO68
CO2 (DRY ICE)	77	100	0,051 +/- 0,001	> 20,	LBL
CO2 (DRY ICE)	195	800	0,058 +/- 0,009	---	GM68
CO2 (DRY ICE)	195	3500	0,046 +/- 0,009	---	GM68
FE2 (SO4)3	300	4500	0,253 +/- 0,003	4,47 +/- 0,13	LBL
CS I	300	50	0,031 +/- 0,013	---	SW58
SILVER NITRATE	300	4500	0,237 +/- 0,003	> 20,	LBL
TITANIUM HYDRIDE	300	100	0,316 +/- 0,006	5,09 +/- 0,26	LBL
NICKEL OXIDE POWDER	300	4500	0,004 +/- 0,001	> 20,	LBL

SATURATED ORGANIC COMPOUNDS

TARGET SUBSTANCE	TEMP(K)	FIELD(G)	ASYMMETRY	T2(MICROSEC)	REF
CARBON TETRACHLORIDE	300	50	0,237 +/- 0,012	---	BB66
CARBON TETRACHLORIDE	300	100	0,271 +/- 0,001	> 20,	LBL
BROMOFORM	300	50	0,223 +/- 0,008	---	BB66
BROMOFORM	300	271	0,219 +/- 0,009	---	BB66
BROMOFORM	300		0,280 +/- 0,006	---	MY67
BROMOFORM	300		0,286 +/- 0,004	---	MY69
CHLOROFORM	300	50	0,184 +/- 0,015	---	SW58
CHLOROFORM	300	50	0,190 +/- 0,009	---	BB66
CHLOROFORM	300	100	0,229 +/- 0,010	> 20,	LBL
C H2 I2	300	50	0,227 +/- 0,009	---	BB66
CH2 CL2	300	100	0,176 +/- 0,003	> 20,	LBL
CH3NO2(NITROMETHANE)	300	100	0,144 +/- 0,002	> 20,	LBL
METHANOL	300	50	0,137 +/- 0,009	---	BB66
METHANOL	300	50	(0,60 +/- 0,02)A	---	GM71
METHANOL	300	50	0,133 +/- 0,002	> 20,	LBL
METHANOL	300	90	(0,61 +/- 0,03)A	---	GM71
METHANOL	300	100	0,140 +/- 0,002	> 20,	LBL
METHANOL	300	1000	0,136 +/- 0,001	> 20,	LBL
METHANOL	300	3400	(0,62 +/- 0,05)A	---	GM71
METHANOL	300	4500	0,140 +/- 0,003	> 20,	LBL
METHANOL (LIQUID)	175	50	0,203 +/- 0,006	> 20,	MR70
METHANOL (SOLID)	77	50	0,154 +/- 0,009	4,5 +/- 1,4	MR70
CH3CH2OH (ETHANOL)	300	100	0,148 +/- 0,002	> 20,	LBL
N-PROPYL ALCOHOL	300	100	0,151 +/- 0,001	> 20,	LBL
C2 H4 CL2	300	50	0,152 +/- 0,010	---	BB66
CH3 CH2 OH	300	100	0,149 +/- 0,003	> 20,	LBL
C2 H5 O C2 H5(LIQ)	157	50	0,180 +/- 0,009	> 20,	MR70
C2 H5 O C2 H5(SOLID)	77	50	0,111 +/- 0,011	6,7 +/- 3,3	MR70
LIQUID PROPANE	193	50	0,170 +/- 0,020	---	SW58
GLYCEROL (C3H8O3)	300	100	0,179 +/- 0,003	> 20,	LBL
HEXANE	300	50	(0,62 +/- 0,03)A	---	GM71
HEXANE	300	100	(0,57 +/- 0,06)A	---	GM71
MIXED HEXANES	300	100	0,146 +/- 0,002	> 20,	LBL
HEXANE	300	3400	(0,67 +/- 0,08)A	---	GM71
HEXANE	300	11000	0,170 +/- 0,001	> 20,	LBL
HEXENE	300	100	0,119 +/- 0,001	> 20,	LBL
2-HEXENE	300	11000	0,140 +/- 0,001	> 20,	LBL
HEXYNE (C6H10)	300	100	0,103 +/- 0,002	> 20,	LBL
1-HEXYNE	300	11000	0,119 +/- 0,001	> 20,	LBL
HEPTANE	300	50	(0,57 +/- 0,06)A	---	GM71
OCTANE	300	7	0,142 +/- 0,054	---	BB66
OCTANE	300	50	0,147 +/- 0,008	---	BB66
CYCLOHEXANE	300	100	0,160 +/- 0,004	> 20,	LBL
CYCLOHEXANE	300		0,196 +/- 0,007	---	MR67
CYCLOHEXANE	77		0,080 +/- 0,005	---	MY67
CYCLOHEXANE	300		0,20 +/- 0,005	---	MY69
C6 H11 F	300		0,197 +/- 0,005	---	MY69
C6 H11 CL	300		0,203 +/- 0,005	---	MY69
C6 H11 BR	300		0,248 +/- 0,005	---	MY69
C6 H11 I	300		0,275 +/- 0,005	---	MY69
CYCLOHEXANOL(C6H11OH)	300		0,200 +/- 0,004	---	MY69
CYCLOHEXANONE(C6H10O)	300		0,181 +/- 0,004	---	MY69

UNSATURATED ORGANIC COMPOUNDS

TARGET SUBSTANCE	TEMP(K)	FIELD(G)	ASYMMETRY	T2(MICROSEC)	REF
CARBON DISULFIDE	300	50	0,029 +/- 0,003	> 20,	LBL
BENZENE	300	50	0,046 +/- 0,012	---	SW58
BENZENE	300	50	0,036 +/- 0,006	---	BB66
CYCLOHEXANE	300	50	0,160 +/- 0,009	---	BB66
CYCLOHEXANE	300		0,197 +/- 0,006	---	MY67
BENZENE	300	50	0,036 +/- 0,002	> 20,	LBL
BENZENE	300	100	0,042 +/- 0,001	> 20,	LBL
BENZENE	300	200	0,038 +/- 0,001	> 20,	LBL
BENZENE	300	271	0,034 +/- 0,007	---	BB66
BENZENE	300		0,052 +/- 0,005	---	MY69
BENZENE (LIQUID)	300	100	0,033 +/- 0,003	> 20,	LBL
BENZENE (SOLID)	77	100	0,018 +/- 0,002	> 20,	LBL
C6 H5 F	300		0,074 +/- 0,007	---	MR67
C6 H5 CL	300	50	0,063 +/- 0,007	---	BB66
C6 H5 CL	300		0,098 +/- 0,007	---	MR67
C6 H5 BR	300	50	0,106 +/- 0,010	---	BB66
C6 H5 BR	300		0,142 +/- 0,007	---	MR67
C6 H5 I	300		0,164 +/- 0,007	---	MR67
C6H5 CH2 CL	300		0,118 +/- 0,005	---	MY69
C6H5 CH CL2	300		0,158 +/- 0,005	---	MY69
C6H5 C CL3	300		0,193 +/- 0,005	---	MY69
C6H5CH3 (TOLUENE)	300	50	0,052 +/- 0,003	> 20,	LBL
C6H5CH3 (TOLUENE)	300	100	0,052 +/- 0,001	> 20,	LBL
TOLUENE (C6H5CH3)	300		0,076 +/- 0,005	---	MY69
C6H5OH (PHENOL)	300	50	0,089 +/- 0,006	> 20,	LBL
C6H5OH (PHENOL)	300	100	0,089 +/- 0,001	> 20,	LBL
C6H5NH2 (ANILINE)	300	50	0,088 +/- 0,004	> 20,	LBL
C6H5NH2 (ANILINE)	300	100	0,084 +/- 0,002	> 20,	LBL
C6H5NO2(NITROBENZENE)	300	50	0,090 +/- 0,001	> 20,	LBL
C6H5NO2(NITROBENZENE)	300	100	0,082 +/- 0,001	> 20,	LBL
C6 H5 C2 H5	300		0,090 +/- 0,005	---	MY69
C6 H5 C4 H9	300		0,115 +/- 0,005	---	MY69
C6H5CH(C2H5)C3H7	300		0,112 +/- 0,005	---	MY69
XYLENE/C6H4(CH3)2	300		0,082 +/- 0,007	---	MY69
C6H3(CH3)3	300		0,090 +/- 0,005	---	MY69
DUROL/C6H2(CH3)4	300		0,087 +/- 0,006	---	MY69
C6 (CH3)6	300		0,13 (APPROX)	---	MY69
C6 H10	300	50	0,113 +/- 0,009	---	BB66
C6 H10	300	271	0,116 +/- 0,008	---	BB66
CYCLOHEXENE (C6H10)	300		0,16 +/- 0,005	---	MY69
1-4 CYCLOHEXADIENE	300		0,135 +/- 0,005	---	MY69
1-3 CYCLOHEXADIENE	300		0,105 +/- 0,005	---	MY69
TOLAN(C6H5C=CC6H5)	300	267	0,031 +/- 0,013	---	BB66
ANTHRACENE(C14H10)	300	267	0,025 +/- 0,011	---	BB66
PHENYLCYCLOHEXANE	300	50	0,084 +/- 0,011	---	SW58
POLYETHYLENE	300	50	0,146 +/- 0,012	---	SW58
POLYSTYRENE	300	50	0,070 +/- 0,010	---	SW58
POLYSTYRENE	300	50	0,044 +/- 0,007	---	BB66
POLYSTYRENE	300	271	0,034 +/- 0,007	---	BB66
PLEXIGLAS	300	50	0,093 +/- 0,011	---	BB66
NUCLEAR EMULSION	300	50	0,087 +/- 0,009	---	SW58
NUCLEAR EMULSION	300	800	0,080 +/- 0,010	---	GM68
NUCLEAR EMULSION	300	1700	0,092 +/- 0,010	---	GM68
NUCLEAR EMULSION	300	3500	0,097 +/- 0,012	---	GM68
NUCLEAR EMULSION	300	4000	0,082 +/- 0,009	---	GM68
TEFLON	300	1300	0,175 +/- 0,015	---	GM68
TEFLON	300	4000	0,174 +/- 0,013	---	GM68
GELATIN	300	800	0,156 +/- 0,011	---	GM68
GELATIN	300	3500	0,139 +/- 0,011	---	GM68
SCINTILLATOR	300	800	0,056 +/- 0,009	---	GM68
SCINTILLATOR	300	3500	0,049 +/- 0,009	---	GM68
POLYETHYLENE	300	800	0,179 +/- 0,009	---	GM68
POLYETHYLENE	300	3500	0,153 +/- 0,009	---	GM68
DPPH	300	4500	0,149 +/- 0,03	7,7 +/- 2,0	LBL
DPPH	310	4500	0,151 +/- 0,004	10,19 +/- 1,29	LBL

MUONIUM SIGNALS IN INERT MATERIALS

TARGET SUBSTANCE	TEMP(K)	FIELD(G)	ASYMMETRY	T2(MICROSEC)	REF
ARGON (40 ATM)	300	2,0 (MU)	0,04 +/- 0,005	5, +/- 4,	MO67
NITROGEN (40 ATM)	300	2,0 (MU)	< 0,01	---	MO67
S F6 (40 ATM)	300	2,0 (MU)	< 0,01	---	MO67
LIQUID NITROGEN	77	7,2 (MU)	< 0,03	---	MO68
FUSED QUARTZ	1800	0,5 (MU)	0,039 +/- 0,011	5,1 +/- 0,8	BO72
FUSED QUARTZ	300	0,5 (MU)	0,040 +/- 0,008	6,2 +/- 1,1	BO72
FUSED QUARTZ	300	7,2 (MU)	0,161 +/- 0,012	1,3 +/- 0,2	MO68
FUSED QUARTZ	77	7,2 (MU)	0,148 +/- 0,014	0,5 +/- 0,1	MO68
FUSED QUARTZ	300	10,0 (MU)	0,104 +/- 0,008	---	GM68
FUSED QUARTZ	300	50,0 (MU)	0,046 +/- 0,030	> 1,	LBL
FUSED QUARTZ	300	95,0 (MU)	0,097 +/- 0,005	1,5 (APPROX)	GI71
FUSED QUARTZ	300	100,0 (MU)	0,072 +/- 0,005	3,0 (APPROX)	LBL
FUSED QUARTZ	300	150,0 (MU)	0,122 +/- 0,05	> 0,5	LBL
QUARTZ CRYSTAL	300	7,2 (MU)	0,167 +/- 0,013	0,4 +/- 0,1	MO68
QUARTZ POWDER	300	7,2 (MU)	< 0,04	---	MO68
CO2 (DRY ICE)	195	7,2 (MU)	0,070 +/- 0,015	0,4 +/- 0,1	MO68
CO2 (DRY ICE)	77	7,2 (MU)	0,075 +/- 0,015	0,6 +/- 0,1	MO68
H20 (ICE)	77	7,2 (MU)	0,16 (APPROX)	0,08 (APPROX)	MO68
AL2 03 POWDER	300	7,2 (MU)	< 0,09	---	MO68
SI CRYSTAL (B DOPED)	77	50,0 (MU)	0,053 +/- 0,010	0,45 +/- 0,10	LBL
SI CRYSTAL (B DOPED)	77	100,0 (MU)	0,042 +/- 0,005	0,315+/- 0,05	LBL
SI XTAL(HI B DOPING)	77	150,0 (MU)	0,022 +/- 0,010	1,09 +/- 0,52	LBL
GE CRYSTAL	77	7,0 (MU)	0,123 +/- 0,026	0,16 +/- 0,07	AM69
GE CRYSTAL	77	98,0 (MU)	0,082 +/- 0,012	0,1 (APPROX)	GI71
NA CL (CRYSTALLINE)	300	(MU)	< 0,023	---	MS67
LI F (FUSED)	300	7,2 (MU)	< 0,021	---	MO69
K CL CRYSTAL	300	(MU)	< 0,013	---	MS67
BENZENE	300	2,7 (MU)	< 0,011	---	BB66
BENZENE (SOLID)	77	7,2 (MU)	< 0,05	---	MO68
FUSED B203	300	7,2 (MU)	< 0,05	---	MO68
FUSED B203	77	7,2 (MU)	< 0,04	---	MO68
POLYETHYLENE	77	7,2 (MU)	< 0,03	---	MO68
PARAFFIN	77	7,2 (MU)	< 0,03	---	MO68
SILICON XTAL /P1	77	100,0 (M')	0,046 +/- 0,005	0,765+/- 0,25	LBL

(FOR HIGH FIELD MU SIGNALS, SUM OF AMPLITUDES IN 2 FREQUENCIES)

Ref. "LBL" corresponds to published or unpublished results of the Lawrence Berkeley Laboratory group.

Table VI. 1 – Parameters of the Theory

$[X]$ = concentration of reagent "X"

$[S]$ = concentration of pure solvent "S" (density/molecular weight)

h = fraction of muonium reacting epithermally to form a Diamagnetic Compound (D)

r = fraction of muonium reacting epithermally to form a Radical (R)

k_{mxd} = chemical rate constant for the reaction $Mu + X \rightarrow D$

k_{msd} = chemical rate constant for the reaction $Mu + S \rightarrow D$

k_{mxr} = chemical rate constant for the reaction $Mu + X \rightarrow R$

k_{msr} = chemical rate constant for the reaction $Mu + S \rightarrow R$

k_{rxd} = chemical rate constant for the reaction $R + X \rightarrow D$

k_{rsd} = chemical rate constant for the reaction $R + S \rightarrow D$

In each case, the rate (in sec^{-1}) at which reaction "i" occurs is given by $\Lambda_i = k_i[Z]$, where "Z" is either "X" or "S", whichever is the appropriate reactant.

The "lifetime" with respect to reaction "i" is given by $\tau_i = 1/\Lambda_i$. The following "lifetimes" are then defined:

$\tau_{md} = [1/\tau_{mxd} + 1/\tau_{msd}]^{-1}$

$\tau_{mr} = [1/\tau_{mxr} + 1/\tau_{msr}]^{-1}$

$\tau_{rd} = [1/\tau_{rxd} + 1/\tau_{rsd}]^{-1}$ = "chemical lifetime" of the radical

$\tau_m = [1/\tau_{md} + 1/\tau_{mr}]^{-1}$ = "chemical lifetime" of the muonium

ν_m = rate of depolarization of muonium electron (sec^{-1})

ν_r = rate of depolarization of unpaired electron in the radical (sec^{-1})

ω_r/ω_o = ratio of hyperfine frequencies in radical and muonium.

TABLE VII. 1 — Comparison of Mu and H reaction rates in gases at 300°K.[a]

A. Two-body collision cross sections

Reaction	Cross Section (10^{-16} cm^2)	
	Muonium	Hydrogen
(Mu, H) + O_2 spin exchange	~1	21 ± 2.1[b]
(Mu, H) + NO spin exchange	$2.4^{+5.1}_{-2.0}$	25 ± 2.5[b]
(Mu, H) + H_2 → (MuH, H_2) + H	< 0.01	~10^{-5}[d]
(Mu, H) + NO_2 → (MuO, HO) + NO	> 23	1.8 ± 0.2[c]
(Mu, H) + C_2H_4 → (C_2H_4Mu*, C_2H_5*)	0.27 ± 0.06	~0.02

B. Three-body third-order rate constants

Reaction	κ (10^{10} liters^2/mole^2-sec)	
	Muonium	Hydrogen
(Mu, H) + O_2 + Ar → (MuO_2, HO_2) + Ar	15.3 ± 3.5	1.1
(Mu, H) + NO + Ar → (MuNO, HNO) + Ar	$6.8^{+6.5}_{-2.4}$	0.9

[a] H atom cross sections and rate constants taken or derived from the review by Thrush Ref. TH 65, unless otherwise specified.

[b] H. C. Berg, Phys. Rev. 137, A1621 (1965).

[c] L. F. Phillips and H. I. Schiff, J. Chem. Phys. 37, 1233 (1962).

[d] I. Shavitt, J. Chem. Phys. 31, 1359 (1959).

TABLE VII. 2 — Asymmetry normalization and comparison of fit quality with and without radicals.

Solvent	Reagent	Field (gauss)	A_o	χ^2/degree of freedom No radicals	With radicals
CH_3OH	I_2	103	0.25 ± 0.01	0.8	0.4
		1000	0.27 ± 0.01	1.1	Same
		4500	0.27 ± 0.01	0.6	Same
C_6H_6	Br_2	200	0.271 ± 0.005	27	2.3
	I_2	200	0.272 ± 0.03	11	0.4
H_2O	H_2O_2	100	0.26 ± 0.01	7.4	0.8
	HNO_3	100	0.277 ± 0.01	11	1.0
		4500	0.30 ± 0.01	1.9	Same
	$FeCl_3$	4500	0.31 ± 0.01	0.6	Same
	$Fe(ClO_4)_3$	100	0.29 ± 0.03	8.3	0.6
		4400	0.30 ± 0.02	0.6	Same
	$Fe(NO_3)_3$	11000	0.35 ± 0.02	7.7	Same

TABLE VII.3-Results of best fits. Errors are approximate.

Solvent	Reagent	Field (gauss)	Radical	$\frac{\omega_r}{\omega_0}$	h	Rate constants (liter/mole sec) $\times 10^{-10}$ k_{mxd}	(Z)	k_{mzr}	k_{rxd}
CH_3OH	I_2	103	None	-	0.54 ±0.02	13.4±2	-	-	-
		1000	None	-	0.51 ±0.02	13±3	-	-	-
		4500	None	-	0.53 ±0.02	13.4±2	-	-	-
C_6H_6	Br_2	200	$C_6H_6Mu^\cdot$	0.095	0.134±0.01	9.4±0.3	S	0.125±0.05	0.36±0.1
	I_2	200	$C_6H_6Mu^\cdot$	0.095	0.133±0.07	5.7±1	S	0.054±0.03	0.2 ±0.1
H_2O	H_2O_2	100	$MuO^\cdot$	0.083	0.59 ±0.01	0.24±0.05	X	0.85 ±0.1	0.14±0.02
	HNO_3	100	?	0.125±0.05	0.545±0.01	3±1	X	10±5	0.1 ±0.01
	$Fe(ClO_4)_3$	100	?	$0.010^{+0.040}_{-0.005}$	0.52 ±0.03	$0.57^{+0.8}_{-0.4}$	X	3.8 ±0.8	0.02±0.002
	$FeCl_3$	4500	None(?)	-	0.51 ±0.02	2.1 ±0.2	-	-	-

TABLE VII. 4 — Comparison of overall rate constants of H and Mu with various reagents. Rate constants are in units of liters/mole-sec. Source of values for H is Anbar and Neta (AN 67) except where otherwise specified.

Reagent	Hydrogen		Muonium		$\frac{k_{Mu}}{k_H}$
	Solvent	k_H	Solvent	k_{Mu}	(approx.)
CH_3OH	H_2O	$(1.6\pm0.1)\times10^6$	CH_3OH	$< 10^7$	-
C_6H_6	H_2O	$(7 \pm 3) \times 10^8$ [a]	C_6H_6	$(8^{+5}_{-3})\times10^8$	1
H_2O	H_2O	Nil	H_2O	$< 10^7$	-
I_2	H_2O	4×10^{10}	CH_3OH	$(13.3 \pm 1) \times 10^{10}$	3
			C_6H_6	$(5.7 \pm 1) \times 10^{10}$	1
Br_2	H_2O	$(12\pm6) \times 10^{10}$ [b]	C_6H_6	$(9.4\pm0.3) \times 10^{10}$	1
H_2O_2	H_2O	$(9\pm5) \times 10^7$ [c]	H_2O	$(1.09\pm0.15)\times10^{10}$	100
NO_3^-	H_2O	$(9\pm5) \times 10^6$ [d]	H_2O	$(13\pm6) \times 10^{10}$	10^4
ClO_4^-	H_2O	Nil	H_2O	$\sim 4\times10^{10}$	?

[a] Sauer and Ward (SW 67) and Michael and Hart (MH 70).

[b] Farhataziz (FA 67).

[c] Sweet and Thomas (ST 68).

[d] Navon and Stein (NS 65).

Table VIII.1-Formulas for relaxation times of paramagnetic impurity spins in ionic crystals due to phonon process (B = magnetic field strength; T = temperature).

Process	Relaxation rate
Direct process: one-phonon exchange	$\frac{1}{T_1} \approx C B^4 T$
Raman process: two-phonon exchange	$\frac{1}{T_1} \approx D_1 T^9 + D_2 B^2 T^2$
Orbach process	$\frac{1}{T_1} \approx E \exp\left(-\frac{\Delta_c}{kT}\right)$

Table VIII.2. Residual polarization of positive muons stopped in samples of silicon at various dopings and temperatures and in other targets, from (EP 66). Measurements were made using a gated scaling technique in transverse field. Except where indicated, data were taken with the samples in a cryostat; corrections have been made only for muons stopping in the walls of the empty cryostat. Residual polarization is expressed relative to aluminum, in which a muon decay asymmetry of $A_0 = 0.27 \pm 0.01$ was measured.

Sample	Resistivity (Ω cm)	Phosphorus donors per cm³	Boron acceptors per cm³	Residual polarization 300°K	77°K	4.2–10°K
Silicon:						
No. 4	0.05		4×10^{18}	0.90±0.01	0.67±0.08	0.45±0.01
No. 14	3000		3×10^{12}	0.52±0.05	0.24±0.03	0.24±0.08
No. 10	350	4×10^{12}		0.45±0.08	0.15±0.04	0.19±0.05
No. 11	50	4×10^{13}		0.07±0.03	0.10±0.03	0.15±0.03
No. 13	0.3	2×10^{16}		0.09±0.03	0.12±0.03	0.16±0.04
No. 15	0.03	3×10^{17}		0.10±0.05		
No. 16	0.01	1.5×10^{18}		1.00±0.15		
No. 5	0.003	1.5×10^{19}		1.07±0.10	0.92±0.09	0.89±0.10
Germanium		10^{15}		0.92±0.08	0.23±0.07	0.18±0.07
Alumina				0.24±0.16	0.24±0.16	0.12±0.10
Sulfur				0.14±0.01 0.00±0.02[a]	0.22±0.01	0.20±0.02
LiF				0.52±0.12[a]		
MgO				0.44±0.12[a]		
Red P				0.07±0.14[a]		
Black P				0.72±0.16[a]		

[a] Indicates measurement outside cryostat, other measurements made with sample in cryostat.

Table IX.1 – Comparison between relaxation measurements and calculations for different orientations of the gypsum crystal. The crystal axes are given in the Onorato convention: (100) $=\hat{x}$, (010) $=\hat{y}$, and $\hat{z} \perp (\hat{x},\hat{y})$. The measured T_2^* are independent of magnetic field strength.

Position	Crystal orientation	Muon - NMR spectrum [scale = gauss]	Calculated T_2^* from NMR spectrum	Measured T_2^* (μsec)
1	$\vec{B}, \hat{z} = 90°$ $\vec{B}, \hat{x} = 94°$ $\vec{B}, \hat{y} = 57.5°$	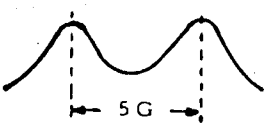	5.6	5.50 ±.50
2	$\vec{B}, \hat{z} = 90°$ $\vec{B}, \hat{x} = 146°$ $\vec{B}, \hat{y} = 62.5°$	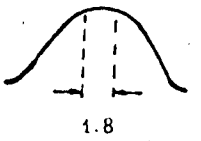	9.0	10.45 1.00
3	$\vec{B}, \hat{z} = 90°$ $\vec{B}, \hat{x} = 176°$ $\vec{B}, \hat{y} = 32.5°$		10.50	10.50 1.00
4	$\vec{B}, \hat{z} = 0$ $\vec{B}, \hat{x} = 90°$ $\vec{B}, \hat{y} = 90°$	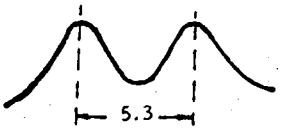	5.3	4.80 ±.30
5	$\vec{B}, \hat{z} = 40°$ $\vec{B}, \hat{x} = 142°$ $\vec{B}, \hat{y} = 111°$	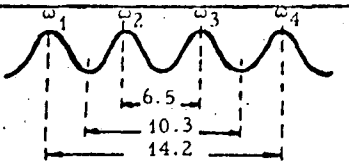	2.9	3.09 ±.20
6	$\vec{B}, \hat{z} = 24°$ $\vec{B}, \hat{x} = 90°$ $\vec{B}, \hat{y} = 66°$	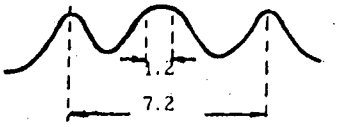	5.60	5.50 ±.40
Polycrystal, powder			5.3	5.30 ±.20
Polycrystal, anhydrous			---	60. ±20.

FIGURE CAPTIONS

Fig. 2.1. μ^+-decay spectrum: isotropic contribution for the energy spectrum of the decay positron, C (upper curve), and energy dependence of the asymmetry factor D, assuming $\xi = 1$ (lower curve).

Fig. 2.2. Angular relations between detector axis, spin orientation of the stopped μ^+, and a coplanar positron emission direction.

Fig. 2.3. Typical experimental setup. Top and side views of stopping target, counter arrangement, and magnet coils for transverse field. Not to scale.

Fig. 2.4. A typical experimental histogram for muon precession in a transverse magnetic field. The target is carbon tetrachloride at 100 G; the data is binned into 10-μsec bins. The mean muon lifetime, $\tau_\mu = 2.20$ μsec, is indicated.

Fig. 3.1. Flow diagram showing the processes involved for positive muons slowing down and thermalizing in matter.

Fig. 3.2. Evidence that protons approach the end of their range as H atoms. The critical velocity is $\alpha c = 2.2 \times 10^6$ m/sec. (From Ref. CH 72.)

Fig. 4.1. Energy eigenstates of $\ell = 0$ muonium in an external magnetic field, as a function of the dimensionless "specific field"

$$x = 2\omega_+/\omega_o = (g_e\mu_o^e - g_\mu\mu_o^\mu)\,|\vec{B}|\;/\;(\hbar\omega_o).$$

For graphical clarity, an unphysical value of $|\mu_o^e/\mu_o^\mu|$ is used to generate the plot. The four allowed transitions ($\Delta m = \pm 1$) are indicated.

Fig. 4.2. Evolution of muon polarization in free muonium in 100-G transverse field. P_x^μ = projection of μ^+ polarization along original polarization direction.

Fig. 5.1. "Two-frequency precession" of the muon (a) in fused quartz with a transverse field of 95 G (upper graph) and (b) in germanium at 98 G (lower graph). The smooth curves represent the best fits of the theoretical

dependence to the data. The theoretical function N(t) and the data are corrected for the decay exponential $\exp(-t/\theta_\mu)$. (From Ref. GI 71.)

Fig. 6.1. Proper muonium mechanism in 100-G transverse field: dependence of magnitude and phase of residual polarization upon chemical lifetime τ of free muonium. Positive phase is defined as being in the direction of μ^+ precession. Dashed curves: no hot chemistry; solid curves: hot fraction $h = 0.5$.

Fig. 6.2. Proper muonium mechanism in several transverse fields: dependence of $P_{\perp\,res}$ upon reagent concentration $[X]$ when $\tau_m^{-1} = k[X]$ with $k = 10^{10}$ liters/mole-sec; hot fraction $h = 0.5$. Solid curves; $B = 100$ G; dotted curves: $B = 10$ G; dashed curves: $B = B_o = 1593$ G.

Fig. 6.3. Flow chart model of depolarization mechanism in liquids.

Fig. 6.4. Various mechanisms in 100-G transverse field. Effect of radicals on $P_{\perp\,res}$ ($[X]$). Hot fraction $h = 0.5$, $\omega_r = 0.1\,\omega_o$, $r = \nu_m = \nu_r = 0$, and $k_{mxd} = k_{rxd} = 10^{10}$ liters/mole-sec in each case. Solid curves: proper muonium mechanism (no radical formation); dotted curves: $[S]\,k_{msr} = 10^{11}$ sec^{-1}; dashed curves: $k_{mxr} = 10^{11}$ liters/mole-sec.

Fig. 7.1. Time-dependent variation (in %) of the ratio of the positron detection rate to the muon decay probability in a transverse field set up for different runs. The soild curves are fits to the data. (From Ref. MO 67.)

Fig. 7.2. Observed values of λ/n [$\propto$ k (liters/mole-sec)] versus magnetic field for NO, O_2, C_2H_4, and NO_2 in units of 10^{-16} (μsec molecules/cm^3)$^{-1}$. The solid curves for NO and O_2 are fits of Eq. (7.6) to the data. (From Ref. MO 67.)

Fig. 7.3. Residual muon polarization in methanol as a function of the concentration of dissolved iodine. Best fit to the data for the proper muonium mechanism.

Fig. 7.4. Residual muon polarization in benzene as a function of the concentration of dissolved bromine. Uncertainties of $|P_{\perp\,res}|$ data are less than the dimensions of the points. Dashed curves: best fit without radicals; solid curve: best fit with radicals.

Fig. 7.5. Residual muon polarization in water as a function of the concentration of dissolved hydrogen peroxide. Dashed curve: best fit without radicals; solid curve: best fit with radicals.

Fig. 7.6. Residual muon polarization in water as a function of the concentration of dissolved nitric acid. Dashed curve: best fit without radicals; solid curve: best fit with radicals.

Fig. 7.7. Residual muon polarization in water as a function of the concentration of dissolved ferric perchlorate. Dashed curve: best fit without radicals; solid curve: best fit with radicals.

Fig. 7.8. Temperature dependence of the μ^+ precession signal asymmetry in H_2O at a transverse magnetic field of 100 G. The asymmetry scale for the Berkeley results (right-hand side) is different from that of the Dubna measurements (MY 67) because of different experimental setups. The asymmetry is proportional to the muonium hot-atom reaction efficiency in water.

Fig. 7.9. Asymmetry ($A = P_{\perp\,res} \cdot A_o$) and overall phase ($\phi = \theta_o + \Delta\phi$) for mixtures of methanol and chloroform. Mole fraction equals number of $CHCl_3$ molecules per total number of molecules. Dashed line (phase) shows best fit for a constant phase ($\Delta\phi = 0$).

Fig. 7.10. Quenching of the depolarization in sulfur by longitudinal field at three temperatures (From Ref. EP 66.)

Fig. 8.1. Muonium precession signal in fused quartz at 30°C and -196°C for a transverse magnetic field of 7.2 G. The rate N is corrected for the exponential decay of the muon. (From Ref. MO 68.)

Fig. 8.2. Muonium precession signal in crystalline quartz at 20°C for a transverse magnetic field of 7.2 G. The rate N is corrected for the exponential decay of the muon. (From Ref. MO 68.)

Fig. 8.3. Observed longitudinal residual muon polarization $P_{\parallel\,res}$ versus field strength in Al_2O_3. The solid curve corresponds essentially to the quenching of the depolarization for vacuum-like muonium [Eq. (4.6)]. (From Ref. MM 70.)

Fig. 8.4. Longitudinal residual muon polarization $R_{\parallel}$ (excluding contributions from epithermal reaction channels) versus field strength for single crystals of KCl. (From Ref. IM 72.)

Fig. 8.5. Frequency spectra (square of the Fourier amplitudes, arbitrary units) of muons in fused quartz at room temperature and in p-type silicon at 77°K. In both cases the applied transverse field is 100 G. The prominent peaks (from left to right) are: the free muon precession signal at 1.36 MHz; a characteristic background signal at 19.2 MHz, due to rf structure in the cyclotron beam; the two anomalous frequencies at 43.6 ± 2.9 MHz (silicon only); and the two 1s muonium peaks centered about 139 MHz. The wider splitting of the two 1s muonium lines in silicon is due to the weaker hyperfine coupling. (From Ref. BC 73.)

Fig. 8.6. Dependence of anomalous frequencies in silicon upon field strength and crystal orientation. Round points and solid lines are data and best fit for [111] crystal axis along the field; triangular points and dashed lines are data and best fits for [100] axis along the field. Free muon, 1s muonium,

and cyclotron background signals are not shown. A number of peaks appear in the spectra in addition to the fitted "proper" anomalous frequencies; these are unexplained. They are indicated by square points (for prominent peaks) and horizontal bars (for weak or questionable peaks). The higher of the "proper" anomalous frequencies is missing at several fields. This is because the spectra showed no statistically significant peaks at those positions.

Fig. 8.7. Hypothetical comprehensive model of the possible fates of muons in mildly p-type silicon crystal at 77°K.

Fig. 8.8. Experimental values of a, the μ^+ asymmetry parameter: (a) versus free electron concentration in n-type silicon and free hole concentration in p-type silicon at room temperature; (b) in one sample of n-type germanium (phosphorus-doped) at room temperature and liquid nitrogen temperature; and (c) in a graphite sample for which the maximum value of $a = 0.33$ is assumed to correspond to full muon polarization. The abscissas for n-type and p-type silicon have been joined at the value of the intrinsic concentration for room temperature ($\sim 10^{10}$ cm^{-3}). Since the product of the numbers of free holes and electrons in thermal equilibrium with the lattice is constant at a given temperature (i.e. $\sim 10^{20}$ for silicon at room temperature), the entire abscissa represents an increasing free electron concentration to the right (or an increasing hole concentration to the left). (From FP 60).

Fig. 8.9. Left graph: temperature dependence of the initial experimental asymmetry of the μ^+ precession signal in a transverse field, A(0), for undoped Ge single crystals (curve 1) and for As doped Ge (curve 2). The upper dashed line represents the maximal asymmetry A_0; the lower dashed line corresponds to the residual asymmetry $A_0 \times R_\perp$ measured at low field. Right graph: temperature dependence of the depolarization rate ($\lambda = 1/T_2$) of the μ^+ in undoped Ge. (From Ref. AM 69.)

Fig. 9.1. Muon-proton dipole-dipole interaction in a single crystal of gypsum: schematic representation of the effect of the muon-proton situation relative to the magnetic field direction on the μ^+ spin precession. $\overline{\omega^\mu}$ corresponds to the precession frequency unperturbed by dipole-dipole interactions; it is split by that interaction into two symmetrically shifted frequencies (one per proton spin orientation for each μ^+ - p pair. The line broadening produced by the magnetic dipoles farther away is indicated by the dashed curves.

Fig. 9.2. (a) Observed μ^+ precession signal asymmetry $A(0)\cdot F(t)$ for a gypsum crystal orientation showing two NMR lines. The asymmetry values are determined for 0.5-μsec intervals. The solid curve represents the theoretical $A(0)\cdot F(t)$ dependence.

(b) For a second crystal orientation showing four NMR lines, the agreement between the observed asymmetry values and the calculated curve is marginal, suggesting that the actual crystal orientation is slightly off the assumed one. The determination of these angles is uncertain to ~ 10°. (From Ref. SC 71.)

Fig. 9.3. Temperature dependence of the μ^+ depolarization rate Λ in copper. $\Lambda = 1/\tau_r$, where τ_r is the time at which the measured F(t) had decreased by a factor of e. (From Ref. GM 72.)

Fig. 9.4. Dependence $\ln(1/\tau_c) = f(1/T)$ obtained from F(t) measurements (GM 72) of the μ^+ spin relaxation in copper. In the graph the "hopping time" values τ_c are entered in μsec. The straight line corresponds to the theoretical relation (9.18) with $E/\mathbf{k}_B = 540°K$.

Fig. 9.5. Local field B_μ at the muon site and line widths ΔB observed in polycrystalline and single-crystal nickel by various techniques. The solid curve is from normalized magnetization data in Ni of Ref. WF 26.

Fig. 9.6. Local field B_μ at the muon site in nickel versus B_{ext}, the external field measured with target out. D is the sample demagnetizing factor. The points denoted by triangles are from data on an approximately spherical single crystal with the [111] axis parallel to B_{ext} at 300 and 77°K. Other points are from data on a polycrystalline ellipsoid (4.5×2×0.5 in.). Solid and open circles refer to the 4.5-in. axis parallel to B_{ext} (D = 0.69) at 523 and 573°K respectively. Solid and open squares refer to the 2-in. axis parallel to B_{ext} (D = 2.24) at 523 and 573°K. B_μ and B_{ext} have been normalized to bring measurements at various temperatures to the same vertical level and to exhibit saturation for all samples at zero on the horizontal scale.

Fig. 9.7. Temperature dependence of the μ^+ residual polarization $P_\perp$ in polycrystalline Ni. The solid line corresponds to the measured sample permeability divided by B_μ and normalized to the data. The dashed line indicates the assumed drop in $P_\perp$ near the Curie temperature. (From Ref. FH 73.)

Fig. 9.8. Concentration dependence of the transverse relaxation time for μ^+ depolarization in $FeCl_3$, $Fe(ClO_4)_3$, and $Fe(NO_3)_3$ solutions. For the $Fe(NO_3)_3$ solution, the T_2 dependence for proton NMR is indicated by the upper solid line. (From Ref. SC 70.)

Fig. 9.9. (a) Transverse muon relaxation times in $MnCl_2$ solutions. The dashed lines represent the spin-exchange and dipole-dipole terms. The solid line is the combined result.

(b) Plot of τ_s^* versus Mn^{2+} concentration at 295°K. The solid line was obtained from Ref. HM 66.

Fig. 9.10. (a) Plot of $1/T_2P$ versus Mn^{2+} concentration. The solid curve is obtained by combining NMR and ESR results. The dashed curves show separately the contributions from spin-exchange and dipole-dipole interactions.

(b) Plot of $1/(T_2P)$ versus temperature. The dotted curve is the fit obtained for 11 kG without modifications. The solid curves result from further analysis at 4.5 and 11 kG (considering a new V_r value). The dashed curves represent the spin-exchange and dipole-dipole contributions separately for the analysis at 11 kG with the modified V_r value.

Fig. 10.1. Ranges of various relaxation rates and sensitive regions for different detection techniques.

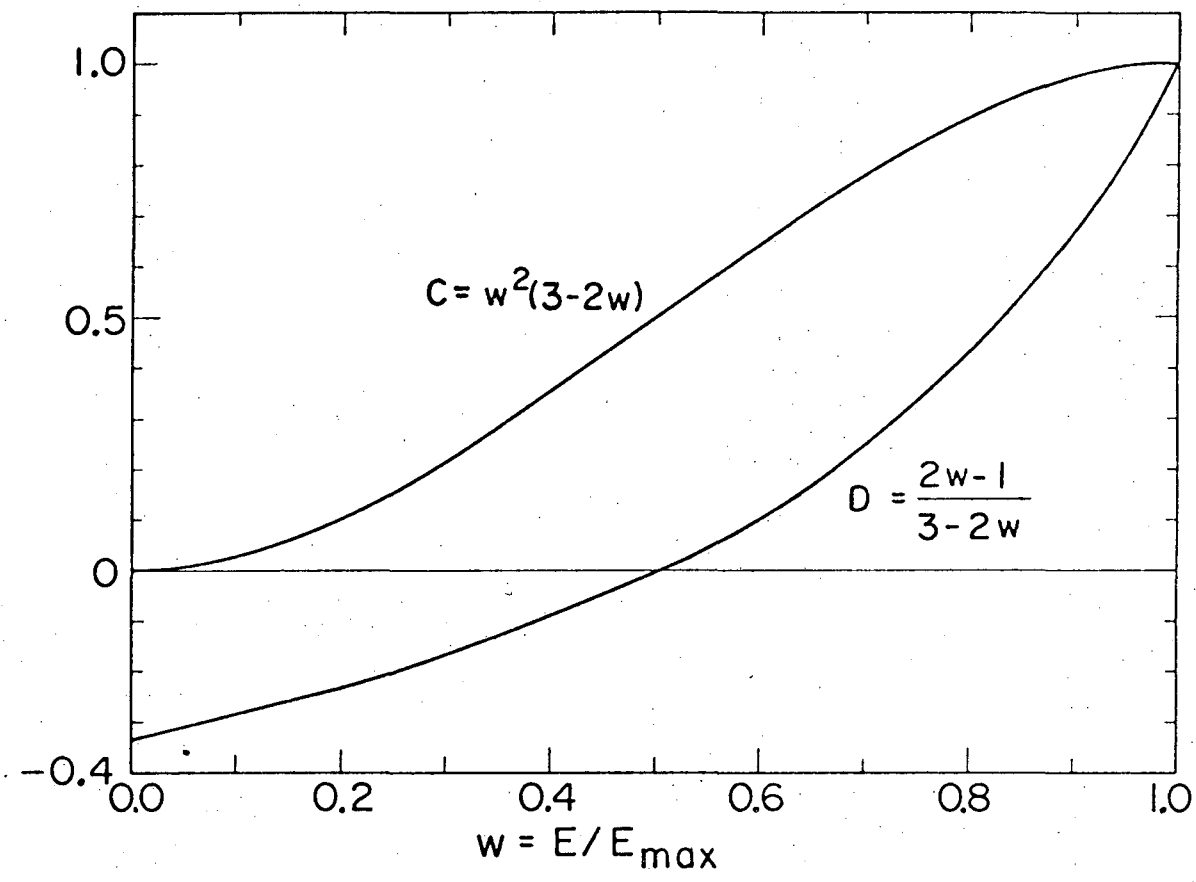

Fig. 2.1.

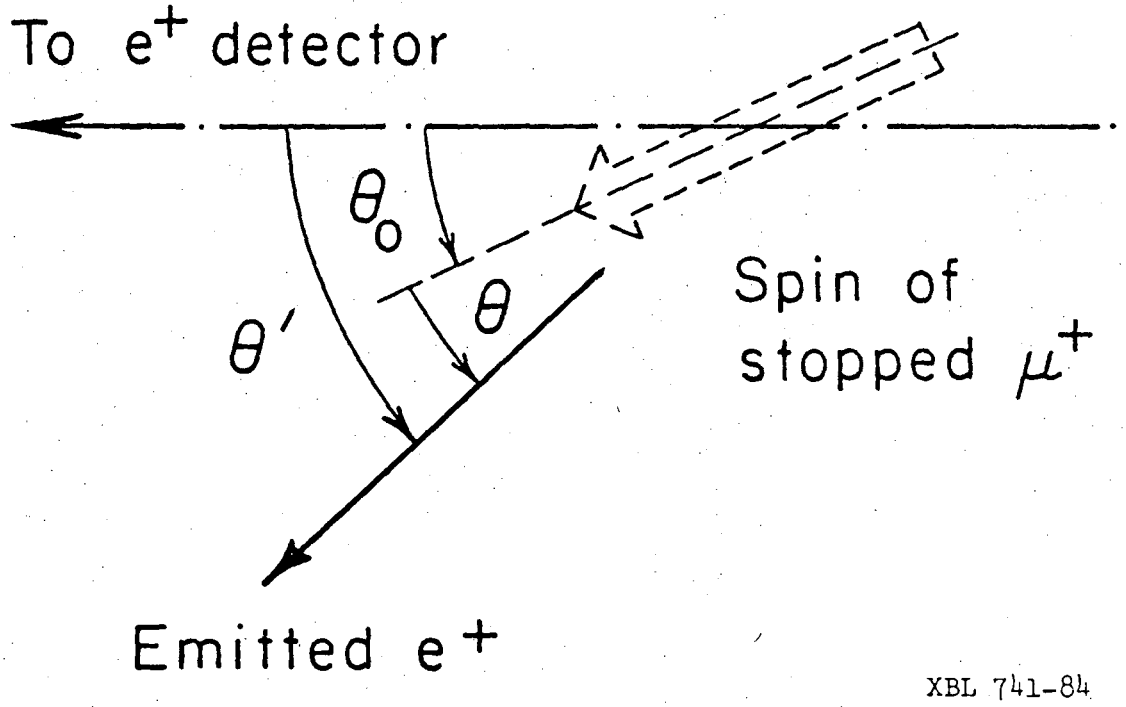

XBL 741-84

Fig. 2.2.

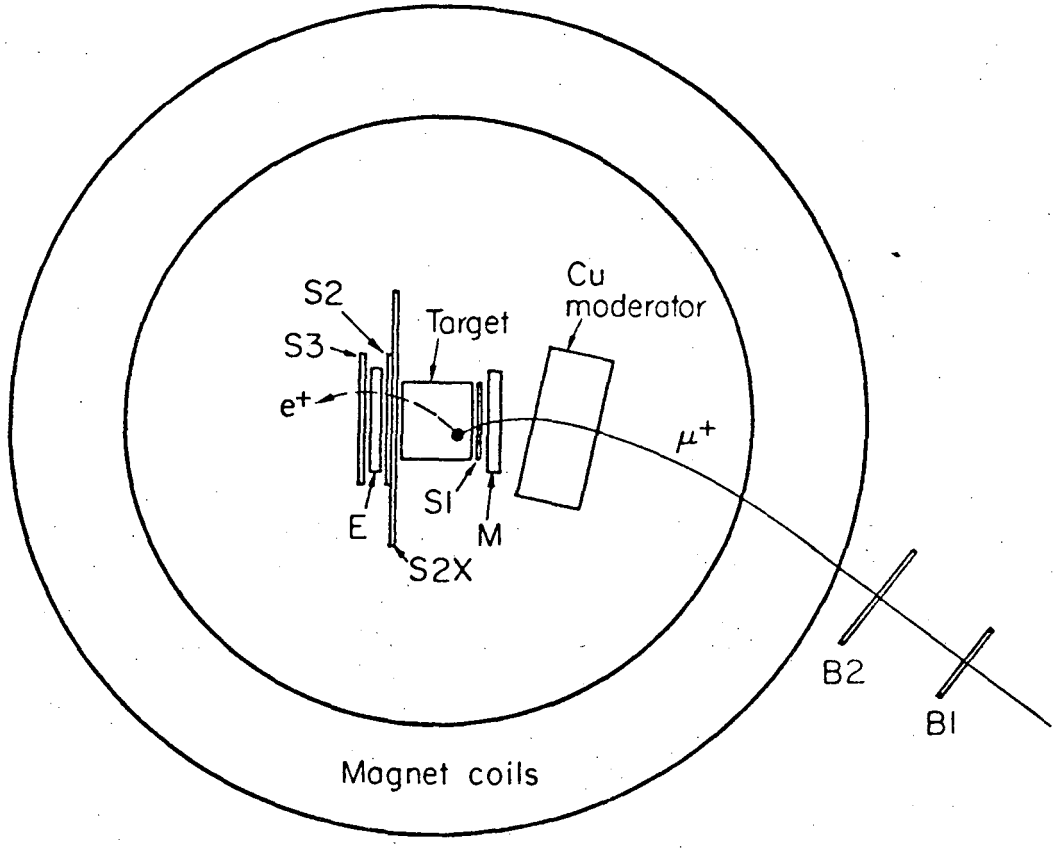

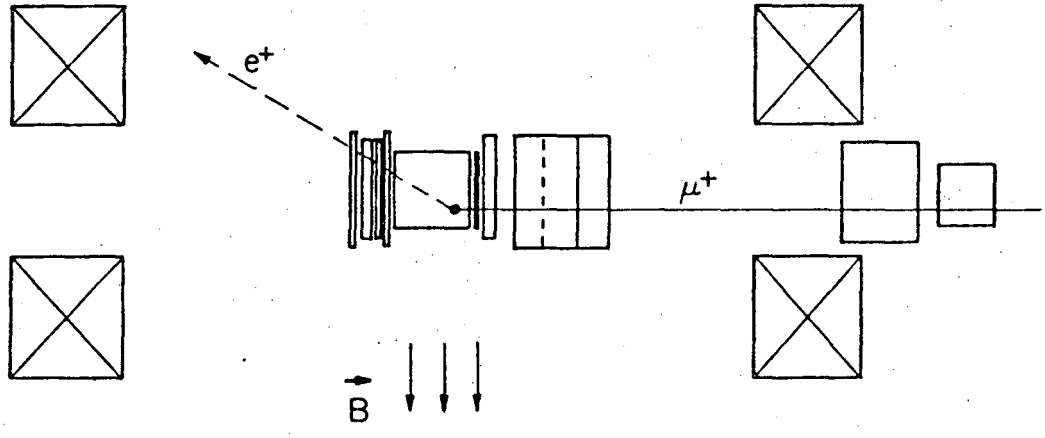

Fig. 2.3.

XBL735-2916

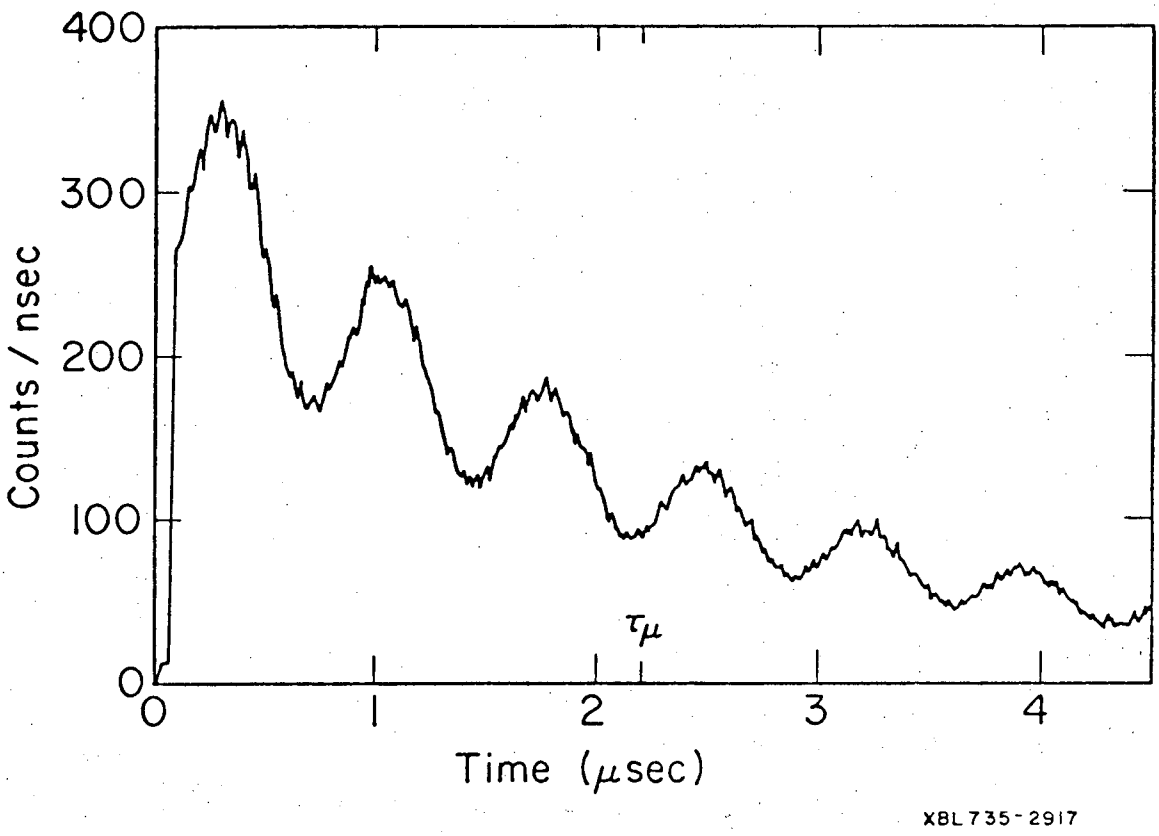

Fig. 2.4.

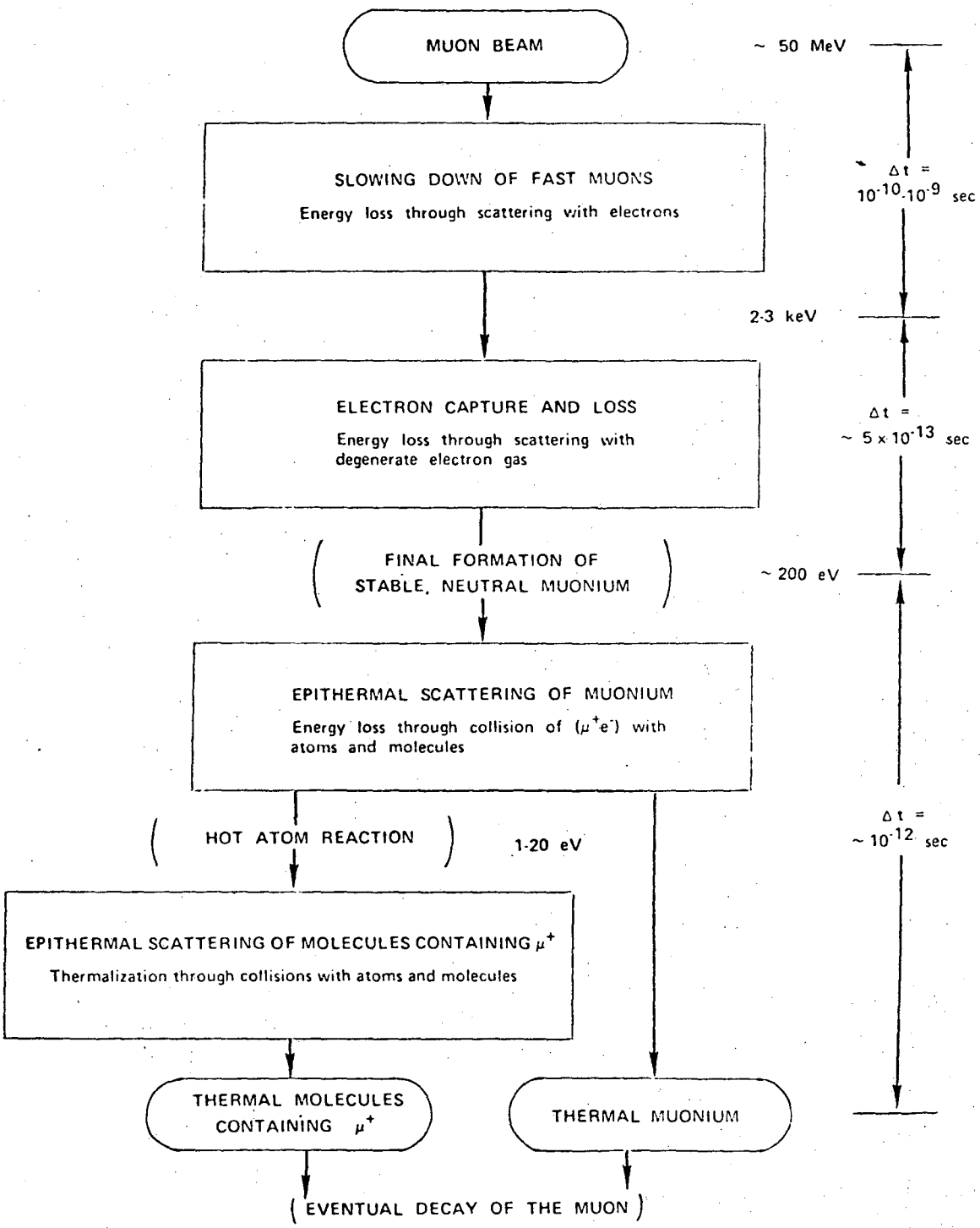

XBL 741-85

Fig. 3.1.

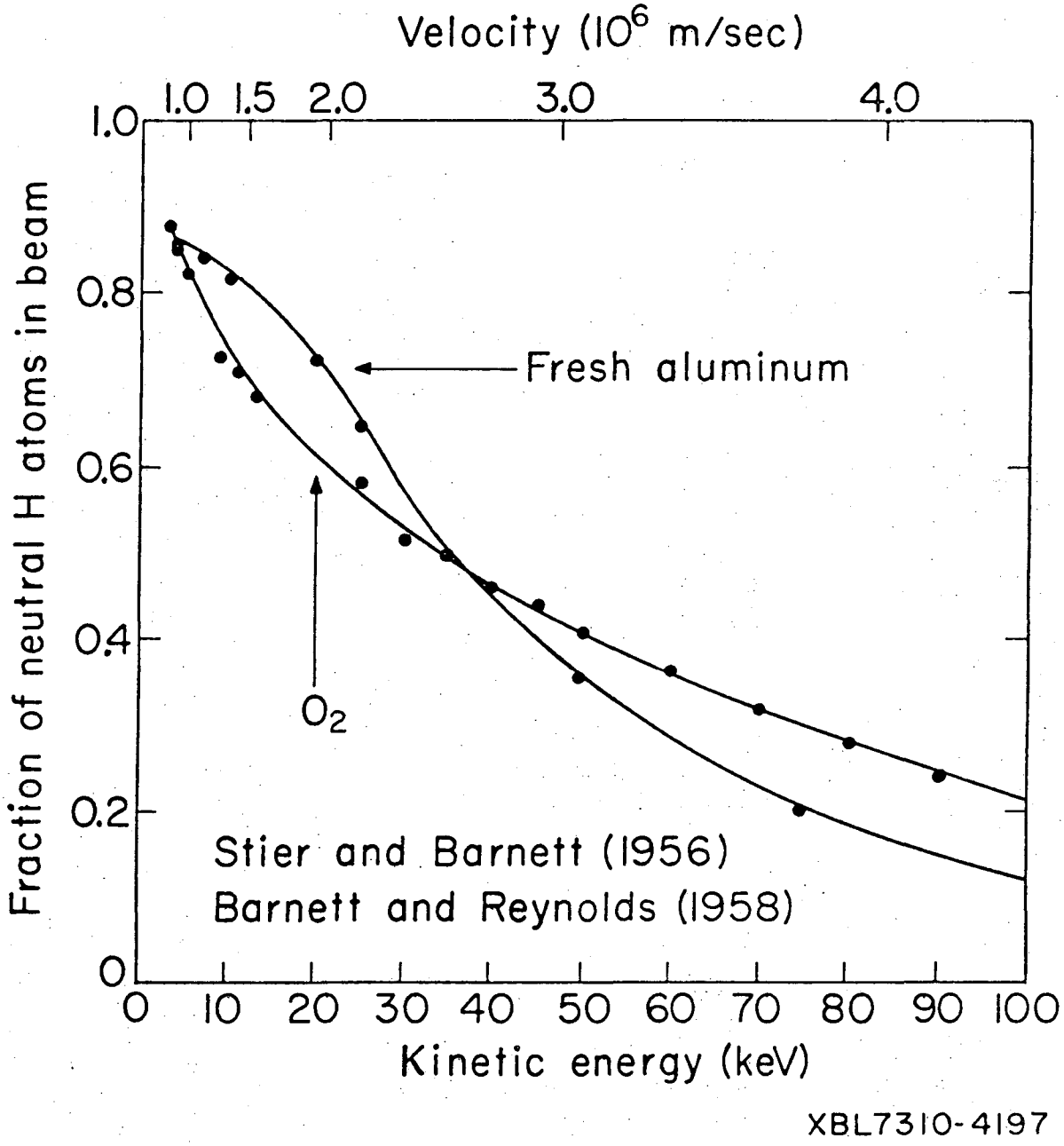
Velocity (10^6 m/sec)
1.0
1.5
2.0
3.0
4.0
Fraction of neutral H atoms in beam
1.0
0.8
0.6
0.4
0.2
0
Fresh aluminum
O_2
Stier and Barnett (1956)
Barnett and Reynolds (1958)
0
10
20
30
40
50
60
70
80
90
100
Kinetic energy (keV)
XBL7310-4197

Fig. 3.2.

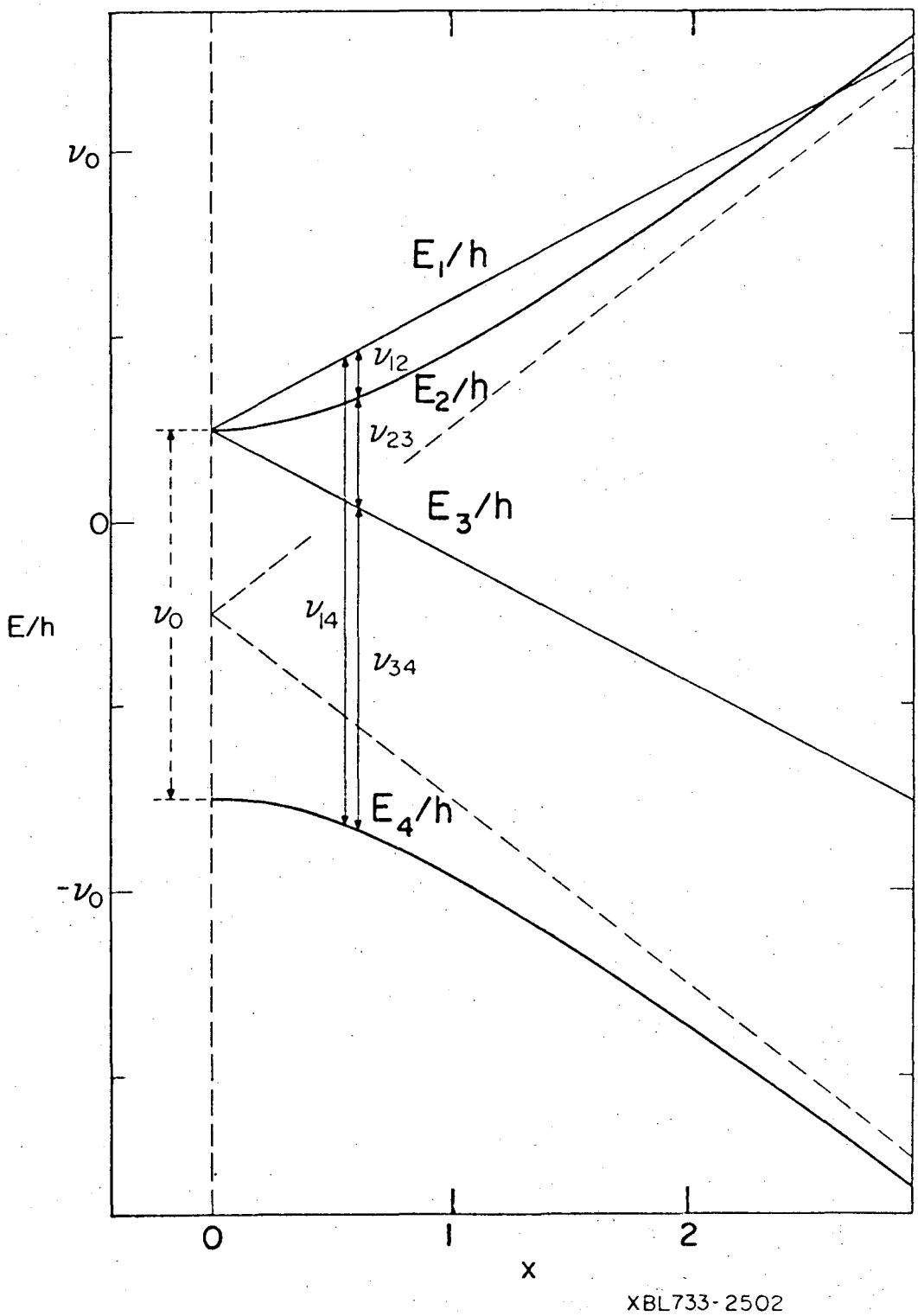
ν_0
0
$-\nu_0$
E/h
E_1/h
E_2/h
E_3/h
E_4/h
ν_{12}
ν_{23}
ν_{14}
ν_{34}
ν_0
0
1
2
x
XBL733-2502

Fig. 4.1.

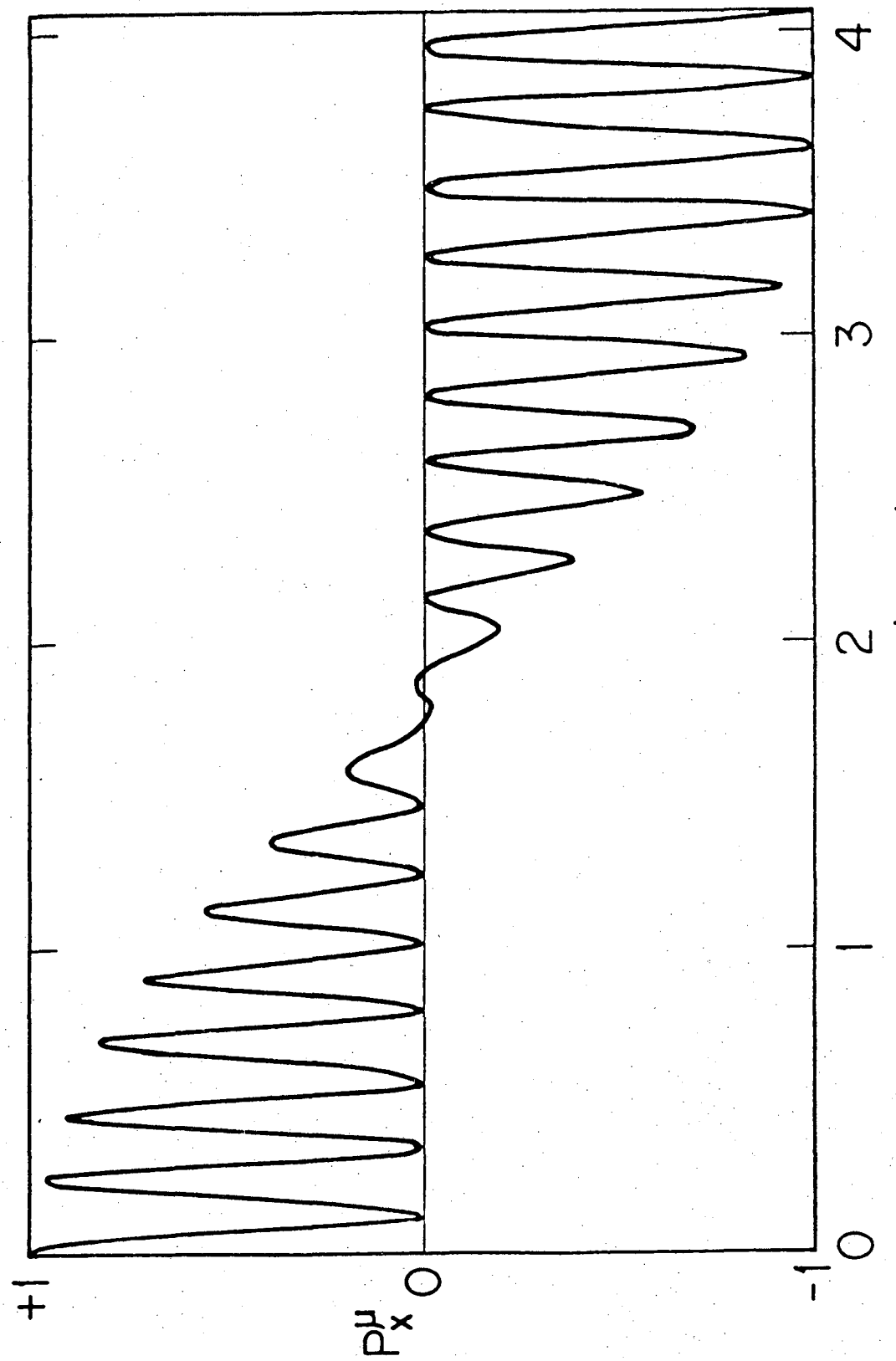

XBL7210-4190

Fig. 4.2.

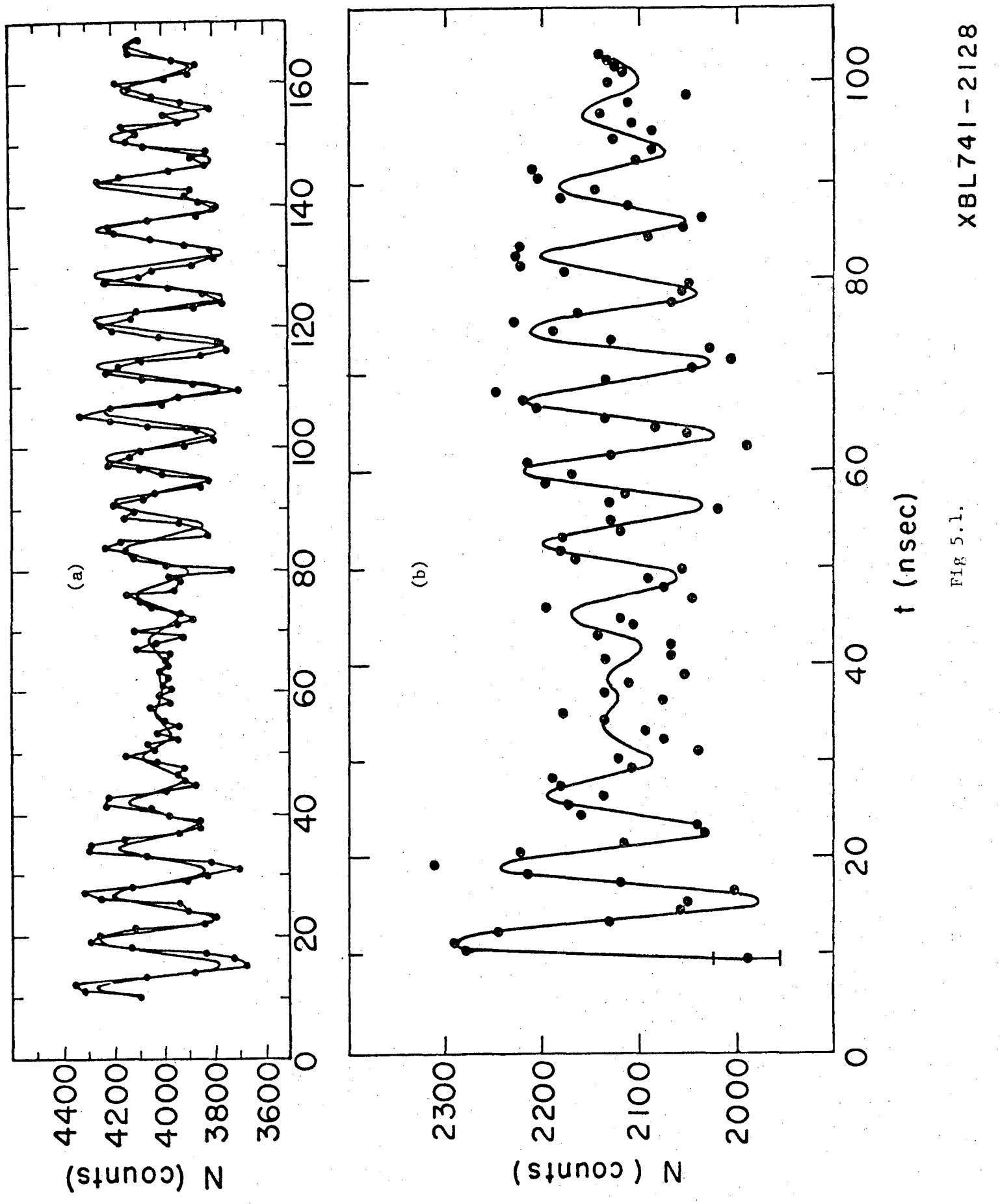

XBL741-2128

Fig 5.1.

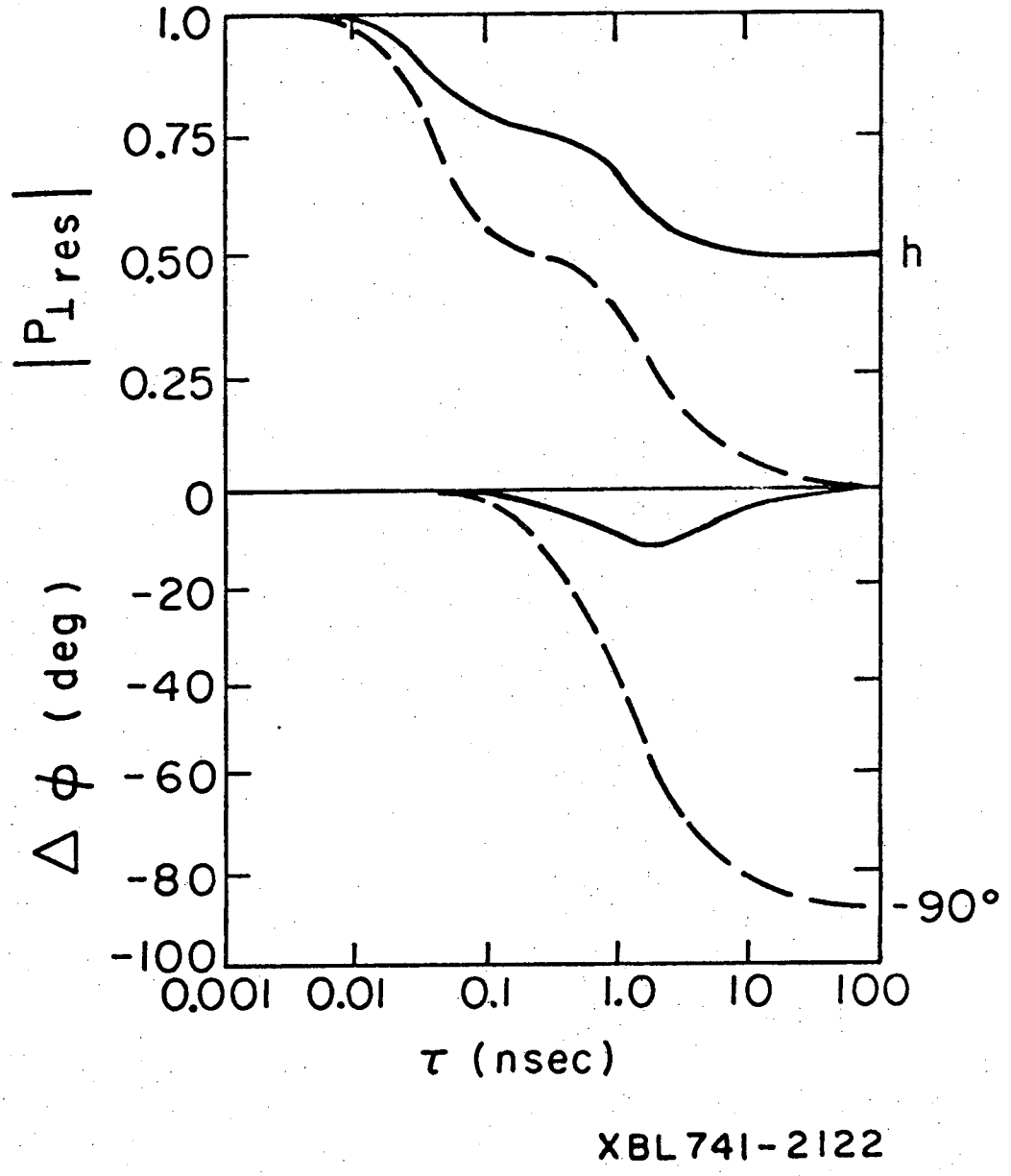
1.0
0.75
0.50
0.25
0
-20
-40
-60
-80
-100
$|P_{\perp res}|$
$\Delta\phi$ (deg)
h
-90°
0.001
0.01
0.1
1.0
10
100
τ (nsec)
XBL741-2122

Fig. 6.1.

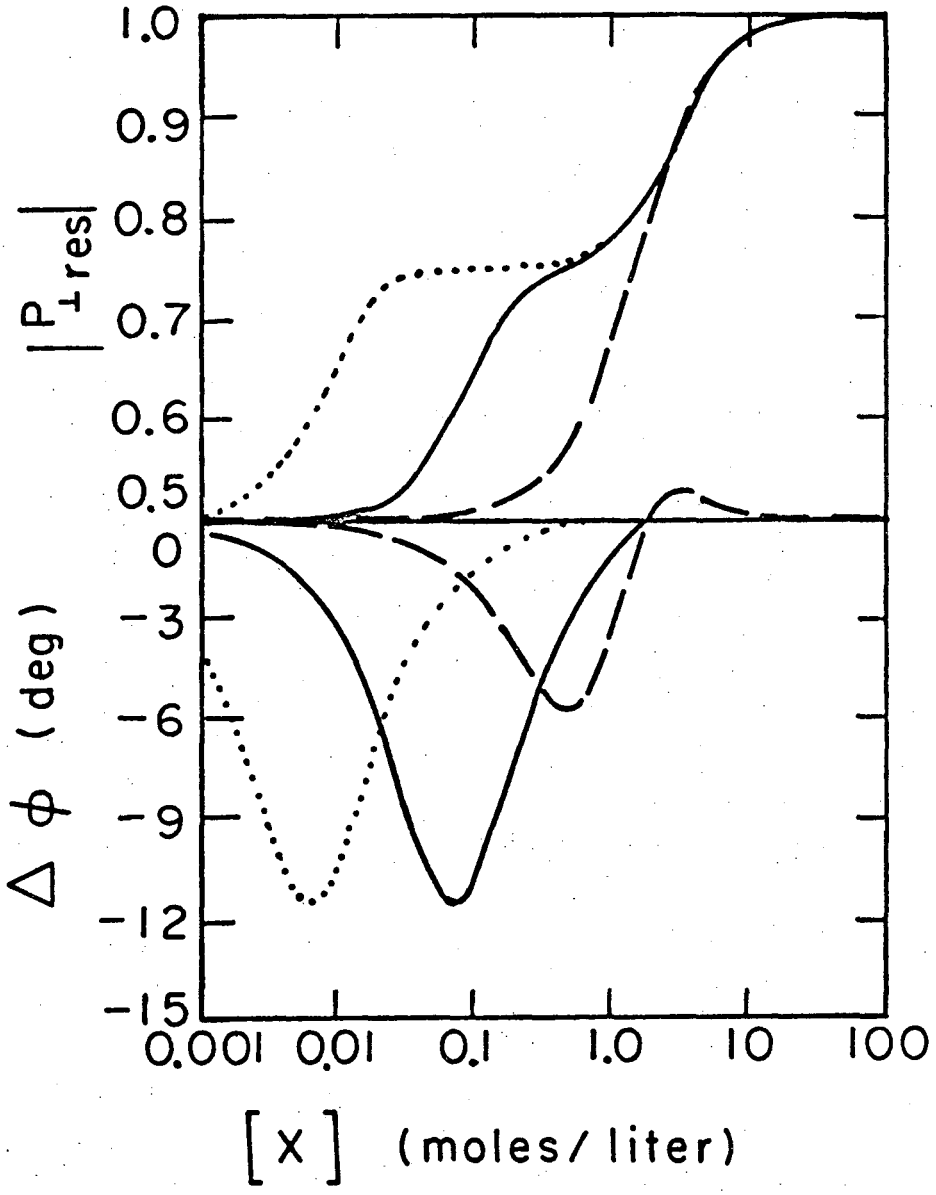
1.0
0.9
0.8
0.7
0.6
0.5
0
-3
-6
-9
-12
-15
$|P_{\perp res}|$
$\Delta\phi$ (deg)
0.001
0.01
0.1
1.0
10
100
[X] (moles/liter)
XBL741-2132

Fig. 6.2.

FLOW CHART OF DEPOLARIZATION MECHANISM

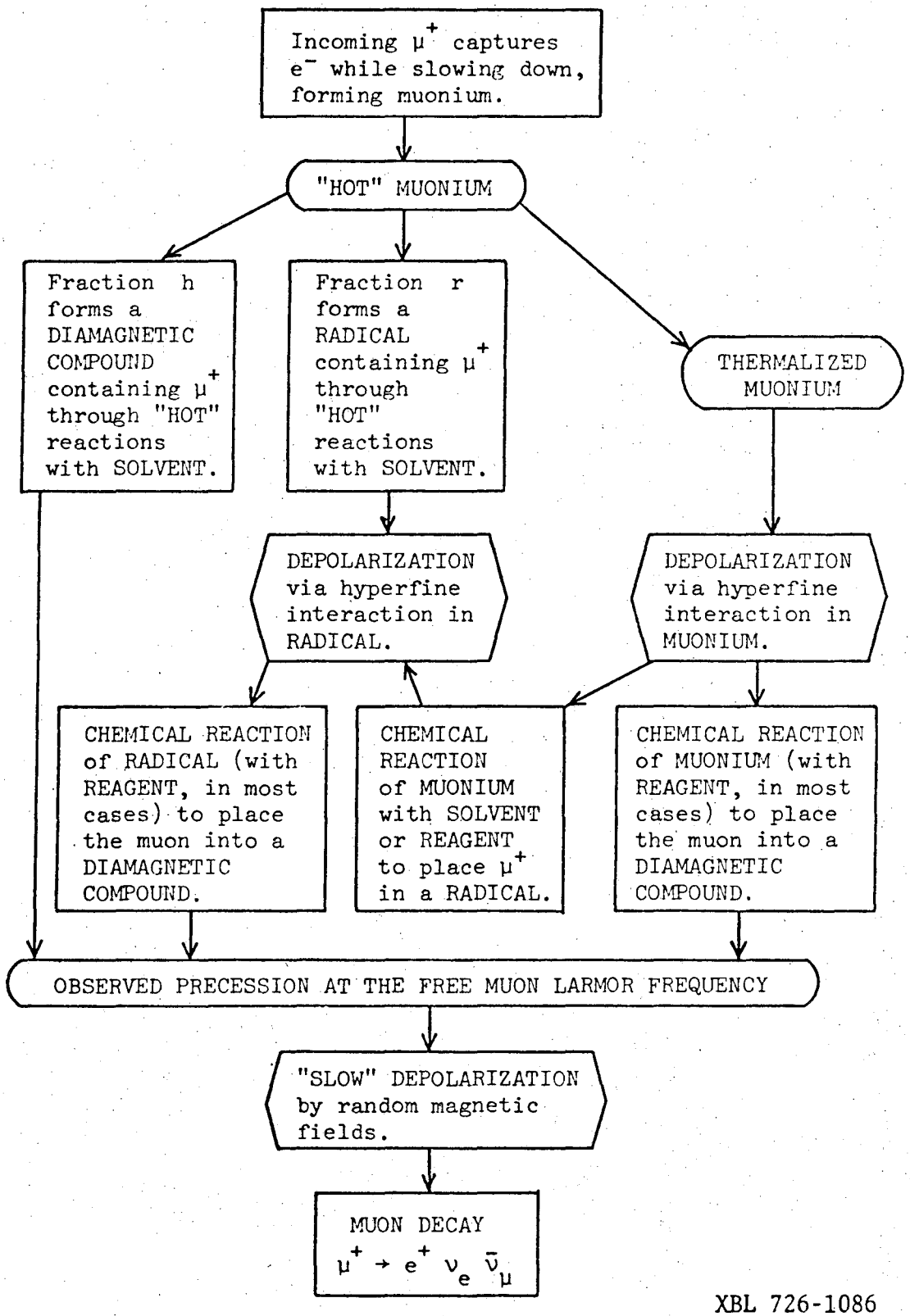

XBL 726-1086

Fig. 6.3.

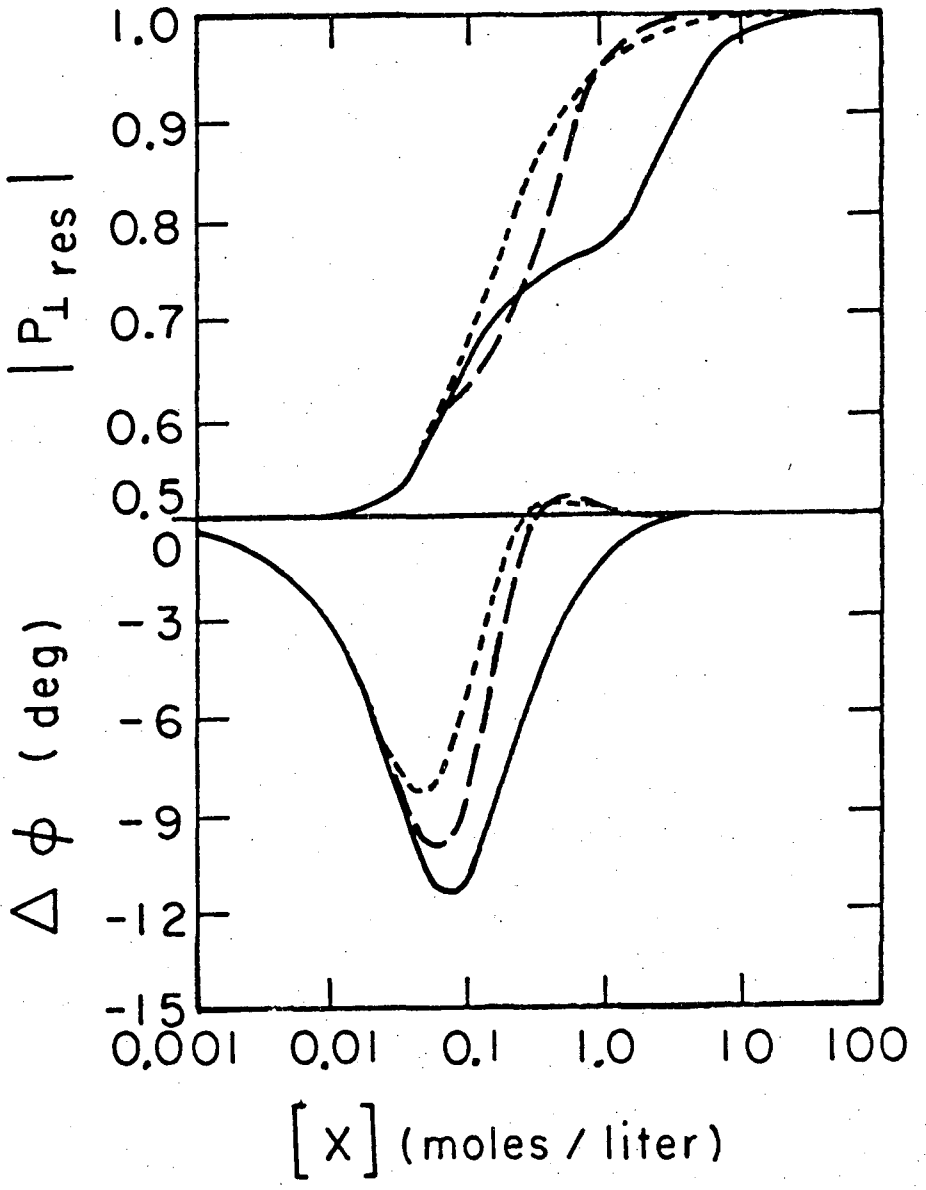
1.0
0.9
0.8
0.7
0.6
0.5
$|P_{\perp res}|$
0
-3
-6
-9
-12
-15
$\Delta\phi$ (deg)
0.001
0.01
0.1
1.0
10
100
[X] (moles / liter)
XBL741-2131

Fig. 6.4.

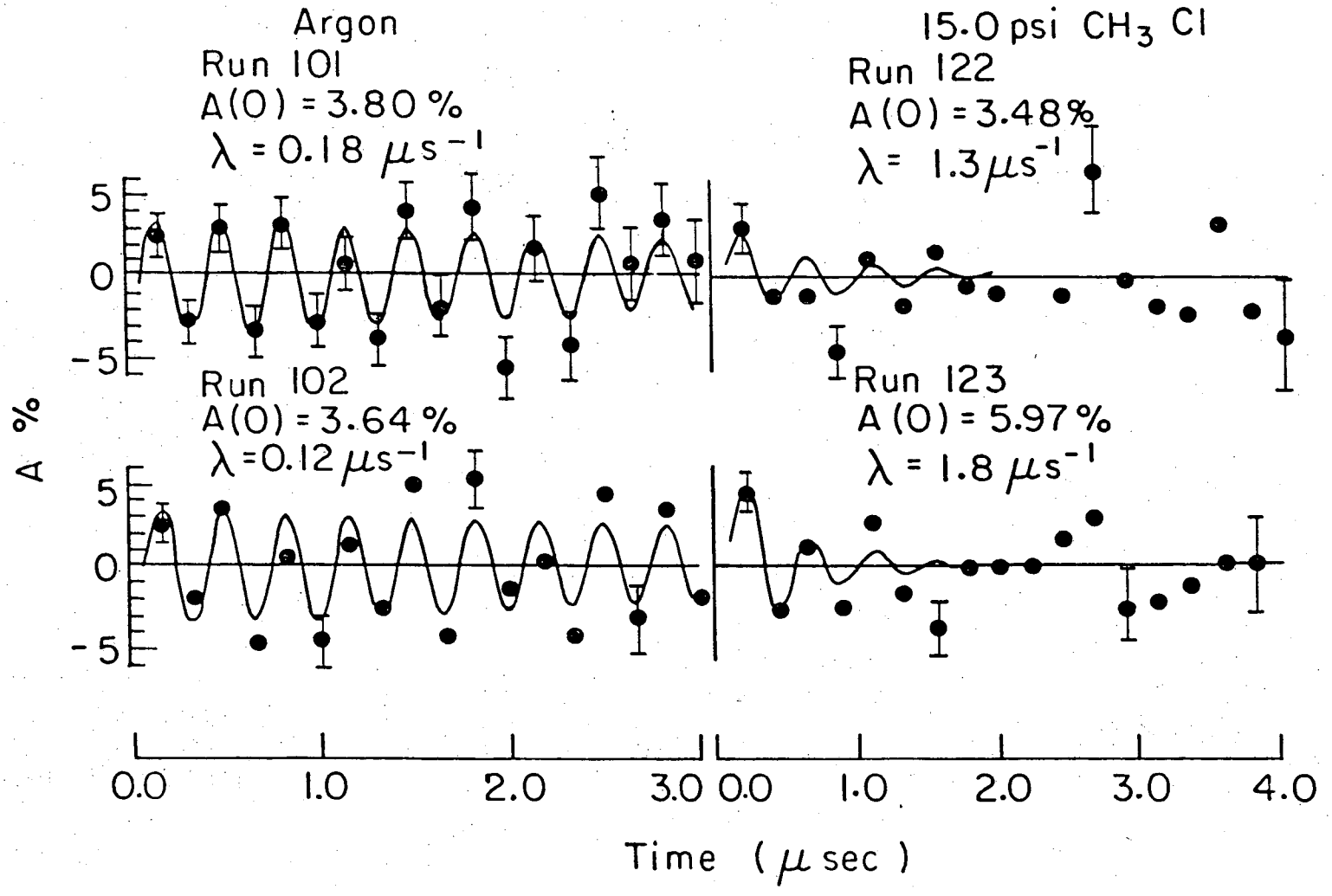
Argon
Run 101
A(0) = 3.80 %
λ = 0.18 μs⁻¹
15.0 psi CH3 Cl
Run 122
A(0) = 3.48%
λ = 1.3 μs⁻¹
Run 102
A(0) = 3.64 %
λ = 0.12 μs⁻¹
Run 123
A(0) = 5.97 %
λ = 1.8 μs⁻¹
A %
5
0
-5
0.0
1.0
2.0
3.0
4.0
Time (μ sec)
XBL741-2152

Fig. 7.1.

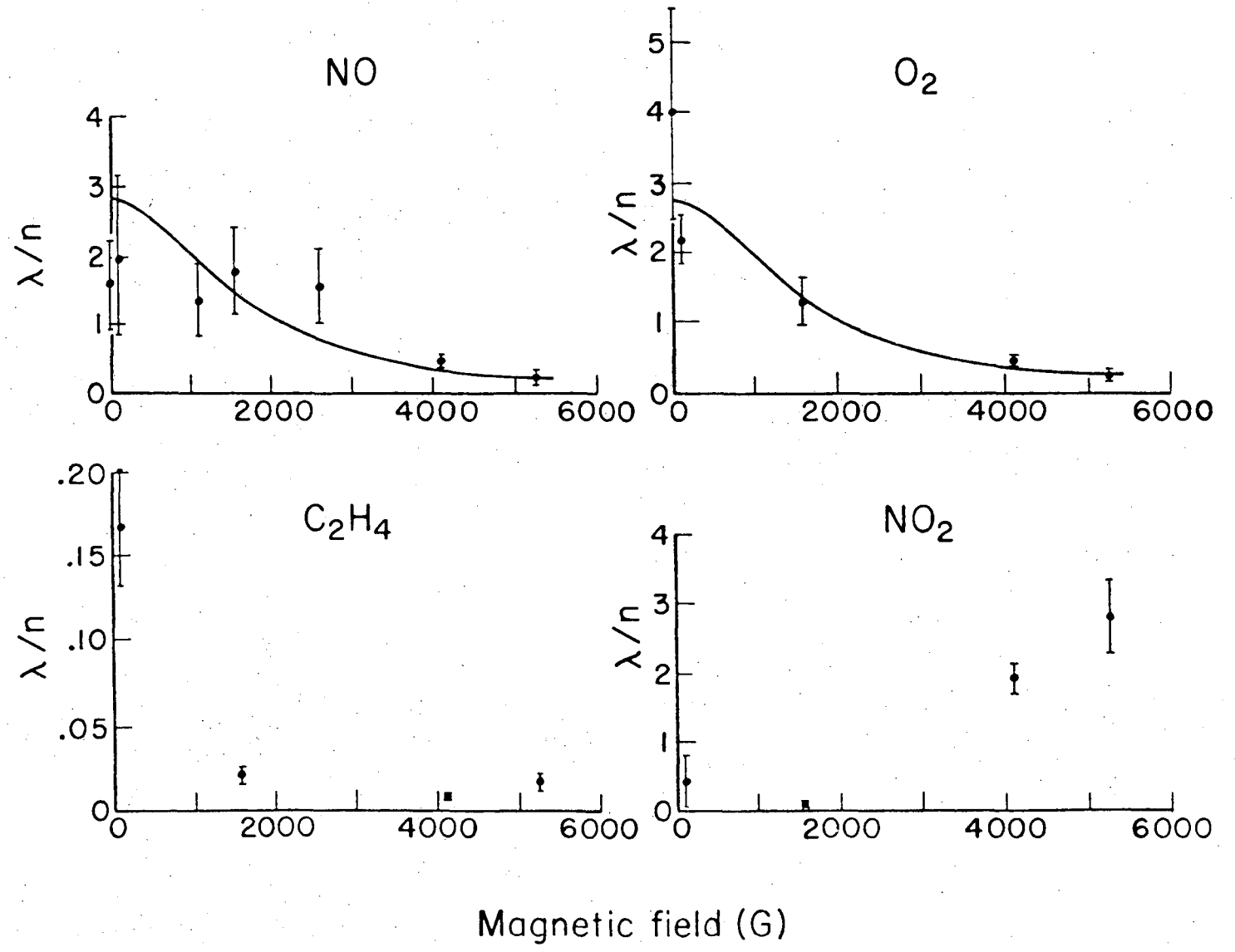
NO
O_2
C_2H_4
NO_2
λ/n
Magnetic field (G)
0
2000
4000
6000
XBL741-2153

Fig. 7.2.

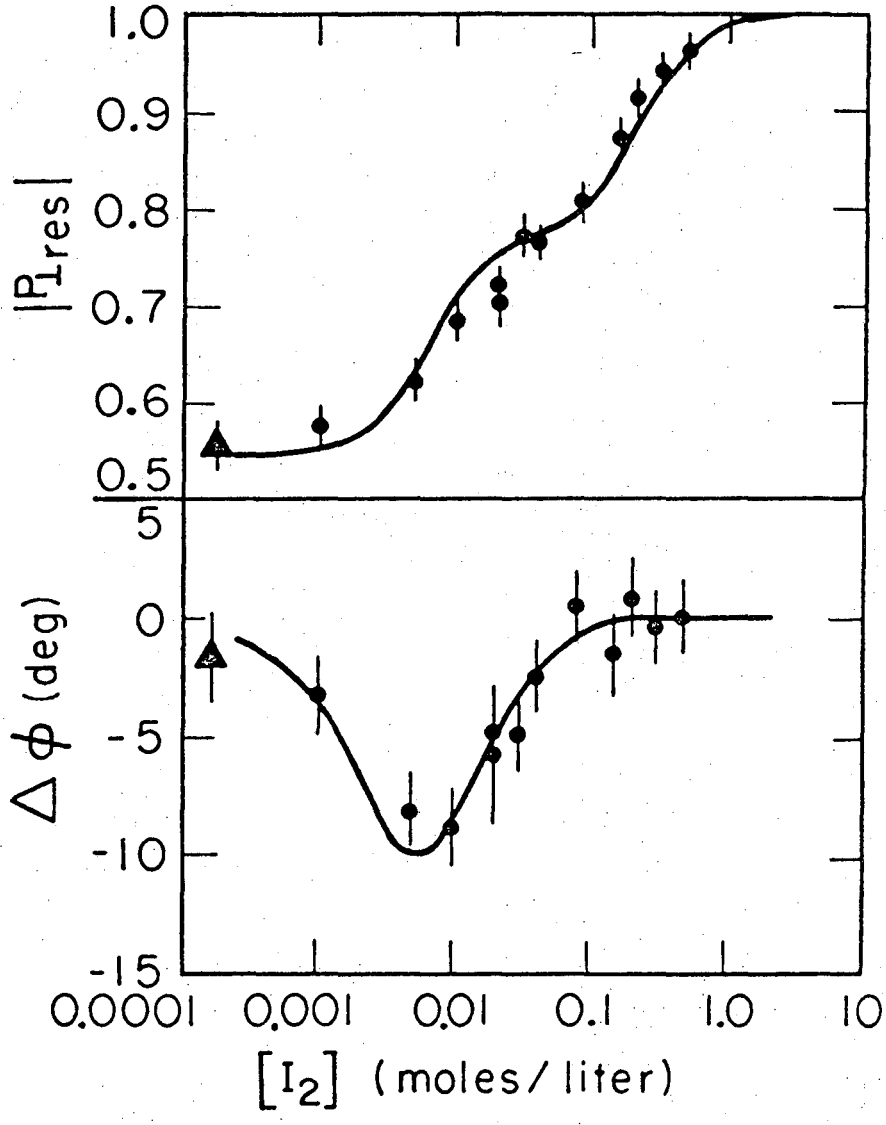

XBL734-2763

Fig. 7.3.

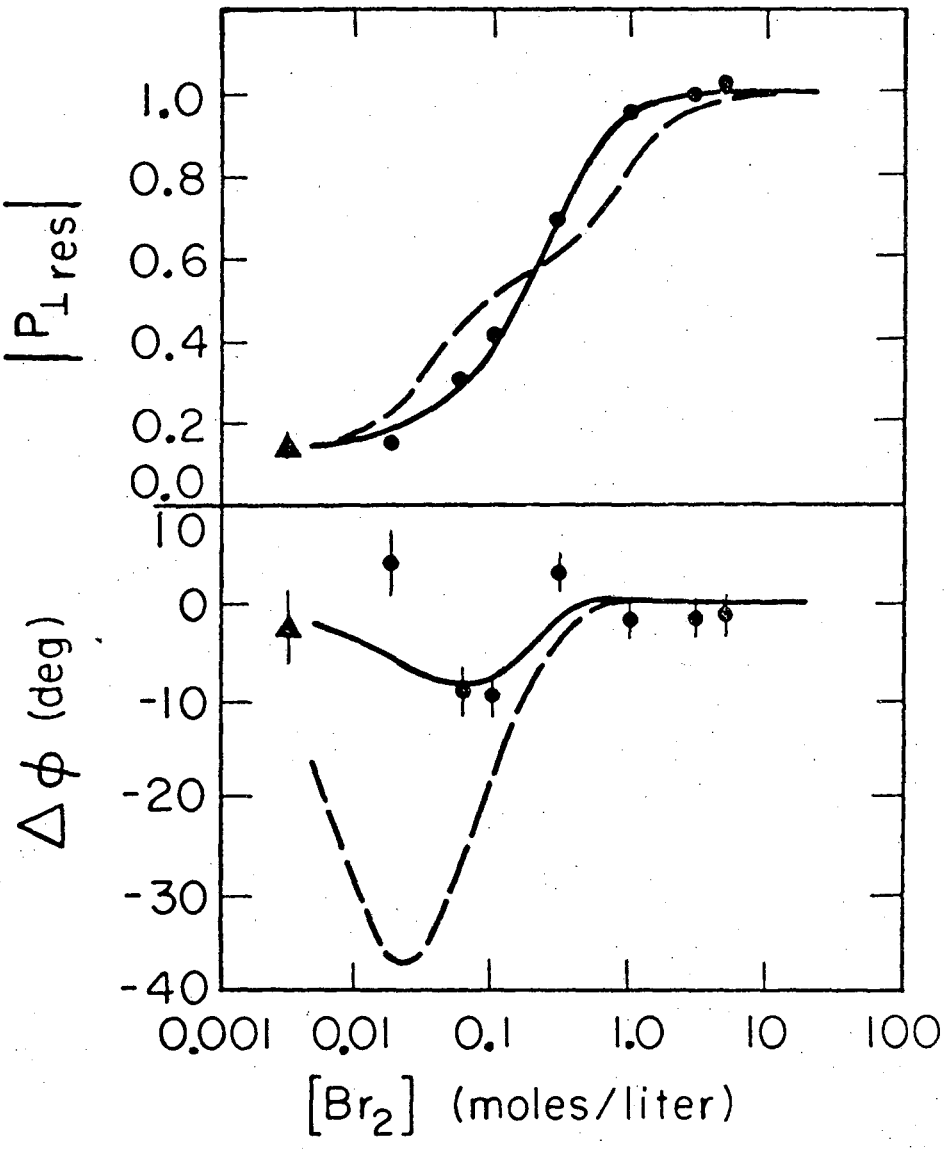

XBL7210-4167

Fig. 7.4.

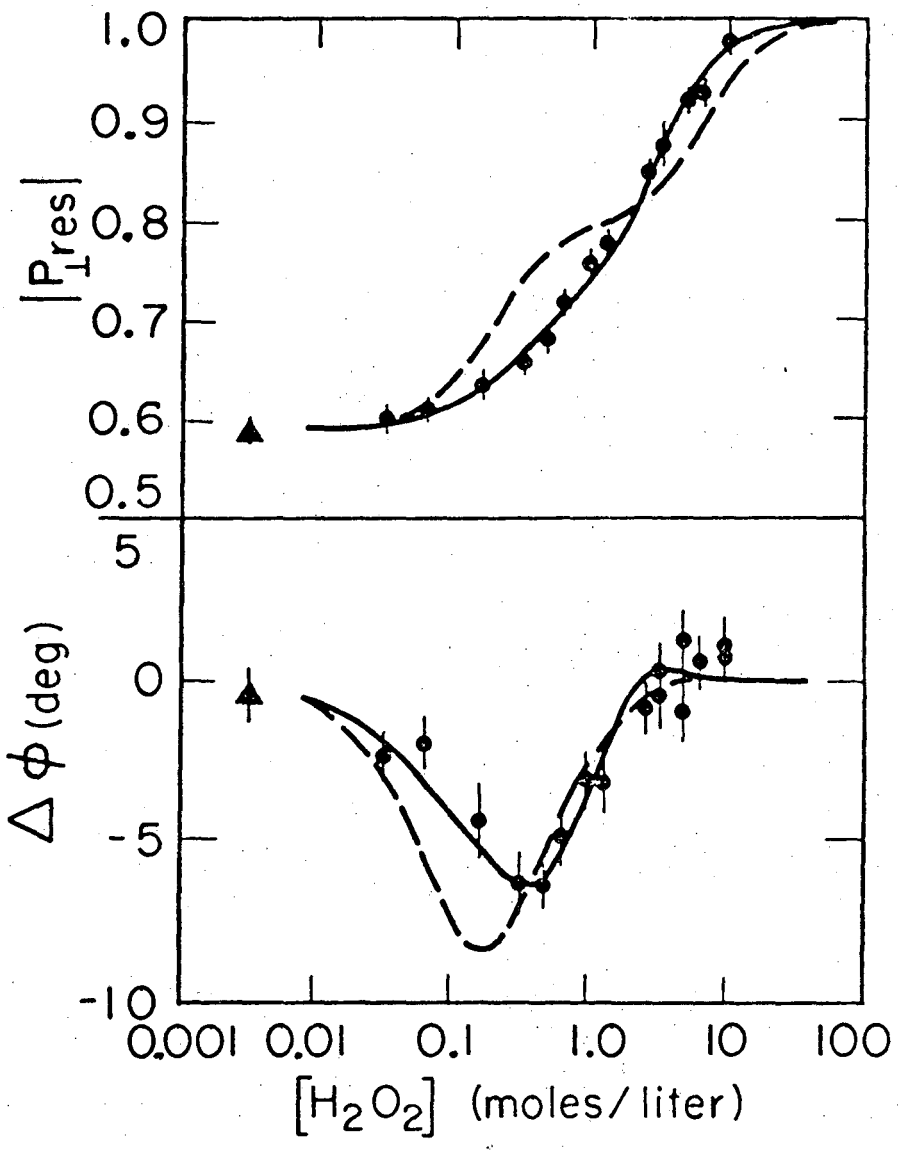

XBL 7210-4166

Fig. 7.5.

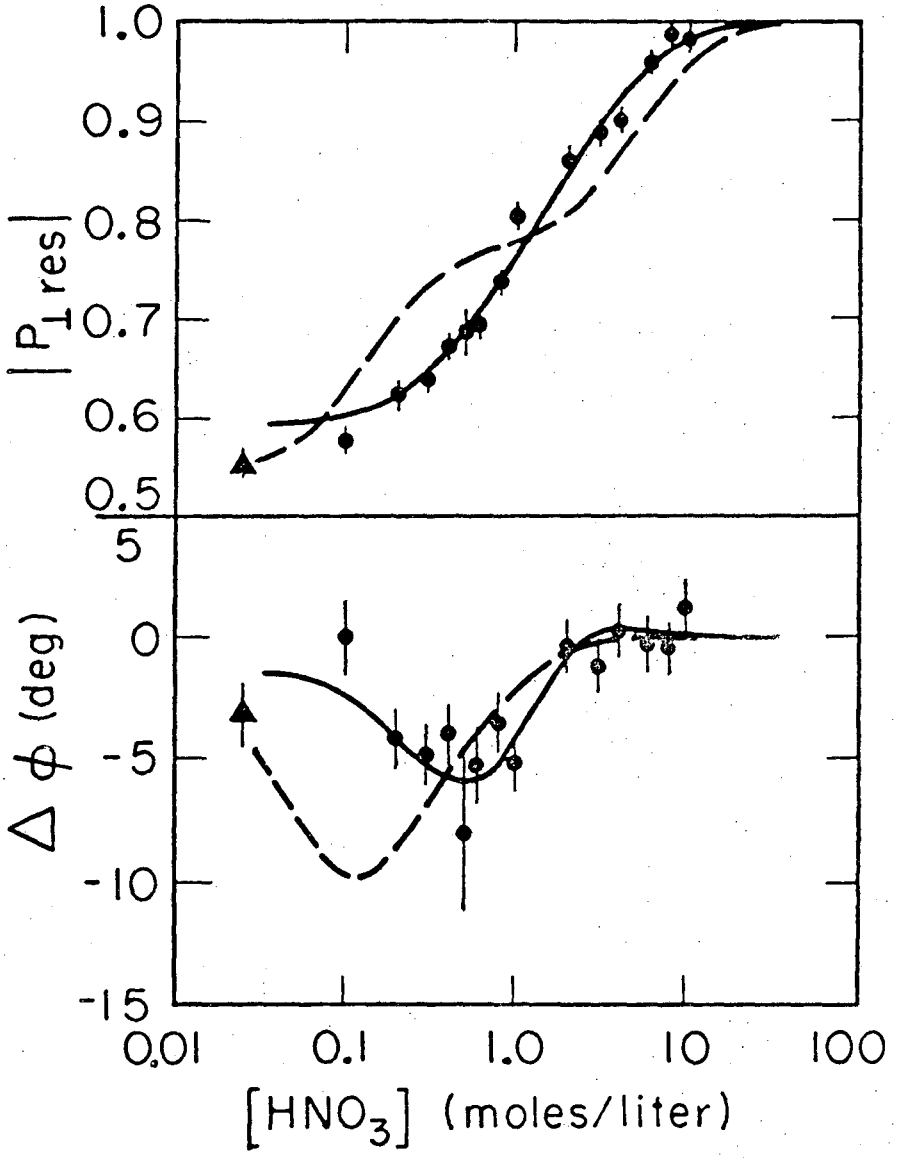
1.0
0.9
0.8
0.7
0.6
0.5
$|P_{\perp res}|$
5
0
-5
-10
-15
$\Delta\phi$ (deg)
0.01
0.1
1.0
10
100
$[HNO_3]$ (moles/liter)
XBL7210-4165

Fig. 7.6.

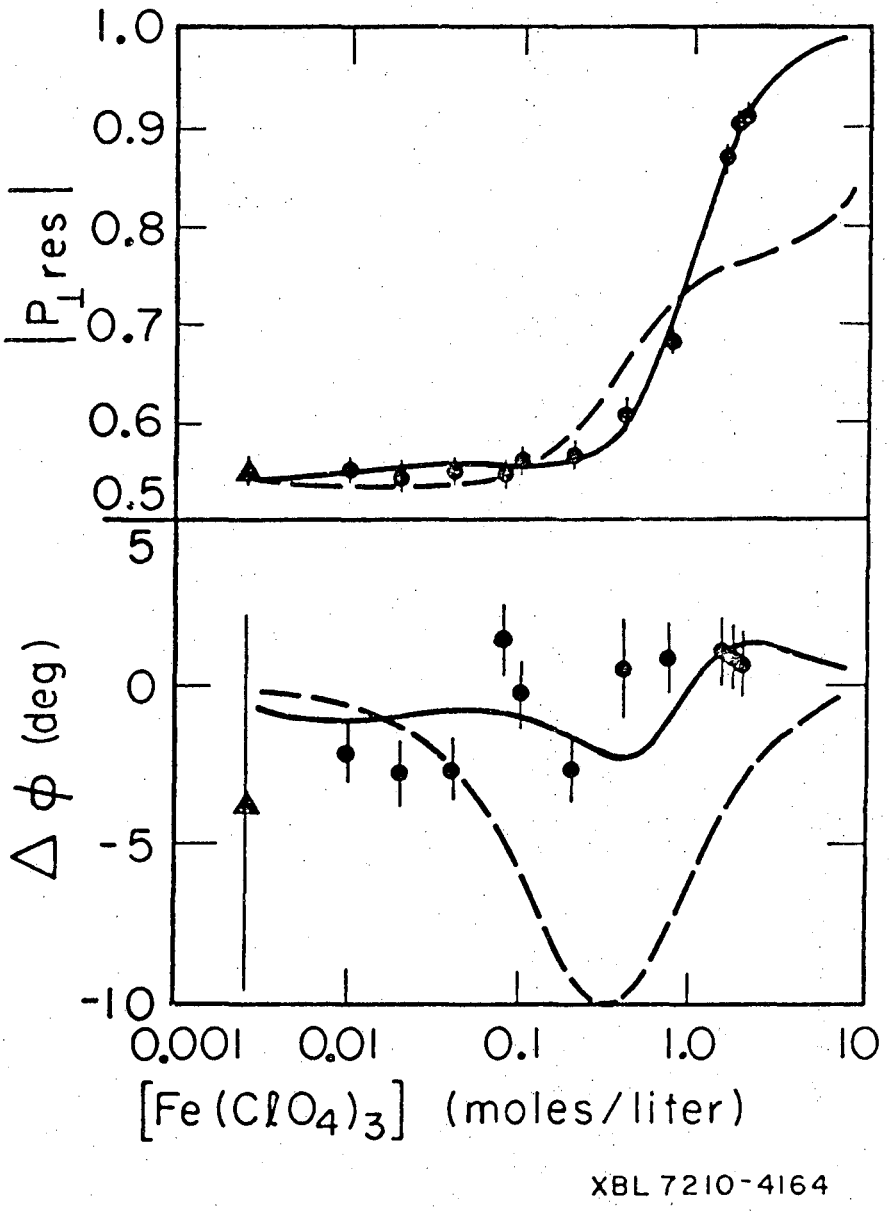
1.0
0.9
0.8
0.7
0.6
0.5
|P⊥res|
5
0
-5
-10
Δφ (deg)
0.001
0.01
0.1
1.0
10
[Fe(ClO4)3] (moles/liter)
XBL 7210-4164

Fig. 7.7.

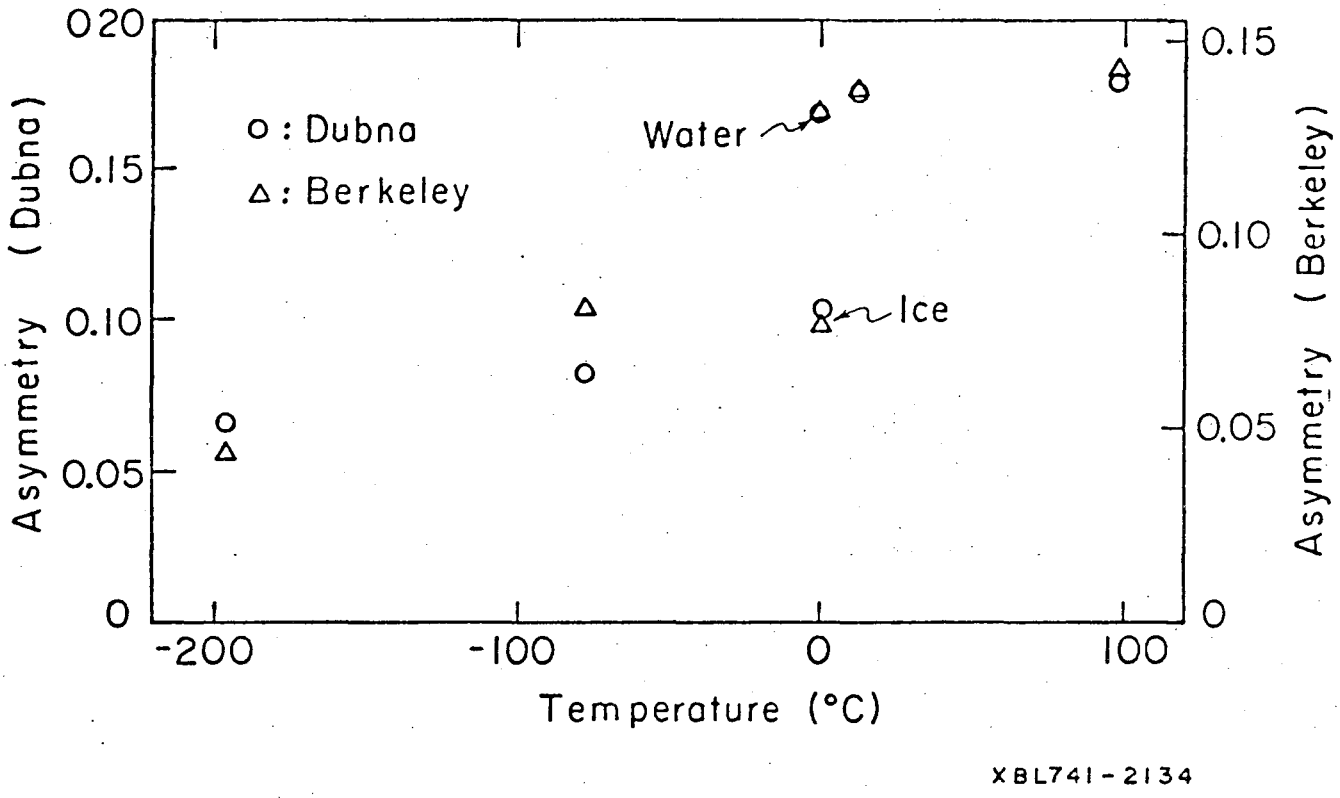
020
0.15
0.10
0.05
0
Asymmetry (Dubna)
o : Dubna
Δ : Berkeley
Water
Ice
0.15
0.10
0.05
0
Asymmetry (Berkeley)
-200
-100
0
100
Temperature (°C)
XBL741-2134

Fig. 7.8.

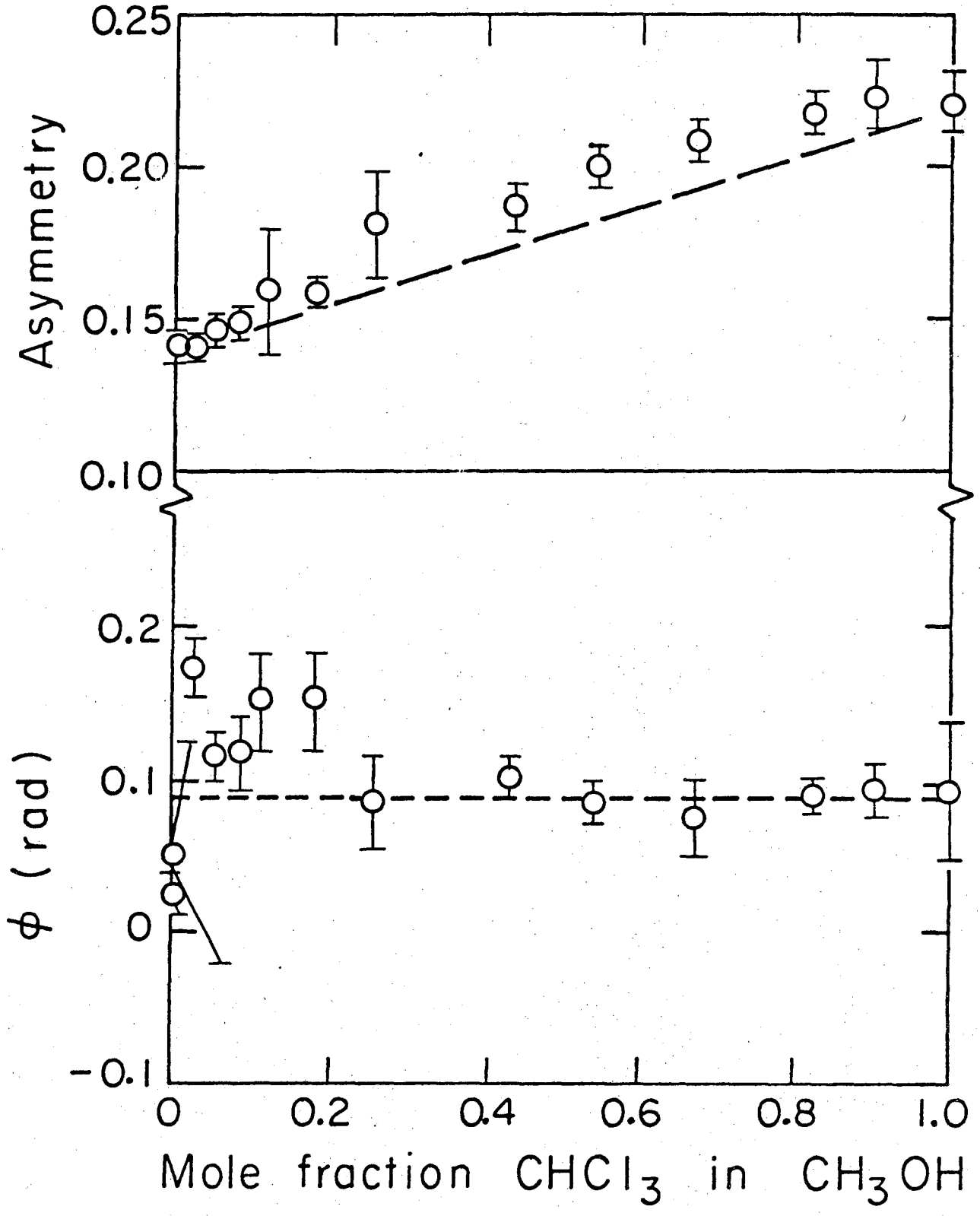
0.25
0.20
0.15
0.10
Asymmetry
0.2
0.1
0
-0.1
ϕ (rad)
0
0.2
0.4
0.6
0.8
1.0
Mole fraction $CHCl_3$ in CH_3OH
XBL741-2130

Fig. 7.9.

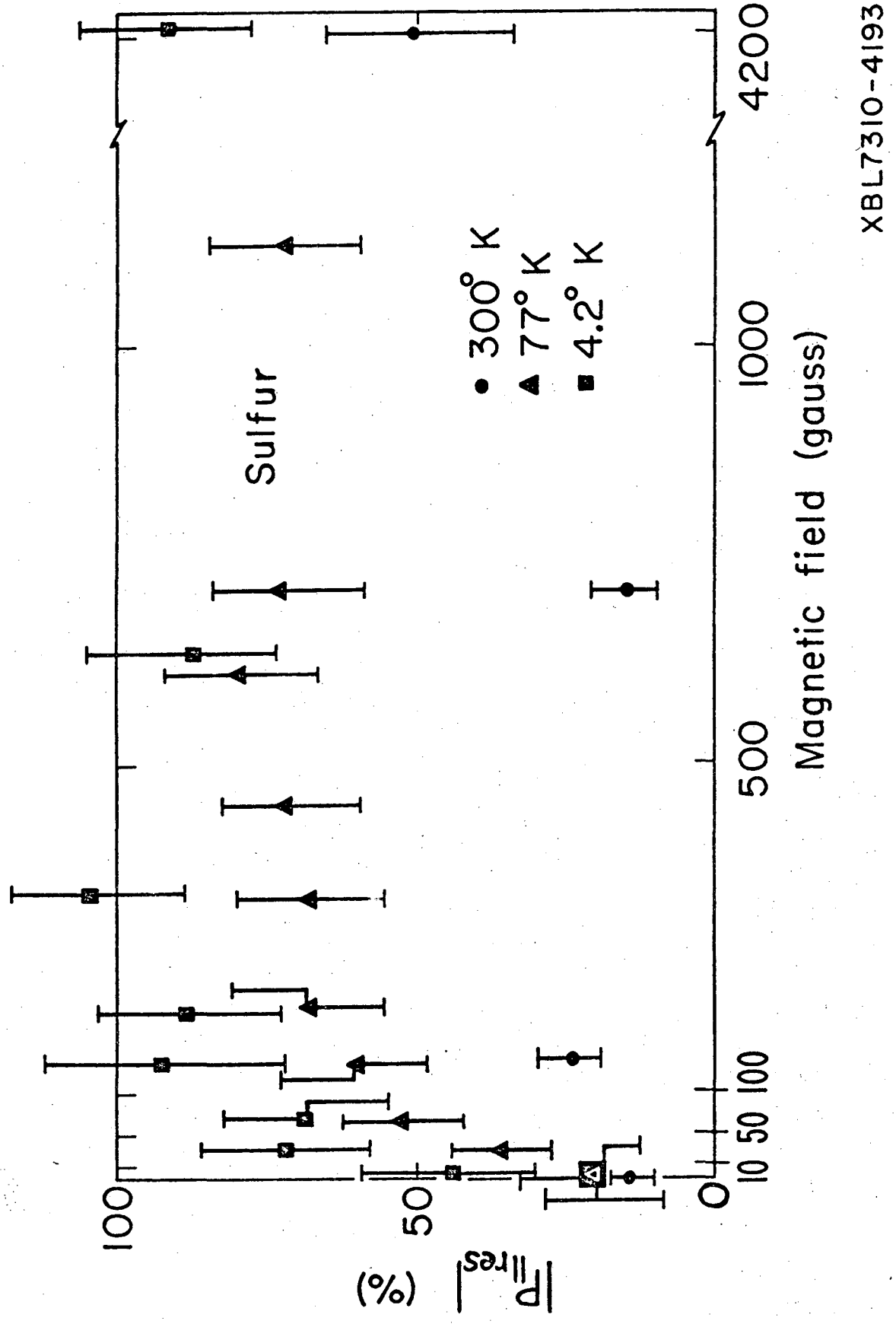
Sulfur
• 300° K
▲ 77° K
■ 4.2° K
Magnetic field (gauss)
0
10 50 100
500
1000
4200
100
50
|P⊥res| (%)
XBL7310-4193

Fig. 7.10.

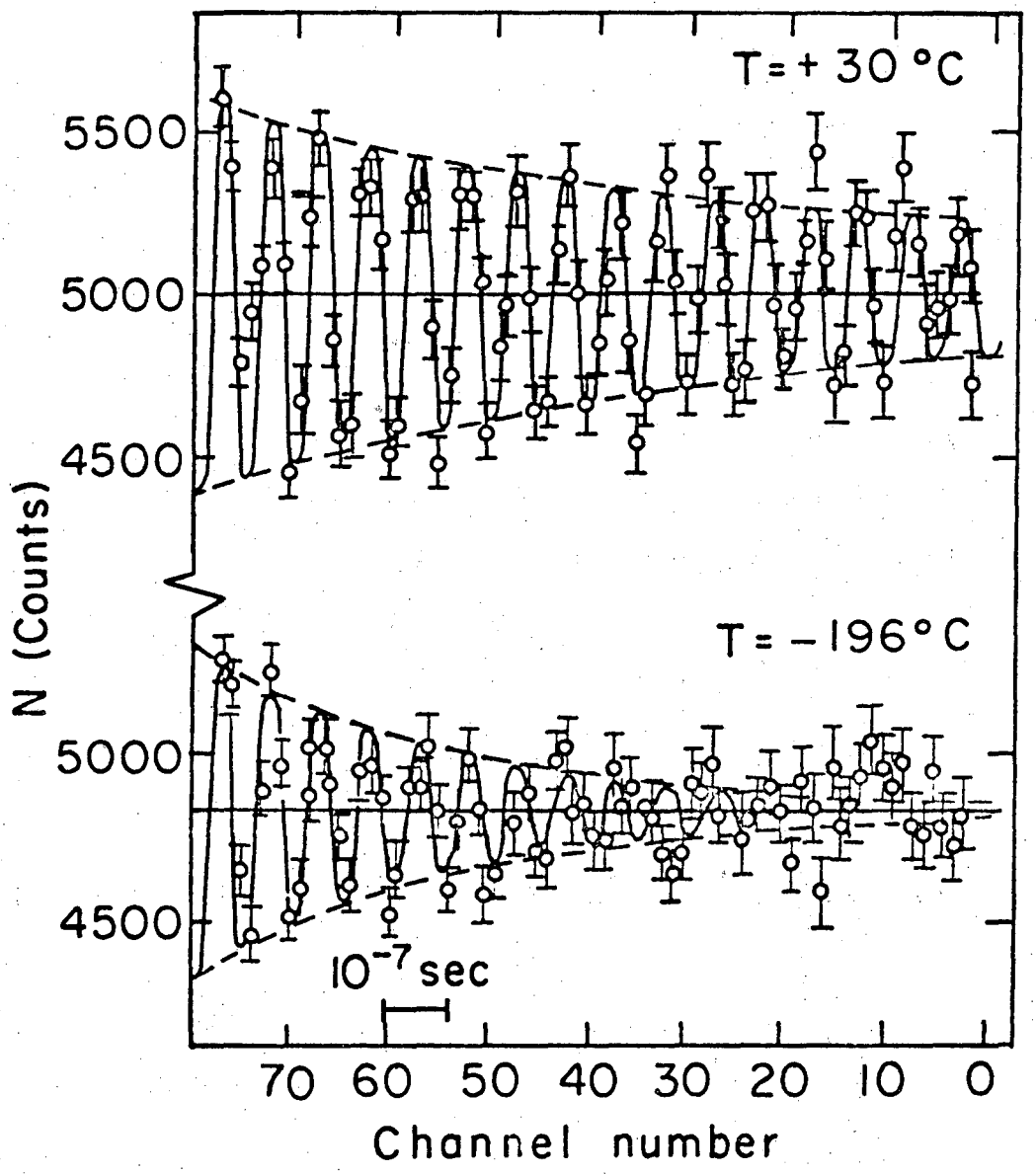
T = + 30 °C
T = − 196 °C
5500
5000
4500
5000
4500
N (Counts)
10⁻⁷ sec
70 60 50 40 30 20 10 0
Channel number
XBL741-2145

Fig. 8.1.

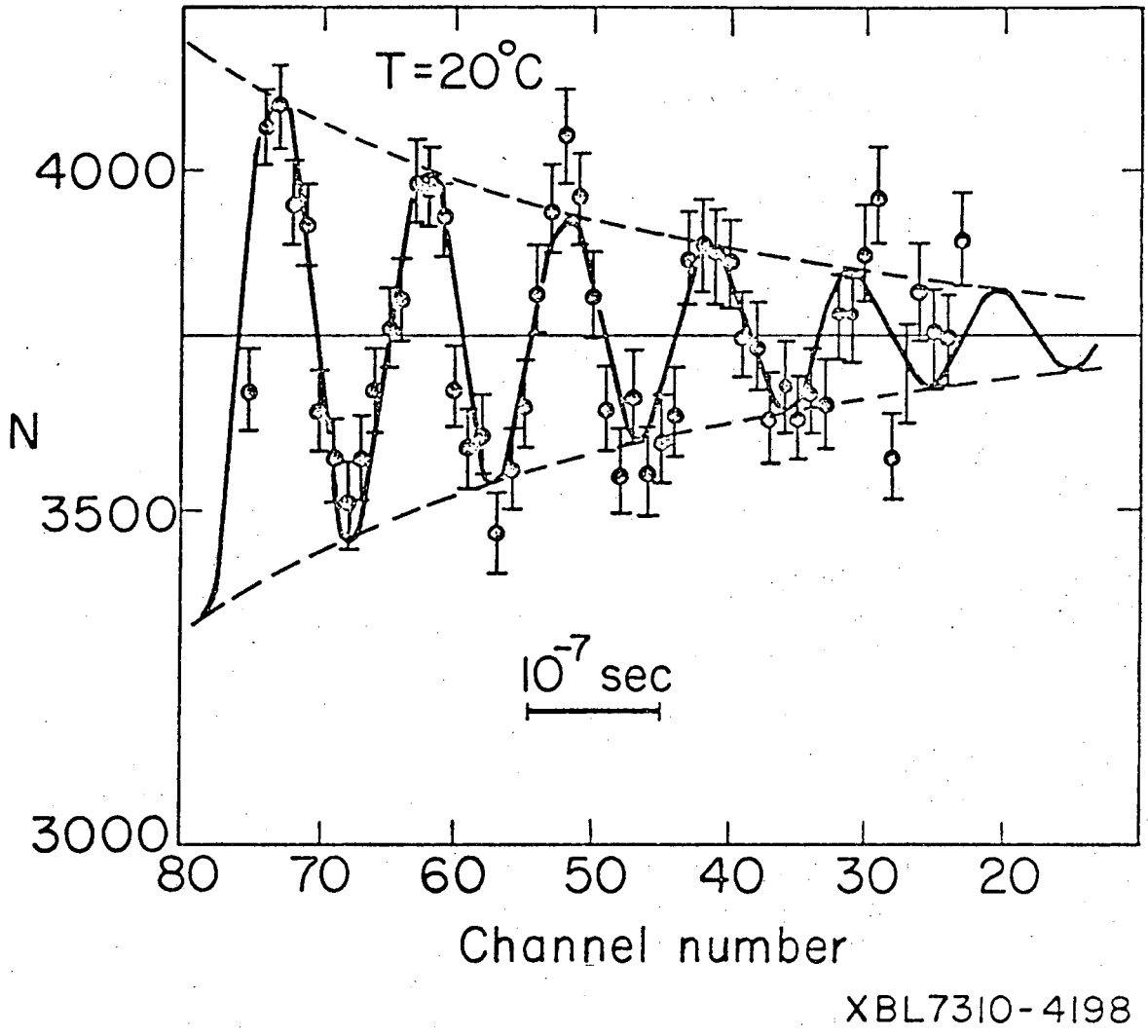
T=20°C
4000
N
3500
3000
10^{-7} sec
80
70
60
50
40
30
20
Channel number
XBL7310-4198

Fig. 8.2.

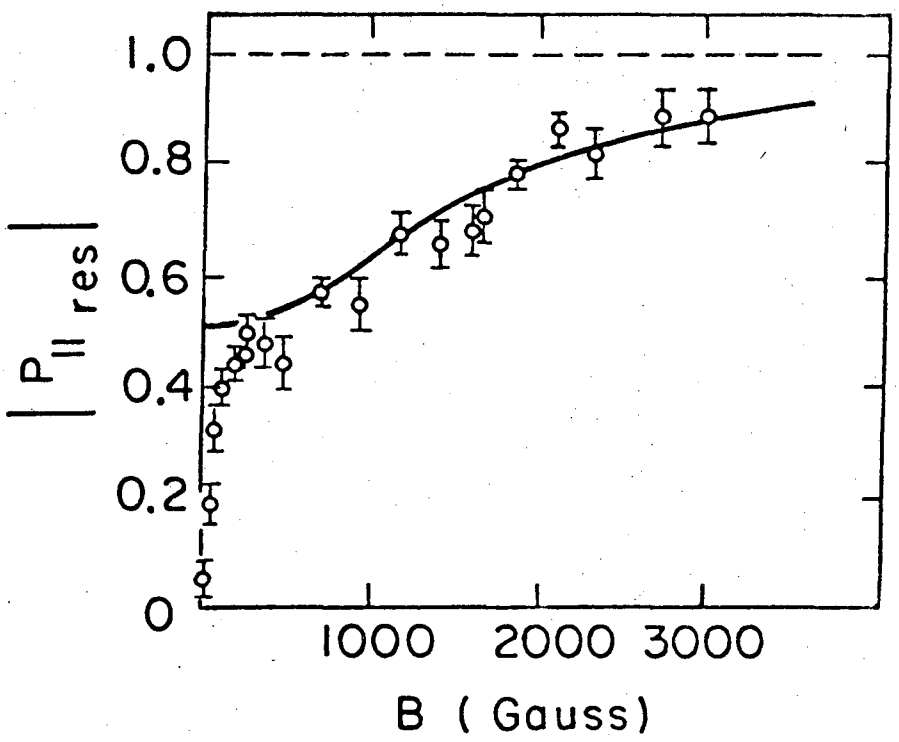

XBL741-2143

Fig. 8.3.

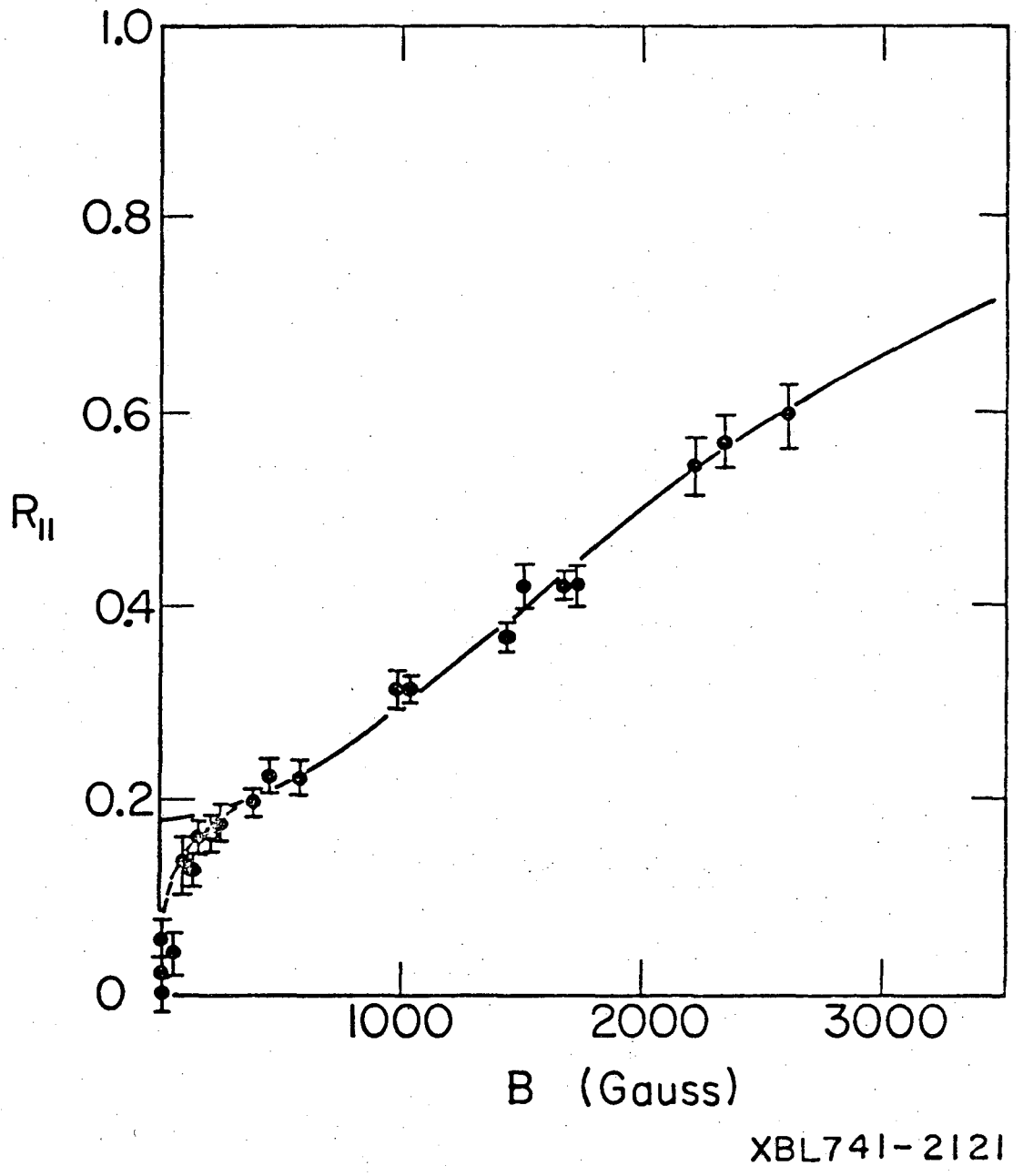

Fig. 8.4.

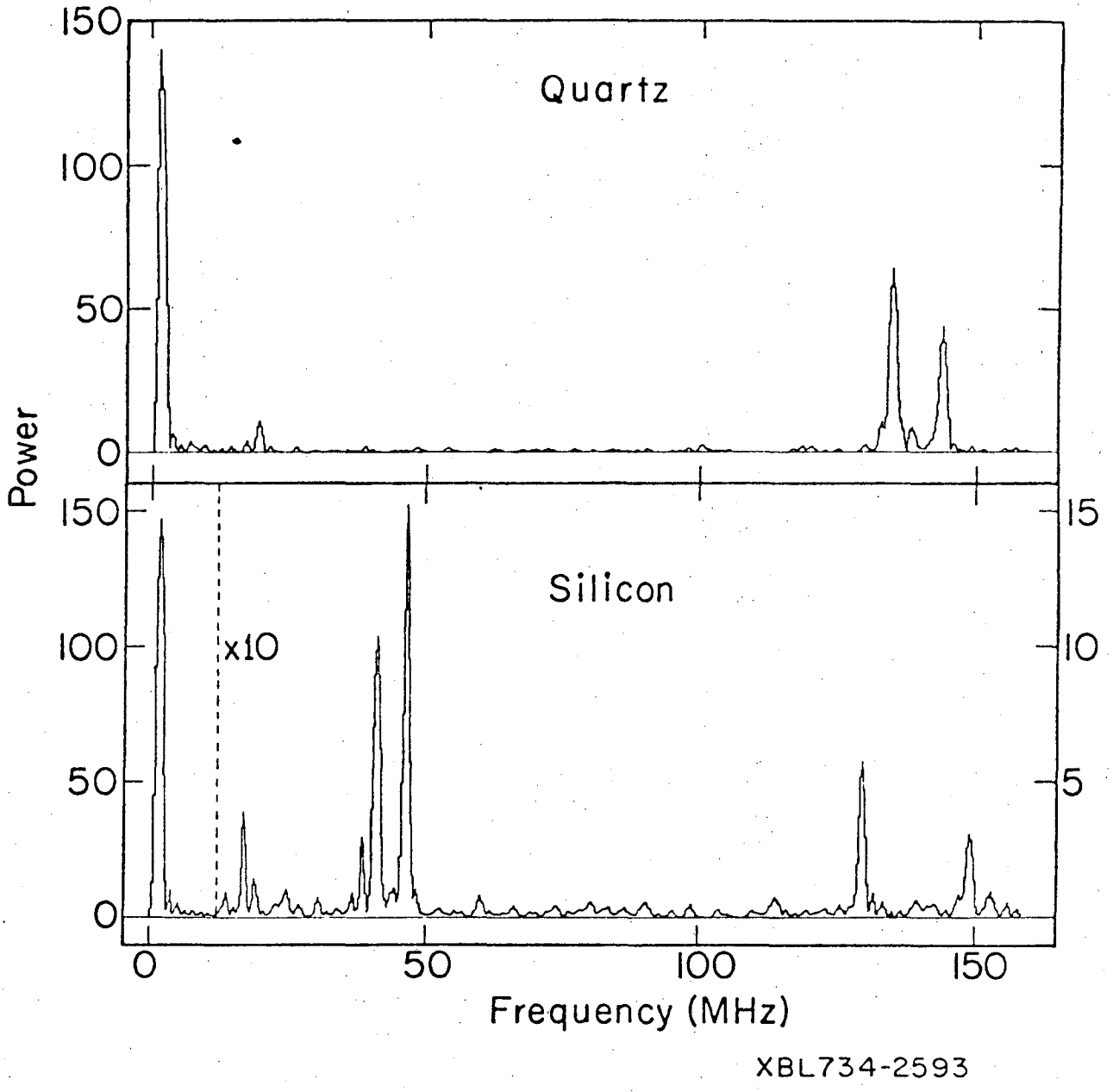
Quartz
Silicon
x10
Power
Frequency (MHz)
150
100
50
0
15
10
5
XBL734-2593

Fig. 8.5.

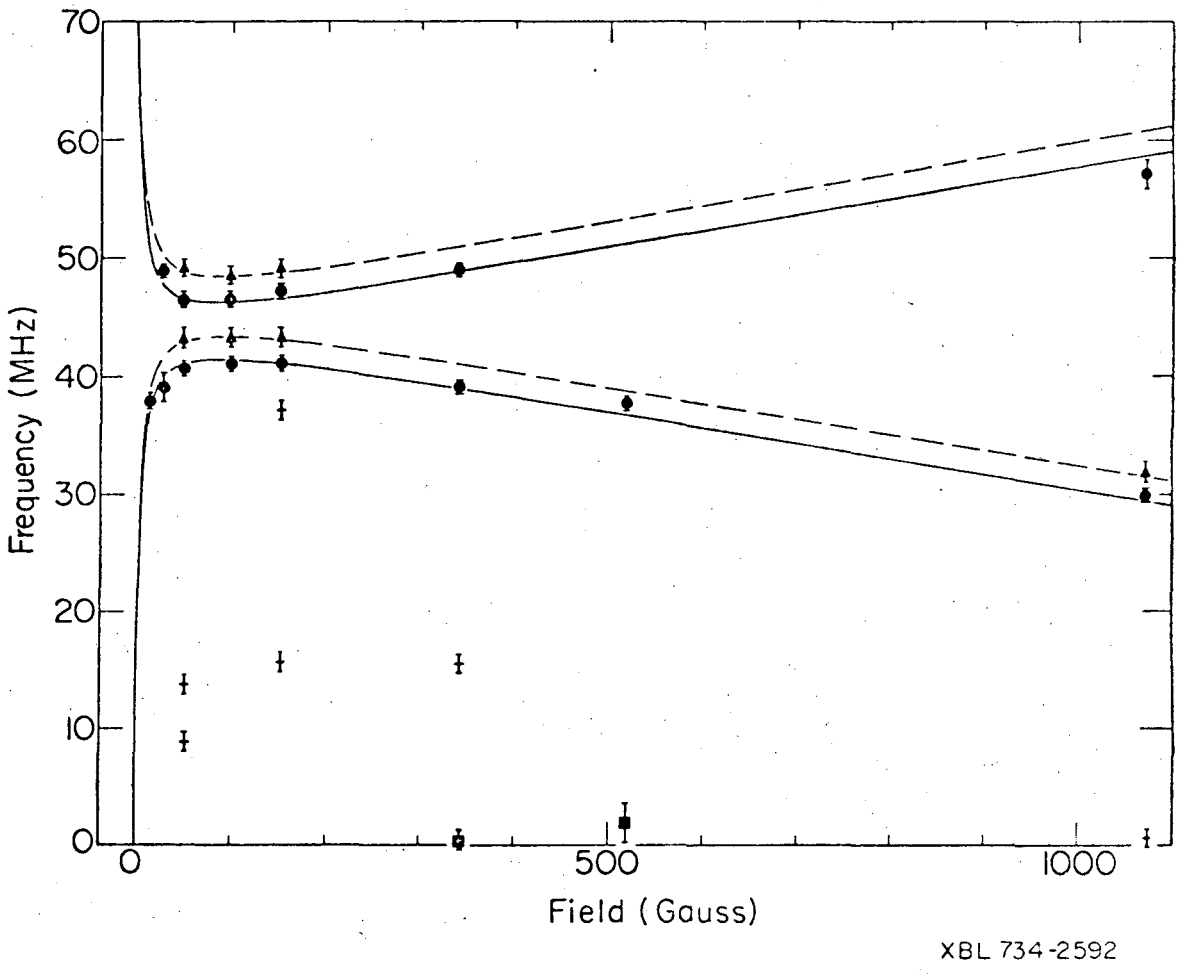
70
60
50
40
30
20
10
0
Frequency (MHz)
0
500
1000
Field (Gauss)
XBL 734-2592

Fig. 8.6.

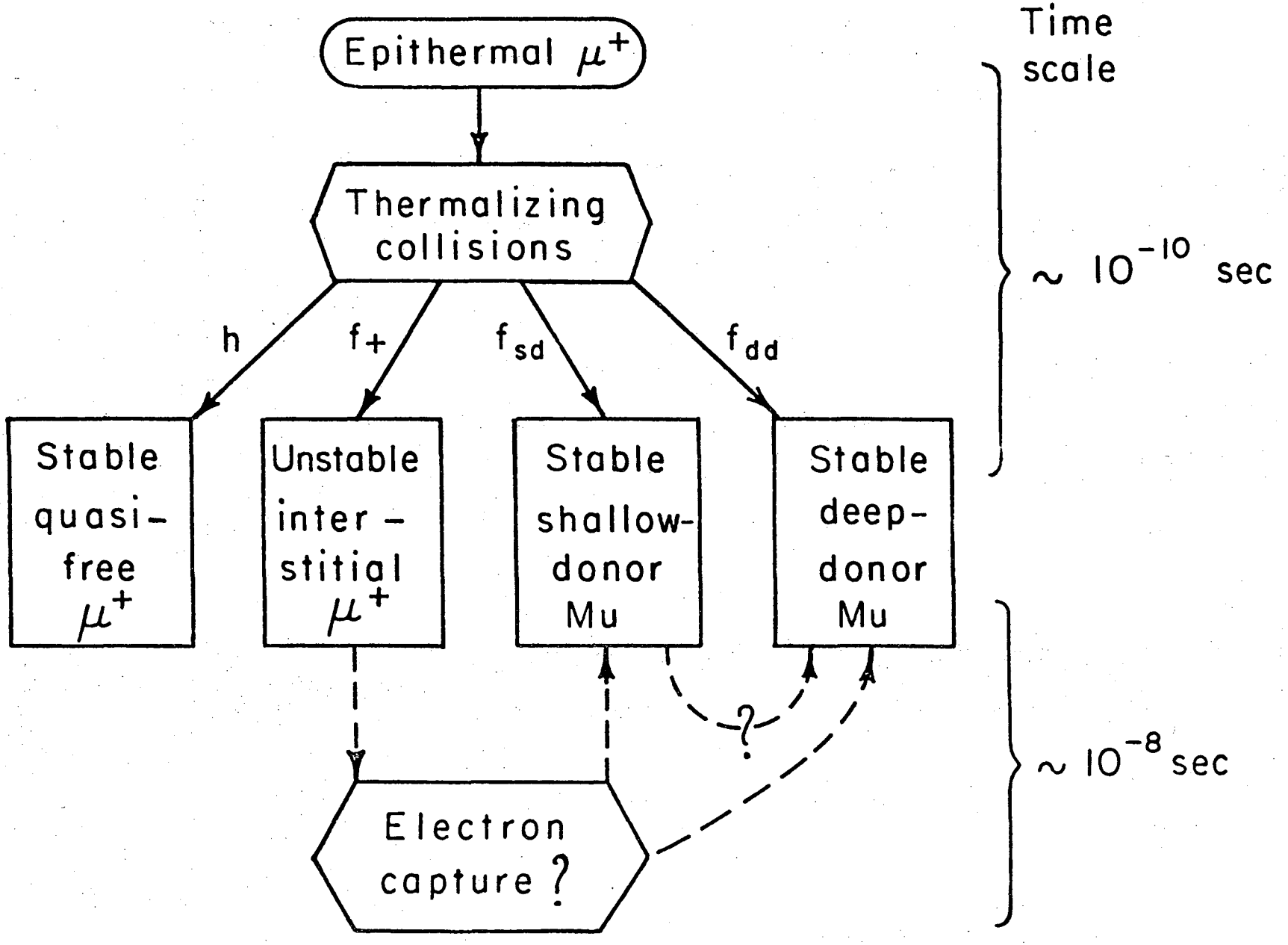

Fig. 8.7. XBL741-2125

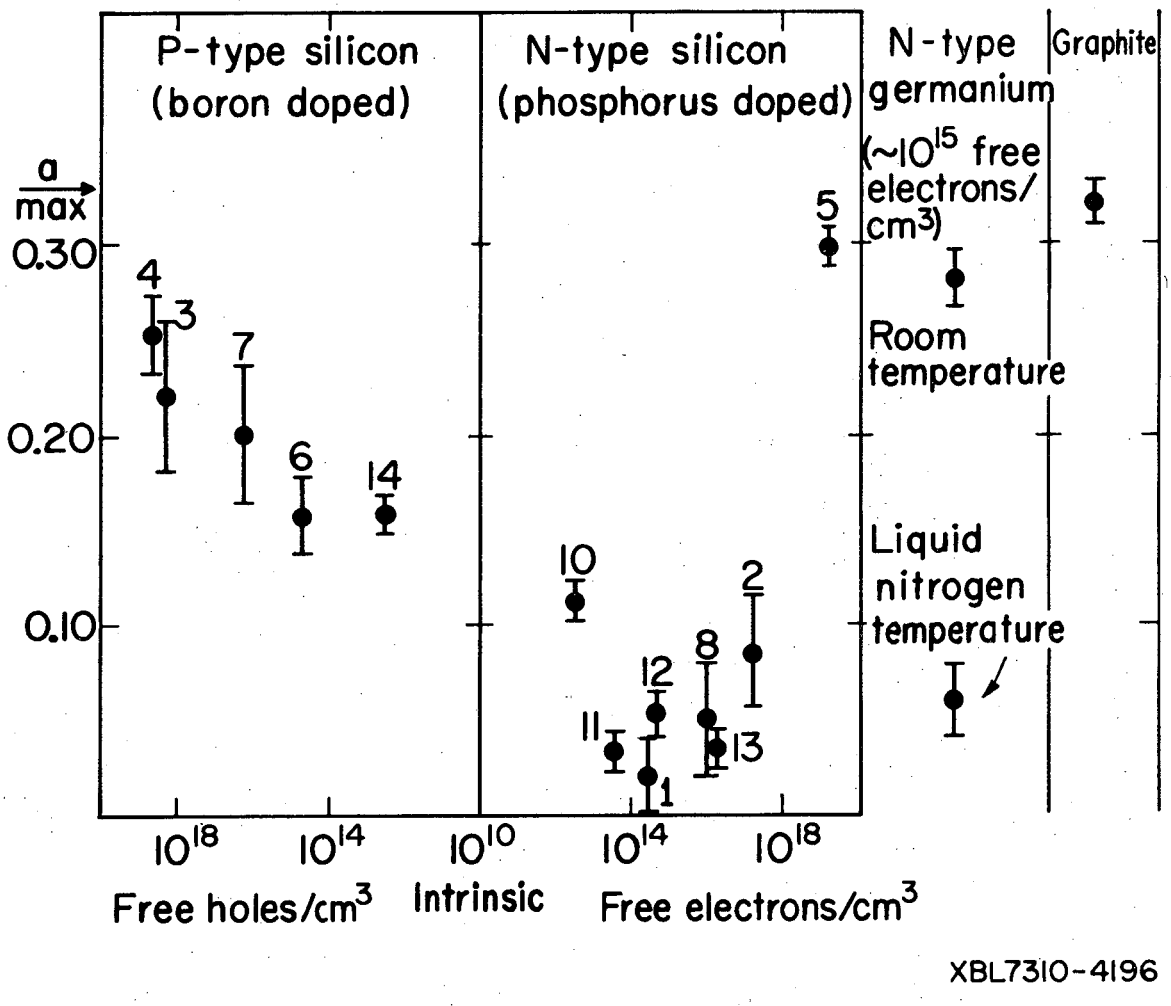
P-type silicon
(boron doped)
N-type silicon
(phosphorus doped)
N-type
germanium
(~10^15 free
electrons/
cm^3)
Graphite
a/a max
0.30
0.20
0.10
4
3
7
6
14
5
10
2
8
12
11
13
1
Room
temperature
Liquid
nitrogen
temperature
10^18
10^14
10^10
10^14
10^18
Free holes/cm^3
Intrinsic
Free electrons/cm^3
XBL7310-4196

Fig. 8.8.

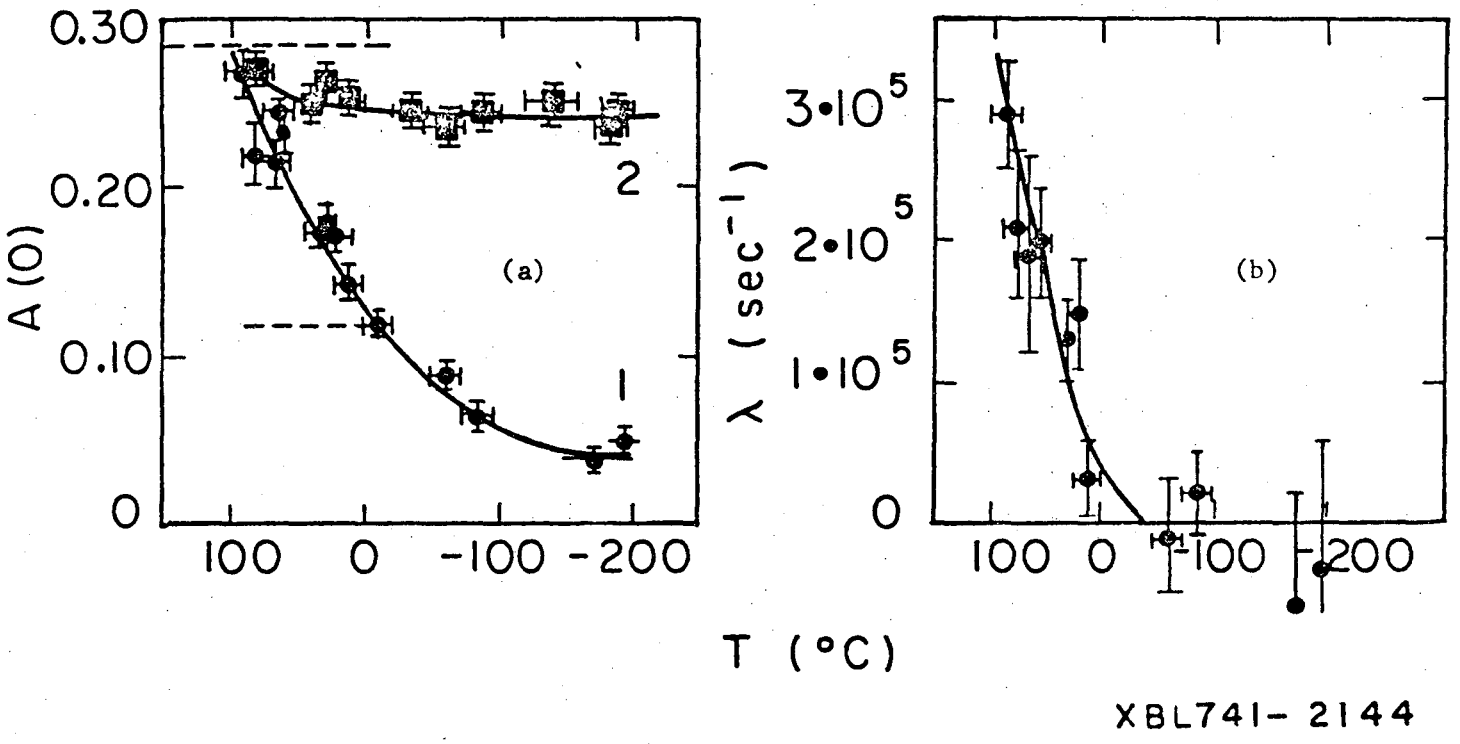
0.30
0.20
0.10
0
A (0)
(a)
2
1
100
0
-100
-200
λ (sec⁻¹)
3•10⁵
2•10⁵
1•10⁵
0
(b)
100
0
-100
-200
T (°C)
XBL741-2144

Fig. 8.9.

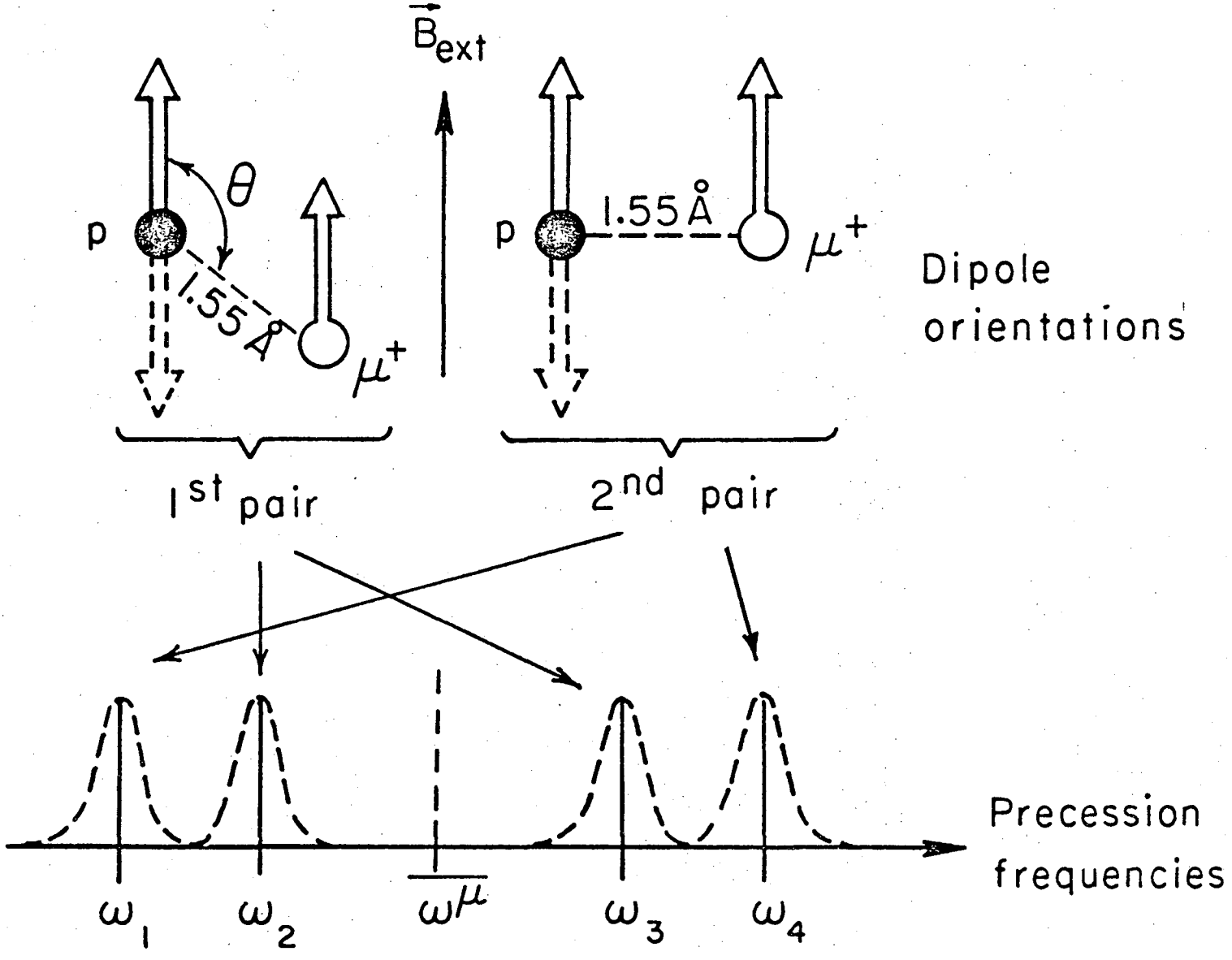
$\vec{B}_{ext}$
p
θ
1.55 Å
μ^+
p
1.55 Å
μ^+
Dipole orientations
1st pair
2nd pair
Precession frequencies
ω_1
ω_2
$\omega\mu$
ω_3
ω_4
XBL741 -2124

Fig. 9.1.

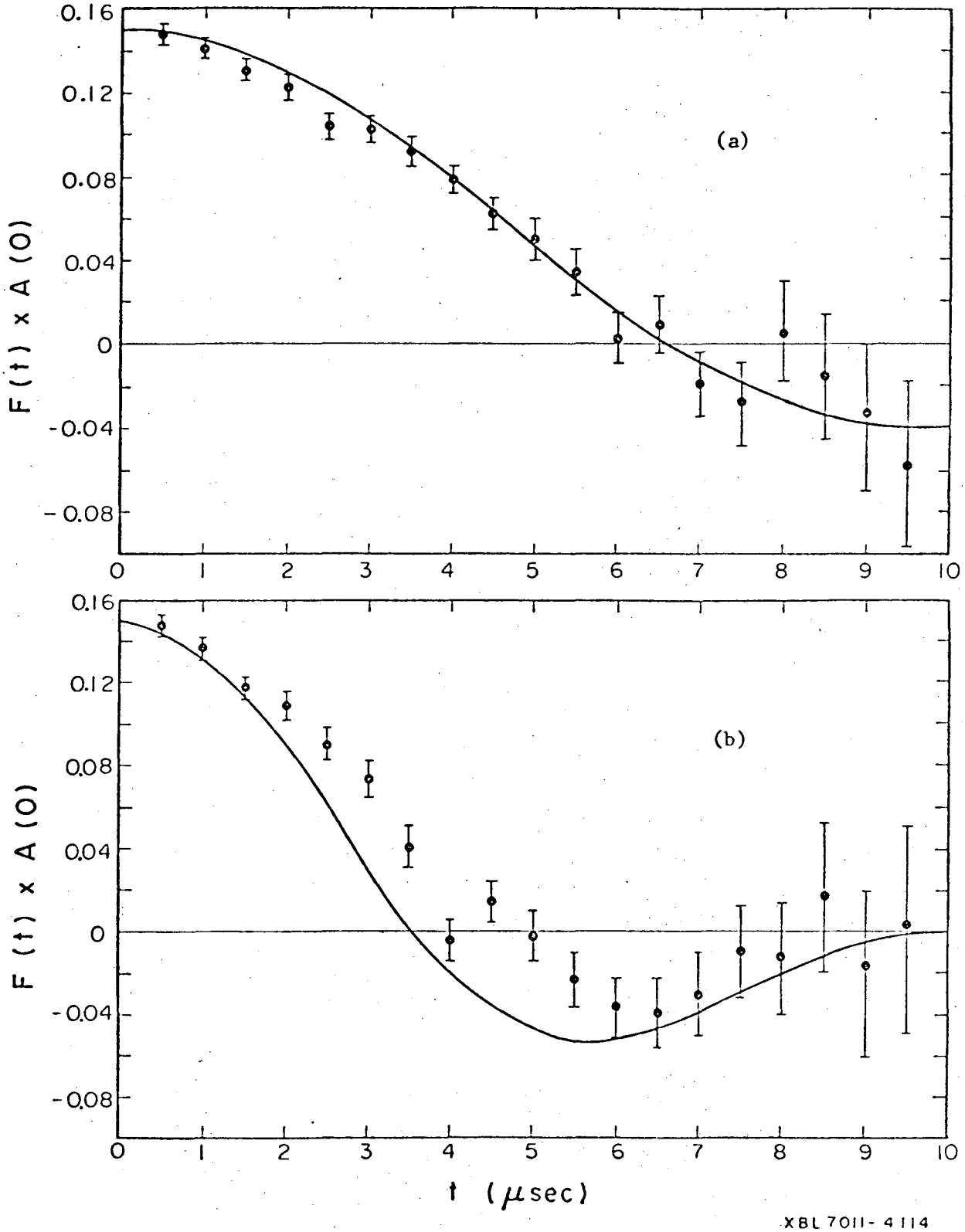
0.16
0.12
0.08
0.04
0
-0.04
-0.08
F(t) x A(0)
(a)
0 1 2 3 4 5 6 7 8 9 10
(b)
t (μsec)
XBL 7011-4114

Fig. 9.2.

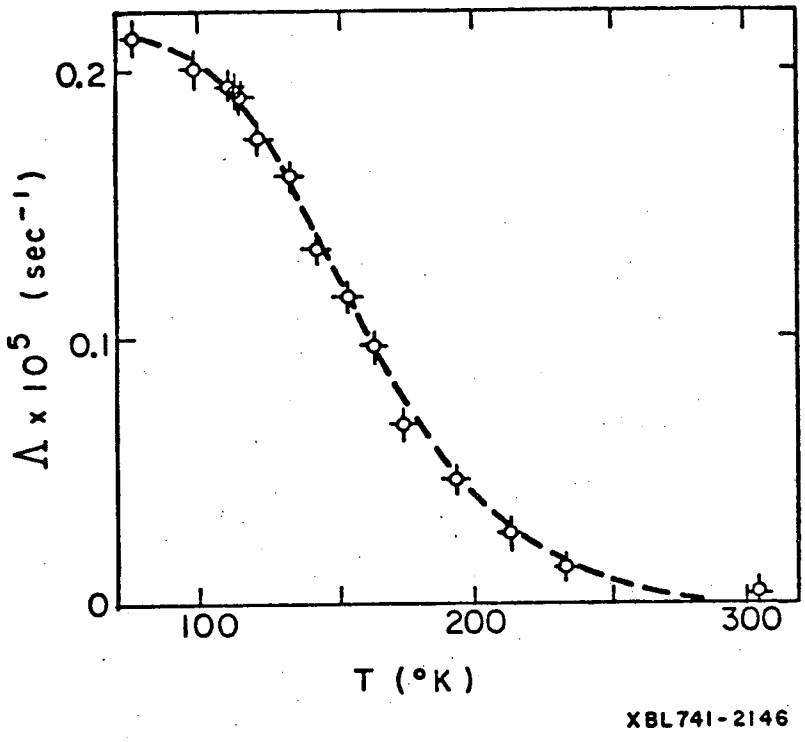
0.2
0.1
0
$\Lambda \times 10^5$ (sec^{-1})
100
200
300
T (°K)
XBL741-2146

Fig. 9.3.

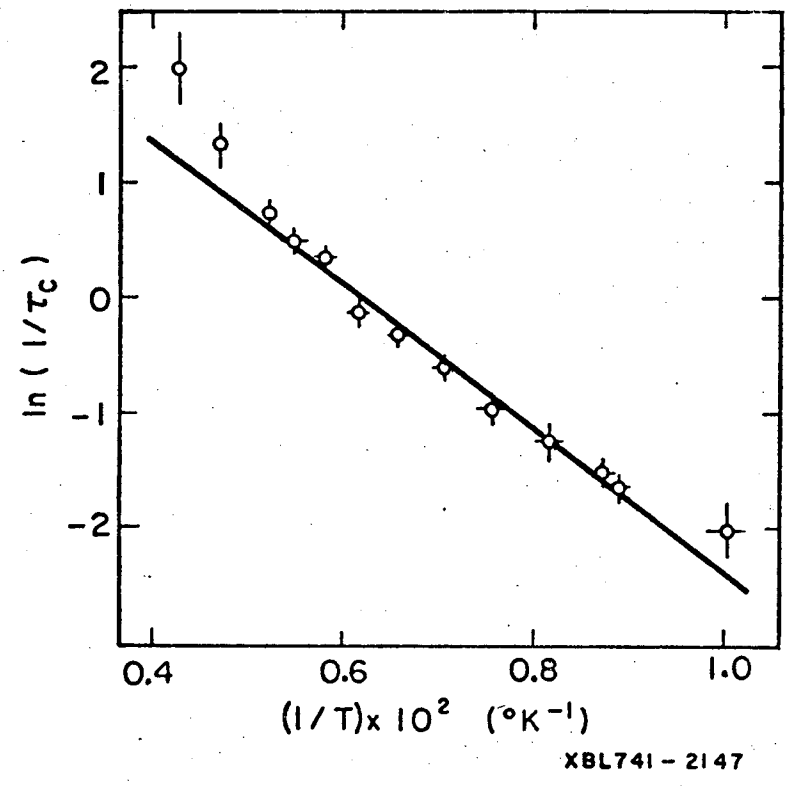
2
1
0
-1
-2
ln (1/τ_c)
0.4
0.6
0.8
1.0
(1/T)x 10^2 (°K^{-1})
XBL741-2147

Fig. 9.4.

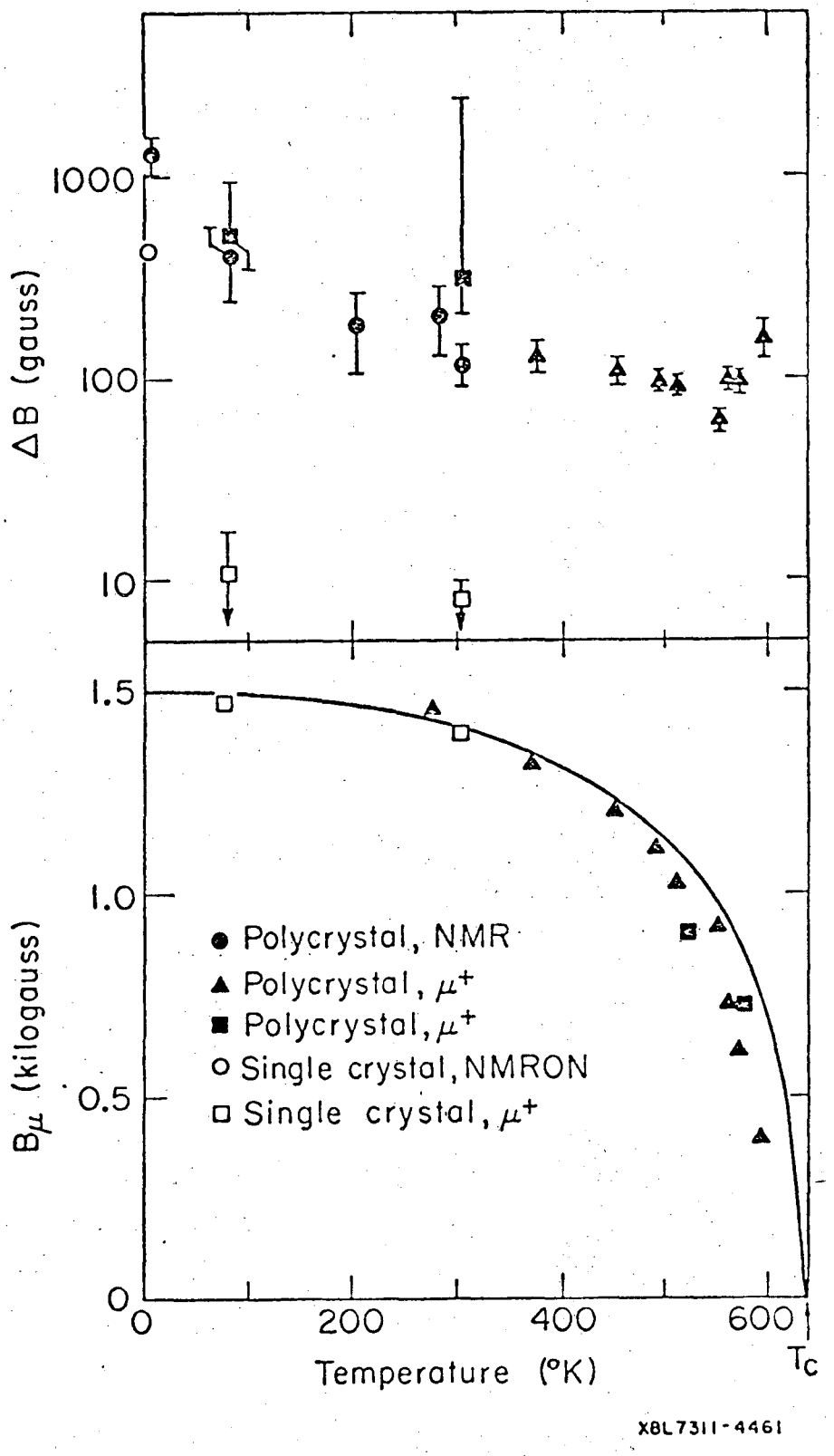
1000
100
10
ΔB (gauss)
1.5
1.0
0.5
0
B_μ (kilogauss)
Polycrystal, NMR
Polycrystal, μ^+
Polycrystal, μ^+
Single crystal, NMRON
Single crystal, μ^+
0
200
400
600
Temperature (°K)
T_c
XBL7311-4461

Fig. 9.5.

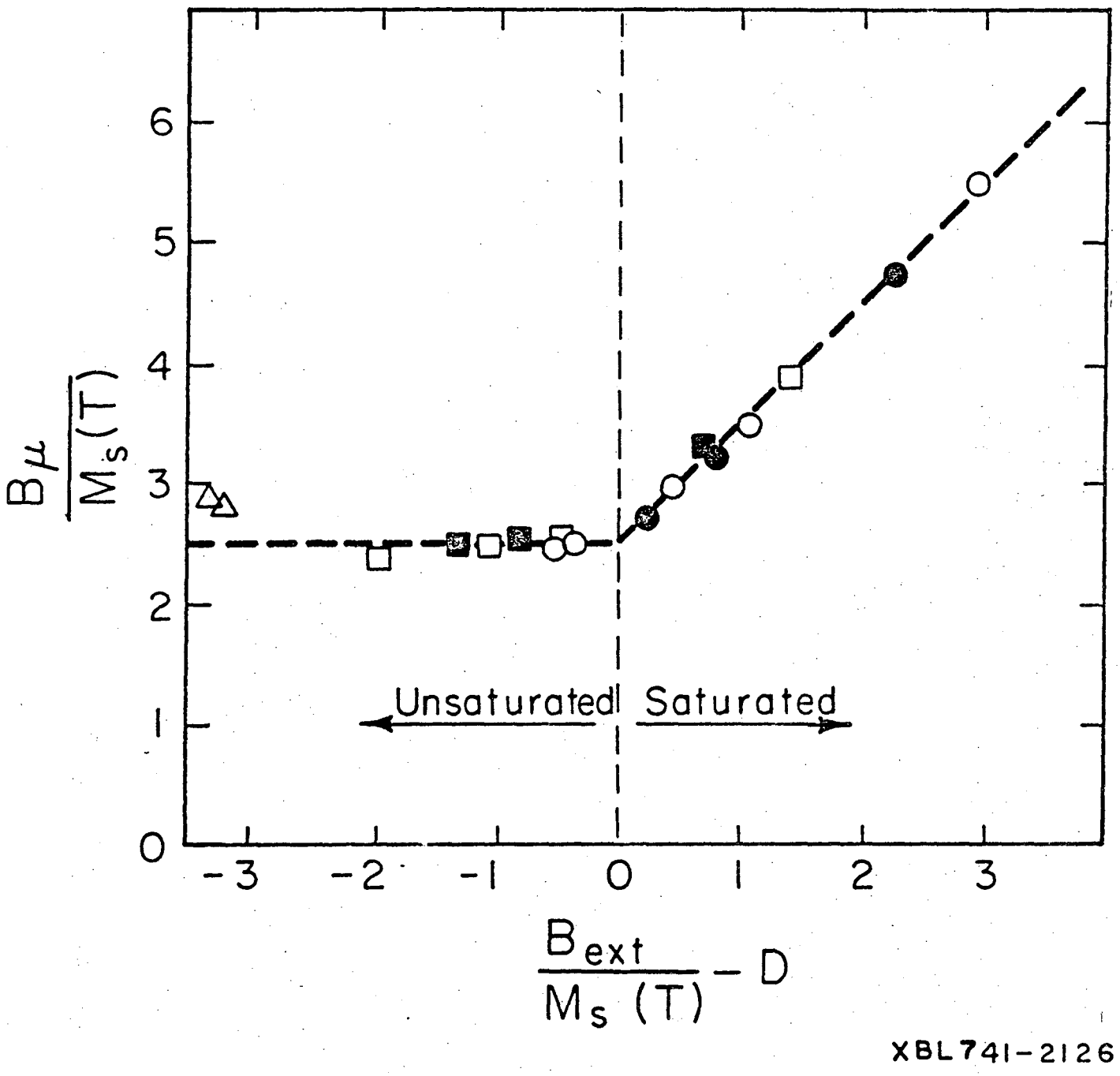
$\frac{B\mu}{M_s(T)}$
6
5
4
3
2
1
0
-3
-2
-1
0
1
2
3
Unsaturated
Saturated
$\frac{B_{ext}}{M_s(T)} - D$
XBL741-2126

Fig. 9.6.

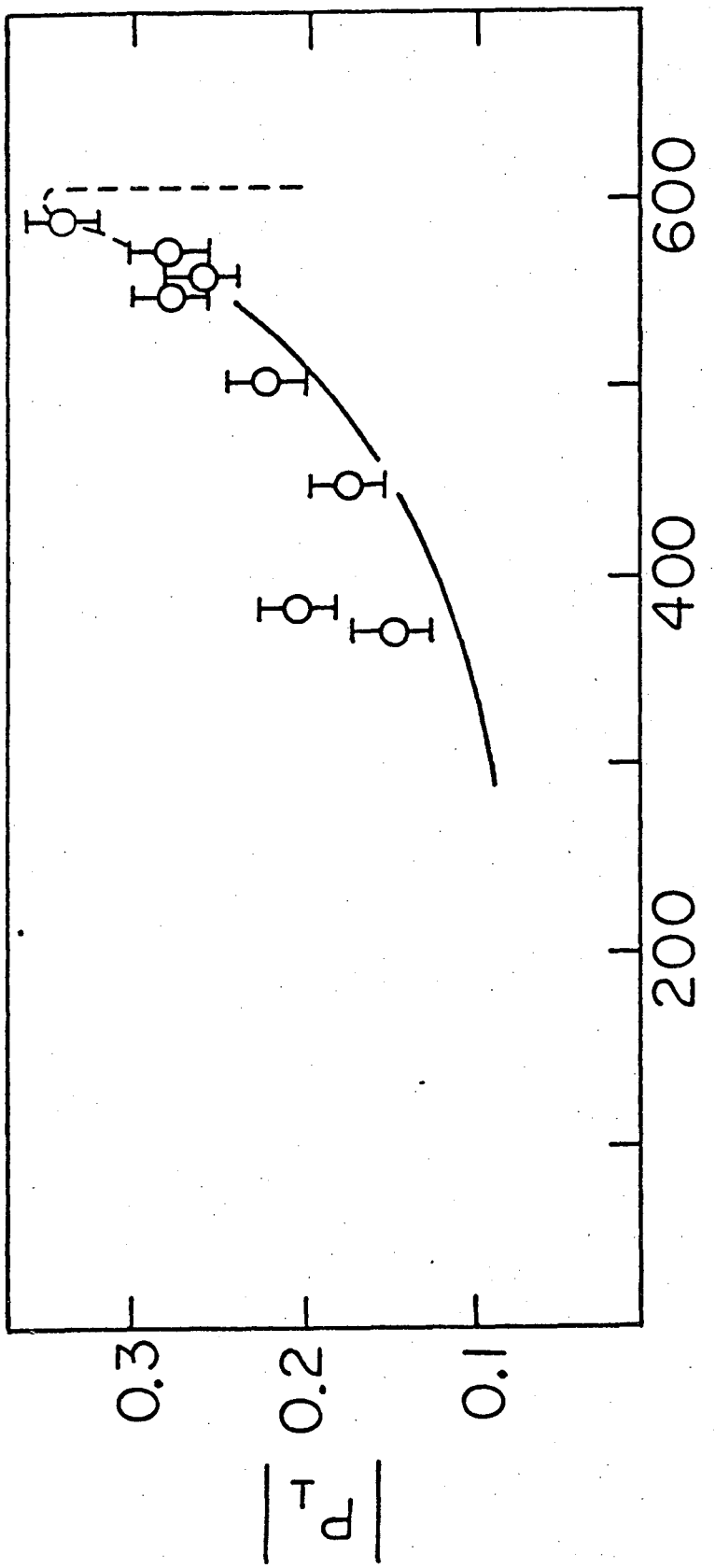

XBL741-2129

Fig. 9.7.

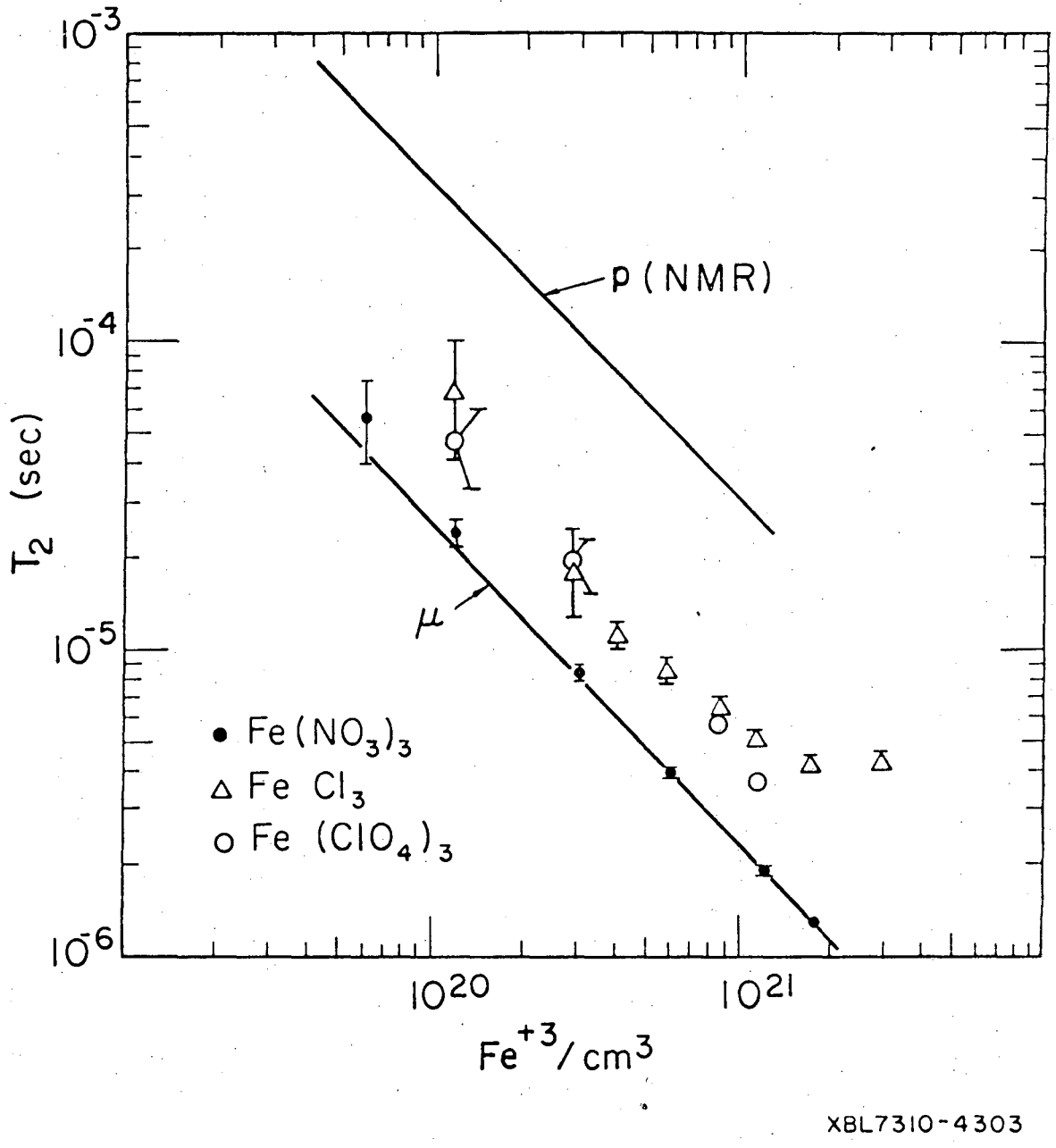
10^{-3}
10^{-4}
10^{-5}
10^{-6}
T_2 (sec)
p (NMR)
μ
● Fe $(NO_3)_3$
△ Fe Cl_3
○ Fe $(ClO_4)_3$
10^{20}
10^{21}
Fe^{+3}/cm^3
XBL7310-4303

Fig. 9.8.

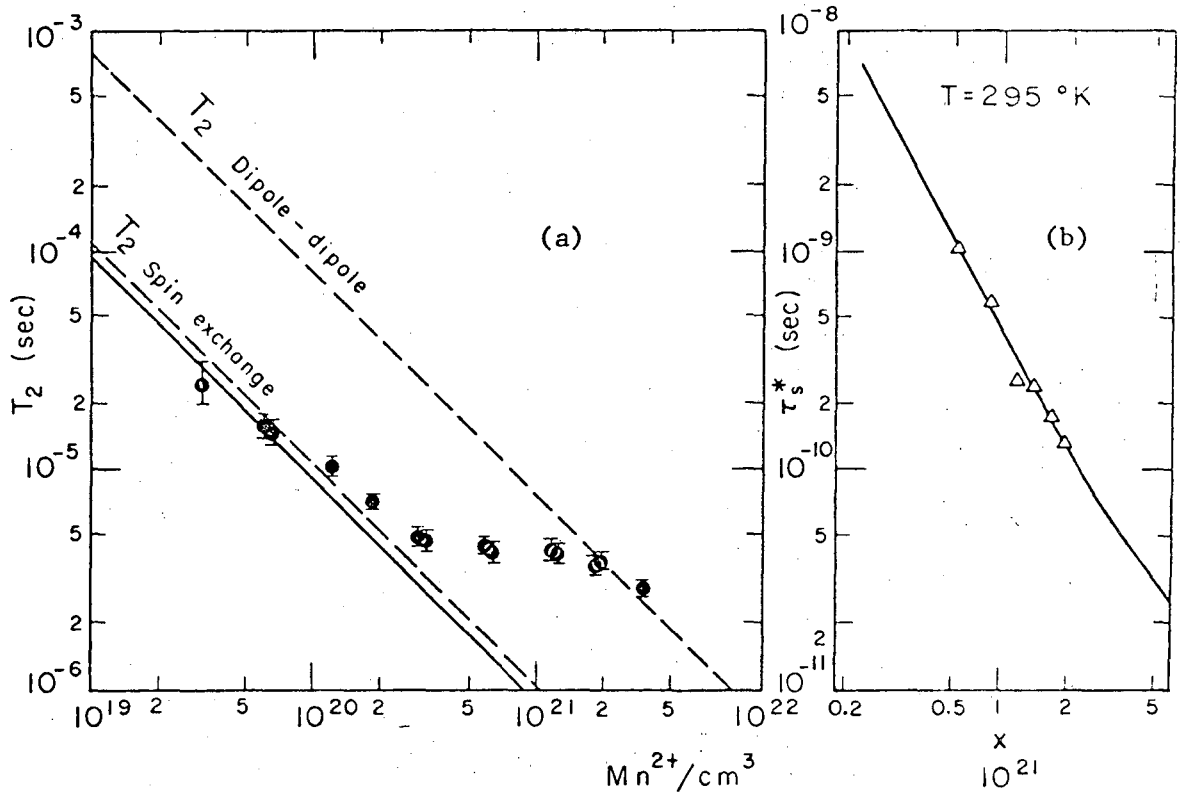
T_2 Dipole - dipole
T_2 Spin exchange
(a)
T_2 (sec)
Mn^{2+}/cm^3
T = 295 °K
(b)
τ_s^* (sec)
x
10^{21}
XBL718-4008

Fig. 9.9.

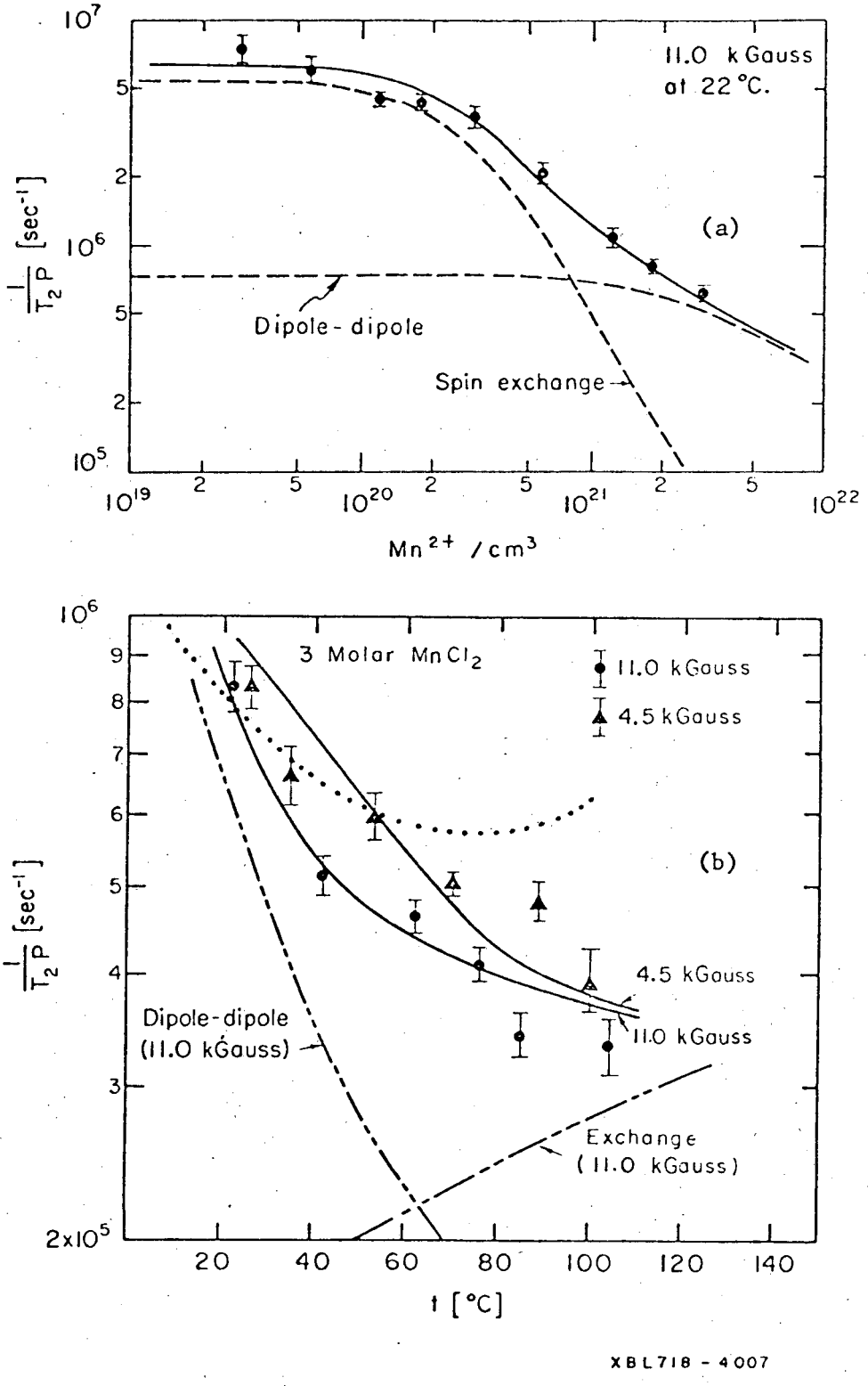
11.0 kGauss
at 22 °C.
(a)
Dipole - dipole
Spin exchange
$\frac{1}{T_2 P}$ [sec^{-1}]
Mn^{2+} /cm^3
3 Molar MnCl$_2$
11.0 kGauss
4.5 kGauss
(b)
Dipole-dipole
(11.0 kGauss)
Exchange
(11.0 kGauss)
t [°C]
XBL718 - 4007

Fig. 9.10.

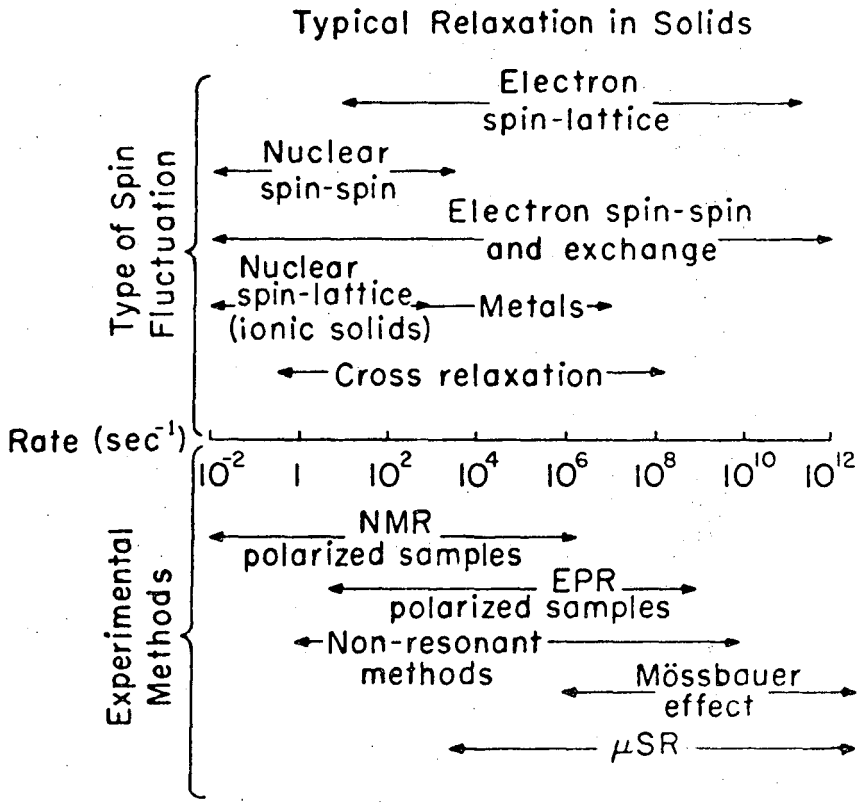
Typical Relaxation in Solids
Type of Spin Fluctuation
Electron spin-lattice
Nuclear spin-spin
Electron spin-spin and exchange
Nuclear spin-lattice (ionic solids)
Metals
Cross relaxation
Rate (sec⁻¹)
10⁻² 1 10² 10⁴ 10⁶ 10⁸ 10¹⁰ 10¹²
Experimental Methods
NMR polarized samples
EPR polarized samples
Non-resonant methods
Mössbauer effect
μSR
XBL741-2133

Fig. 10.1.

TECHNICAL INFORMATION DIVISION
LAWRENCE BERKELEY LABORATORY
UNIVERSITY OF CALIFORNIA
BERKELEY, CALIFORNIA 94720